# Geophysical Studies of Aseismic Ridges in Northern Indian Ocean- Crustal Structure and Isostatic Models

*Thesis Submitted to the Goa University for the Degree of*

**Doctor of Philosophy**
*in*
**Marine Science**

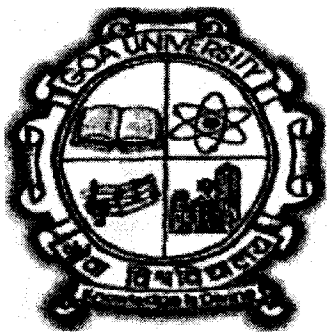



*by*

**Sreejith K.M.**

**National Institute of Oceanography (CSIR)**
Dona Paula, Goa - 403004, India

*and*

**Space Applications Centre (ISRO)**
Ahmedabad, Gujarat - 380015, India

March 2011

*Dedicated to.....*

*My Achan and Amma*

# Statement

As required under the University Ordinance 0.19.8 (vi), I state that the present thesis entitled "**Geophysical Studies of Aseismic Ridges in Northern Indian Ocean-Crustal Structure and Isostatic Models**" is my original research work carried out at the National Institute of Oceanography, Goa and Space Applications Centre, Indian Space Research Organization, Ahmedabad, and that no part thereof has been submitted for any other degree or diploma in any university or institution. The literature related to the problem investigated has been cited. Due acknowledgements have been made wherever facilities and suggestions have been availed of.

**Sreejith K. M.**

Space Applications Centre
Indian Space Research Organization
Ahmedabad-380 015

# Certificate

This is to certify that the thesis entitled "**Geophysical Studies of Aseismic Ridges in Northern Indian Ocean-Crustal Structure and Isostatic Models**" submitted by **Sreejith K. M.** for the award of the degree of Doctor of Philosophy in the Department of Marine Sciences is based on his original studies carried out by him under my supervision. The thesis or any part thereof has not been previously submitted for any degree or diploma in any university or institution.

**Dr. K. S. Krishna, FASc, FNASc**

Scientist G
National Institute of Oceanography
Council of Scientific and Industrial Research
Dona Paula, Goa- 403 004

All the corrections suggested by the referees have been incorporated

19/8/2011

19/8/2011.

# *Acknowledgements*

I hereby express my heartfelt gratitude to my research supervisor Dr. K. S. Krishna, Scientist G, National Institute of Oceanography (NIO), Goa for his inspiring guidance and constant encouragements throughout research work. I am also greatly indebted to Dr. Krishna for introducing me to outstanding geophysical problems related to evolution of major aseismic ridges of the Indian Ocean and plume-oceanic lithosphere interactions, for scientific discussions and for critical comments. It would not have been possible to complete this research work with out his constant motivation and support during the course of work both at NIO, Goa and SAC, Ahmedabad.

I am grateful to Prof. M. Radhakrishna, Department of Earth Science, Indian Institute of Technology, Mumbai (IIT-B) for his valuable guidance for development of process oriented modeling technique and for lengthy scientific discussions which I had for many weekends at IIT-B. I am also thankful to Dr. A. R. Bansal, National Geophysical Research Institute (NGRI) for his support in developing admittance analysis technique.

I thank Council of Scientific and Industrial Research (CSIR), New Delhi for awarding NET-JRF for carrying out research at NIO, Goa. This work is a part of major scientific project that was supported by Department of Science & Technology, New Delhi (project: ESS/16/174/2002) and Indian Space Research Organization (Meteorology and Oceanography Program-II).

I am also grateful to Prof. G. N. Nayak, Co-guide, Department of Marine Science, Goa University for his valuable comments and instructions from time to time. I thank Dr A. K. Chaubey, NIO for his critical reviews and constructive suggestions at various stages of the work. I further thank Dr. T. J. Majumdar, SAC; Dr. Gopala Rao, Osmania University; Dr. K Srinivas, NIO; and Prof. H. B. Menon, Goa University for their discussions and for providing critical comments.

I thankfully acknowledge Dr. S. R. Shetye, Director, NIO for his encouragement and support. I am grateful to Dr. R. R. Navalgund, Director, SAC, for kindly permitting me to continue the Ph.D while working in SAC. I am also grateful to Dr. J. S. Parihar, Deputy Director, EPSA, Dr. Ajai, Group Director, MPSG and Dr. A. S. Rajawat, Head, Geosciences Division for their constant support and encouragement during the course of work at SAC.

I express my sincere thanks to all of my colleagues and friends at NIO for their support and encouragements. From the long list, I may mention the names of Laju, Ajay, Yatheesh, Dileep, Shyju, Jayanth, Shyam, Abu, Pradnya, Sudheesh, Anoop, Nuncio, Sudheesh *chettan*, Rajani, Manoj, Sreekumar, Sijin, Vineesh and Nisha. I specially thank Honey for sending research papers, fruitful scientific discussions and helping me a lot in university matters. I also thank Praveen and Twinkle, IIT-B for their help and support during my visits to IIT-B.

My colleagues at SAC have given me immense support for successful completion of the work. Thanks to Arvind, Phani, Ratheesh, Satadru, Megha, Veera, Ami, Guneswar, Manik, Vanya, Sharad, Sriram and all other lab mates. My SAC friends and football team mates (Dr. Pal, Jidesh, Saji, Bikas, Kaushik, Rakesh, Anoop, Naveen, Ravish, etc.) kept me sane during the course of the work. I specially thank Rajesh *Chettan,* Kamala *Chechi,* Ammu and Appu for their hospitality and encouragements.

I am, indeed, short of words to express my inner-feel to my beloved family members. My father and mother always stood behind me for all important decisions, particularly for pursuing PhD after the Masters Degree. I am highly obliged to my parents for giving me constant encouragements and moral support through out the course of work. Therefore, I dedicate this thesis to them.

# PREFACE

The Indian Ocean is youngest in age and smallest in area relative to the other major oceans, Atlantic and Pacific Oceans. But its structure and evolution are very complex and the ocean encompasses with almost all varieties of geological processes. The structural framework of the northeastern Indian Ocean is unique as the region includes numerous oceanic fracture zones, aseismic ridges, seamounts, abandoned spreading centers, Sunda subduction zone, etc. Besides, the ocean floor is carpeted by enormously thick pre- and post- continental collision sediments discharged from the rivers of east coast of India and Ganges and Brahmaputra. Three aseismic ridges: 85°E Ridge, Ninetyeast Ridge and Comorin Ridge and other major features of the northeastern Indian Ocean have largely contributed in shaping the oceanic and sedimentary basins in the region. It is generally accepted that the Ninetyeast Ridge was formed by the Kerguelen hotspot activity during the rapid northward drift of Indian Plate over the hotspot. Whereas in the case of 85°E Ridge, varied opinions do exist for the evolution of the ridge. The Comorin Ridge is one of the least studied aseismic ridges in the Indian Ocean, thus not much details are available particularly regarding its origin.

The present research work consists of detailed geophysical study of the structure and isostatic compensation mechanisms of the Comorin, Ninetyeast and 85°E ridges. Available ship-borne bathymetry, gravity and magnetic data of the northeastern Indian Ocean extracted from National Geophysical Data Centre (NGDC), are collated with gravity and seismic reflection data generated in various Indian and Russian cruises. The composite geophysical datasets are investigated in detail. The isostasy of the Comorin and Ninetyeast ridges are examined using admittance analysis and two-dimensional gravity forward modeling. In the case of 85°E Ridge, a process oriented modeling technique using seismic and gravity anomaly data was performed as the ridge structure was completely buried under the Bengal Fan sediments. The present research work revealed detailed crustal architecture, isostatic compensation mechanisms and evolutionary models for these three

important aseismic ridges of the northeastern Indian Ocean, thereby the studies have provided new insights to the understanding of the geodynamic evolution of the region.

The thesis comprises seven chapters. A brief description of each chapter is given below:

**Chapter 1** gives an introduction to the concepts of plate tectonics, mantle plumes and isostasy. Some of these basic theories related to the Earth's internal processes are discussed in greater detail as they were extensively used in explaining the evolutionary models of the aseismic ridges. Further, the major objectives of the research work are also described.

**Chapter 2** outlines the structural evolution of the Indian Ocean. A general account of the major aseismic ridges of the Indian Ocean is also described using the up-to-date available geological and geophysical results.

**Chapter 3** describes theoretical and computational aspects of elastic plate model, admittance analysis, backstripping, process oriented gravity modeling and two-dimensional gravity forward modeling. Details of geophysical data sets used in this work are also included.

**Chapter 4** deals with the admittance analysis and forward modeling of gravity and bathymetry data of the Comorin Ridge. Airy model or local compensation with an elastic plate thickness (Te) of about 3 km and crust thickness (t) of 15-20 km are suggested for the southern part of the Comorin Ridge (south of 5°N), whereas for the northern part a flexural plate model with an elastic thickness of about 15 km is obtained. Admittance analysis together with the results from gravity forward modeling reveal that the south part was emplaced on relatively weak oceanic crust with both surface and sub-surface loading, while the north part was emplaced on the continental crust. For the first time, an attempt has been made to demarcate the Continent-Ocean Boundary on west of Sri Lanka and southern tip of India. The present studies coupled with published plate kinematic models suggested that the Comorin Ridge may have evolved at about 90 Ma during the rift-phase

of the Madagascar fragment from the southwest of the Indian subcontinent, possibly triggered by the Marion hotspot volcanism. A portion of this chapter has been published in "Geophysical Journal International" (Sreejith et al., 2008. Geophy. J. Int., 175, 729-741).

**Chapter 5** address two important geophysical aspects of the 85°E Ridge i) isostasy, ii) the contrasting gravity anomalies of the ridge: negative anomaly for the northern part (north of 5°N) and positive for the southern part. The morphology, extent, trend and characteristic gravity signatures are studied in detail using seismic reflection, satellite and ship-borne gravity data of the northeastern Indian Ocean. Multichannel seismic reflection and gravity data along four profiles crossing the 85°E Ridge at 14.7°, 14°, 13° and 4.5°N latitudes are modeled using process oriented method in order to determine the structure, isostasy and long-term mechanical properties of the lithosphere beneath the ridge. The results suggest that the 85°E Ridge was emplaced on approximately 10-15 km thick elastic plate (Te) and in off-ridge tectonic setting. The change of gravity anomalies through time from its inception (positive anomaly) to present (negative anomaly) is demonstrated by computation of gravity anomalies for different mantle-crust-sediment structural models of the ridge existent at three geological ages, late Cretaceous, early Miocene and Recent. The present results and published plate reconstruction information together opines that the 85°E Ridge was emplaced by a short-lived hotspot from 85 to 55 Ma in an intraplate geological setting. Recently, a portion of this chapter has been accepted for publication in "Journal of Earth System Science".

**Chapter 6** deals with the isostatic compensation mechanism and crustal structure of the Ninetyeast Ridge. Seventy two bathymetry and gravity profiles (ship-born and satellite derived) running across the Ninetyeast Ridge, spread between 28°S and 8°N latitudes with an interval of approximately 50 km, are utilized for the admittance analysis and flexural modeling in order to determine the elastic plate thickness (Te) beneath the ridge. The southern (south of 22°S latitude) and northern (north of 2°N latitude) parts of the ridge are flexurally compensated with elastic plate thickness (Te) values of >10 and >18 km, respectively. Admittance analysis suggests that the central part of the ridge (between latitudes 20°S and 2°N) has Airy type compensation with crustal thickness 15-20 km.

However, Te values derived along profiles using flexural modeling, revealed that that central part of the ridge could be further divided into 1) south-central part (18°S to 8°S), where the Te values constantly decrease from 20 to 5 km and 2) north-central part (8°S to 2°N), where Te values randomly vary between 2 and 25 km. Further, the ridge crustal structure was derived along five representative profiles (with different Te values) by using gravity forward modeling under the constraints of seismic reflection and refraction results. Based on the present results and published plate reconstruction results, a convincing evolutionary model is proposed for the evolution of the underneath oceanic lithosphere and emplacement of the Ninetyeast Ridge. The southern part of the ridge was emplaced on a lithosphere of intermediate strength possibly along the edge of the Indian plate, whereas northern part of the ridge was emplaced in an intraplate setting. The highly variable isostatic compensation mechanism in the central part of the ridge could be a manifestation of complex interactions between the Kerguelen hotspot and spreading ridge segments. The north-central part of the ridge may have emplaced on a crust of highly variable age produced by multiple southward ridge jumps, whereas the south-central part was emplaced on a crust of uniformly increasing age towards south produced as a result of a major southward ridge jump.

**Chapter 7** summarizes and synthesizes important results with future outlook.

# CONTENTS

# List of Tables

# List of Figures

# CHAPTER 1

# Introduction

# Introduction

## 1.1 General

The Indian Ocean is youngest in age and smallest in area relative to the other major oceans, Atlantic and Pacific Oceans. But its structure and evolution are very complex and the ocean encompasses with almost all varieties of geological processes. A systematic scientific study of the Indian Ocean has started after successful completion of the International Indian Ocean Expedition (IIOE) during the period 1960-65. Geological and geophysical data of the IIOE and subsequent major scientific expeditions including the Deep Sea Drilling Project (DSDP) and the Ocean Drilling Program (ODP) have brought out broader understanding of geodynamic evolution of the Indian Ocean since the break-up of eastern Gondwanaland in early Cretaceous. However, major scientific aspects like precise timing of continental brake-up, continental margin evolution, hotspot activity, formation of aseismic ridges etc. are not fully understood.

The structural framework of the northeastern Indian Ocean is unique as the region includes numerous oceanic fracture zones, aseismic ridges, seamounts, abandoned spreading centers, Sunda subduction zone, etc. Besides, the ocean floor is carpeted by enormously thick pre- and post- continental collision sediments discharged from the rivers of east coast of India, Ganges and Brahmaputra. Three aseismic ridges, 85°E Ridge, Ninetyeast Ridge and Comorin Ridge are the major structural features in the northeastern Indian Ocean. The Ninetyeast Ridge is a product of the Kerguelen hotspot activity, whereas varied opinions exist for the origin of the 85°E Ridge. The Comorin Ridge is one of the least studied aseismic ridges and a little is known regarding its origin and isostasy. Crustal structure, isostasy and origin of these aseismic ridges are key elements to better understand the tectonic evolution of the Indian Ocean lithosphere.

## 1.2 Plate Tectonics

The theory of *Plate Tectonics* in earth science is a relatively new scientific postulation and it has revolutionized our understanding of the dynamic planet Earth, upon which we live. In geology the word "plate" refers to thin and rigid slab of rocks, whereas "tectonics" term comes from the Greek root "to build". Plate tectonic theory suggests that outer most layer of the Earth is fragmented into numerous segments of varying size and the segments are being moved relative to each other over a fluid substratum (asthenosphere). These segments are called lithospheric or tectonic plates. The average thickness of the lithospheric plate is 100 km and consists of crust and upper part of mantle. The fluid layer below the lithosphere up to a depth of ~ 670 km is referred as asthenosphere. The asthenosphere is being heated by radioactive elements such as Uranium, Thorium, and Potassium and the rocks are partially molted and led to convection currents, which eventually drive the rigid lithospheric plate over the asthenosphere with relatively little resistance. The disposition of major tectonic plates of the Earth is illustrated in Figure 1.1.

The idea of moving continents was existing much before the advent of plate tectonic theory. In 1912 Alfred Lothar Wegener postulated that continents were once compressed into a single protocontinent, which he called Pangaea (meaning "all lands"), and over the time they have drifted apart and reached to the current distribution. Wegener's continental drift hypothesis (Wegener, 1922) was mainly based on the observation that most of the continents appears to fit together like a puzzle such as the West African coastline seems to snuggle nicely into the east coast of South America. A more close fit is observed if submerged continental shelf is considered rather than the present-day coastline. The other evidences supporting the hypothesis includes 1) occurrence of same fossilized plants and animals from the same time period across continents 2) similarity in rock formations 3) striae left by the scraping of glaciers over the land surfaces. Further, Wegener's drift hypothesis has provided an explanation for mountain building process; the leading edge of the drifting continents would encounter resistance and thus compress and fold upwards for forming mountains. Wegener also suggested that India drifted northward into the Asia forming the Himalayas.

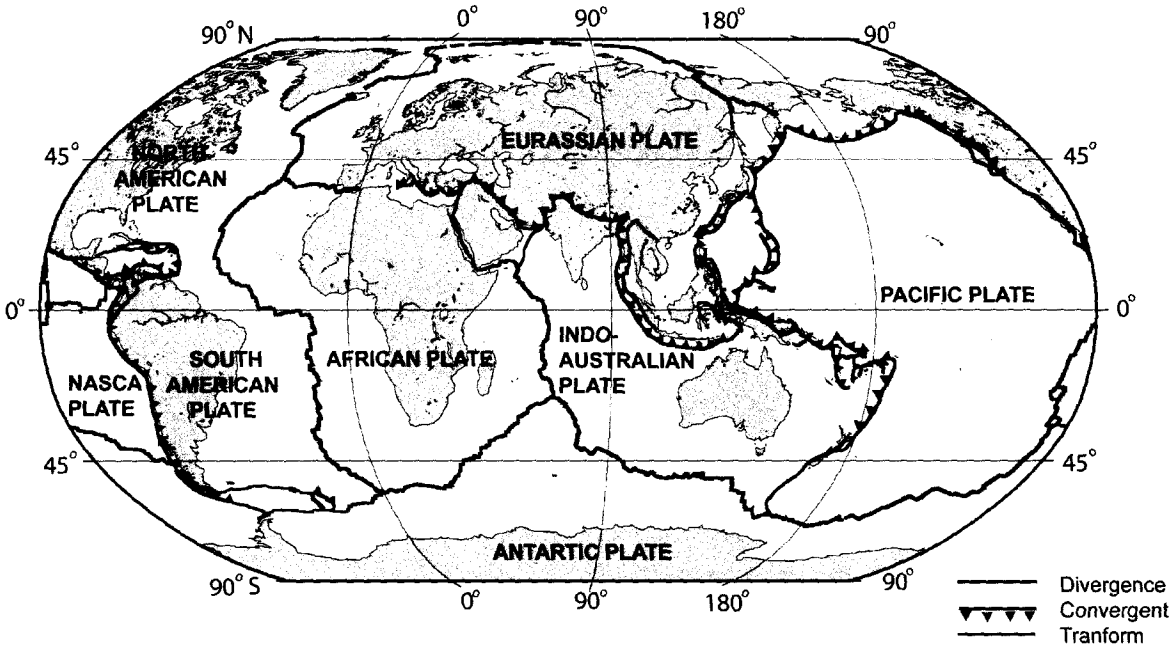


**Figure 1.1** Disposition of major tectonic plates on the Earth. Divergent, convergent and transform plate boundaries are also shown.

Though the theory of continental drift would become the spark that ignited a new way of viewing the Earth, it terribly failed to explain the nature of forces, which propelled giant and massive continents around the surface of the Earth. Wegener's model of continental movement over ocean floor, like boat on the surface of water, was rejected by the scientific community and then theory remained dormant until the discovery of *Seafloor Spreading* theory (Hess 1960, 1962; Dietz, 1961). This theory suggests that new magma from deep within the Earth rises easily through the weak zones and eventually erupts along the ridge crest to create a new oceanic crust. Further, the new oceanic crust generated at the ridge crust moves away like a conveyer belt motion, and finally descends down to mantle along deep-trenches, hence the total surface area of the Earth essentially remains constant. The most definitive evidence for seafloor spreading process comes from study of the linear magnetic anomalies that characterizes the ocean floor. The Earth's magnetic field in the geological past has flip-flopped several times, when the magna cools down through Curie temperature it acquires the Earth's prevailing magnetic polarity leading to zebra-like magnetic strips of normal and reverse polarity parallel to the ridge system. This hypothesis was supported by several lines of evidence: (1) at or near the crest of the ridge, the rocks are very young, and they become progressively older away from the ridge crest; (2) the youngest rocks at the ridge crest always have present-day (normal) polarity; and (3) stripes of rock parallel to the ridge crest alternated in magnetic polarity recording the history of the Earth's magnetic field reversals. Vine and Mathews (1963) and independently by Morley and Larochelle explained the seafloor spreading theory in the light of Earth's magnetic reversals, and later the theory was known as Vine and Mathews seafloor spreading hypothesis.

Thus, the continental drift hypothesis with strong support from seafloor spreading hypothesis framed the basic concepts of tectonic plates and their internal dynamics. The actual mechanism of plate motion was explained by the mantle convection phenomena by Tuzo Wilson (1965, 1966). Below the lithospheric plates, at some depth the mantle is partially molten and can flow, albeit slowly, in response to steady forces applied for long periods of time. Hot magma rises below the mid-oceanic ridge system, spreads latterly

carrying the plates and finally cold plates decent down to mantle, where the plate material is reheated and leading to another cycle. Though mantle convection and seafloor spreading provided a basic mechanism of plate tectonics, recent studies show that "slab pull" created by the sinking lithospheric plates at subduction zones are more prominent driving forces.

### 1.2.1 Plate Boundaries

Plate boundaries are geodynamically active deformed zones, where a large fraction of earthquakes, volcanic eruptions and mountain building take place. Plate boundaries are broadly classified as divergent, convergent, transform and diffuse (Figures 1.1 and 1.2).

Along the divergent boundaries lie along the spreading centers, lithospheric plates are created by the up-welling of magma from the mantle. The two plates from either side of the ridge crest move away in opposite direction with almost equal velocities of few centimeters per year. The gap generated by the diverging plate is filled by the hot, molten rocks from the mantle. The up-welled mantle rocks subsequently cool down due to conductive heat rocks and accrete to the base of the spreading plates. As the plates move away from the spreading centre, they cool down, become denser and thicker leading to subsidence. The divergent boundary or the ridge crest is topographically elevated due to greater buoyancy of the thinner and hotter lithosphere. A component of the gravitational body force of the elevated lithosphere drives the plates away from the accretionary boundary. This gravitational sliding forms an important force called "ridge push" which eventually drives the plates. The lithospheric plates created at the divergent plate boundaries are being destroyed almost at the same rate to keep the total surface area of the Earth constant. Away from the ridge crest, the old, dense and thick lithosphere becomes gravitationally unstable and sinks into the mantle along oceanic trenches or convergent plate boundaries. The descending plate creates negative buoyancy forces which get transmitted to the surface of the entire plate casing pulling towards the trench. This is the most important force that drives the plates and hence causes continents to move and known as "slab pull". The immense stress involved in the subduction dynamics results numerous high-magnitude earthquakes along the subduction zones. The locations of these deep

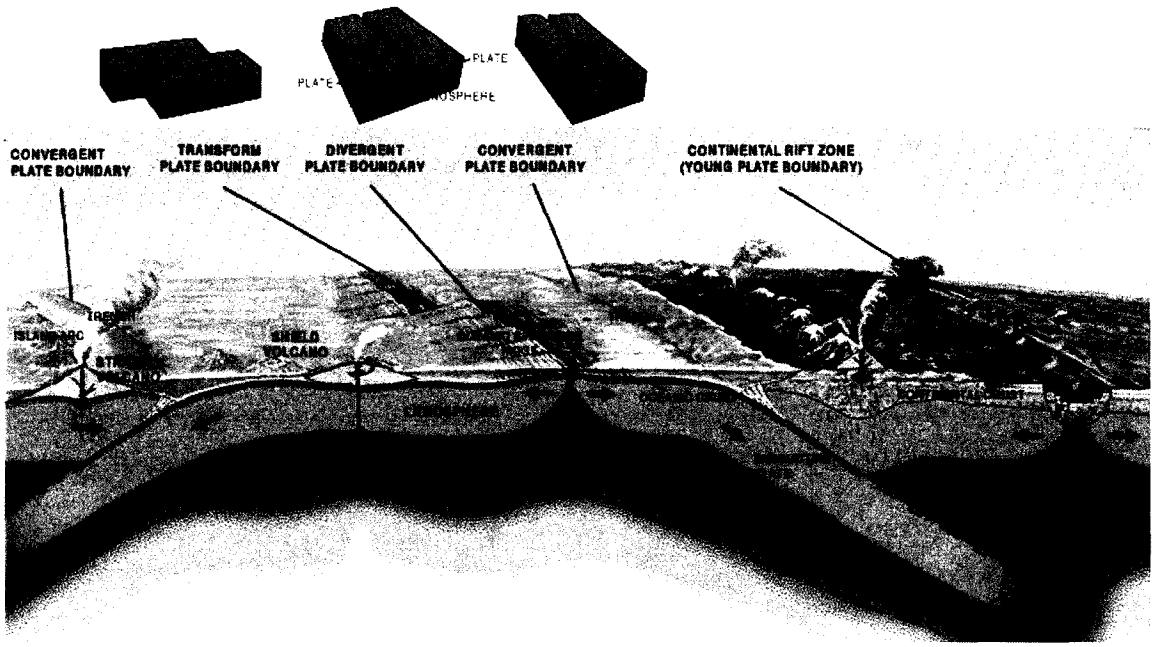


**Figure 1.2** Schematic sketch of vertical cross-section through lithospheric plates illustrating different plate boundaries (after Kious and Tilling, 2008)

earthquakes define the structure of descending plate and are known as Wadati-Benioff Zone.

Convergence can occur between oceanic and continental plates, between two oceanic plates and between two continental plates. An oceanic-continent convergence leads to the subduction of denser oceanic plate under the lighter continental plate, for example, off west coast of South America the Nazca plate is being subducted under continental part of the South American plate along the Peru-Chile trench. When two oceanic plates converge, the older and denser plate subducts beneath the other. Subduction processes in oceanic-oceanic plate convergence also result in the formation of chain of volcanoes and island arcs. The Mariana Islands were created due to the excessive volcanism when fast moving Pacific plate converges against the slower moving Philippine plate along the Mariana trench. When two continents converge, they resist downward motion and tend to buckle and push upwards as continental rocks are relatively lighter. The slow continuous convergence of the Indian and Eurasian plates over millions of years resulted the formation of the Himalayan ranges.

The zone between two divergent plates or between the spreading centers, where sliding takes place horizontally is called transform-fault boundary. Most of the transform faults are found on ocean floor offsetting mid-oceanic ridge into numerous segments. The ridge segments lie perpendicular to the spreading direction, whereas transform faults lie parallel to the spreading direction. The relative velocity across the fault segments causes earthquakes, which are more intense than the spreading related seismicity. The transform fault can also connect two trench segments or can terminate at a triple junction of three lithospheric plates.

Diffuse plate boundaries are broad zones, in which boundaries are not very well defined and the effects of plate interaction are unclear. Diffuse plate boundary mapped in the central Indian Ocean is the best example of such plate boundary zones. It has divided the traditionally believed Indo-Australian plate into three component plate; India, Australia and Capricorn (Royer and Gordon et al., 1997; Gordon et al., 1998)

### 1.2.2 Continental Margins and Ocean Basins

Ocean basins and continental platforms are most dominant physiographic domains on the surface of the Earth (Kenneth, 1982). These are linked by continental margins, where the oceanic and continental crust merges along a narrow transition zone. Continental margins form about 20% of the total area of oceans. Morphologically continental margin is divided into continental shelf, slope and rise. Continental shelf consists of gently sloping flat laying area and extends from shoreline to shelf edge. The shelf is a seaward extension of continent and covered by the sediments derived from the land. At the edge of the continental shelf, the water depth abruptly increases from 100-200 m to 1500-3500 m within a short horizontal distance and form a continental slope. The low relief-gently dipping province between the continental slope and ocean basin is called continental rise. The continental margins are best store houses of sediment accumulations transported from the continents.

Continental margins are broadly classified into two types, Passive or Atlantic and Active or Pacific. Passive continental margins develop when continents break and rift apart and allow forming the ocean floor between the rifted continental blocks. Initially the passive margins form at divergent plate boundaries and with time they move apart due to the commencement of seafloor spreading and also subside with cooling. Eventually they become sites of massive sedimentation and subsidence. A well-developed shelf-slope-system is observed in most of the passive continental margins. Active continental margins are formed at convergent plate boundaries. They are associated with a narrow shelf and a deep trench or island arch system and are regions of intense seismic activity.

Ocean basins lie between continental margins and to the vicinity of mid-oceanic ridges, include abyssal planes, oceanic rises and seamounts and seamount chains. Abyssal plains, in general, lie in the regions of flattest portions of Earth's surface with a slope less than a meter per km horizontal distance. The topographic undulations of the ocean floor are covered with sediments mainly derived from the continents. They extend from 200 km to 2000 km long with a depth ranging from 3000 m to 6000 m. Abyssal hills are small,

sharply defined topographic rises of elevation less than 1000 m and with a few tens of kilometers horizontal extents. They occur in groups between abyssal plains and mid-oceanic ridges. Abyssal hills are integral part of the mid-oceanic ridge system, but are morphologically distinct with smaller dimensions, deeper occurrence and often buried under sediments. Volcanic edifies in the ocean basin that rise above 1000 m from the adjacent ocean floor are called seamounts. They occur either in cluster or distributed randomly in the ocean basins. Seamounts rise abruptly from the ocean floor with deeply buried base and usually have steep slopes with conical shape. Seamounts, which were formed above sea surface, becomes flat topped due to erosion and sinks at later period to form Guyots or table mountains. Guyots are commonly found in the Pacific Ocean.

### 1.2.3 Fracture Zones

Fracture zones are long, arcuate and narrow geological features on ocean floor. A typical fracture zone is of about 60 km wide with several hills and valleys aligned along the overall trend (Cox and Hart, 1986). Fracture zones cut across major features of ocean floor including rises, abyssal plains and mid-oceanic ridges. They resemble strike-slip faults in topography and large off-sets when cut across magnetic isochrones and mid-ocean ridges. Unlike active faults, fracture zones are mostly devoid of seismic activity all along their length. However, portion of the fracture zone, which offset the ridge axis is seismically very active and this portion is called transform fault. This is due to the intense shearing between the ridge segments along the transform fault. In other words, transform fault becomes a part of a plate boundary and allows the plates to move in opposite directions. Identification of fracture zones on ocean floor is extremely important as they provide explicit clues to reveal the tectonic history of the continents and oceans.

### 1.2.4 Age of the Ocean Floor

Plate tectonic theory explains the strips of positive and negative marine magnetic anomalies as the thermal remnant magnetism of oceanic crust produced during episodic reversals of the Earth's magnetic fields. The strips of seafloor with positive magnetic anomalies were created during periods of normal polarity of the Earth's magnetic field and

those with negative magnetic anomalies were produced during periods of reversed polarity of the Earth's magnetic field. The magnetic anomaly pattern is used to date the ocean floor by correlating with the ages of magnetic field reversals obtained by paleomagnetic and isotopic dating results. The distribution of ocean floor ages determined by magnetic anomaly identifications, have been subsequently validated using dates of basaltic rocks and deep sediment cores obtained from Deep Sea Drilling Project. Isochrone or portion of ocean crust formed at same age is parallel and symmetrical to the mid-oceanic ridge. However, they are at places offset by hundreds of kilometers by fracture zones.

## 1.3 Mantle Plumes and Hotspots

Mantle plumes are quasi-cylindrical concentrated upwelling of hot mantle rock and they represent a basic form of mantle convection, whereas hotspots are anomalous areas of surface volcanism that cannot be linked with plate tectonic processes (Morgan, 1971, 1972). Hotspots are caused by upwelling of mantle rocks from a deep thermal boundary layer below the upper mantle; they are driven by thermal bouncy rather responding to plate tectonics and subduction. The classical hotspot model proposed by Wilson (1963) and Morgan (1971, 1972) requires magma source deep in the mantle and thus the rising magma are chemically distinct from those of mid-oceanic ridges. Further, their nearly stationary mantle plumes on the base of moving lithospheric plate could explain the age progression of volcanic chains.

Numerical simulation and laboratory experiments show that the plumes initiate with a leading plume head followed by a narrow conduit or plume tail connecting the plume head to the source region (Turcotte and Schubert, 2002). Supporting this result, observational evidences suggest that flood basalt eruptions mark the initiation of hotspots. For example, the Reunion hotspot track originates from Deccan flood basalt province of western India (White and McKenzie, 1989).

However, recent studies shows that very few hotspots are associated with upper or lower mantle tomographic anomalies, but majority lack prominent swells or surface volcanism

(Anderson, 2007; and references therein). Among the prominent swell hotspots many are lacking geochemical evidences for its deeper origin. Most significant and geochemically distinct hotspots like Hawaii, Iceland and Reunion are not underlined by lower mantle P-wave seismic anomalies. These studies have lead to an alternate hypothesis that the anomalous volcanism is attributed to plate tectonic processes at the Earth's top thermal boundary layer. Below the tectonic plates the mantle is at near melting point temperature, and it is inhomogeneous by the recycling of crustal rocks, these two conditions can cause volcanism and this is controlled by the stress conditions of the plate. The most significant processes that cause stress to vary in the lithosphere are differential cooling and variable plate boundary types. Thus according to this model, anomalous volcanism occurs, where the stress field is extensional and mantle is unusually fusible, therefore this model does not requires temperature anomalies deep in the mantle. A comparison of these two contrasting models of hotspot formation is given in Figure 1.3.

### 1.3.1 Three Distinct Types of Hotspots

Courtillot et al. (2003) made an attempt to classify 49 hotspots on the Earth based on geochemichal, geochronological, geophysical results (Figure 1.4). The characteristic features of deep origin hotspots are presence of linear volcanic chain, flood basalts at the origin, prominent buoyancy, high He isotopic ratios and low shear wave velocities at the mantle. Only seven out of 49 hotspots meet at least three of the above criteria and classified as primary hotspots. Around twenty hotspots are classified as secondary-type hotspots as they originate at shallow depths from the transient stems of super plumes. The remaining hotspots must have originated by stress related cracking of lithosphere as suggested by Anderson (2007). It is interesting to note that the three different hotspots are, in general, associated with three different thermal boundaries within the Earth. Hence, these hotspots should be studied independently keeping their different mechanisms of formation to avoid controversies.

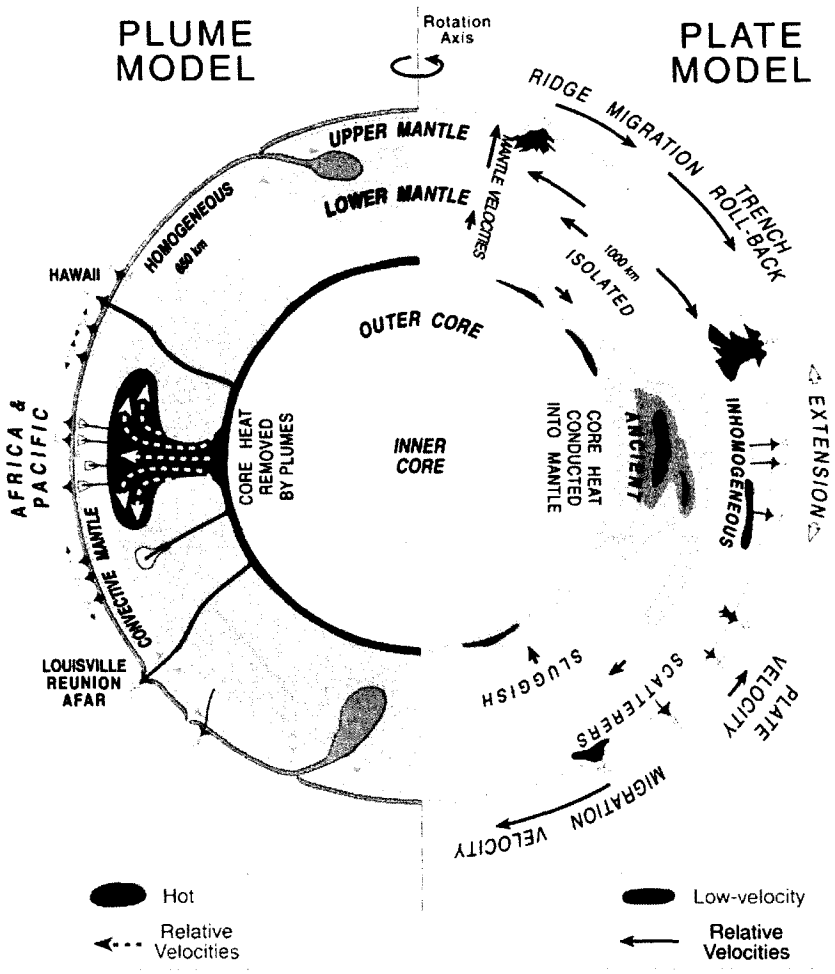


**Figure 1.3**. A schematic cross section of the dynamic earth along its rotational axis. Plume and Plate models of hotspot formation are demonstrated in left and right halves of the earth (after Anderson, 2007).

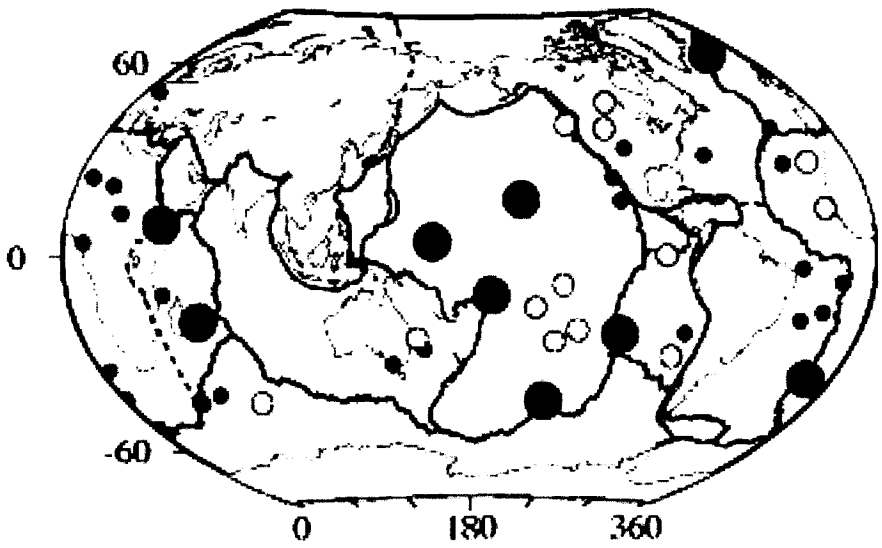


**Figure 1.4** Global distribution of three types of hotspots; Primary and likely to be primary (Red), secondary (yellow) and stress related (green) (after Courtillot et al., 2003).

### 1.3.2 Hotspot Expressions on Lithospheric Plates

Hotspots originate due to the gravitational instability of a lower thermal layer in the lower mantle and propelled by its own buoyancy and can stuck at any part of the Earth's surface. The interaction between the upwelling magma and oceanic lithosphere produces hotspot features like seamount chains, swells, volcanic islands, underplating, etc. On Earth surface hotspots can exist near or away from the plate boundaries. The Iceland was formed by a hotspot activity on the spreading ridge; this causes excessive thickening of oceanic crust and its elevation above sea surface. The Hawaii hotspot, which had formed the Hawaiian-Emperor island-seamount chain extending about 4000 km from Aleutian Islands to the active Kilauea volcano on the island of Hawaii, is an example of mid-plate volcanism. Hotspots can also form topographic swells of elevation up to 3 km and width up to 1000 km. The swell is parabolic in shape and extent upstream from the active hotspot. The excess elevation associated with the swell decays slowly with the hotspot track. The pacific swell is associated with the Hawaii hotspot.

The hotspot initial eruptions on continental lithosphere, in general, produce volcanic provinces with massive flood basalts. These are interpreted as plume heads marking the initiation of hotspot activity, which in subsequent phases, may leave trace on oceanic crust. The major hotspot related flood basalt provinces are Reunion-Deccan, Iceland-Tertiary North Atlantic, Tristan da Cunha-Parana and Prince Edward-Karoo (Turcotte and Schubert, 2002). Deccan volcanic province provides spectacular evidence for pressure-release melting of Deccan plume head as it impinged on the Indian plate. Within a short span of 1 Myr about $1.5x10^6$ $km^3$ magma material was pored in to form a large Deccan volcanic province. This volcanism continued approximately for next 65 Myrs, over which the Indian plate moved northward resulting the formation of the Chagos-Laccadive Ridge and Mascarene Ridge, and currently the hotspot is right below the Reunion Island on African plate (White and McKenzie, 1989). The Rajmahal traps present in the eastern part of India is considered as product of the Kerguelen hotspot about 117 Ma, which later formed the Ninetyeast Ridge in the northeastern Indian Ocean (Weis and Frey, 1991).

### 1.3.3 Fixity of Hotspots

The classical idea of deep anchored hotspot provides a fixed reference system for measuring the absolute plate motions in addition to the relative plate motions. This model has successfully been used to explain the age progressions along the linear volcanic chains. The bend in the hotspot track is explained by the change in direction of plate motion over the fixed hotspot. The sharp bend in the Hawaiian hotspot track between Hawaii and Emperor Islands is a result of abrupt change in the direction of Pacific plate motion over the hotspot. However, the concept of fixed plumes to explain the hotspots activity is currently shaking and not universally accepted. Studies on inter-hotspot movements suggest that the primary hotspots in Pacific and Indo-Atlantic hemispheres currently move very slowly (<5 mm/yr), but in the geological past prior to 50 Ma, they had moved relatively faster (Courtillot et al., 2003). Molnar and Stock (1985, 1987) showed that average velocities between the Hawaiian hotspot and those in the Indo-Atlantic hemisphere for the last 65 Ma have been 10-20 mm/a. In subsequent studies Koppers et al. (2001) argued that motions between certain Pacific hotspots must have reached much higher velocity of more than 60 mm/yr. Later Courtillot et al. (2003) made a significant observation that these higher rates were estimated with the hotspots of specific type (non-primary), but in the case of primary hotspots the analysis could not find evidences for significant inter-hotspot motion greater than 5 mm/yr. This clearly implies that the proposition of fixed hotspot theory is still acceptable for the primary plumes and for other types of hotspots the moments need to be studied in detail.

## 1.4 Aseismic Ridges

A long linear or broad-plateau like structural highs with a relief of 2 to 3 km lie on the ocean floor, are termed as aseismic ridges. The ridges were emplaced on oceanic crust under various tectonic settings: near or on spreading centre, near to the subduction zones or as isolated features away from plate boundaries. Following the mode of origin, aseismic ridges are classified as volcanic ridges, seamount chains, plateaus, continental fragments, etc. Major aseismic ridges in the global oceans in order of decreasing total volume, are the Ontong-Java Plateau, the Kerguelen Plateau, the Caribbean, the Ninetyeast Ridge, the

Chagos-Laccadive Ridge and the Mid-Pacific Mountains. These six major features constitute 54% of the total crustal volume of all oceanic plateaus of the Earth (Schubert and Sandwell, 1989). A substantial fraction of crustal volume of global oceanic plateaus was subducted and some part was accreted onto the continents, leading to the formation of new continental lithosphere.

Most of the volcanic ridges and seamount chains are formed by the hotspot interaction with the oceanic plates. Confirmation of hotspot origin for the ridges/ seamount chains comes from radiometric dating of basalt samples of the aseismic ridges. The age progression along the aseismic ridges is an important constraint to understand the plate motions over the hotspots. The importance of aseismic ridges in understanding the tectonic histories of lithospheric plates is described in detail in section 1.4.1.

The other type of aseismic ridges are submarine plateaus or rifted pieces of continental blocks. Schubert and Sandwell (1989) have mapped submarine plateaus in world oceans and estimated that submarine continental plateaus accounts about 3.2% of the total continental crustal volume. Significant continental plateaus, in decreasing order of volume, are the Falkland Plateau, the Lord Howe Rise, the Campbell Plateau, the Arctic Ridges, the Mascarene Plateau and the Chatham Rise. These six plateaus constitute 75% of the continental crustal volume on the ocean floor. The age of continental submarine plateaus are generally much greater than the surrounding seafloor age, which generally marks the age when the fragment detached from the parent continent. Some of the submarine plateaus together with the oceanic lithosphere have subducted into the mantle in the past, forming an important rout for returning of continental crust to mantle.

### 1.4.1 Aseismic Ridges- Record of Absolute and Relative Plate Motions

The kinematic theory of plate tectonics is based upon Euler's theorem, it states that motions on a sphere can be expressed as a rigid rotation about an axis (Cox and Hart, 1986). The motion of any lithospheric plate on the surface of a spherical approximation of the Earth can be described by a rotation about an axis called as Euler pole. The plate motion with

reference to the Euler pole is called finite rotation and these rotations in series are generally used to describe the movement of a lithospheric plate over a period. The plate motions can be relative or absolute: the relative plate motion is described by keeping one plate fixed and moving the other one, whereas absolute plate motion is described with respect to a stationary point deep inside the Earth. If a lithospheric plate moves over a hotspot that is considered as fixed relative to the mantle, the hotspot will create a line of volcanism that follows the trace of a small circle about an Euler pole. This trace of volcanism can then be used to determine the Euler pole and opening angle that describes the plates motion relative to the fixed hotspot i.e., absolute plate motion (APM). Morgan (1971, 1972) was the first to use the geometry and age progressions along the Hawaiian-Emperor, Tuamotu-Line, and the Austral-Gilbert-Marshall chains to develop an absolute plate motion model for the Pacific plate. He used two poles of rotation to describe Pacific APM since 100 Ma with a major change in APM occurring at 43 Ma, reflected by the Hawaiian-Emperor bend.

## 1.5 Concept of Isostasy

The term "isostasy" is derived from Greek words "iso" and "stasis" meaning "equal standing". The term is used to describe an equilibrium to which the Earth's crust and mantle tend, in the absence of disturbing forces (Watts, 2001). Geological processes like volcanism, sedimentation, glacial movements, etc., disturb the equilibrium or static state of the Earth's outer shells - the crust and mantle. In general, Isostasy explains how Earth's crust and mantle responds to volcanic loads to maintain its state of equilibrium for a range of spatial and temporal scales. Isostatic observations are important tools to study the Earth's rheology, composition, structure and dynamics.

The idea of isostasy was first put forwarded by Leonardo Da Vinci in fifteenth century, wherein he had explained the rise of mountain with the removal of materials. However, the development of isostasy further grew in eighteenth century, that was the time scientists have attempted to estimate the mean density and shape of the Earth. One notable contribution has come from the French scientist, Pierre Bouguer, who had attempted to

determine the Earth's mean density by measuring the deflection of the plumb-line (vertical direction) by the mass of a nearby mountain. His experiments ended with contrasting results; the ratio of density of crust to the mean density of the Earth estimated for Mt. Chimborazo in Ecuador, is quite higher than half to that of Mt. Quito in Peru. The erroneous result indicated that the deflection of the vertical caused by the mountain was too small for its estimated mass.

In the first half of the nineteenth century (1806-1843), the English geodesist George Everest carried out triangulation surveys in India. He observed that the distance measured by triangulation between Kalianpur on the Indo-Ganges plain and Kaliana in the foothills of the Himalayas differed substantially from the separation of the sites computed from the elevations of stars (Everest, 1857-59). He opined that that the discrepancy must have caused by errors in geodetic measurements. However, Pratt (1855) attributed the discrepancy to deflection of the plumb-line by the mass of the Himalayas and observed that the minimum deflection of the plumb-line that might be caused by the mass of the Himalayas, is about three times larger than the observed deflection. These observations further lead to a conclusion that the attraction of the mountain range on the plumb-line was not as large as it should have been.

### 1.5.1 Isostatic Compensation Mechanisms

The plumb-line deflection problem was explained with two contrasting mechanisms by Airy (1855) and Pratt (1855). Both mechanisms suggest local compensation of the extra mass of a mountain above sea-level by a less-dense region (or root) below sea-level, but they differ in the way the compensation is achieved. Hayford (1909) derived a mathematical model to describe the Pratt hypothesis. As a result, this theory of isostasy is often called the Pratt–Hayford scheme of compensation. Whereas, Heiskanen (1931) derived sets of tables for calculating isostatic corrections based on the Airy model. This concept of isostatic compensation has since been referred to as the Airy–Heiskanen scheme. In 1889 C. E. Dutton referred to the compensation of a topographic load by a less-dense subsurface structure as *isostasy*. In the first half of twentieth century Putnam (1912)

and Barell (1914) put forward the idea of regional isostasy, in which the geological loads are supported by the rigidity of the crust. Further, Vening Meinesz worked on these aspects and proposed a third model, in which the crust acts as an elastic plate. As in the other models, the crust floats buoyantly on a substratum, but its inherent rigidity spreads topographic loads over a broader region.

### *1.5.1.1 Airy–Heiskanen Model*

Airy–Heiskanen model assumes that the crust is thin and lighter and floats on a thicker and denser substratum like ice bergs floating in water. The height of a mountain above sea-level is much less than the thickness of the crust underneath it, just as the visible tip of an iceberg is much smaller than the subsurface part. The densities of the crust and mantle are assumed to be constant; the thickness of the root-zone varies in proportion to the elevation of the topography. The thickness of continental crust is 30-35 km and the compensation take place below this depth. Oceanic crust is thinner with an average thickness of 6-8 km and the region below forms anti-roots.

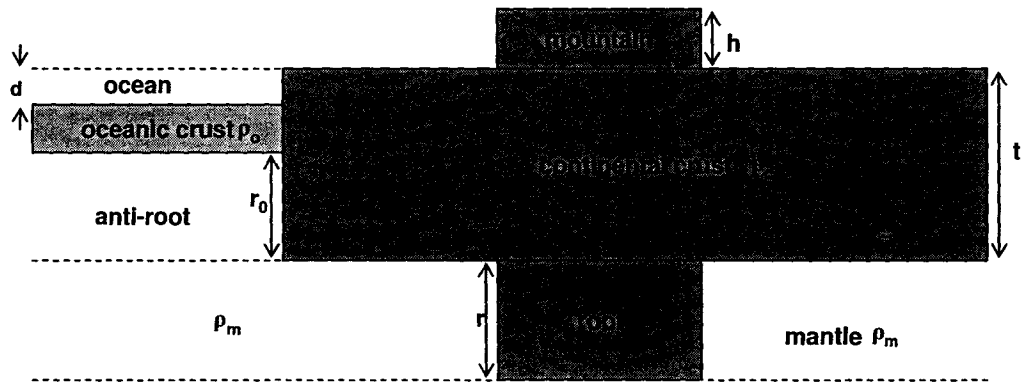


**Figure 1.5** Isostatic compensation according to Airy- Heiskanen model.

According to this model the isostatic compensation is complete and hydrostatically balanced. The thickness of the root zone of a mountain of thickness h with density $\rho_c$ (Figure 1.5) is given by (Lowrrie, 2007)

$$r = \frac{\rho_c}{\rho_m - \rho_c} * h \qquad \text{... (1.1)}$$

where $\rho_m$ is the density of mantle. The thickness $r_o$ of the anti-root of the oceanic crust under an ocean basin of water depth $d$ and density $rw$ is given by

$$r_o = \frac{\rho_c - \rho_w}{\rho_m - \rho_c} * d \qquad \text{...(1.2)}$$

*1.5.1.2 Pratt–Hayford Model*

The Pratt–Hayford isostatic model is based on the contraction theory; the depressions and elevations on the Earth's surface are considered as the product of thermal contractions and expansions. This implies that the isostatic compensation is locally attained at a particular depth of compensation by lateral density variations. The elevated regions are underline by low density rocks whereas depressed regions are underline by high density rocks.

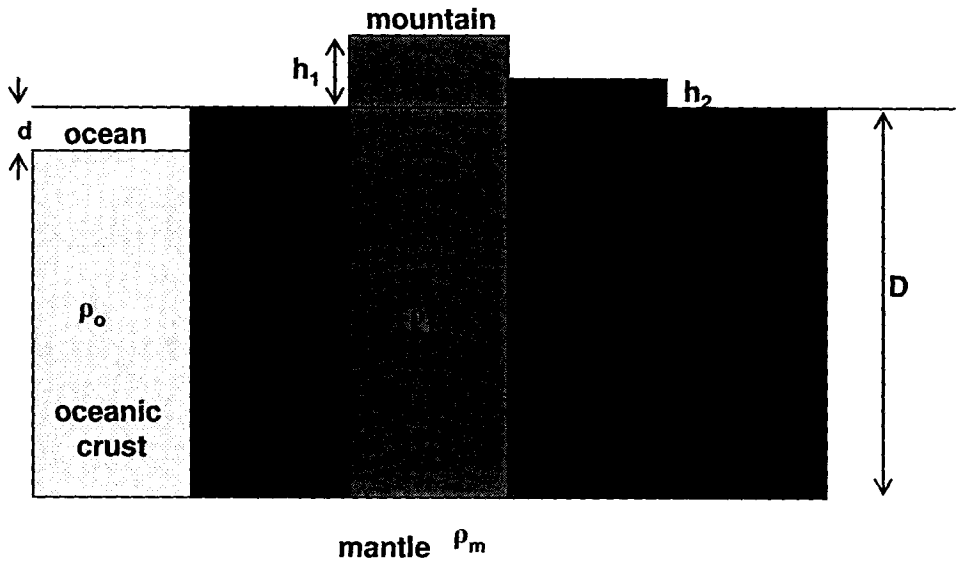


**Figure 1.6** Isostatic compensation according to Pratt–Hayford model

If the rock beneath a mountain of height *hi* ($i$=1, 2,...) has density $\rho_i$, and if the rock columns are in equilibrium at a depth D (Figure 1.6), Then the density below a topographic elevation $h_i$ is given by (Lowrrie, 2007)

$$\rho_i = \frac{D}{h_i + D} * \rho_c \qquad \ldots(1.3)$$

where $\rho_c$ is the mean density of the crust. The density under an oceanic basin of depth d is given by

$$\rho_i = \frac{\rho_c D - \rho_w d}{D - d} \qquad \ldots(1.4)$$

*1.5.1.3 Vening Meinesz Elastic Plate Model*

The Pratt–Hayford and Airy–Heiskanen models are both idealized with regard to the density distributions and behavior of the Earth's materials. These models assume that Earth's upper part offers no resistance to shear stress leading to vertical adjustments between adjacent columns. Like earlier models the Vening Meinesz model also considers a two-layer Earth model, but the upper layer behaves like an elastic plate overlying a weak fluid (Vening Meinesz, 1939). The strength of the plate distributes the load of a surface feature (e.g., an island or seamount) over a horizontal distance wider than the feature (Figure 1.7).

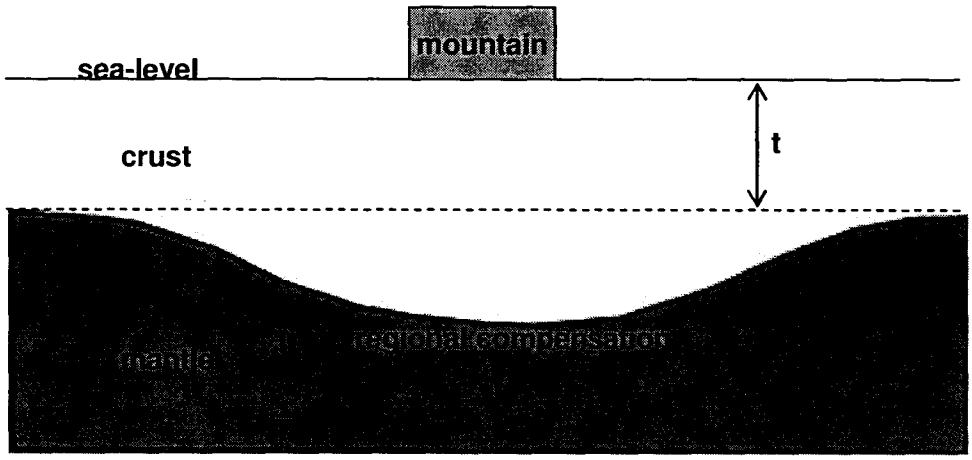


**Figure 1.7** Isostatic compensation according to Vening Meinesz elastic plate model

The topographic load bends the plate downward into the fluid substratum, which is pushed aside. The buoyancy of the displaced fluid forces it upward, giving support to the bent

plate at distances well away from the central depression. The bending of the plate which accounts for the regional compensation in the Vening Meinesz model depends on the elastic properties of the lithosphere.

## 1.6 Elastic Plate Thickness and Flexural Rigidity

The elastic properties of the lithosphere are studied by applying the theory of plate bending in response to applied forces. This model describes the lithospheric as an elastic thin plate that flexes elastically in response to loads. The parameter that characterizes the apparent flexural strength of the lithosphere is the flexural rigidity which is an important factor when parameterizing flexural isostasy. Flexural rigidity is commonly expressed in terms of elastic plate thickness, Te, which approximates the Earth's uppermost, elastically deforming layer as a thin elastic plate. If the plate is continuous, homogeneous, and elastic, the flexural rigidity of the plate is defined in terms of Young's modulus *E*, the Poisson's ratio v and the effective elastic thickness Te with the following equation (Watts, 2001)

$$D = \frac{ETe^3}{12(1-\nu^2)} \qquad \text{...(1.5)}$$

The deflection of the plate depends on the properties of the plate, or in other words, how resistant is the material of the plate against a deformation. A flexural model where the plate has no strength (Te=0) approximates the classical Airy model for local compensation. The theory of elastic plates and methods of Te estimation are described in detail in Chapter 3.

## 1.7 Isostatic Compensation of Aseismic Ridges and Seamounts

Elastic plate model is a simple and powerful tool for understanding the deformation caused by loading and unloading related to various geological processes like post-glacial rebound, mountain orogeny, submarine volcanism, evolution of sedimentary basins etc (Watts, 2001 and references therein). Isostasy and structure of numerous aseismic ridges and seamounts that occur in World's Oceans are studied using flexural modeling (McKenzie and Bowin 1976; Watts 1978; Detrick and Watts 1979; Watts, 1982). They are mainly volcanic in

origin and exist in various tectonic settings. The response of aseismic ridges indicate the long-term mechanical (>$10^6$ yrs) properties of the oceanic lithosphere, which are expressed in terms of the effective elastic thickness. The value of Te depends on mineralogy, temperature, and state of stress of the lithosphere. Oceanic lithosphere, with a thin and mafic crust, generally behaves like a single mechanical layer. Oceanic mantle is relatively homogeneous, and the ocean geotherm is dominated by plate cooling, so Te of oceanic lithosphere increases with thermal age of the lithosphere at the time of loading (Watts, 1978). This important property of the Te has been used to date aseismic ridges and to infer the tectonic setting of its origin. Further details of Te-age relation and its tectonic interpretation are discussed in Chapters 4, 5 and 6.

## 1.8 Objectives

The present work consists of a detailed geophysical study of the structure and isostatic compensation mechanisms of three major aseismic ridges; The Comorin Ridge, The 85°E Ridge and Ninetyeast Ridge of the northeastern Indian Ocean. The major objectives of the study are

1. **The Comorin Ridge**

    a) to determine the elastic plate thickness (Te), crustal thickness and isostatic compensation mechanism of the Comorin Ridge
    b) to demarcate the Continent-Ocean Boundary (COB) on the southwest margin of Sri Lanka and southern tip of India
    c) to outline the tectonic setting of the ridge

2. **The 85°E Ridge**

    a) to develop a process oriented modeling technique for determining the elastic plate thickness of the ridge
    b) to determine the crustal structure and isostatic compensation mechanism of the ridge

c) to investigate the changes in ridge gravity anomaly through time since its formation and discuss the geological processes.

### 3. The Ninetyeast Ridge

a) to study the variation in elastic plate thickness along Ninetyeast Ridge using admittance analysis and forward model techniques

b) to determine crustal structure and isostatic compensation mechanism of the ridge.

c) to discuss the spatial variations in the Te in the light of complex interactions between the Kerguelen hotspot and oceanic lithosphere.

# CHAPTER 2

# Aseismic ridges of the northeastern Indian Ocean

# Aseismic ridges of the northeastern Indian Ocean

## 2.1 Evolution of the Indian Ocean

The initiation of the Indian Ocean commenced with the breakup of the Gondwanaland super-continent into two groups of continental masses during the Mesozoic period (Norton and Sclater, 1979). The first split of the Gondwanaland may possibly have associated with the Karoo mega-plume (Lawver and Gahagan, 1998). Followed by this rifting phase, during the late Jurassic, the Mozambique and Somali basins have formed by seafloor spreading activity of series of east-west trending ridge segments. Thus, the Gondwanaland super-continent divided into western and eastern continental blocks. The Western Gondwanaland consisted of Africa, Arabia and South America, whereas the East Gondwanaland consisted of Antarctica, Australia, New Zeeland, Seychelles, Madagascar and India-Sri Lanka (Figure 2.1). After initial break-up, the East Gondwanaland moved southwards from the West Gondwanaland and led to gradual enlargement of the intervening seaways between them (Bhattacharya and Chaubey, 2001). Both West and East Gondwanaland masses have further sub-divided during the Cretaceous period. Approximate reconstructions of continental masses of the Gondwanaland from Jurassic to Present illustrating the aforesaid rifting events are shown in Figure 2.1 (Royer et al., 1992).

The opening of the western Indian Ocean started in early Cretaceous period with the rifting of Antarctica-Australia from Madagascar-Seychelles-India fragment at about 133 Ma (Holmes and Watkins, 1992). After about 15 Myr, followed by a major change in spreading pattern the Madagascar-Seychelles- India block again joined with the African plate (Besse et al., 1988). Thus, it is believed that the oldest oceanic crust of the Indian Ocean lies along the eastern margin of the African Continent.

The evolution of eastern Indian Ocean consists of three distinct phases of spreading and two major plate reorganizations. The first phase of spreading started during early Cretaceous in NW-SE direction resulting the drifting of Greater India from the Australia-Antarctica block (Curray et al., 1982; Gopala Rao et al., 1997; Gaina et al., 2003; Krishna

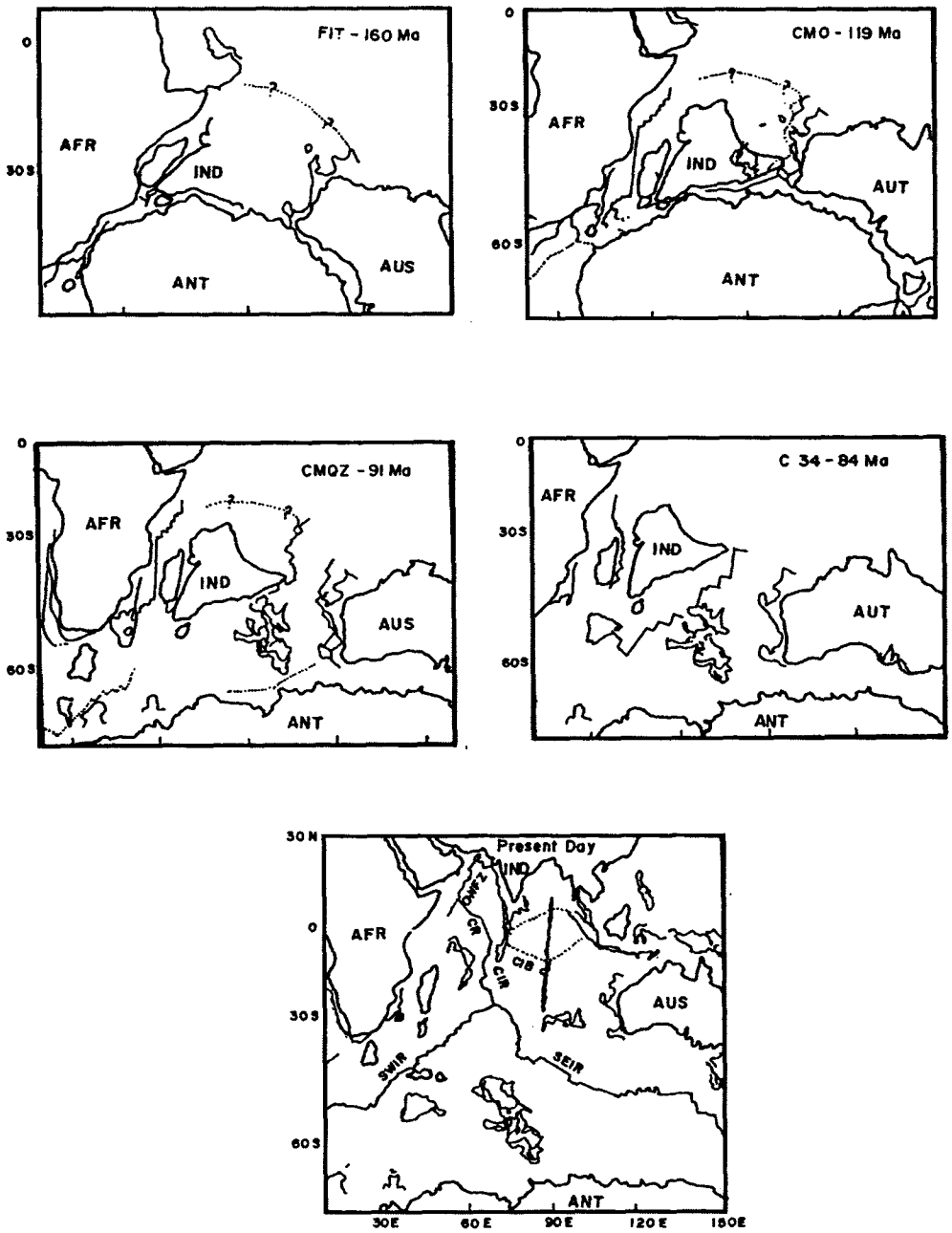


**Figure 2.1** Reconstruction of Gondwana super-continent blocks from Jurassic to Present (after Royer et al., 1992).

et al., 2009a). Subsequently, at about 120 Ma the Elan Bank, a micro-continent, which presently lies on the western margin of the Kerguelen Plateau in the southern Indian Ocean, separated from the present-day eastern margin of India (Gaina et al., 2003, 2007; Borissova et al., 2003; Krishna et al., 2009a). These breakup sequences suggest that most part of the oceanic crust in the Bay of Bengal was evolved during the Cretaceous Magnetic Quite Period (120-83 Ma) as shown in Figure 2.1.

During the mid-Cretaceous, the second phase of spreading initiated approximately in north-south direction causing the first major plate organization in the Indian Ocean. Since then, India drifted northward from Antarctica continent (McKenzie and Slater, 1971), while Australia drifted away from Antarctica in NE direction by the spreading processes of Australia-Antarctica Ridge (Cande and Mutter, 1982; Veevers, 1986). During this period, spreading along India-Madagascar Ridge caused drifting of India from Madagascar-Seychelles (Norton and Sclater, 1979). These processes eventually led to the opening of Crozet, Wharton, Mascarene and Central Indian Basins (White and McKenzie, 1989; Storey et al., 1995) and establishment of a three-plate system: Antarctica, Africa and Indo-Australian, with a triple junction (Rodriguez Triple Junction) at a geographical position, 25°S latitude and 69°E longitude.

During the period close to the K-T boundary age, Seychelles rifted away from the Western India paving the way for the formation of the Carlsberg Ridge (McKenzie and Sclater, 1971; Norton and Sclater, 1979; Naini and Talwani, 1983; Royer et al., 2002; Chaubey et al., 2002). Concurrently, spreading along the Carlsberg Ridge led to the opening of conjugate Arabian and Eastern Somali basins. During this period the Indian and Arabian plates were moving along a fracture zone, the ancestor of Owen Fracture Zone, which connected the Carlsberg Ridge System and the Subduction zone in the Neo-Tethys region (Bhattacharya and Chaubey, 2001).

The northward flight of Greater India slowed down due to the collision of Indian Continent with southern Asian subduction zone in early Eocene. The first encounter, probably a soft collision between the greater India and an Island arch seaward of a marginal basin must

have occurred about 53 Ma (Curray et al., 1982). Subsequently at about 42 Ma, Wharton Spreading Ridge became inactive and jumped towards south (Liu et al., 1983; Krishna et al., 1995), and this led to the unification of India-Antarctica Ridge and Australia-Antarctica Ridge into the present day Southeast Indian Ridge (SEIR). In this process, Australian plate did merge with the Indian plate and formed a single Indo-Australian plate, resulting the second major plate reorganization in the Indian Ocean. The third phase of spreading (middle Eocene to Present) started in NE-SW direction along SEIR, which resulted the opening of Australian and Antarctic basins, north Crozet basin and southern part of the Central Indian Basin (Schilich, 1982).

After the India-Eurasia collision tectonics, the spreading centers in western Indian Ocean reorganized. Spreading along the Central Indian Ridge (CIR) and some ridge jumps during the early Oligocene resulted the separation of Chagos Bank from Nazareth Bank (Duncan, 1990). The continued spreading along CIR and Southwest Indian Ridge (SWIR) led to move the African plate towards northeast direction.

The next major event took place during the middle Miocene - the Carlsberg Spreading Ridge propagated westward as Sheba Ridge and led to the opening of the Gulf of Aden (Laughton et al., 1970). The oceanic crust north of the Indian subcontinent has largely subducted, as a result the Indian subcontinent collided with the Eurasian continent, generally referred as "Hard Collision", which resulted the initial upliftment of the Himalayas (Curray et al., 1982). The rapid uplift and subsequent erosion of Himalayas resulted huge sediment deposition in both ocean regions: Bay of Bengal and Arabian Sea, adjoining the Indian continental regions. Within the central Indian Ocean, the collision tectonics and rapid upliftment of Himalayas accumulated compressional stresses leading to periodic deformation of oceanic lithosphere between India and Australia since about 15.4-13.9 Ma (Krishna et al., 1998, 2009b). The subduction of northeastern Indian plate below the South Asian plate resulted the Andaman Island Arch – trench system (Curray et al., 1982). The extrusive tectonics, rifting and seafloor spreading activity since 4 Ma resulted the formation of Andaman backarc basin (Kamesh Raju et al., 2004).

Several mantle plumes have significantly influenced the evolution of the Indian Ocean lithosphere at different geological ages. Initial plume head interaction with continental lithosphere caused Large Igneous Provinces (LIP), subsequently in oceanic region plume trails produced aseismic ridges, seamount chains and plateaus. Marion, Kerguelen and Reunion hotspots are the most prominent among the Indian Ocean hotspots, which had major role on the geodynamic history of the ocean. The locations of major hotspots along with tectonic and physiographic features of the Indian Ocean are shown in Figure 2.2.

The Marion hotspot is believed to be the most ancient one (over 184 m.y age) among the present day global hotspots and believed to have formed the Karoo flood basalts in South Africa (Morgan, 1981). During the late Cretaceous period the Marion hotspot was under India-Madagascar block and caused for wide spread volcanism in Madagascar and southwest India (Storey, 1995; Kumar et al., 2001). Further, it is generally believed that the Marion hotspot volcanism was a main cause for the India-Madagascar breakup and formation of Madagascar Ridge on African plate (Storey, 1995).

The Kerguelen hotspot activity started at around 130 m.y ago when the continental blocks of India-Australia-Antarctica were together. The hotspot has caused wide spread volcanism during the Cretaceous and Cenozoic period in continental as well as in oceanic regions (Duncan, 1978). The volcanic activity resulted the formation of large widespread igneous provinces of Rajmahal, Bunbury and lamprophyre dikes in Indian, Australian and Antarctic margins, and plateaus and aseismic ridges such as Kerguelen Plateau, Broken Ridge, Ninetyeast Ridge, recent expressions on Kerguelen Archipelago, Heard and McDonald Islands, etc. (Coffin et al., 2002). After the break up, the plates motion have dispersed the igneous rock complexes from their original site of emplacement to present locations (Müller et al., 1993).

The Reunion hotspot formed the Deccan Traps at about 69-65 Ma on northeastern Indian Shield (Duncan, 1990). The volcanic rocks of Seychelles Bank and adjacent Seychelles-Saya de Malha saddle area are also considered as the products of Deccan plume (Plummer and Belle, 1995). Subsequently India separated from Seychelles and moved northwards,

resulting in formation of the Laccadive-Maldives-Chagos Ridge and on African plate, the Seychelles-Mascarene ridge, Nazareth Bank and the island of Mauritius (O' Nail et al., 2003).

## 2.2 Major Aseismic Ridges

Aseismic ridges in the Indian Ocean were generally evolved either by volcanic activity or by continental fragmentation. In this section, a short description of some of the important aseismic ridges of the Indian Ocean is given. However, a detailed account of the structure, isostasy, geophysical signatures and evolutionary history of the Comorin, 85°E and Ninetyeast ridges are given in Chapters 4, 5 and 6, respectively.

### 2.2.1 The Ninetyeast Ridge

The Ninetyeast Ridge is one of the longest linear aseismic ridges in the world oceans. It stretches for more than 5000 km in north-south direction from 17°N to 30°S in eastern Indian Ocean (Figure 2.2). The average elevation of the ridge is 2-3 km and width varies from 100 to 200 km. The southern part of the ridge (south of 15°S) is generally broader and wider than the northern part (Sclater and Fisher, 1974; Krishna et al., 1995). The northern portion of the Ninetyeast Ridge (north of 10°N) is buried under the Bengal Fan sediments (Curry et al., 1982; Gopala Rao et al., 1997; Micheal and Krishna, 2011), whereas the southern end of the ridge joins with the Broken Ridge.

### 2.2.2 The Chagos-Laccadive Ridge

The Chagos-Laccadive ridge extends for about 2500 km from 14°N to 9°S along 73°E meridian in western Indian Ocean (Figure 2.2). The entire ridge system is broadly divided into three parts: the northern segment is referred as the Laccadive Ridge, the middle segment as Maldive Ridge and the southern segment as Chagos Bank. The Laccadive Ridge consists of a group of twenty islands and Banks, together known as Laccadive Islands. In general, this part of the ridge is associated with negative gravity signature with a belt of positive anomalies over the ridge crest (Naini and Talwani, 1983). The basement,

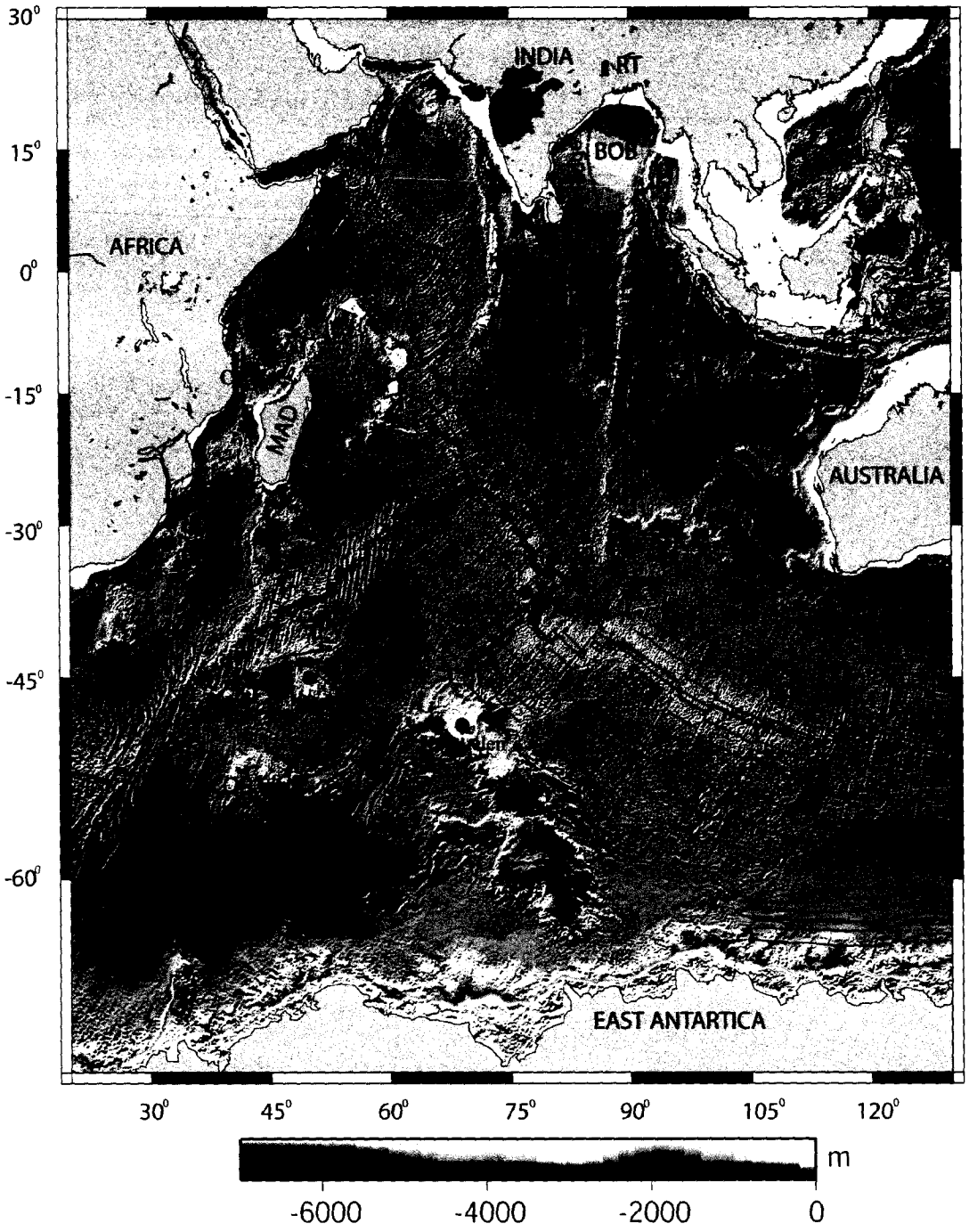


**Figure 2.2** General bathymetric map of Indian Ocean (ETOPO-1) showing mid-oceanic ridge system, aseismic ridges, plateaus, fracture zones, and magnetic lineations (after Royer et al., 1989; Müller et al., 1997). Locations Major hotspots are shown as pink dots. SWIR, Southwest Indian Ridge; SEIR, Southeast Indian Ridge; CIR, Central Indian Ridge; CBR, Carlsberg Ridge; NER, Ninetyeast Ridge; CR, Comorin Ridge; CLR, Chagos Laccadive Ridge; MR, Madagascar Ridge; S-M-P, Seychelles-Mascarene-Plateau; MOZR, Mozambic Ridge; BR, Broken Ridge; GR, Gunnerus Ridge; KP, Kerguelen Plateau; CP, Crozet Plateau; COR, Conrad Rise; EB, Elan Bank; OFZ, Owen Fracture Zone; RT, Rajmahal Traps; DT, Deccan Traps; ANS, Afanasy Nikitin seamount.

in general, forms a dome with several individual peaks. These peaks are devoid of sediments and some of them reach close to the sea surface. Seismic refraction results indicate that the Moho boundary lies at about 17-18 km and suggest an over thickened oceanic crust (Naini and Talwani, 1983). The Maldive Ridge lies between 7°N and 1°S is associated with subduded free-air gravity anomalies (Avraham and Bunce, 1977). A deep-water channel lying at a depth of about 4800 m separates Maldive Ridge from the Chagos Bank. The Chagos Bank is the southern part of the ridge system and lies south of 4°S. Free-air gravity anomaly over the bank is almost close to zero. Seismic and ODP results suggest volcanic crust with small sedimentary cover (Backman and Duncan, 1988).

Various theories have been proposed for the origin of the Chagos-Laccadive Ridge system, viz, leaky transform fault, continent-ocean boundary, hotspot trace, composed of structural elements of various origin, etc. (Bhattacharya and Chaubey, 2001; and references therein). The results of ODP Leg 115 suggested that the Chagos-Laccadive Ridge might have formed during the northward flight of the Indian plate over the Reunion hotspot (Whitmarsh, 1974; Duncan, 1981). However, the Laccadive Ridge segment is considered as continental fragment with volcanic intrusions (Chaubey et al., 2002; 2008).

### 2.2.3 The 85°E Ridge

The 85°E Ridge stretches from the Mahanadi Basin (~19°N) to the Afanasy Nikitin seamount (4°S) in northeastern Indian Ocean (Figure 2.2). The northern part of the ridge in Bay of Bengal is completely buried under Bengal Fan sediments and associated with prominent negative gravity anomaly signature, whereas south of 7.5°S the ridge is partly exposed to the seafloor and associated with positive gravity anomaly signature. Seismic reflection studies reveal the presence of buried ridge in the Bay of Bengal and divide the region into two basins: the Western Basin lies between the ECMI and the 85°E Ridge, and the Central Basin lies between the 85°E and Ninetyeast ridges (Curray et al., 1982). The average width of the ridge is about 100 km with variable relief and morphology. It is generally believed that the ridge was emplaced by hotspot activity. However, there are

many contradicting views existing on the origin of the ridge. Detailed discussions regarding the origin of the 85°E Ridge are included in Chapter 5.

### 2.2.4 The Comorin Ridge

The Comorin Ridge trends in NNW-SSE direction in deep-water region of west of Sri Lanka and south of India, was named as Comorin Ridge because of its vicinity close to the place called Cape Comorin, southern tip of India (Figure 2.2). The ridge stretches for about 500 km with an average width of 50 km and relief of 1 km. In general, the ridge is associated with a subdued gravity anomaly, but no specific magnetic signature is noticed. Using marine geophysical data, Khale et al. (1982) suggested that the eastern edge of the Comorin Ridge might represent a continent-ocean boundary.

### 2.2.5 The Broken Ridge

The Broken Ridge in eastern Indian Ocean trends approximately in E-W direction and its western end joins the southern part of the Ninetyeast Ridge (Figure 2.2). The ridge stretches for about 1000 km with an average width of 100 km. Over the Broken Ridge the water depths are <2000 m and the southern edge of the ridge is steeper than the northern edge. The free-air gravity anomaly observed over the Broken Ridge suggests that the topography is basically uncompensated, in the sense that the Moho topography approximately follows the trend of the bathymetry. It is also suggested that Broken Ridge and central part of the Kerguelen Plateau were emplaced together due to intraplate volcanism during the mid-Cretaceous period and were separated during the middle Eocene (Weissel and Karner, 1989). The ODP Leg 121 results suggested that the Broken Ridge was formed initially above the sea level and subsequently subsided to the present position (Weissel and Karner, 1989).

## 2.3 Other Major Structural Features

The Indian Ocean, besides aseismic ridges discussed above, posses number of plateaus, seamounts, banks, etc. Most prominent among them are the Kerguelen Plateau, the

Mascarene Plateau, the Conrad Rise, the Nazareth Bank, the Elan Bank, the Afanasy Nikitin seamount, the Osborn Knoll, etc., (Figure 2.2). Some of the features relevant to the present research work are discussed below.

### 2.3.1 The Kerguelen Plateau

The Kerguelen Plateau, an assemble of several geological provinces, consists of Kerguelen-Gaussberg Ridge, sub-aerial Kerguelen Archipelago, Elan Bank, Skiff Bank, Heard Island (Frey et al., 2000). The plateau extends from 46°S to 64°S in a NNW-SSE direction with an average width of 450 km (Figure 2.2). The Kerguelen-Gaussberg Ridge is bounded north and east by the Crozet Basin, SW by the Enderby Basin, and SE by the Australia-Antarctic Basin. A trough with a deep of 3600 m, named as Challenger Channel (Vanney and Johnson, 1982), separates the Kerguelen-Heard Ridge from the Antarctic margins. The Kerguelen-Gaussberg Ridge is associated with low amplitude positive gravity anomalies, suggesting its structural compensation at deeper depths (Houtz et al., 1977). However seismic studies show that isostatic compensation is achieved by a low density mantle beneath the ridge. This scheme implies an upwelling of partially melted mantle. The magnetic anomaly pattern demonstrates that the Kerguelen-Gaussberg Ridge and Broken Ridge were joined prior to seafloor spreading anomaly 18 (40-42 Ma) and the present day separation between them is a result of the initial interplateau rifting followed by seafloor spreading since 42 Ma (Mutter and Cande, 1983; Royer and Sandwell, 1989)

### 2.3.2 The Elan Bank

The Elan Bank, a relatively small elongated approximately E-W oriented feature, lies on the western margin of the Kerguelen Plateau (Figure 2.2). The ODP Leg 183 (Site 1137) results of the Elan Bank revealed that the bank consists of continental nature crust, therefore the bank is considered as a micro-continent (Frey et al., 2000). Using marine magnetic data, Gaina et al. (2003, 2007) and Krishna et al. (2009a) have suggested that the Elan Bank was separated from the present day Eastern Continental Margin of India at about 124 Ma. According to this interpretation, the seafloor spreading in the Enderby Basin ceased at about 124 Ma and the ridge segments jumped towards the Eastern

Continental Margin of India and caused for the detachment of the Elan Bank and its subsequent transfer to the Antarctic plate.

### 2.3.3 The Afanasy Nikitin seamount

The Afanasy Nikitin seamount (ANS) stretches along 83°E between 2°S and 6°S with a relief of more than 2 km (Figure 2.2). The ANS is elongated for about 450 km in the north-south direction with an average width of 150 km. However, in the central part its width is narrower by ~50 km. The basement platform of the ANS rises to 3800 m water depth, on which a cluster of elongated peaks exists (Krishna, 2003). ANS is associated with positive but low amplitude free-air gravity anomaly. Plate reconstruction and magnetic studies have shown that the ANS is laying on 80-73 Ma aged oceanic crust (Müller et al., 1993; Krishna et al., 2011a). The magnetic anomalies over the ANS are low amplitude and short wavelength in nature, which are superimposed over the seafloor spreading anomalies.

# CHAPTER 3

# Methodology and Geophysical Data

# Methodology and Geophysical Data

## 3.1 Introduction

Gravitation is the attractive force existing between any two objects that have mass in the universe. According to Newton's law of universal gravitation the magnitude of this force between two bodies of masses $m_1$ and $m_2$ kilograms separated by a distance r meter is given by

$$F = \frac{Gm_1m_2}{r^2} \qquad \ldots (3.1)$$

Where, G is the universal constant of gravitation ($6.7 \times 10^{-11}$ $Nm^2/kg^2$). In Geophysics, the gravitational acceleration (g) - the gravitational force per unit mass- is often considered more important than the absolute magnitude of the force. If the planet Earth were a non-rotating spherically symmetrical body, the gravitational acceleration on its surface would remain constant. The Earth behaves as an elastic body and deform in response to the forces generated by its rotation, therefore it becomes slightly flattened at the poles and with a compensating bulge at the equator. The equatorial bulge and the effects of centrifugal force together cause an increase in mean that sea-level gravitational acceleration of about 0.5% from equator to poles.

The figure of the Earth is the shape of an equipotentional surface of gravity, in particular the one that coincides with mean sea level, which is called geoid (Li and Gőtze, 2001). The best mathematical approximation to the shape of the Earth is an oblate ellipsoid, or spheroid. In 1980, the International Association of Geodesy adopted the Geodetic Reference System (GRS 80) in which the International Reference Ellipsoid or the Normal Earth has an equatorial radius (a) equal to 6378.137 km and a polar radius (c) equal to 6356.752 km (Moritz, 1980).

The gravity field due to this equipotential ellipsoid of revolution is referred as theoretical or normal gravity. The normal gravity field at any point on the Earth's surface can be computed using the International Gravity Formula (IGF) as given below (Moritz, 1980)

$$g_n = g_e(1+\beta_1 \sin^2\phi + \beta_2 \sin^2 2\phi) \quad \ldots (3.2)$$

The constants in the formula for GRS80, are: $g_e$=9.780327 $ms^{-2}$; $\beta_1 = 5.302441\times10^{-3}$; $\beta 2 = -5.810\times10^{-6}$. They are used in calculation of normal gravity at any latitude with an accuracy of 0.1 mGal.

## 3.2 Gravity Measurements at Sea

The gravity measurements at sea surface are severely effected by the vertical and horizontal accelerations generated by the wave action of sea water and movement of the ship/ boat corresponding to sea conditions. The ship's vertical and horizontal accelerations are compensated by mounting the gravimeter sensors on gimbals or stabilized platforms. The Vening-Meinesz pendulum is the earliest instrument that has measured gravity at sea to an accuracy of 5-15 mGal on board submarines, which could handle small and long period accelerations (Telford et al., 1990). The Graf Askania gravimeters mounted on elaborate gyro-stabilized platform have been successful in measuring gravity readings onboard surface-ships with an accuracy of 2 mGal. The new Lacoste-Romberg gravity meters which are being routinely used onboard research vessels have good accuracies of ~1 mGal.

## 3.3 Gravity Anomaly Computation

The reduction of the gravity data acquired at sea requires knowledge of absolute gravity field at the location generally referred as a base station value. This is the location where the ship/ boat is berthed prior to the start of data acquisition. The measured values are tied to this base station value in order to calculate the gravity values along the traverse. The gravity values, thus computed must be corrected for latitude, elevation and topography in order to obtain the gravity values corresponding to some datum like geoid or ellipsoid. In addition the corrections for instrumental drift, Earth tide and the motion of ship are also necessary to carry out. A short description of important gravity correction applied for marine gravity measurements is given below.

### 3.3.1 The Latitude Correction

The theoretical gravity at given latitude position is calculated by the normal gravity formula (Eq. 3.2). If the measured gravity is an absolute value, then the latitude correction is made by subtracting the value calculated using the normal gravity formula. Gravity surveys are often carried out with a gravimeter, which measures the gravity difference relative to a base station. Therefore, the normal reference gravity $g_n$ may then be replaced by a latitude correction, obtained by differentiating Eq. (3.2) (Telford et al., 1990)

$$\Delta g_L / \Delta s = \left(1 / R_e\right) \frac{\Delta g}{\Delta \phi} \qquad \ldots (3.3)$$

Where, $\Delta s = R_e \Delta \phi$ is the N-S distance and Re is the radius of Earth (6368 km). Therefore Eq.3.3 becomes

$$\Delta g_L / \Delta s \approx 0.811 \sin 2\phi \quad mGal/km \qquad \ldots (3.4)$$

This correction is zero at poles and equator and maximum at 45°.

### 3.3.2 The Free-air Correction and Free-air Gravity Anomaly

The Free-air correction accounts for the height of the gravity station above the ellipsoid 'h'. The free-air correction is given by the second approximation of international 1924 ellipsoid (Moritz, 1980)

$$\partial g_{FC} = -(0.30877 - .00045 \sin^2 \phi)h + 0.000072h^2 \qquad \ldots (3.5)$$

Ignoring the second order term and setting $\phi$ = 45°, the first approximation of the height correction is

$$\partial g_{FC} = -0.30877h \text{ mGal} \qquad \ldots (3.6)$$

Thus, the free-air correction formula suggests that for every 1 m change in height, the gravity value changes by a factor of 0.30877 mGal. Free-air correction is positive for the gravity stations lie above the datum plane and negative for stations lie below the datum. In general, elevation or height above the geoid is used rather than ellipsoidal height for computing the free-air correction. The gravity anomaly derived after applying free-air correction is known as free-air anomaly and is expresses as

$$F.A.A = (g_{obs} - g_{ellipsoid}) \pm \partial g_{FC} \quad \ldots (3.7)$$

Where, $g_{obs}$ and $g_{ellipsoid}$ are observed and ellipsoidal gravity respectively. Marine gravity measurements are done at mean sea level; hence no free-air correction is required to be considered. The small changes caused by sea surface elevations due to tides are generally ignored (Nettleton, 1976).

### 3.3.3 The Eótvós Correction

During the marine gravity surveys, the motion of research vessel generates additional centrifugal force which affects the gravity measurements. An eastward component of velocity adds to the rotation of the Earth and causes slight increase in the centrifugal force and thus causes a reduction in measured gravity, whereas the westward component has the opposite effect. The Eótvós correction for a ship moving with a velocity V heading at angle θ from true north at a latitude φ is given by (Telford et al., 1990)

$$\partial g_{eotvos} = 4.04V \cos\phi \sin\theta + 0.0012V^2 \text{ mGal} \quad \ldots (3.8)$$

## 3.4 Interpretation of Gravity Anomaly using Two-Dimensional Gravity Forward Modeling

The gravity anomalies after applying corrections, in general, represent density inhomoginities within the Earth. The simple way to interpret these anomalies is by forward modeling, which involves computation of gravity effect of assumed causative bodies and compare with observed anomalies. For bodies of regular geometry, forward modeling is carried out using standered anomaly equations. Models of arbitrary shape are, in principle, divided in to several bodies of regular shape and then their individual gravity contributions are calculated and added. In a classic paper, Talwani et al., (1959) presented a method to compute the gravity effect of any two-dimensional body of arbitrary shape by approximating it to an n-sided polygon. The polygons are defined in terms of coordinates of vertices and the gravity anomaly is computed using line integral method.

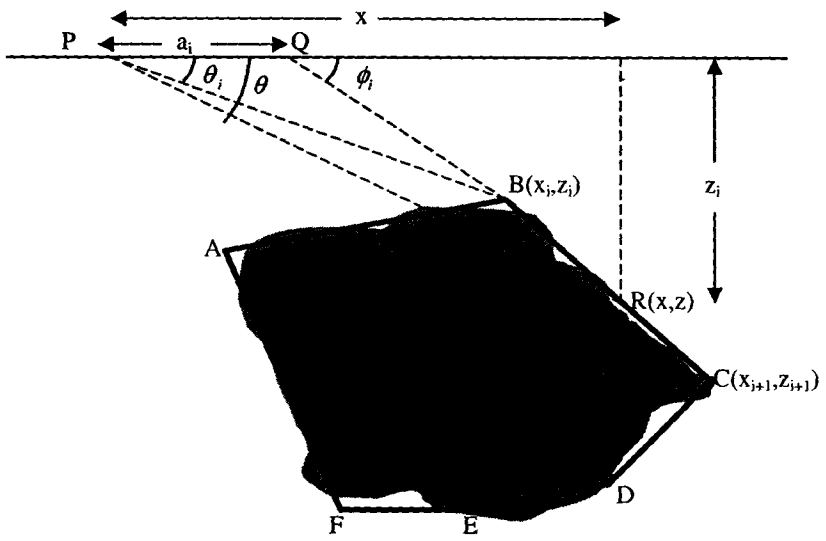


**Figure 3.1** Polygon approximation of irregular vertical section of two-dimensional body. Geometrical elements involved in the gravity computation are depicted.

The polygon ABCDFF approximates an arbitrary shaped body (Figure 3.1). The gravity effect of the polygon at the observation point P is given by (Hubbert, 1948)

$$g = 2G\rho z d\theta \qquad \ldots (3.9)$$

Where, G is the universal gravitational constant and ρ is the volume density. From geometry (Figure (3.1) it follows that

$$z = x\tan\theta = (x - a_i)\tan\phi_i = \frac{(a_i \tan\theta \tan\phi_i)}{(\tan\phi_i - \tan\theta)} \qquad \ldots (3.10)$$

The line integral for the side BC is given by

$$\int_{BC} z d\theta = \int_{B}^{C} \frac{(a_i \tan\theta \tan\phi_i)}{(\tan\phi_i - \tan\theta)} d\theta = Z_i \qquad \ldots (3.11)$$

Thus, for an n sided polygon Eq. 3.11 can be written as

$$g = 2G\rho \sum_{i=1}^{n} Zi \qquad \ldots (3.12)$$

The general solution of the above equation is

$$Z_i = a_i \sin\phi_i \cos\phi_i \left[ (\theta_i - \theta_{i+1}) + \tan\phi_i \log\left\{ \frac{\cos\theta_i (\tan\theta_i - \tan\phi_i)}{\cos\theta_{i+1} (\tan\theta_{i+1} - \tan\phi_i)} \right\} \right] \qquad \ldots (3.13)$$

Where, $\theta_i = \tan^{-1}\left(\frac{Z_i}{x_i}\right)$, $\phi_i = \tan^{-1}\left(\frac{Z_{i+1}-Z_i}{x_{i+1}-x_i}\right)$ and $a_i = x_{i+1} - Z_{i+1}\cot\phi_i$

The gravity forward model studies described in chapters 4, 5, and 6 have been carried out using the above method as implemented in the GM-SYS software.

## 3.5 Theoretical Basis of Isostatic Compensation

The isostasy of geological features is modeled by applying the theory of bending elastic plate in response to applied forces. The response of a thin, continuous, homogeneous elastic plate floating on a fluid mantle that is subjected to a line load can be represented with the following differential equation (McKenzie and Bowin, 1976; Watts, 2001)

$$D\frac{dy^4}{dx^4} + (p - q) = 0 \qquad \ldots (3.14)$$

where, q is the downward pressure, p is the restoring upward force, y is the deflection produced, g is the acceleration due to gravity and D is the flexural rigidity of the plate. The flexural rigidity depends on the Young's modulus E, and Poisson's ratio ν of the plate and could be expressed as

$$D = \frac{ETe^3}{12(1-\nu^2)} \qquad \ldots (3.15)$$

Where, Te is the approximate thickness of Earth's uppermost, elastically deforming elastic layer and commonly referred as effective elastic thickness or elastic plate thickness.

If we consider that the depression produced by the bending of plate is filled by crustal rocks of density $\rho_c$, and it displaces mantle of density $\rho_m$, then the force terms p and q in the Eq. (3.14) could be expressed as

$$q = \rho_c yg \qquad \ldots (3.16)$$

$$p = \rho_m yg \qquad \ldots (3.17)$$

Substituting Eq. 3.16 and Eq.3.17 on Eq. 3.14

$$D\frac{dy^4}{dx^4} + (\rho_m - \rho_c)yg = 0 \qquad \ldots (3.18)$$

### 3.5.1 Isostatic Response Functions

Elastic plate theory suggests that the lithosphere does not respond locally to long-term geological loads, as the Airy and Pratt models would predict. The compensation takes place regionally by a flexure over a wide region. Thereby the lithosphere behaves like a

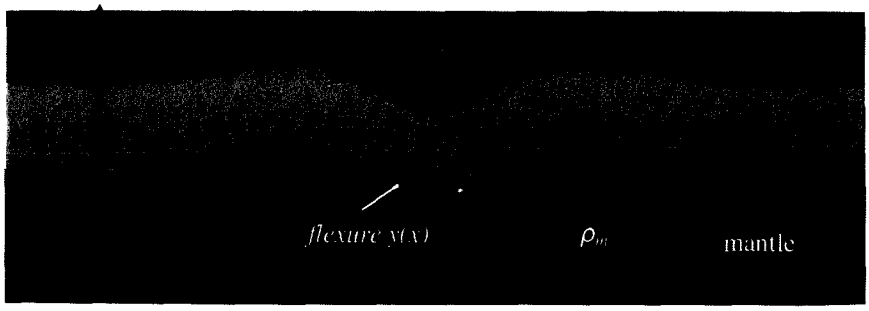


**Figure 3.2** Elastic plate approximation of the bending oceanic lithosphere under load.

linear space-invariant filter that suppress the short-wavelength and high amplitude deformation associated with local models of isostasy and passes the long-wavelength deformation (small amplitude) corresponding to the flexural behavior of the lithospheric plate (Watts, 2001). Therefore, if the input load is periodic, then the output flexure is also periodic. The elastic response of a plate to a periodic load (Figure 3.2) is given for one dimension by (Watts, 2001)

$$D\frac{dy^4}{dx^4}+(\rho_m-\rho_c)yg=(\rho_c-\rho_w)gh\cos(kx) \qquad \ldots (3.19)$$

Where h is the amplitude of the load, k is the wavenumber of the load along x direction. The solution of Eq.19 is periodic and of the form

$$y=\frac{(\rho_c-\rho_w)h\cos(kx)}{(\rho_m-\rho_c)}\left[1+\frac{Dk^4}{g(\rho_m-\rho_c)}\right]^{-1} \qquad \ldots(3.20)$$

Let us consider that the plate is extremely weak, i.e. $D \rightarrow 0$, then $y \rightarrow \frac{(\rho_c - \rho_w)h\cos(kx)}{(\rho_m - \rho_c)}$, this is Airy isostatic response to the periodic loading. If we assume that the plate is of enormous strength, i.e. $D \rightarrow \infty$, then $y \rightarrow 0$ which is the Bouguer isostatic response. If the plate has a finite strength, then it responds by flexure.

The wavenumber parameter which modifies the Airy response to give flexure is known as Isostatic Response Function ($\Phi_e(k)$).

$$\Phi_e(k) = \left[1 + \frac{Dk^4}{g(\rho_m - \rho_c)}\right]^{-1} \quad \ldots (3.21)$$

For low wavenumber loads ($k \rightarrow 0$), the plate behaves as a weak body and deforms with Airy response, whereas for high-wavenumber loads ($k \rightarrow \infty$), the plate becomes rigid. For intermediate wavenumbers (0.001<k<0.1), the response is flexural and is called diagnostic waveband for flexure.

Eq. 3.20 yields only the flexural response to a load at a particular wavenumber. However, using Fourier analysis, the load can be split into its individual spectral components to compute the response to any arbitrarily shaped load.

$$Y(k) = \frac{-(\rho_c - \rho_w)}{(\rho_m - \rho_c)} H(k)\Phi_e(k) \quad \ldots (3.22)$$

where, H(k) and Y(k) are wavenumber domain representation of the load, $h\cos(kx)$ and the flexure (y(x)).

### 3.5.2 The Gravitational Admittance

The state of isostasy or the lithospheric flexure beneath the geological features is not always directly observable. Gravity anomalies are sensitive to both magnitude of load and flexure and act as proxies of the flexural response of the lithosphere to geological loads. As in the case of flexural studies, Fourier transform method provides an efficient way to

compute the gravity anomalies. The gravity anomaly at a point p caused by an undulating density interface is calculated as (Parker, 1972)

$$\Delta g_p(k) = e^{-kp} 2\pi G\rho \Delta H(k) \quad \ldots (3.23)$$

Where, $\Delta g_p(k)$ is the Fourier Transforms of gravity anomaly, $\Delta H(k)$ is the Fourier Transforms of the undulating surface with a uniform density contrast $\rho$ and G is the universal gravitational constant. Gravitational Admittance, the wavenumber parameter which modifies the topography to produce gravity may be expressed as

$$Z(k) = \frac{\Delta g(k)}{\Delta H(k)} \quad \ldots (3.24)$$

### 3.5.3 Gravitational Admittance and Isostatic Models

The gravitational admittance is an important parameter as it can be used to infer the state of isostasy of geological loads. The formulation of admittance function for sea-floor topography in three different isostatic cases (Watts, 2001) is given below

*Case-1: uncompensated topography*

The gravitational effect of the topography at sea-floor ($\Delta g(k)_{topo}$) could be expressed as

$$\Delta g(k)_{topo} = 2\pi G(\rho_c - \rho_w) e^{-kd} H(k) \quad \ldots (3.25)$$

and the admittance due to uncompensated topography ($Z(k)_{uncomp}$) is given by

$$Z(k)_{uncomp} = 2\pi G(\rho_c - \rho_w) e^{-kd} \quad \ldots (3.26)$$

Where d is the average water depth

*Case-2: Airy model*

For Airy model, the isostatic compensation of topographic highs and lows are obtained by forming "roots" and "anti-roots" in the mantle. Hence, the gravity anomaly is the sum of two effects: one from topography ($\Delta g(k)_{topo}$) and the other from compensation ($\Delta g(k)_{comp}$)

$$\Delta g(k)_{total} = \Delta g(k)_{topo} + \Delta g(k)_{comp} \quad \ldots (3.27)$$

Where the gravity effect of compensation ($\Delta g(k)_{comp}$) can be expressed as

$$\Delta g(k)_{comp} = 2\pi G(\rho_c - \rho_w) e^{-k(d+t)} R(k) \quad \ldots (3.28)$$

Where t is the oceanic crust thickness and R(k), the Fourier transform of the root r(x) is expressed as $R(k) = -H(k)\frac{(\rho_c - \rho_w)}{(\rho_m - \rho_c)}$

$$\Delta g(k)_{total} = 2\pi G(\rho_c - \rho_w) e^{-kd}\left(1 - e^{-kt}\right) H(k) \quad \ldots (3.29)$$

The admittance function is given by

$$Z(k)_{airy} = 2\pi G(\rho_c - \rho_w) e^{-kd}\left(1 - e^{-kt}\right) \quad \ldots (3.30)$$

*Case3: Elastic plate (flexure) model*

Flexural isostasy assumes a definite strength for the lithosphere and the compensation is distributed over broader region. The gravity effect of the flexure ($\Delta g(k)_{flex}$)is computed as

$$\Delta g(k)_{flex} = 2\pi G(\rho_c - \rho_w) e^{-k(d+t)} Y(k) \quad \ldots (3.31)$$

The total gravity anomaly due to flexure and topography ($\Delta g(k)_{total}$) could be expressed as

$$\Delta g(k)_{total} = 2\pi G(\rho_c - \rho_w) e^{-kd}\left(1 - \phi_e(k) e^{-kt}\right) H(k) \quad \ldots (3.32)$$

The admittance function is given by

$$Z(k)_{flex1} = 2\pi G(\rho_c - \rho_w) e^{-kd}\left(1 - \phi_e(k) e^{-kt}\right) \quad \ldots (3.33)$$

The above formulation considers constant densities for the load, infill material and the oceanic crust is single layered. If the load of density $\rho_l$ is emplaced on a two layered crust with densities $\rho_2$, $\rho_3$ and thicknesses $t_2$, $t_3$ where the infill material has a density $\rho_i$ (Figure 3.3), then the admittance equation becomes

$$Z(k)_{flex2} = 2\pi G(\rho_l - \rho_w) e^{-kd}\left\{1 - \phi_e(k)\left[\frac{(\rho_2 - \rho_i) + (\rho_3 - \rho_2) e^{-kt_2} + (\rho_m - \rho_3) e^{-k(t_2+t_3)}}{(\rho_m - \rho_i)}\right]\right\} \quad \ldots (3.34)$$

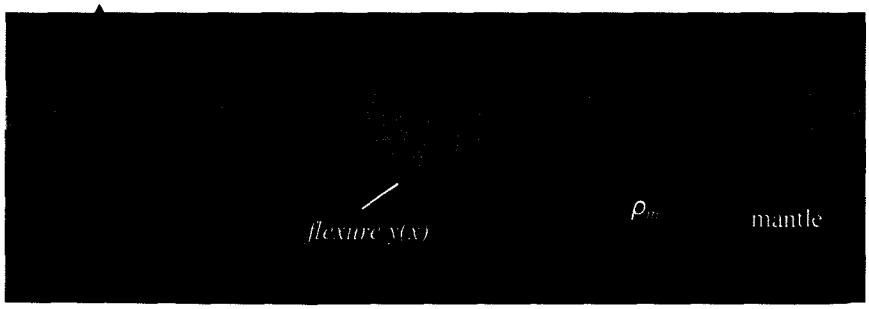


***Figure 3.3*** *Elastic plate model for layered oceanic crust.*

*Case 4: flexure with subsurface load*

Elastic plate model with surface and subsurface loads can provide information on underplating or presence of high density volcanic material beneath volcanic ridges and seamounts. Following McAdoo and Sandwell (1989) hypothesis, the admittance for the subsurface or buried load having a density $\rho_b$ at a depth z below the mean depth z could be expressed as

$$Z_{burried}(k) = Z_0(k)\left[1+\left(\frac{\rho_m-\rho_b}{\rho_b-\rho_w}\right)e^{-kh}-\left(\xi(k)\frac{\rho_m-\rho_w}{\rho_b-\rho_w}\right)e^{-kz}\right] \quad \ldots (3.35)$$

Where

$\xi(k) = 1+\frac{Dk^4}{g(\rho_m-\rho_w)}$, $Z_o(k) = 2\pi G(\rho_2-\rho_w)e^{-kd}$, and h is the average crustal thickness

Following Equation 3.34, the expression for admittance in the case of surface load for $\rho_l=\rho_i=\rho_2$ is

$$Z(k)_{surface} = 2\pi G(\rho_2-\rho_w)e^{-kd}\left\{1-\phi_e(k)\left[\frac{(\rho_3-\rho_2)e^{-kt_2}+(\rho_m-\rho_3)e^{-k(t_2+t_3)}}{(\rho_m-\rho_2)}\right]\right\} \quad \ldots (3.36)$$

The equation for combined loading: subsurface and surface can be expressed as

$$Z_{combained}(k) = \frac{\beta^2 Z_{burried}(k)+Z_{surface}(k)}{\beta^2+1} \quad \ldots (3.37)$$

Where, $\beta = f\left[\frac{\rho_3 - \rho_w}{\rho_m - \rho_3 + Dk4/g}\right]$

Where, f is the subsurface to surface load ratio

## 3.6 Computation of Admittance from Observed Data

Admittance analysis investigates the relationship between bathymetry and gravity anomaly in the discrete Fourier transform domain (McKenzie and Bowin, 1976; Watts, 1978). This essentially involves computation of admittance function from the observed bathymetry and gravity data and compare with the theoretical admittance to derive isostatic parameters, such as Te, t, d and $\rho_c$.. The admittance between gravity and bathymetry data can be calculated as suggested by McKenzie and Bowin (1976),

$$Z(k) = \frac{C(k)}{E_t(k)} \quad \ldots (3.38)$$

where, k is the wavenumber, Z(k) is gravitational admittance between gravity and topography; C(k) is cross spectrum of the gravity and topography, $E_t(k)$ is power spectrum of the topography and could be expressed as

$$C(k) = \frac{1}{N}\sum_{m=1}^{N} \Delta g_m(k) H^*_m(k) \quad \ldots (3.39)$$

$$E_t(k) = \frac{1}{N}\sum_{m=1}^{N} H_m(k) H^*_m(k) \quad \ldots (3.40)$$

Where, $\Delta g(k)$, $H(k)$ are now the Fourier transforms of the observed free-air gravity anomaly and topography ,N is the number of ship tracks and the asterisk denotes the complex conjugate.

A key parameter in the admittance analysis is coherence, which gives the measure of gravity produced by seafloor topography. The coherence can be computed using the following equation (Watts, 2001)

$$\gamma^2(k) = \frac{C(k)C^*(k)}{E_g(k)E_t(k)} \quad \ldots (3.41)$$

where, $E_g(k)$ the power spectrum of free-air gravity field and can be expressed as

$$E_g(k) = \frac{1}{N}\sum_{m=1}^{N} \Delta g_m(k) \Delta g^*_m(k) \quad \ldots (3.42)$$

The coherence can be used to separate energy spectrum into two parts (Watts, 1978)

$$CohrentEnergy = \gamma^2(k) E_g(k) \quad \ldots (3.43)$$

$$IncohrentEnergy = \left(1 - \gamma^2(k)\right) E_g(k) \quad \ldots (3.44)$$

Coherent energy is defined as the part of the energy in the gravity signal that is caused by bathymetry, therefore the most confident determination of the admittance function can be carried out.

The admittance is complex parameter, but in general, the real part is only used for analysis. However, phase of admittance θ is also important as it is an indicator of the coherence between free-air gravity and seafloor topography. The phase in the range of high coherence is expected to be close to zero. The phase of admittance can be computed using the following equation (Louden, 1981).

$$\theta = \arctan\left[\mathrm{Im}\,Z(k) \Big/ \mathrm{Re}\,Z(k)\right] \quad \ldots (3.45)$$

The plus/ minus standard deviation (σ) in the admittance is computed from the variance of the coherence estimator as (Louden, 1981)

$$\sigma = \left[\frac{(\gamma(k))^{-2} - 1}{2n}\right]^{1/2} Z^2(k) \quad \ldots (3.46)$$

Where n is the number of discrete samples in the wavenumber band.

The application of admittance analysis for the study of isostatic response of the Comorin Ridge and the Ninetyeast Ridge is described in detail in Chapter-4 and Chapter-6, respectively.

## 3.7 Process Oriented Gravity Modeling

Process oriented gravity modeling is an extremely useful and widely accepted technique in order to investigate the geologically complex regions, where the gravity anomalies have

been changed through geological ages. Earlier Watts (1988) and Watts and Fairhead (1999) have used this technique to study the complex rifted continental margins in terms of crustal structure, subsidence history and long-term mechanical properties of the crust. In this analysis, the observed gravity anomaly was considered as a sum of several processes those were involved during the evolution of continental margins such as rifting, underplating, sediment loading, flexure, erosion, etc. The technique essentially involves 2D flexural backstripping and computation of gravity anomalies corresponding to relevant processes at the margin.

The aim of backstripping is to reconstruct the basement configuration of the basin prior to the sediment and water loading. The 2D backstripping procedure consists of flexural

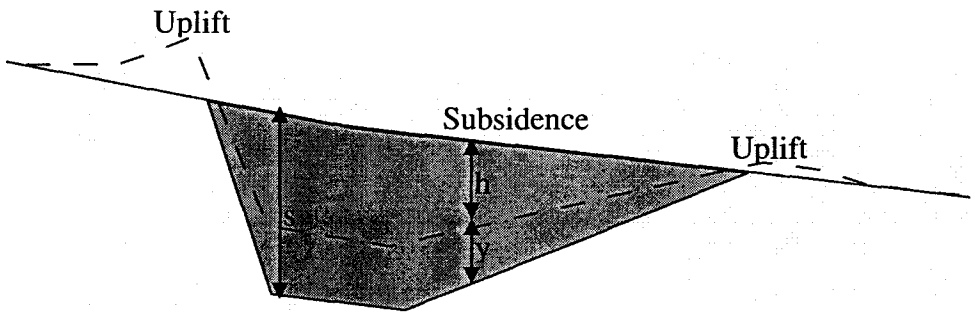


**Figure 3.4** The principle of backstripping. The shaded region represents the wedge of sediments. The dashed line is backstripped basement in the absence of sediment loading.

unloading of each sedimentary layer identified from seismic section from the top downwards. The flexure of basement due to sediment loading is computed using elastic plate theory as described in section (3.5). The flexure y(x) due to a sediment load of present day thickness s(x) and density $\rho_s$ (Figure 3.4) is expressed as (Watts, 2001)

$$Y(k) = \frac{-(\rho_s - \rho_w)}{(\rho_m - \rho_w)} S(k)\Phi_e(k) \qquad \ldots (3.47)$$

Y(k), S(k) are Fourier representations of y(x) and s(x) and and $\Phi_e$(k) is the isostatic response function. The backstrip h(x) is calculated from

$$h(x) = s(x) - y(x) \qquad \ldots (3.48)$$

This concept of process oriented modeling is used for investigating the structure and isostatic compensation of the 85°E Ridge. The details of the method are discussed in detail in Chapter 5.

## 3.8 Geophysical Data

In this study, ship-borne bathymetry, gravity and magnetic profiles available in NGDC database are compiled with data collected on various Indian and Russian cruises in eastern Indian Ocean. From this database selected geophysical profiles crossing the Comorin Ridge, 85°E Ridge and Ninetyeast Ridge were used for the study in this research work.

Multichannel Seismic reflection data along with gravity and bathymetry data collected on board *MV Sagar Sandhani* (profiles MAN-01 and MAN-03), *ORV Sagar Kanya* (profile SK107-7) and *RV Issledovatel* (Profile 98791) are used for the model studies of 85°E Ridge (Chapter 5). Geophysical data acquisition were carried out using similar instruments during *MV Sagar Sandhani* and *ORV Sagar Kanya* cruises; Integrated Navigation System (Magnavox 1107) along with Global positioning System for position fixing, DFS V system for seismic data, KSS-30, 31 Bodenseewerk system for gravity data and Honeywell Elac narrow beam echosounder system for bathymetric data. Free-air gravity anomalies are computed from the acquired gravity data by applying Eotvos correction and normal gravity (GRS 67 reference ellipsoid). Seismic data processing was done at Interra Exploration Company (India) Pvt. Ltd., Bombay for profiles MAN-01 and MAN-03, at SPIC, ONGC, Mumabi for profile SK107-07 and on-board *RV Issledovatel* for profile 98791.

These data sets along with their profile locations and other details are presented in Chapters 4, 5 and 6. Additionally, satellite-derived gravity (Sandwell and Smith, 1997, 2009) and bathymetry (Smith and Sandwell, 1997; GEBCO; ETOPO) data sets are also used wherever necessary. GMT software (Wessel and Smith, 1995) is extensively used for data processing and figure preparations.

# CHAPTER 4

## Structure and Isostasy of the Comorin Ridge

# Structure and Isostasy of the Comorin Ridge

## 4.1 Introduction

The presence of the Comorin Ridge in the north Indian Ocean was first reported by Heezen and Tharp (1964) from the compilation of echo-sounding data acquired during the International Indian Ocean Expedition (IIOE). Using marine geophysical data, Kahle et al., (1981) have suggested that the Comorin Ridge was formed on oceanic crust with Airy type compensation and also opined that the eastern edge of the Comorin Ridge could mark a boundary between oceanic crust and rifted/ altered continental crust. Further they concluded that the ridge seems to act as a barrier to the passage of Ganges sediments to the west. Southeast of the Comorin Ridge, Krishna et al. (2001a) have also mapped steep isolated basement rises in seismic reflection data and attributed that the rises were acting as a barrier for limiting the Bengal Fan sediments in western side. All these structures together have encircled the western margin of Sri Lanka and contributed to the formation of a small basin within the Gulf of Mannar (Figure 4.1). The origin of the Comorin Ridge is not clearly known yet. Using marine magnetic data, Desa et al. (2006) opined that it may be a transform ridge formed during the early phase of opening of the Indian Ocean. Later, Shena et al. (2007) have suggested that the ridge could be a product of large-scale volcanism during the onset of seafloor spreading.

Admittance analysis technique was, in general, earlier performed on various geological features of the Indian Ocean to obtain structure and isostatic compensation mechanisms (Detrick and Watts, 1979; Paul et al., 1990; Ashalatha et al., 1991; Chand et al., 2001; Tiwari et al., 2003; Bansal et al., 2005). However, a detailed study of the isostatic behavior of the Comorin Ridge is not yet attempted. The present study investigates the mode of isostatic compensation and nature of the crust underneath the Comorin Ridge using admittance analysis and forward modeling of ship-borne bathymetry and gravity data sets. Also, an attempt has made to mark the Continent-Ocean Boundary (COB) on west of Sri

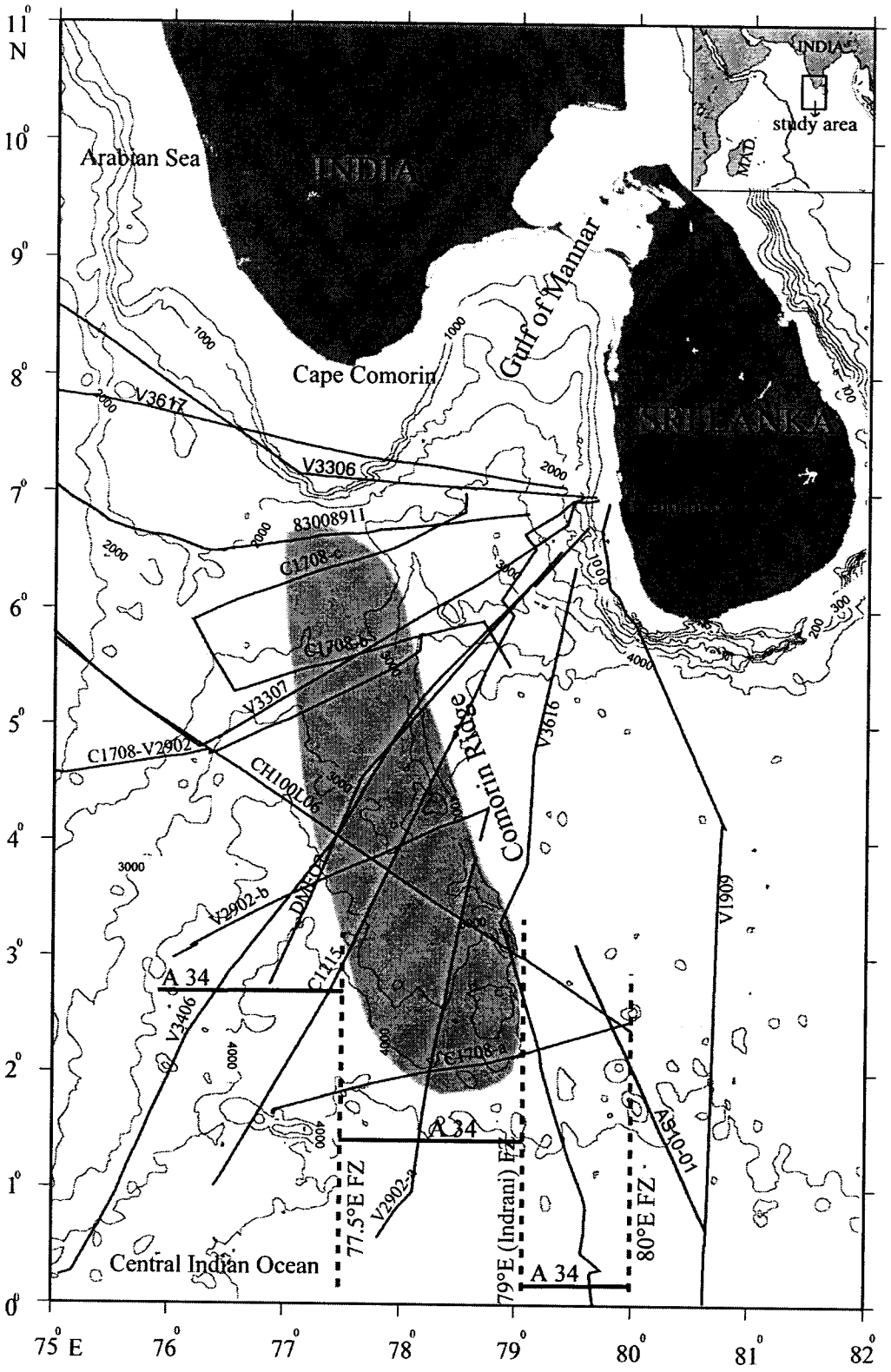


**Figure 4.1.** General bathymetry of the southern tip of India and south and west margins of Sri Lanka (ETOPO5). Light shaded region shows the location of the Comorin Ridge. Solid lines indicate the geophysical profiles. Magnetic lineation A34 and fracture zones shown in this figure are after Müller et al. (1997) and Krishna and Gopala Rao (2000).

Lanka and southern tip of India. Based on new inferences, a plausible tectonic model for the evolution of the ridge is proposed.

## 4.2 Geological Setting of the Region

The eastern continental margins of India and Sri Lanka were evolved in the early Cretaceous after their break-up from the Mac.Robertson Land - Enderby Land, east Antarctica (Rotstein et al., 2001; Kent et al., 2002; Giana et al., 2007; Jokat et al., 2010). At a subsequent stage, after 124 Ma, a continental fragment called Elan Bank was detached from the northeastern margin of India (Gaina et al., 2003). The southwest margin of Sri Lanka and southern margin of India seem to have been rifted initially at around 127 Ma from east Gunnerus Ridge, east Antarctica. During the phase, before the commencement of the first major change in spreading direction in the Indian Ocean, there was a probable ridge jump towards India-Sri Lanka region similar to the ridge jump that occurred on the northeastern margin of India. This implies that the earliest oceanic crust formed near the India-Sri Lanka region was transferred to the west Enderby Basin (Nogi et al., 2004). Therefore, most part of the oceanic crust adjacent to the India-Sri Lanka region seems to be evolved during the long Cretaceous normal polarity reversal (120-83 Ma).

It is widely believed that the western margin of India has rifted from the eastern margin of Madagascar during the late Cretaceous period (White and McKenzie 1989; Storey et al., 1995, 1997; Torsvik et al., 1998, 2000; Raval and Veeraswamy, 2003a). Also, it is supposed that the rifting process was associated with the Marion hotspot volcanism, which occurred at Volcan de l'Androy, southeast Madagascar and caused the eruption of widespread basalts and rhyolites in Madagascar and Fe-Ti-enriched tholeiites in southwest India. Hence the hotspot source was attributed to the formation of the Comorin Ridge and some basaltic flows and dykes in the southwestern margin of India (Radhakrishna et al., 1994; Anil Kumar et al., 2001) as well as in Madagascar (Storey et al., 1995; Torsvik et al., 1998) before shifting its activity entirely to the African plate. The Comorin Ridge extends in NNW-SSE direction between latitudes 1.5°N and 6.5°N (Figure 4.1) with an average width of 150 km. The southern part of the ridge lies on the oceanic crust evolved older to the age of seafloor magnetic anomaly A34 and is bounded by the 77.5°E and 79°E

(Indrani) FZs. The nature of the crust beneath the northern part of the ridge is not clearly known.

## 4.3 Geophysical Data

Bathymetry, gravity and magnetic data along 17 profiles totaling to 9200 lkm across the Comorin Ridge and in its adjacent parts, acquired during the cruises of Conrad 17, Vema 29, 33, 34, Chain L06, Jean Charcot 83008911, Dimitry Mendeleev 07 (NGDC 1998) and A. A. Sidorenko (AS 10), are used in the present study. Additionally, ETOPO-5 bathymetric data (3D image) are used to study the morphology of the ridge. Sediment isopachs of this region published by Kahle et al. (1981) are also considered for two-dimensional forward modeling of gravity anomalies in order to constrain the sediment thickness along profiles C1215 and V3307.

## 4.4 Bathymetry, Gravity and Magnetic Anomalies of the Ridge

A three-dimensional topographic map of the seafloor is presented in Figure 4.2 for better visualization of the Comorin Ridge morphology and its comparison with the adjacent seafloor. Bathymetry, gravity and magnetic profiles have been stacked with reference to the axis of the Comorin Ridge and are shown in Figure 4.3. The depth to the seafloor along the profiles (Figure 4.3) varies from 2 to 4.2 km. The important geomorphic features in the study area are the Comorin Ridge, another ridge-like structure in the northwest quarter of the region, a steep scarp of up to 1.2 km on the eastern flank of the ridge, and 77.5°E and 79°E (Indrani) FZs. In general the water depth adjacent to the Comorin Ridge is decreasing towards north from 4 km to 2.5 km (Figures 4.2 and 4.3). The southern part of the ridge between 1.5°N and 3°N has an elevation of up to 0.5 km compared to that of adjacent seafloor. In the central part between 3°N and 5°N, the ridge has maximum elevation of 1 km from the surrounding water depths, and in the north between 5°N and 6.5°N, the ridge has an elevation generally on eastern side ranging from 0.4 to 0.7 km (Figure 4.3). On the northern part of the ridge, the western flank does not have any distinct bathymetric expression as it probably merges with the continental rise of the southern tip of India

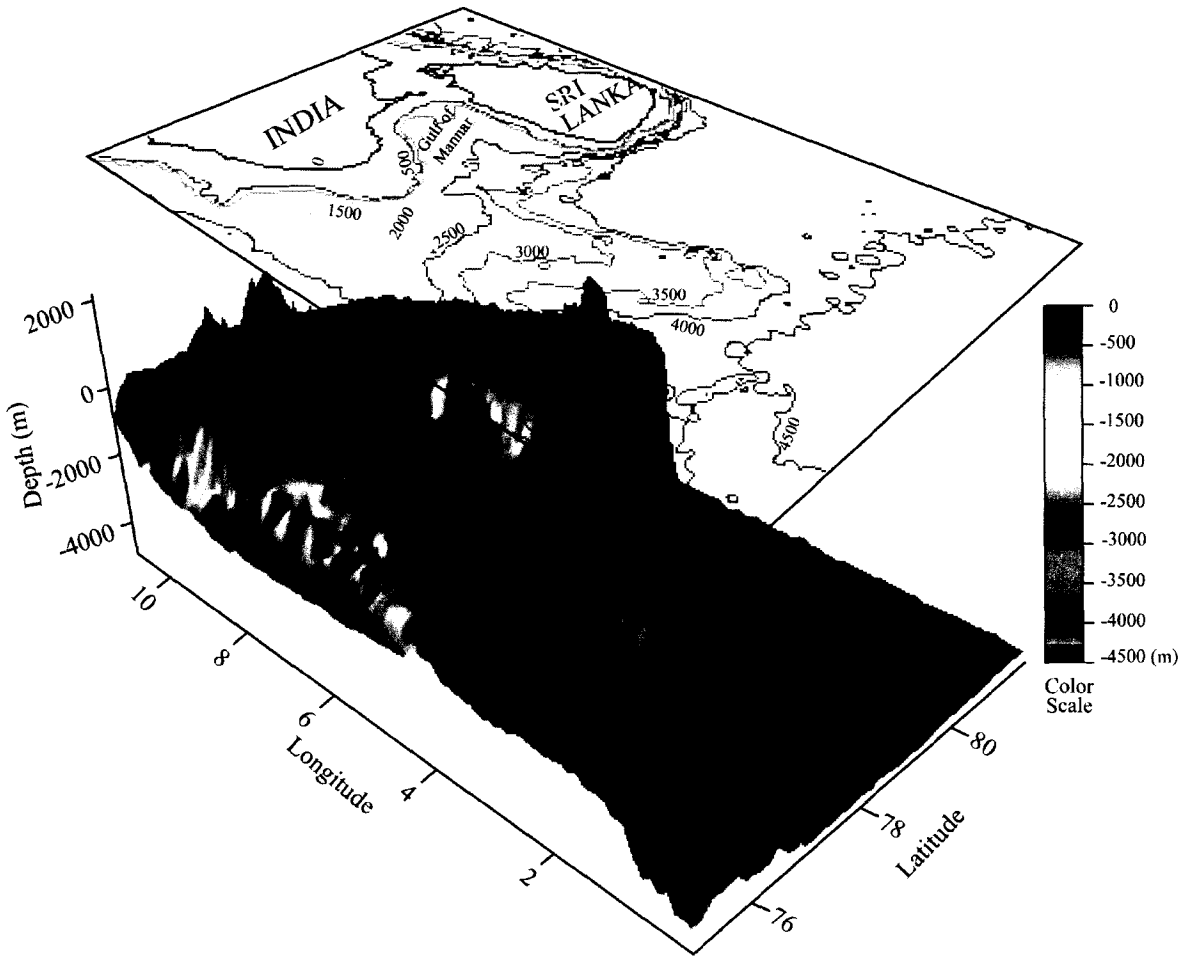


**Figure 4.2** Three dimensional view of the Comorin Ridge surface topography generated from ETOPO5 data.

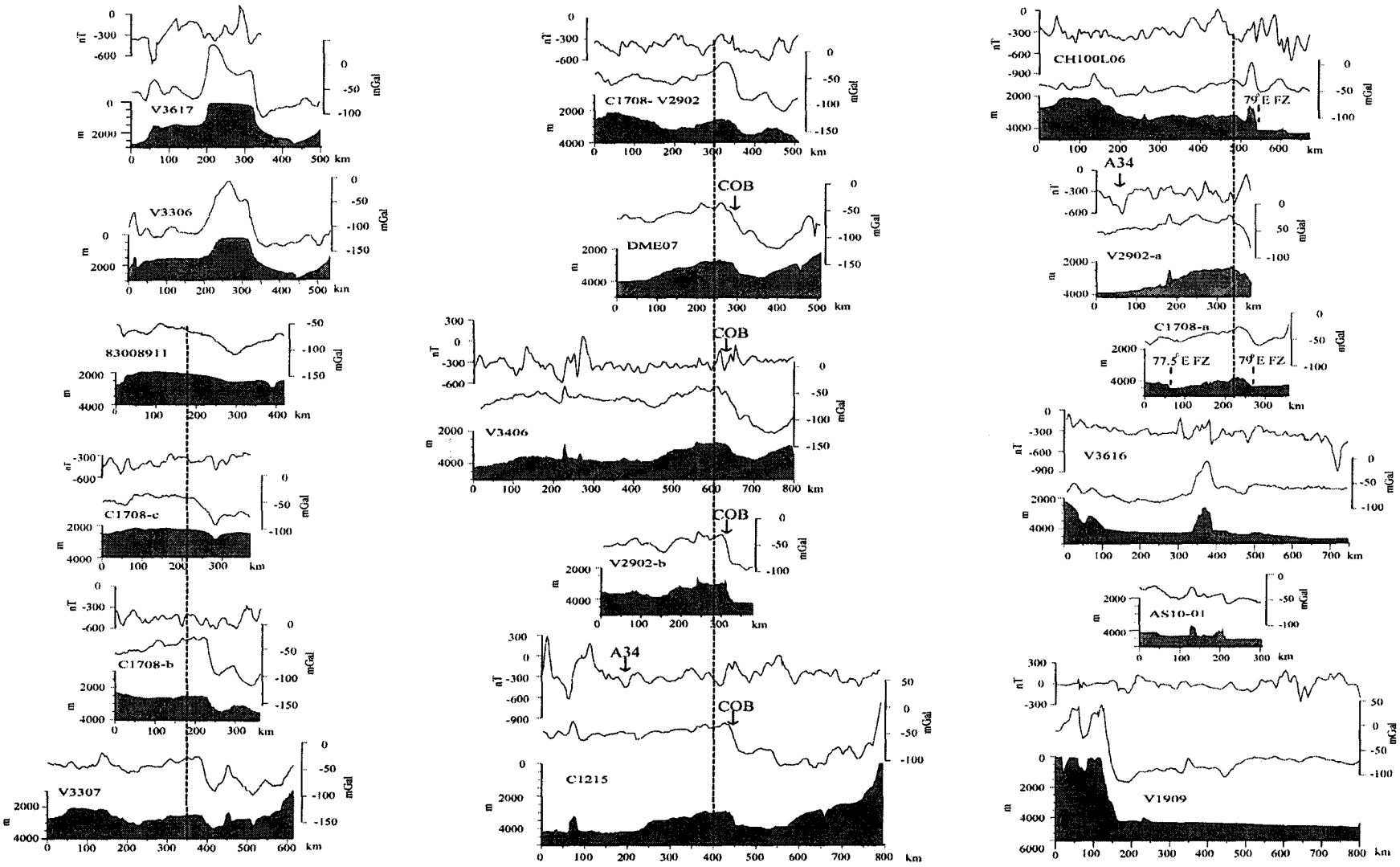


**Figure 4.3** Composite plots of bathymetry, gravity and magnetic profile data across the Comorin Ridge and its vicinity. The dashed line marks the axis of the Comorin Ridge

(Figure 4.2). While in the southern part, the western flank extends for more than 100 km with relatively smooth gradient, the eastern flank comes to an end about 50 km distance with a steep scarp of about 1.2 km (Figure 4.3). North of the ridge, north of 5.5°N the eastern steep scarp is not obviously seen.

The free-air gravity anomalies of the Comorin Ridge region, in general, follow the topography of the seafloor with variable amplitudes (Figure 4.3). From satellite gravity data of the central Indian Ocean, Gopala Rao et al. (2004) found NW trending elongated gravity high closures associated with the Comorin Ridge. From the profile data, it is evident that the ridge is associated with relatively low-amplitude gravity anomalies of about 25 mGal in southern part (1.5°N – 5°N) and 30 mGal in northern part (5°N – 6.5°N) corresponding to its variable elevations (Figure 4.3). The less elevated northern part of the ridge is associated with relatively high-amplitude 30 mGal gravity anomaly, suggesting that this part of the ridge is relatively less compensated in comparison to its southern part. Along the profiles C1215, V2902-b, V3406, DME07, C1708-V2902, V3307 and C1708-b a significant regional gravity anomaly of more than 50 mGal is observed on the eastern flank of the Comorin Ridge (Figure 4.3). Such significant anomaly is absent on other profiles, CH100L06 and C1708-a, in spite of sharp increase in depths to the seafloor (about 500 m) on eastern side of the ridge. Northern most profiles, V3306 and V3617 show bathymetric rise and associated high gravity anomalies (Figures 4.1 and 4.3), which are related to the southern tip of continental margin of India and not associated with the Comorin Ridge.

Most of the present study area is underlined by oceanic crust and was evolved during the period from post-anomaly 34 to younger part of the long Cretaceous magnetic quiet period. The seafloor magnetic anomaly 34 is identified with confidence on profiles V2902-a and C1215 (Figure 4.3). The rest of the anomalies having short-wavelength and low-amplitude are in general non-coherent and may have been formed during the Cretaceous Magnetic Quiet Period. The anomaly identifications (A34) are reasonably acceptable as they are found to be compatible with the earlier anomaly identifications of adjacent region (Krishna

and Gopala Rao, 2000). It is further observed that the Comorin Ridge as one is not associated with any specific magnetic anomaly signatures.

## 4.5 Gravity-Topography Admittance Analysis

The theoretical basis and methodology for admittance analysis are described in detail in Chapter 3. Out of 12 bathymetry and gravity profiles (Figures 4.1 and 4.3), 9 profiles crossing the Comorin Ridge were selected for the admittance analysis. These profiles were projected perpendicular to the strike of the ridge and their length is limited to 300 km keeping the apex of the ridge in the centre. Each profile has been sampled at an interval of 1.172 km representing a spatial wave-number range of $0.0105<k<2.6805 km^{-1}$ ($600>\lambda>2.344$km). The mean including linear trend in the data were removed and the ends of the profiles were tapered using a cosine window of 10% profile length prior to the spectral estimation. The Welch's averaged periodogram method was used to compute cross spectrum and power spectrum because of its improvement over the conventional Fast Fourier Transform (FFT) method (Welch 1967). The method has advantage of having less variance, hence it produces smooth admittance. In this method, bathymetry and gravity data are divided into overlapping segments and each of them is detrended, windowed using Hanning window and discrete Fourier transformed. MATLAB codes are developed for admittance analysis. The inputs to the program are gravity-bathymetry data and model parameters for theoretical admittance computation as listed in Table 4.1. These codes can processes the data sets, generates admittance values, compute theoretical admittance curves, plot them together and finally select the best fit by computing the RMS difference between the two.

### 4.5.1 Elastic Plate Thickness and Crustal Thickness

In admittance analysis, the admittance values generally computed along individual ship-tracks crossing the aseismic ridge, are smoothened by averaging. Thus, the smoothed admittance exclusively represents the overall isostatic state of the ridge structure. In order to examine the variation of the isostasy along the Comorin Ridge, individual admittance estimates are computed and then compared with the Airy and flexure theoretical models

for a wavenumber range of 0.0105<k>0.15, where the isostatic compensation effect is prominent (Figures 4.4a and b). Though the admittance values along the profiles show considerable scatter, the southern profiles show low amplitude admittance compared to the

**Table 4.1** Model parameters used for the calculation of theoretical admittance.

| *Parameter* | *Notation* | *Value* |
|---|---|---|
| Density of Sea-Water | $\rho_w$ | 1.03 gm/cc |
| Density of oceanic layer 2 | $\rho_2$ | 2.70 gm/cc |
| Density of oceanic layer 3 | $\rho_3$ | 2.90 gm/cc |
| Density of mantle | $\rho_m$ | 3.35 gm/cc |
| Thickness of oceanic layer 2 | $t_2$ | 2 km |
| Thickness of oceanic layer 3 | $t_3$ | 5 km |
| Young's modulus | E | 100 Gpa |
| Poissons ratio | $\sigma$ | 0.25 |

northern profiles. A rough estimate of Te and t values along the profiles were made by visual match and presented in Table-4.2. Following the Te and t value ranges, the profiles are combined into two groups: southern profiles (Te range 1-5 km, t range 15-20 km) and northern profiles (Te range 9-20 km and t more than 30 km) and calculated smoothed admittance by averaging individual spectra.

The $\log_{10}$ of the amplitude of admittance, coherence and phase for southern and northern profiles of the Comorin Ridge are presented in Figures 4.5a and b. High coherence ($\gamma_{(k)}{}^2 >$ 0.5), low phase ($\theta$) and smooth admittance values are observed for k<0.314 ($\lambda$> 20.01 km). For this same waveband the coherent gravitational energy caused by topography is dominant over incoherent energy (Figures 4.6a and b). This clearly indicates that for k<0.314 ($\lambda$> 20.01 km) the admittance computation is most reliable and can be used to compare with the theoretical models. The amplitude of the admittance decreases at lower wave-numbers indicating isostatic compensation at deeper depths. At higher wave-numbers the admittance flattens, probably because of instrument noise in the shipboard gravity data. The part of the admittance not caused by isostasy and instrument noise

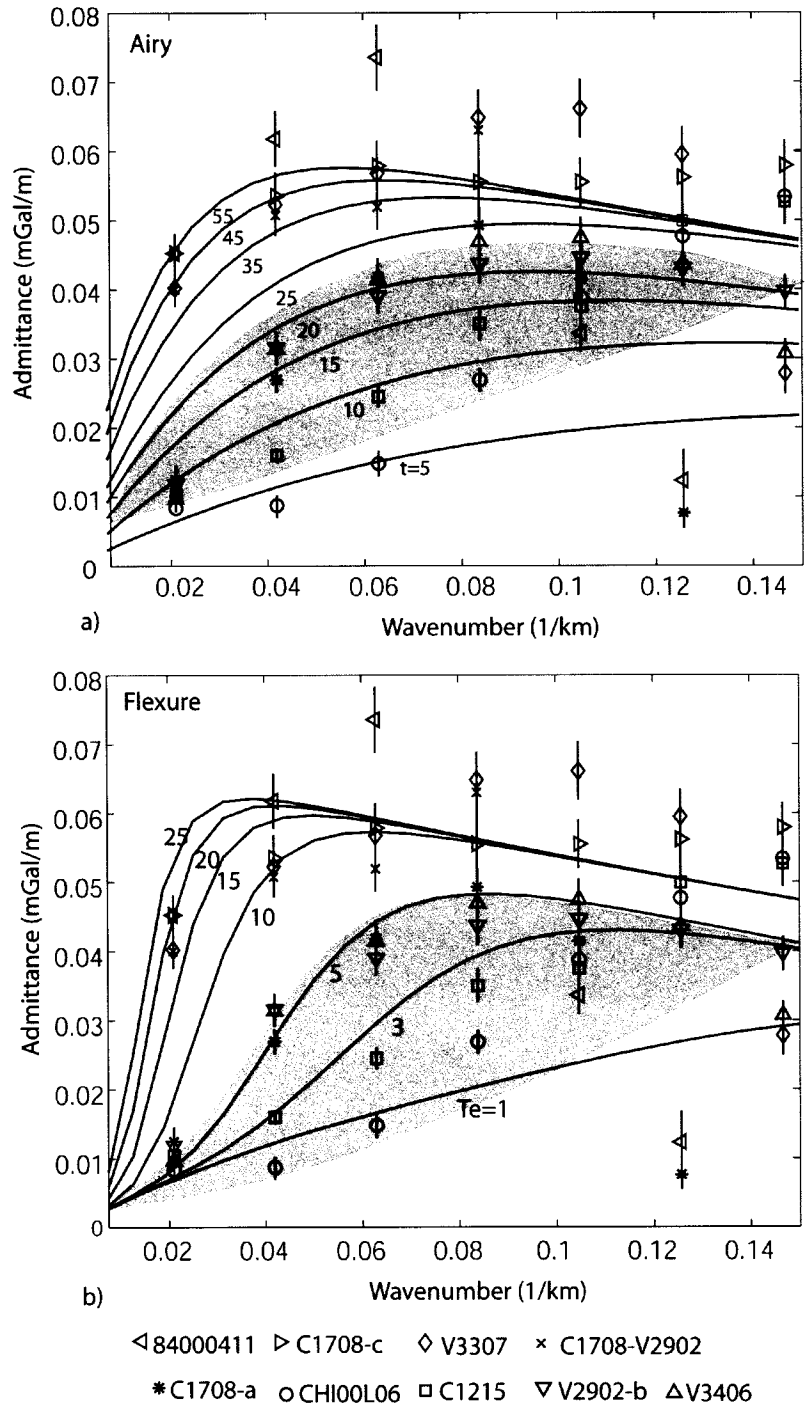


**Figure 4.4a and b** Admittance values computed for individual profiles plotted with theoretical curves for Airy and Flexure models. Southern profiles (blue) matches with Te~1-5 and t~10-20 (shaded region). Northern profiles (red) matches with Te~10-20 and t~30-50. The Te and t values for each profiles are listed in Table 4.2.

**Table 4.2** Elastic plate thickness (Te) and crustal thickness (t) are determined from admittance analysis and approximate age of lithosphere at the time of ridge emplacement is determined for each profile following the relationship of Calmant and Cazenave (1987).

| *S. No.* | *Profile Id* | *Te (km)* | *t (km)* | *Approximate Age (Myr)* | *Remarks* |
|---|---|---|---|---|---|
| 1 | C1708-a | 4-5 | 15 | 2.2-3.5 | Low Te and high t values |
| 2 | CH100L06 | 1-3 | No match | 0.13-1.2 | Low Te value |
| 3 | C1215 | 2-3 | 10-15 | 0.6-1.2 | Low Te and high t values |
| 4 | V2902-b | 3-4 | 20 | 1.2-2.2 | Same as above |
| 5 | V3406 | 3-4 | 20 | 1.2-2.2 | Same as above |
| 6 | C1708-V2902 | 9-15 | 30-40 | 11-31 | High Te and exceptionally high t values |
| 7 | V3307 | 10-15 | 40 | 14-31 | Same as above |
| 8 | C1708-c | 10-15 | >40 | 14-31 | Same as above |
| 9 | 84000411 | 15-20 | >50 | 31-55 | Same as above |

reflects the uncompensated topography ($0.11 < k < 0.8167$ and $0.04 < k < 0.44$ for the southern and northern parts respectively). This part of the spectrum carries the information on the mean water depth and density of the topography. As discussed in Chapter 3, the uncompensated admittance can be expressed as

$$Z(k)_{uncomp} = 2\pi G(\rho_c - \rho_w)e^{-kd}$$

Taking logs on both sides yields

$$\log_{10} Z(k)_{uncomp} = -kd \log_{10} e + \log_{10}(2\pi G(\rho_c - \rho_w))$$

The slope and intercept of the log linear plot of $Z(k)$ against $k$ is d0.4335 and $\log_{10}(2\pi G(\rho_c - \rho_w))$, respectively. Average water depth and density of the crust are calculated from slope and intercept of the linear least square fit to the log10 admittance for $0.11<k<0.8167$ and $0.04<k<0.44$ for the southern and northern parts of the ridge (Figures 4.5a and b). For the southern part the mean calculated water depth, 3.52 km is in agreement with observed water depth of 3.5 km and the estimated density of 2.5 gm/cc is less than the density of normal oceanic crust. Estimated water depth (2.7 km) and density (2.75 gm/cc) for the northern part are comparable with the observed water depth of 2.6 km and density of normal oceanic crust.

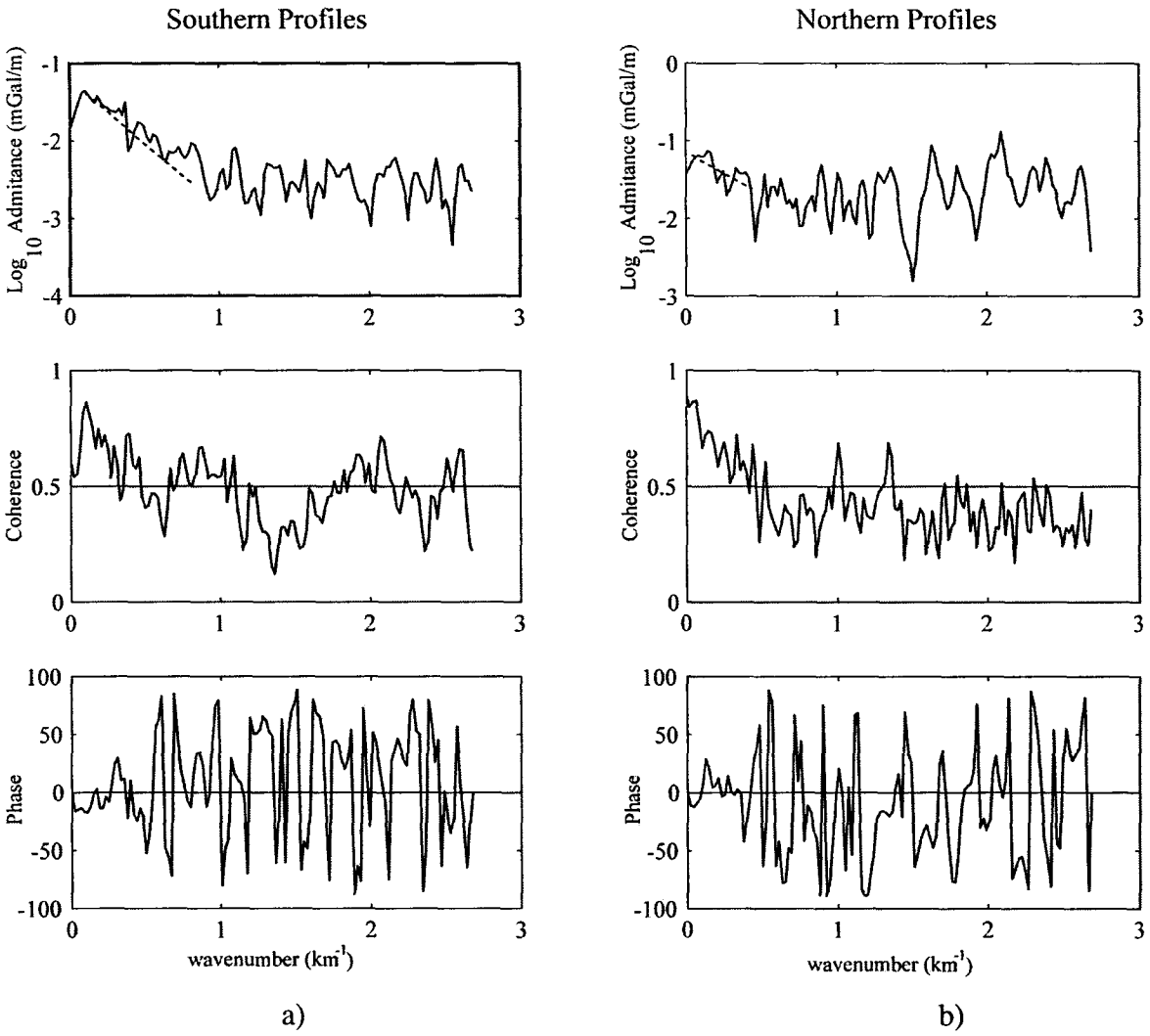


**Figure 4.5a and b** Admittance, coherence and phase in degree generated from a) southern and b) northern set profiles. The dashed line represents the best fit to the observed admittance

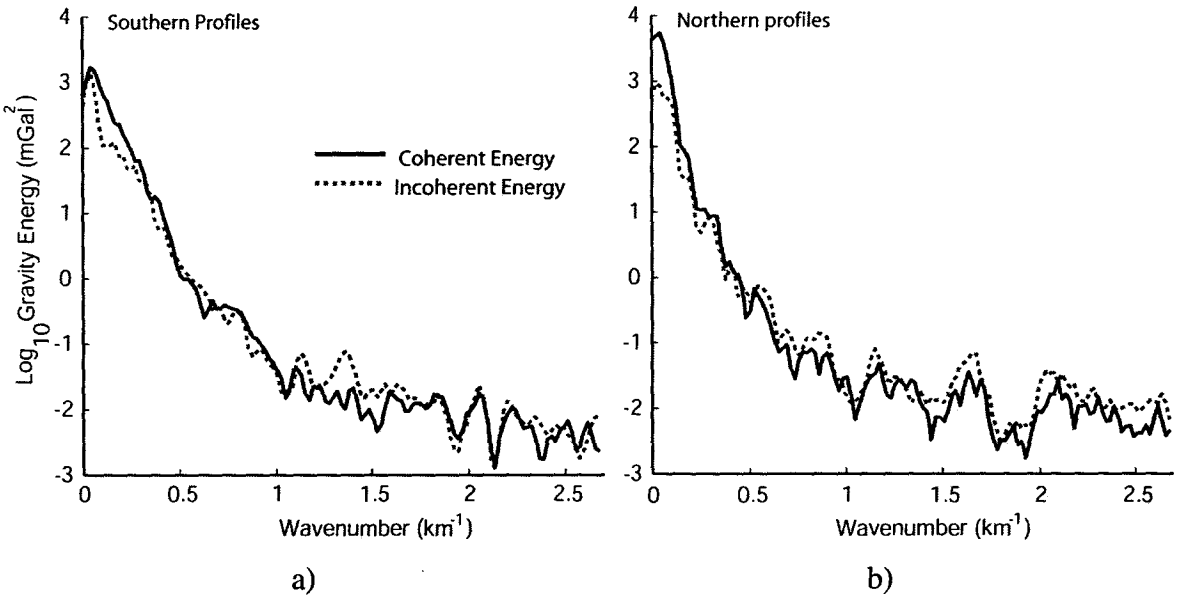


**Figure 4.6a and b** The gravity energy generated from a) southern and b) northern profiles.

Theoretical admittance values and observed admittance values with standard error bars are shown in Figures 4.7a and b. Root Mean Square (RMS) errors between the observed and theoretical admittance for different t and $T_e$ values are also presented (Figures 4.7a and b). Both RMS error and error bounds in the admittance calculation are considered as the criteria for choosing the best fit Te and t. Admittance values calculated for southern part of the ridge (Figure 4.7a) are suitable for Airy model of isostatic compensation with a crustal thickness (t) of 15-20 km and for flexural model with $T_e$ value of ~3 km. The observed admittance for the northern part of the ridge is too high to be explained by the Airy model compensation. Crustal thickness of about 40 km is required for explaining the observed admittance, which is very unlikely to be beneath the ridge. On the other hand a simple flexural model with Te value of ~15 km is reasonably in agreement with the observed admittance (Figure 4.7b). Earlier, Shena et al., 2007 have estimated Te value of 10 km beneath the Comorin Ridge with the consideration of whole Comorin Ridge and a part of the continental shelf of the southern continental margin of the India as a single block.

### 4.5.2 Te and Age of Emplacement of the Comorin Ridge

Watts (1978) proposed that the elastic plate thickness of seamount chains depends on age and temperature gradient of the lithosphere at the time of loading. Further, he has postulated that the elastic plate thickness roughly corresponds to 450±150°C isotherm of the cooling plate model. Therefore, seamounts with low Te values are considered to be emplaced on younger oceanic crust and those with higher Te values on relatively older oceanic crust. Calmant and Cazenave (1987) estimated Te values over the Pacific, Atlantic and Indian Oceans and proposed a simple empirical relationship between Te and age of the oceanic crust (million years) at the time of loading is given as

$$Te = (2.7 \pm 0.15)\sqrt{\Delta t} \qquad \ldots (4.1)$$

The results derived from the above empirical relation suggest that the southern part of the Comorin Ridge (Te = 3 km) was emplaced on young oceanic crust of 2 to 3 Myr old, whereas the northern part of the ridge (Te = 15 km) might have emplaced on an oceanic

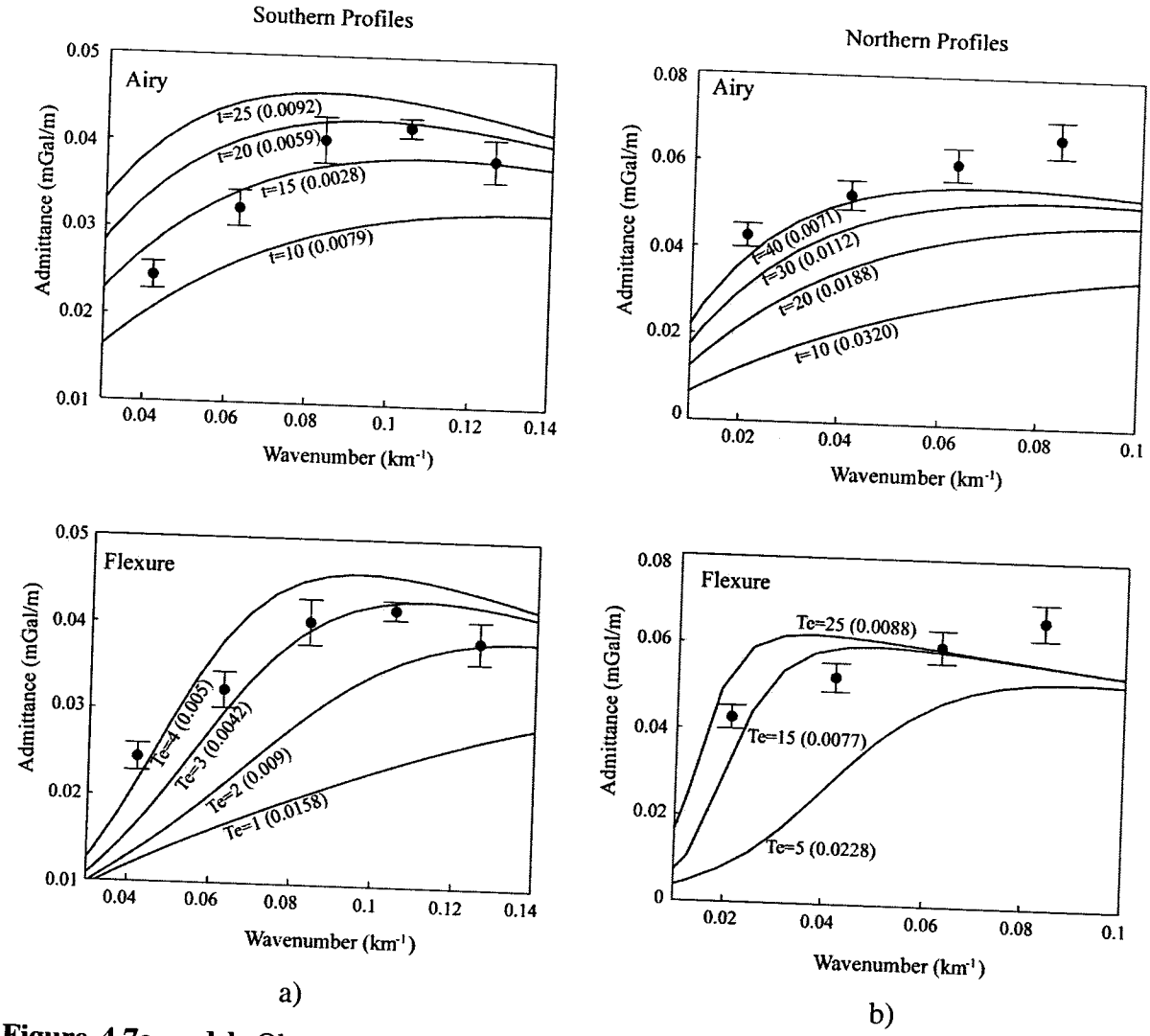


**Figure 4.7a and b** Observed admittance (solid dots) with standard error bars generated from a) southern and b) northern set profiles plotted with theoretical models based on Airy and Flexure models. The RMS error in mGal/m between the observed and theoretical admittance for various t and Te values are shown in bracket.

crust of ~30 Myr. To explain this age difference, extremely slow spreading rates during the emplacement of the ridge are required to be considered. Alternatively, the higher Te value for the northern part of the ridge could be explained by emplacement on altered/ stretched continental crust. Two-dimensional gravity forward modeling is also carried out to obtain the crustal architecture of the Comorin Ridge, and the results are described in the following section.

## 4.6 Crustal structure of the Comorin Ridge- Two-Dimensional Gravity Forward Modeling

Two gravity anomaly profiles, C1215 from southern part and V3307 from northern part of the Comorin Ridge (Figure 4.1) have been chosen to determine the crustal structure using two-dimensional forward modeling technique. These profiles were selected as the admittance results broadly suggested that the ridge was emplaced in two geological settings: southern part of the ridge was formed on weak oceanic crust and the northern part was formed either on old oceanic crust or altered/ stretched continental crust. Sediment layer and oceanic crust layers (2 and 3) thicknesses are considered from sediment isopach map of Kahle et al. (1981) and seismic refraction results of equatorial region published by Bull and Scrutton (1990) and Neprochnov and Gopala Rao et al. (1998), respectively as initial model parameters. The crustal layers are refined moderately to determine the crustal structure of the Comorin Ridge. Seismic velocities obtained from the refraction studies of the equatorial region, 1°S - 2°N (Bull and Scrutton, 1990; Neprochnov and Gopala Rao et al., 1998) were utilized to determine the densities for oceanic crustal layers, whereas for densities of continental crust, seismic velocity results of western continental margin of India (Naini and Talwani, 1983) were consireded. Then these velocities were converted to densities following the velocity-density relationship of Christensen (1977).

### 4.6.1 Crustal Structure of the Southern Comorin Ridge

The gravity model results along profile C1215 reveal that the crust beneath the southern part of the Comorin Ridge is ~17 km thick, consisting of 2 km thick volcanic rocks, 6 km thick oceanic crust and 9 km thick underplated magmatic rocks (Figure 4.8). The crust

beneath the ridge is comparatively thicker than average oceanic crust thickness (7-8 km) lying west of the ridge and nearly equals the thickness of continental crust extending from the southwest of Sri Lanka. The continental crust off southwest of Sri Lanka terminates at eastern flank of the Comorin Ridge, revealing that the ridge was basically emplaced on the oceanic crust lying adjacent to the continental crust. A small flexure to the magnitude of up to 1 km is observed at interfaces within the crust. Beneath other geological features of the Indian Ocean such as Ninetyeast Ridge and Afanasy Nikitin seamount, thick anomalous crustal structures including volcanic and magmatic rocks were determined (Krishna et al., 2001b; Krishna, 2003) and they are comparable with the results of crustal structure of the southern part of the Comorin Ridge.

### 4.6.2 Crustal Structure of the Northern Comorin Ridge

An attempt has been made to model the gravity anomalies of the profile V3307 running across the northern part of the Comorin Ridge, with two types of crust (continental or old oceanic) to determine the nature of crust beneath the ridge (Figures 4.9 and 4.10). In the first computation the underneath crust was assumed as continental and could achieve a reasonably good fit between observed and computed gravity anomalies (Figure 4.9). The crustal structure indicates that the northern part of the ridge was emplaced on continental crust with a crustal thickness of about 18 km. About 3 km thick volcanic rocks are determined on top of the crust, which had eventually contributed to flexure the crustal layers and Moho boundary with a magnitude of about 3 km (Figure 4.9).

In second computation the underneath crust is assumed as old oceanic crust with the consideration of similar geometry for upper/ lower crust and Moho interfaces obtained in the earlier model, but with greater densities and reduced thickness of crustal layers (Figure 4.10). Even with this consideration, a reasonable fit with a crustal thickness of about 13 km beneath the ridge is obtained, but towards east, crust thickness increases up to 20 km (Figure 4.10). This crustal model has two difficulties for acceptance: 1. it is difficult to consider such over thick oceanic crust beneath the northern part of the ridge against usual thickness of 7 km oceanic crust, and 2. high Te value of about 15 km and oceanic crust age of about 30 m.y. (determined from Te value) at the time of volcanic emplacement are not

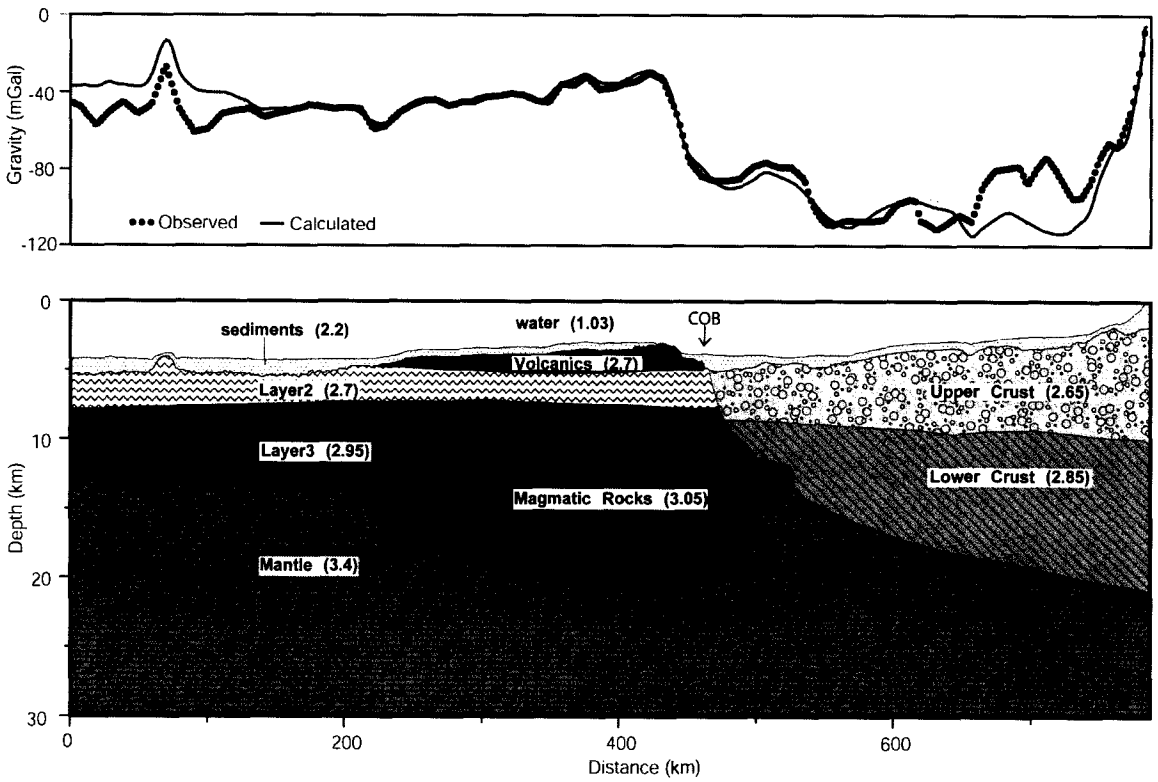


**Figure 4.8** Two-dimensional gravity model with interpreted crustal structure along profile C1215. Numerical values within brackets indicate the densities (gm/cc) of different strata.

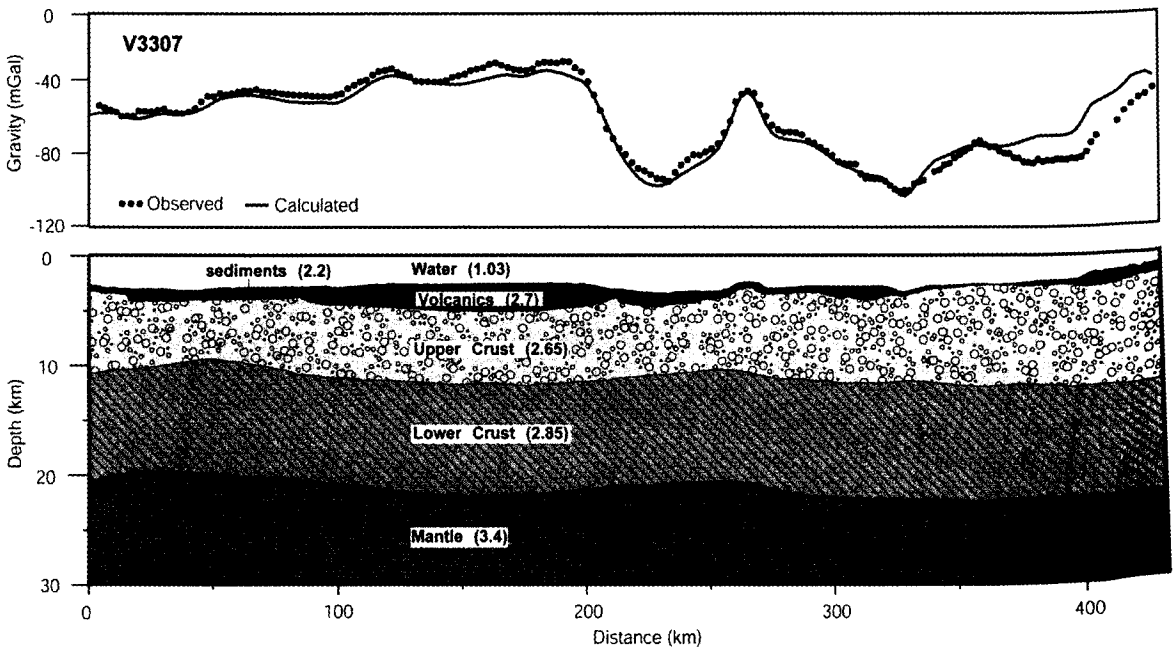


**Figure 4.9** Two-dimensional gravity model with interpreted crustal structure along profile V3307 considering that the underneath crust is continental.

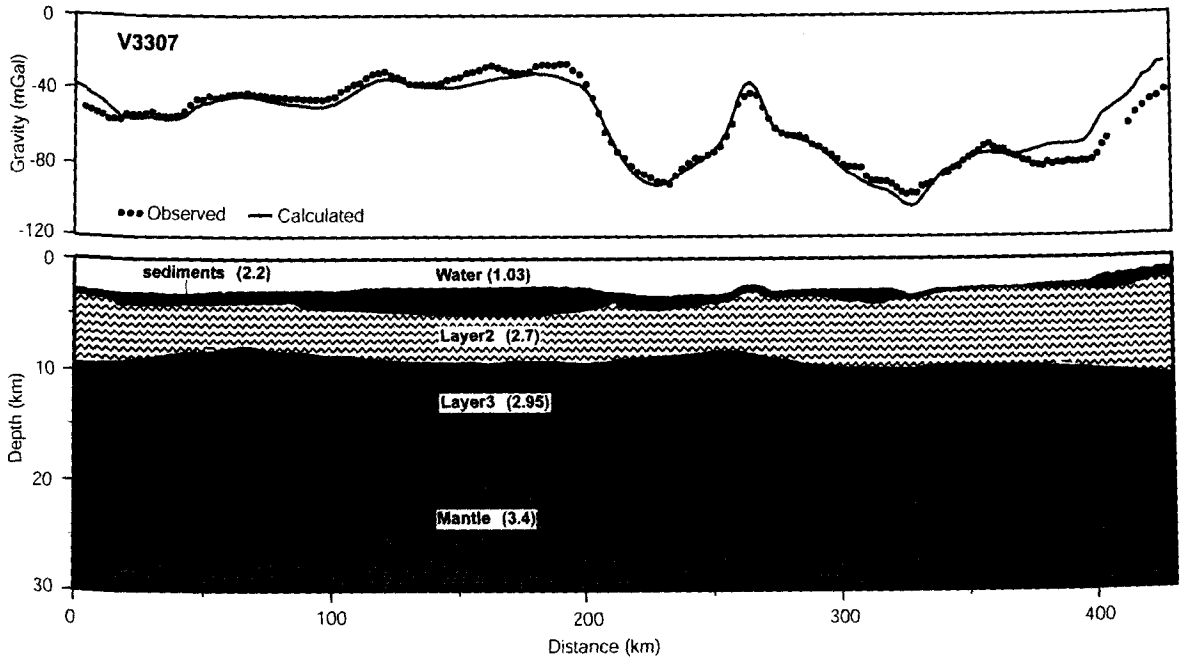


**Figure 4.10** Two-dimensional gravity model with interpreted crustal structure along profile V3307 considering that the underneath crust is oceanic.

in accordance with the plate motion data particularly with reference to the evolution of the southern part of the ridge.

## 4.7 Continent-Ocean Boundary on Western Margin of Sri Lanka and Southern Tip of India

Demarcation of Continent-Ocean Boundary (COB) along the continental margins, in general, provides useful geological information for understanding the evolution of basins, ridges, etc., lying in the vicinity of margins or seaward. The boundary and associated geophysical signatures may further useful for the better understanding of how continental margin segments split from its conjugate margin segments, whether those were in transform motion before they drifted away or in rift phase for longer periods. A steep scarp on seafloor topography and rapid decrease in gravity anomaly are, in general, observed with variable amplitudes on eastern edge of the Comorin Ridge (Figure 4.3). The 79°E FZ in the central Indian Ocean, south of the present study area possess a distinct step-like structure with rapid increase in water depths by about 0.3 km and sudden fall in gravity anomalies by about 20 mGal on east side of the FZ (Kamesh Raju et al., 1993). Keeping these signatures in view, the northward continuity of the 79°E FZ on profiles C1708-a and CH100L06 (Figures 4.1 and 4.3) are mapped. Further north along profiles C1215, V2902-b, V3406 and DME07 steep scarp of about 1.2 km on east side of the ridge is seen associated with lateral shift of ~50 mGal in regional gravity field. But no significant magnetic anomaly is seen coinciding with the steep scarp of the seafloor topography and lateral shift of the gravity field as the oceanic crust of the study area may have evolved during the long interval of Cretaceous Magnetic Quiet Period. The shift in regional gravity field may be interpreted due to the presence of high-density oceanic rocks beneath the volcanic rocks of the Comorin Ridge (Figure 4.8) between latitudes 3.5°N and 5°N. Earlier, following the same criterion of lateral shift in gravity field, Chaubey et al. (2002) ıd Krishna et al. (2006) have demarcated the COB on west of the Laccadive Ridge and xmi Ridge, respectively. On close observation, it is observed that the amplitude of th ·ty anomaly along the eastern edge of the Comorin Ridge varies from ~55 mGal in tl part between 3.5°N and 5°N to ~65 mGal in the northern part between 5°N to 6° 'he depth to the seafloor is nearly constant (~0.9 km). The gravity anomaly

northern part is independently controlled by the undulations of seafloor topography, whereas in the central part the anomaly is contributed by multiple sources such as seafloor undulation and geometry between the Moho, lower crust and magmatic body at deeper depth. In other words the northern part of the ridge was emplaced on rigid continental lithosphere and the central part was evolved nearly in the vicinity of continent-ocean adjoining region, hence the gravity anomaly of the central part of the ridge is isostatically compensated.

From Admittance and gravity forward modeling studies it is found that continental crust lies below the northern part of the Comorin Ridge (north of 5°N latitude), allowing COB to run across the strike of the ridge. The boundary permits the northern part of the ridge on continent and southern part on oceanic crust. Earlier Kahle et al. (1981) have related the eastern edge of the Comorin Ridge to the place of significant change in crustal structure, which they have cautiously attributed to the boundary between oceanic crust on the seaward side and rifted or altered continental crust on the landward side.

The COB and associated magnetic and gravity anomalies of the present study area are compared with that of eastern and western margins of India (Gopala Rao et al., 1997; Krishna et al., 2006) (Figure 4.11), with a view to discussing the possible geological processes associated with COB evolution (Figure 4.11). On eastern margin of India the COB was located at about 70-80 km seaward of the shelf edge, whereas on western margin of India the COB was placed along the west of the Laxmi Ridge about 400 km away from the shelf edge. In the present study area, it is inferred that the COB lies about 250 km off southwest of Sri Lanka and about 300 km off southern tip of India (Figure 4.11). The gravity signature having a lateral shift in regional field is seen associated with the COB on both western margins of India and Sri Lanka, while on the eastern margin of India the COB associates with a different gravity signature of high-amplitude, short-wavelength negative gravity anomaly that rapidly changes to low-amplitude broad regional anomaly (Gopala Rao et al., 1997; Subrahmanyam et al., 2001; Krishna et al., 2009a). South of Sri Lanka, the COB has been placed about 250 km away from the coastline following the changes in regional trend of the gravity field on profiles (V3616 and V1909 in Figure 4.3)

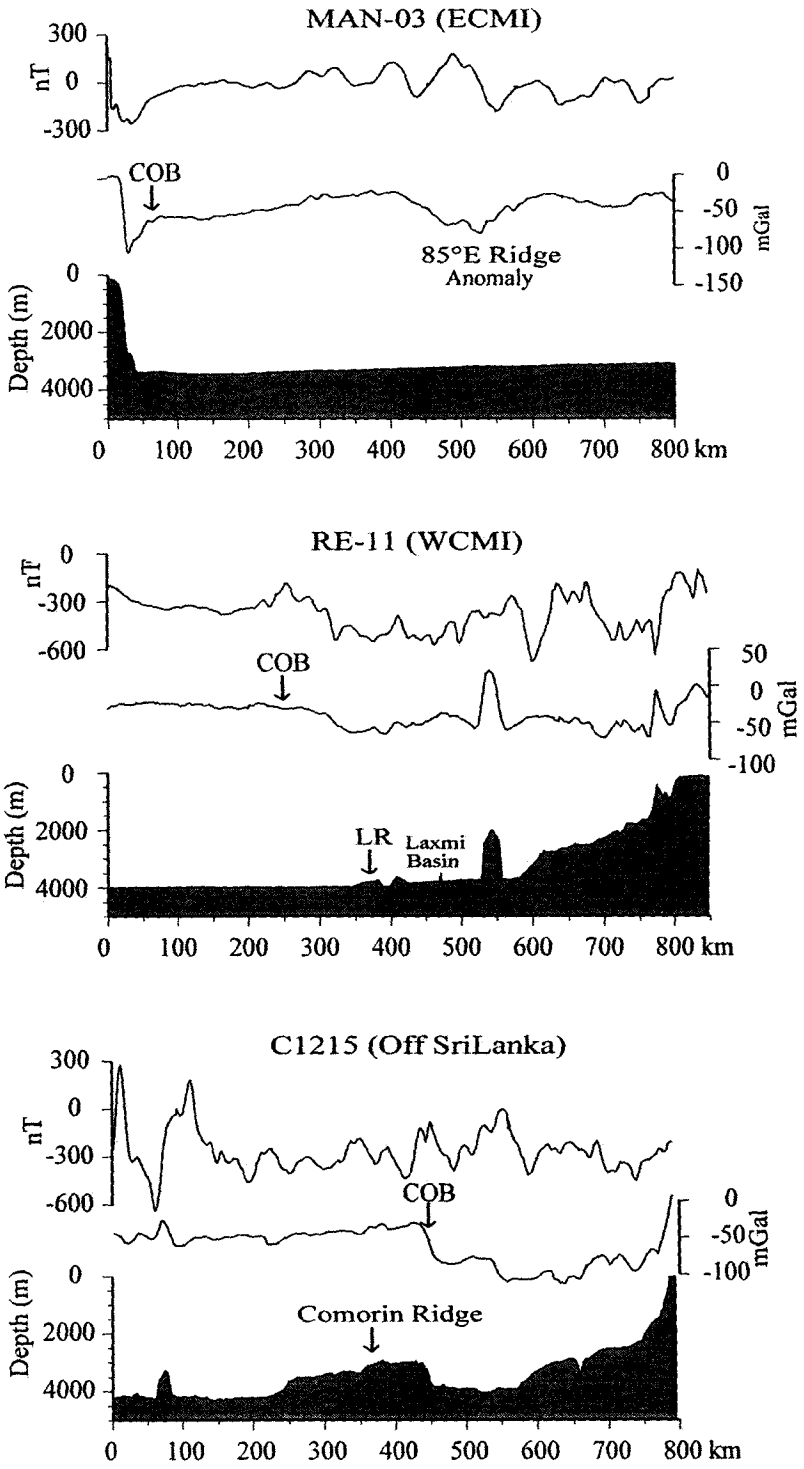


**Figure 4.11** A comparison of bathymetry, gravity and magnetic profile data from western continental margin of India (WCMI), eastern continental margin of India (ECMI) and western margin of Sri Lanka. The diagnostic character of regional shift in gravity anomaly for demarcation of COB is observed in western margin of Sri Lanka and WCMI

as well as in satellite gravity image (Figure 4.12). The boundary is tentatively indicated, but needs to be confirmed by other geophysical results. Off Kron Prinz Olav Kyst and Gunnerus Ridge region, east Antarctica (believed to be conjugate part of Sri Lanka), Stagg et al., (2004) have marked the COB within the Enderby Basin, which is about 250 km away from the coastline and lying in water depths of around 4000 m. Thus the COB on southwest and southern parts of Sri Lanka and their conjugate region, off east Antarctica has evolved approximately in similar geological processes.

## 4.8 Tectonics and Evolution of the Comorin Ridge

The geophysical results obtained from admittance analysis and gravity modeling are explained in light of the tectonic history of the Indian Ocean in order to put forward a plausible geological mechanism for the evolution of the Comorin Ridge. Airy isostatic model beneath the southern part of the ridge, proximity of seafloor spreading anomaly 34 between 77.5°E FZ and 79°E FZ and plate kinematic models suggest that the ridge was formed during the late Cretaceous period. Volcanic rocks, erupted during the late Cretaceous were found on the southwest coast of India (Radhakrishna et al., 1994; Anil Kumar et al., 2001) and southeast of Madagascar (Storey et al., 1995; Torsvik et al. 1998 and 2000) and the rocks were considered as products of the Marion hotspot formed during the rift stage of western margin of India from Madagascar. Earlier investigations: plate motions relative to the Indian Ocean hotspots (Müller et al., 1993), plate reconstructions (Storey et al., 1995; Torsvik et al., 2000) and sub-marine morphological structures of India and Madagascar (Yatheesh et al., 2006) suggest that the breakup between Madagascar and India has occurred at around 90 Ma. The probable location of the Marion hotspot with reference to the continental masses of India, Madagascar, Seychelles and Africa for the late Cretaceous period, just prior to the emplacement of the Comorin Ridge is shown in Figure 4.13 (Torsvik et al., 2000). Keeping these inferences and present geophysical results in view, it is proposed that the Comorin Ridge may have been emplaced by the Marion hotspot volcanic activity in a span of about 6 m.y. from north (88-90 Ma) to south (82-84 Ma).

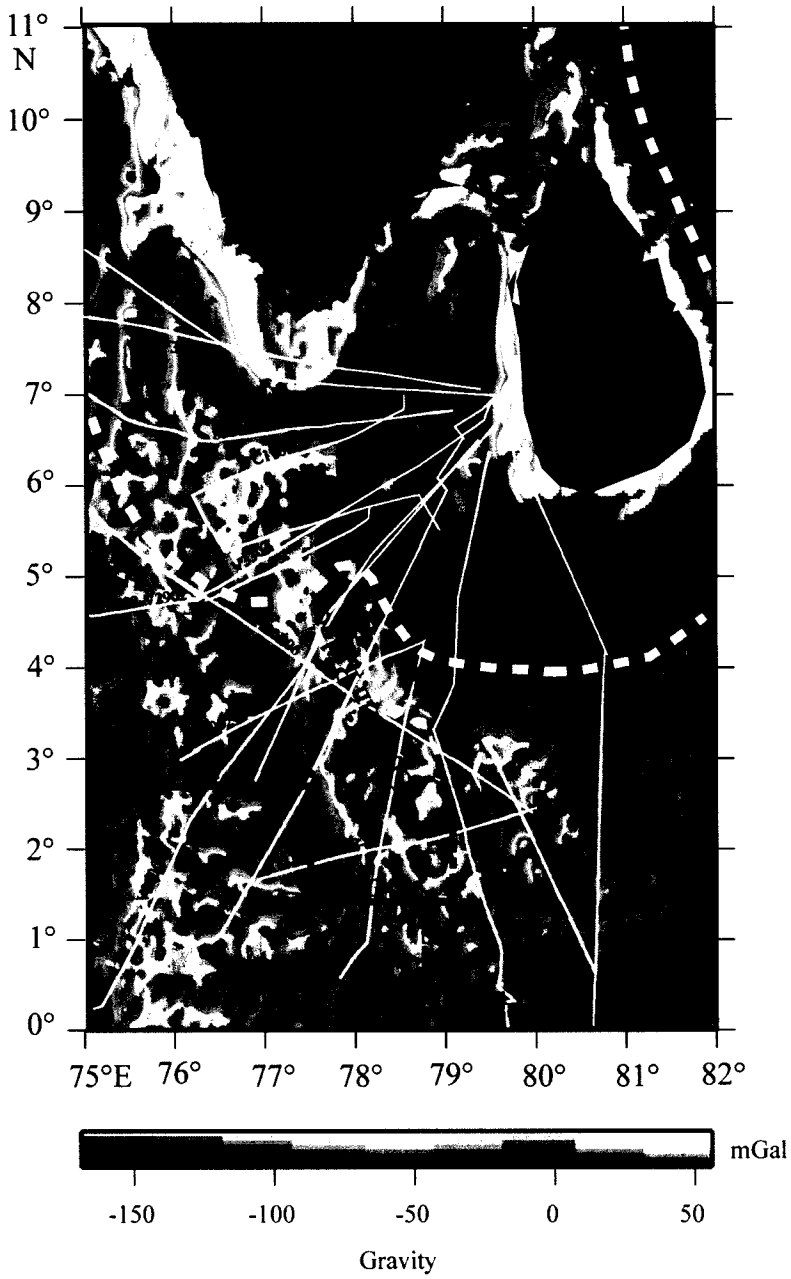


**Figure 4.12** Interpreted COB on western margin of Sri Lanka and southern tip of India, geophysical profiles used in this study, fracture zones and magnetic lineation A34 are superimposed on satellite gravity field (Sandwell and Smith, 1997). Eastern margin of Comorin Ridge is bounded by different tectonic elements.

Te value (about 15 km) beneath the northern part of the Comorin Ridge suggests that the ridge was emplaced either on approximately 30 m.y. old oceanic crust or on rifted/ altered continental crust, whereas the southern part of the ridge was emplaced on 2-3 m.y. old oceanic crust (Te=3 km). It is difficult to reconcile the presence of old oceanic crust beneath the northern part of the ridge as the age spans for the formation of the oceanic crust from north to south beneath the ridge (about 28 m.y.) and for emplacement of the ridge by the Marion hotspot (about 6 m.y.) are not in accordance with the plate motion data with reference to Indian the Ocean hotspots. Therefore, probably the northern part of the Comorin Ridge was emplaced on rifted continental crust. The gravity model studies across the northern part of the ridge (along profile V3307) also suggest the continental nature of the crust beneath this part of the ridge (Figure 4.9).

Geophysical profiles: C1215, V292b, V3406 and DME 07, across the Comorin Ridge show a distinct character of steep downward-scarp on eastern flank of the ridge. The geophysical signatures such as steep seafloor topography and lateral shift in regional gravity field (Figures 4.3 and 4.8) allow to place the Continent-Ocean Boundary on east side of the central part of the ridge (Figure 4.12). The east side of the ridge (entire) is controlled by different tectonic elements, southernmost part (up to 3.5°N) by the 79°E FZ, central part (3.5°N to 5°N) by the COB and northernmost part by the termination of the Gulf of Mannar Basin (Figure 4.12). From geophysical signatures it can be interpreted that continental crust extends on western margin of Sri Lanka up to east side of the ridge and off the southern tip of India up to 5°N latitude, which includes northernmost part of the ridge (Figure 4.12). Model studies of gravity anomalies suggest that about 21 km thick continental crust lies on the western margin of Sri Lanka that is relatively thinner than the normal continental crust. This thin continental crust may have evolved due to the crustal stretching during the rift processes that took place between Sri Lanka and the Gunnerus Ridge part of east Antarctica (Rotstein et al., 2001; Kent et al., 2002) and between India and Madagascar (Storey et al., 1995; Torsvik et al., 2000). Demarcation of the COB on the western margin of Sri Lanka (Figure 4.12) may provide new constraints on the nature of the crust beneath the Gulf of Mannar Basin. Western part of the Greater India (India-Madagascar-Seychelles) had experienced continental rifts several times in the geological

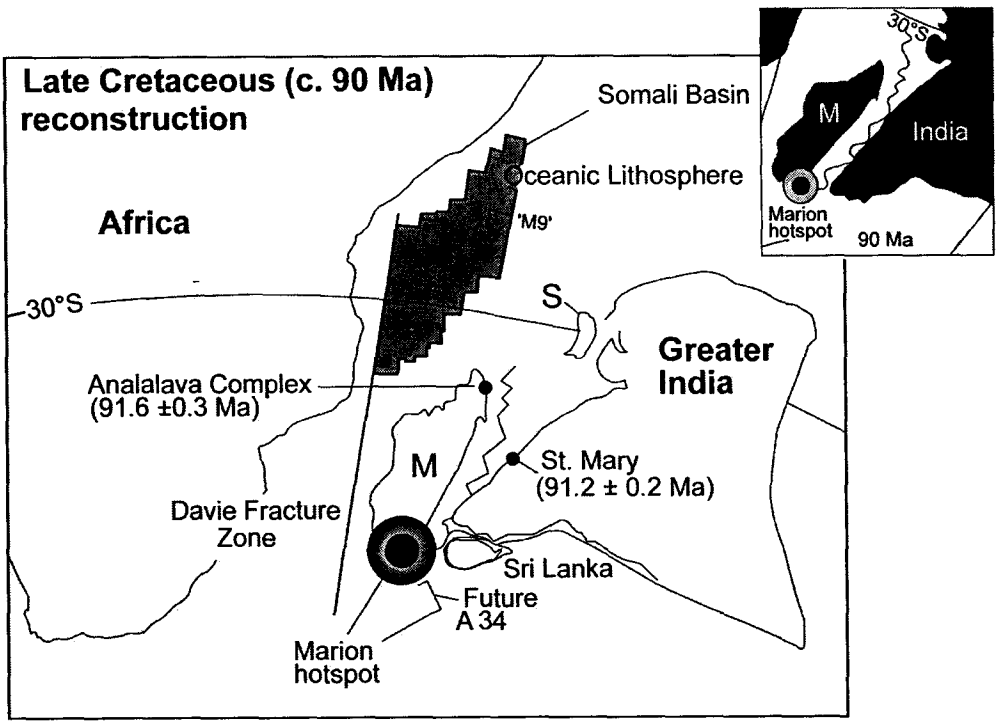


**Figure 4.13** Late Cretaceous reconstruction of India, Madagascar (M), Seychelles (S) and Africa with reference to the Marion hot spot position before emplacement of the Comorin Ridge, reproduced from Torsvik et al. (2000).

past; thereby new basins have formed on continent as well as in offshore regions of western India (Krishna et al., 2006). The stretching process that eventually led to continental splitting contributed to the evolution of rifted basins both on western and eastern margins of India. The basins underlined by thin continental crust did not extend further for continental break-ups. For example Cambay and Kutch rifts on western India (Raval and Veeraswamy, 2003b) and Laxmi Basin on western margin of India (Krishna et al., 2006) have remained as failed rifts due to some changes in geological settings. On the basis of subsidence rates, particularly higher rates during the Neogene, in the Gulf of Mannar Basin and folded and uplifted Bengal Deep-Sea Fan sediments off the SSE continental margin of Sri Lanka, Curray (1984) has suggested a possible continuation of continental stretching in the basin. The stretching process between India and Sri Lanka may have contributed to the initiation of basin in Gulf of Mannar and the basin appears to be widening due to the continuing process of stretching. Hence, probably the basin in the Gulf of Mannar had evolved by extensional tectonics, but underlained by relatively thin continental crust.

On comparison of geophysical signatures of COB obtained from the present study area with those from western margin of India (Krishna et al., 2006) and eastern margin of India (Gopala Rao et al., 1997), it appears that western margins of India and Sri Lanka have rifted margin character and eastern margin of India, south of 15°N latitude has transform-rift character. These observations are supported by earlier results obtained from admittance analysis of bathymetry and gravity data of conjugate margins of southeastern margin of India and Enderby Land of Antarctica (low elastic plate thickness of less than 5 km) (Chand et al., 2001; Subrahmanyam and Chand 2006) and conjugate margins of India and Madagascar (Te values ranging from 8-15 km) (Chand and Subrahmanyam 2003).

# CHAPTER 5

## The 85°E Ridge – Study of Crustal Structure, Isostasy and Negative Gravity Anomaly using Process Oriented Gravity Modeling

# The 85°E Ridge – Study of Crustal Structure, Isostasy and Negative Gravity Anomaly using Process Oriented Gravity Modeling

## 5.1 Introduction

The 85°E Ridge extends from the Mahanadi Basin in the north to the Afanasy Nikitin seamount (ANS) in the south, is a prominent aseismic ridge in the northeastern Indian Ocean (Figure 5.1). The northern part of the ridge (north of 5°N) is buried under thick Bengal Fan sediments, whereas in the south, its structure occasionally rises above the seafloor (Curray et al., 1982; Liu et al., 1982; Curray and Munasinghe, 1991; Müller et al., 1993; Gopala Rao et al., 1997; Subrahmanyam et al., 1999; Krishna, 2003; Krishna et al., 2011a). At around 5°N, southeast of Sri Lanka, a westward shift of 250 km exists, which is not observed along other major hotspot related tracks in the Indian Ocean such as the Ninetyeast and Chagos-Laccadive ridges .

Origin of the 85°E Ridge is enigmatic due to its characteristic negative gravity anomaly and complex magnetic anomaly signatures. Curray and Munasinghe (1991) were the first researchers to postulate that the Rajmahal Traps in the Bengal Basin, 85°E Ridge and ANS form the trace of the Crozet hotspot. However, geochemical results of lava samples of the ANS do not show affinity to the Crozet hotspot volcanism (Mahoney et al., 1996). Though many subsequent researchers favored the hotspot origin for the emplacement of the ridge (Müeller et al., 1993; Gopala Rao et al., 1997; Subrahmanyam et al., 1999; Krishna, 2003), the source of the hotspot volcanism remains speculative. Alternatively, formation of the ridge due to shearing or sagging of crust by horizontal stretching/ compressional forces has also been proposed (Ramana et al, 1997; Anand et al., 2009). Following the analogy of negative gravity signature of the Laxmi Ridge in the Arabian Sea and its continental sliver interpretation (Naini and Talwani 1983; Talwani and Reif 1998; Krishna et al., 2006), it is also possible to think in the direction of continental origin to the 85°E Ridge. This possibility has numerous difficulties for explaining the other aspects: 1. The trend of the 85°E Ridge is not parallel to the configuration of the Eastern Continental Margin of India

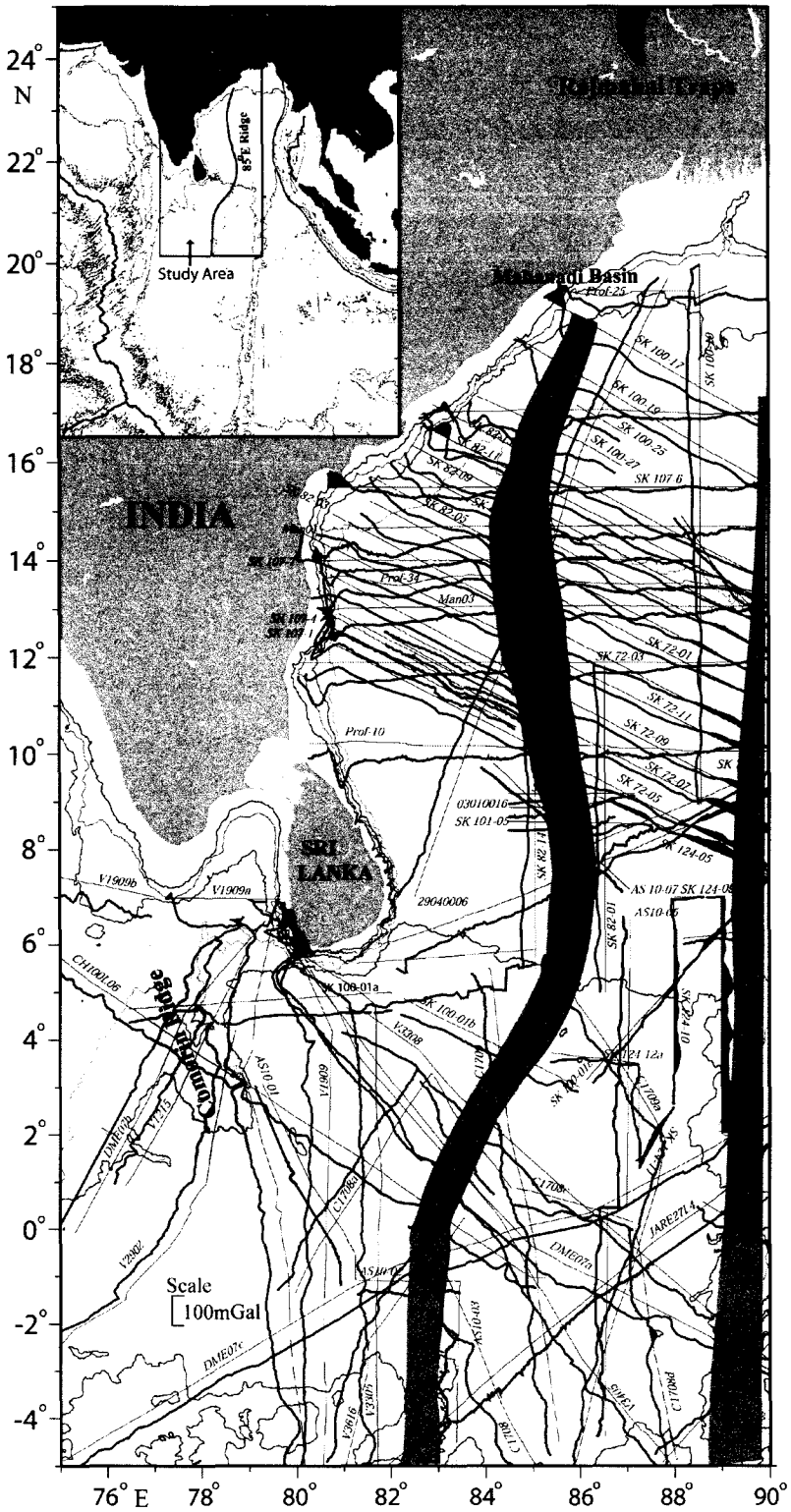


**Figure 5.1** Ship-borne gravity profiles in the 85°E ridge and adjoining areas of the NE Indian Ocean. Free-air gravity anomalies (thick black lines) plotted at right angle to the ship tracks. General bathymetry of the Bay of Bengal is from GEBCO.

(ECMI) and to the identified Continent-Ocean Boundary along the ECMI, 2. The oceanic crust in the Western Basin between ECMI and 85°E Ridge does not provide any evidences for the presence of conjugate parts of the ocean floor evolved by the spreading process after so-called breakup of the 85°E Ridge from ECMI, 3. The NW-SE trending oceanic fracture zones identified in the Western Basin obliquely cross the 85°E Ridge, and these fractures zones were earlier have interpreted as conjugate parts of the fracture zones evolved in the Enderby Basin (Krishna et al., 2009a), and 4. The breakup history of the Elan Bank from the north ECMI becomes more complex in case of consideration of the 85°E Ridge as a continental sliver.

Liu et al. (1982) have modeled the negative gravity anomaly of the 85°E Ridge with consideration of two stage loading; initially emplacement of the ridge on a weak lithosphere (5-15 m.y) leading to excess thickening of the crust and subsequently loading of sediments on a stronger lithosphere of 40-80 m.y old. This model infers approximately 180 times increase in the flexural rigidity between emplacement and burial. Later, Krishna (2003) proposed an alternative model, in which he explained the negative gravity anomaly as a result of density contrast between the metasedimets and less dense ridge material and a broader Moho depression beneath the ridge. However, the above proposed models lack a clear understanding on the timing of emplacement of the ridge as well as flexural characteristics beneath it. The sources/ mass anomalies that gave rise to the negative gravity anomaly, which otherwise expected to have been positive also needs to be understood and quantified.

The admittance analysis is, in general, used for estimation of flexural rigidity and isostatic response of the geological structures; but in the case of the 85° E Ridge, the technique is unsuccessful because of absence of its topographic expression on the seafloor. Therefore the process-oriented gravity modeling, in which the present-day gravity field of the ridge can be divided into different gravity anomaly components, has been carried out. Thereby, an attempt has been made to determine the elastic plate thickness of the ridge at the time of emplacement and its crustal structure and isostatic compensation mechanism.

## 5.2 Tectonic Setting

It is widely accepted that the Greater India separated from East Antarctica during the early Cretaceous period and subsequently formed the conjugate oceanic regions, Bay of Bengal and Enderby Basin. The Indian landmass had witnessed two continental breakups in early stages of eastern Gondwana splitting. The first breakup occurred with separation of Greater India from Australia and East Antarctica during the Early Cretaceous (Curray et al., 1982; Royer and Coffin, 1992; Gopala Rao et al., 1997; Müller et al., 2000). In second stage the Elan Bank, a submerged micro-continent lies presently on the western margin of the Kerguelen Plateau in the southern Indian Ocean, sundered from the present-day eastern margin of India at about 120 Ma (Gaina et al., 2003, 2007; Borissova et al., 2003; Krishna et al., 2009a). The breakup events and their timings suggest that most part of the oceanic crust in the Bay of Bengal was evolved during the Cretaceous Magnetic Quite Period (120-83 Ma).

During the mid-Cretaceous period a major change in the spreading direction occurred from NNW-SSE to N-S, resulted in northward drift of Indian plate followed by collision with Asian plate during the early Eocene. The Indian plate, during the course of its northward movement, recorded the mantle plume expressions on the Indian Ocean seafloor in the form of linear aseismic ridges. The 85°E Ridge is one of the major aseismic ridges formed in this phase in the northeastern Indian Ocean and subsequently buried under the post-collision Bengal Fan sediments.

## 5.3 Geophysical Data

Multichannel Seismic reflection, gravity and bathymetry data collected on board *MV Sagar Sandhani* (MAN-01 and MAN-03), *ORV Sagar Kanya* (SK107-7) and *RV Issledovatel* (Profile 98791) are used for the model studies. Published seismic refraction results (Naini and Leyden, 1973; Curray, 1994) are used to constrain the densities of various sedimentary layers. Additionally, published seismic reflection data across the ridge (Krishna, 2003; Bastia et al., 2010) are also presented to map the continuity of the 85°E Ridge track.

## 5.4 Seismic Structure and Gravity Anomaly of the 85°E Ridge

The overall trend of the 85°E Ridge is seen in satellite gravity anomaly map shown in Figure 5.2 and also in anomaly wiggles along ship-borne gravity profiles (Figure 5.1). The ridge extends from 19°N to 5°S with variable widths range from 100 to 180 km. The width of the ridge is maximum near 14°N latitude and associated with a deep gravity low of ~80 mGal. Further north, between 15°N and 16.5°N latitudes, the gravity anomaly of the ridge is not significant, but shows its presence again near 17°N latitude and appears to continue up to 19°N in the offshore region of Mahanadi Basin. Using aeromagnetic and marine magnetic data Natyak and Rao (2002) and Subrahmanyam et al. (2008) have traced the continuity of the 85°E Ridge trace in offshore Mahanadi Basin and further to the Chilka Lake. With the use of high-quality seismic reflection data Bastia et al. (2010) have strongly confirmed the presence of ridge structure in the Mahanadi Basin (Figure 5.3a). Northward continuation of the ridge onto the continental slope and shelf tracts of the Eastern Continental Margin is clearly observed in these sections. Towards south between 11°N and 2°N, the ridge track bends in clockwise direction, then appears to continues straight-down to join the Afanasy Nikitin seamount (ANS) (Figures 5.1 and 5.2). Using seismic images of the ridge Krishna (2003) has shown the southward continuity of the 85°E Ridge up to the Afanasy Nikitin seamount (Figure 5.3b). It can be clearly observed that the southern track of the ridge joins with the ANS through isolated buried hills and intervening subsurface structures. Thus, seismic sections and gravity anomaly maps unambiguously shows the continuity of 85°E Ridge from the Mahanadi offshore basin in north to the ANS in south. The prominent negative gravity anomaly associated with the 85°E Ridge in the Bay of Bengal region changes to positive south of 5°N and in further south, the ANS is associated with significant positive gravity anomaly (Figure 5.2).

Four seismic reflection and gravity profiles crossing the 85°E Ridge along 14.7°, 14°, 13° and 4.5°N latitudes (Figures 5.3c and d) are analyzed in detail. The ridge structure in the Bay of Bengal region is completely buried below the Bengal Fan sediments of variable thick. For example, along 14.7°N and 13°N latitudes the ridge is carpeted by about 2.8 and

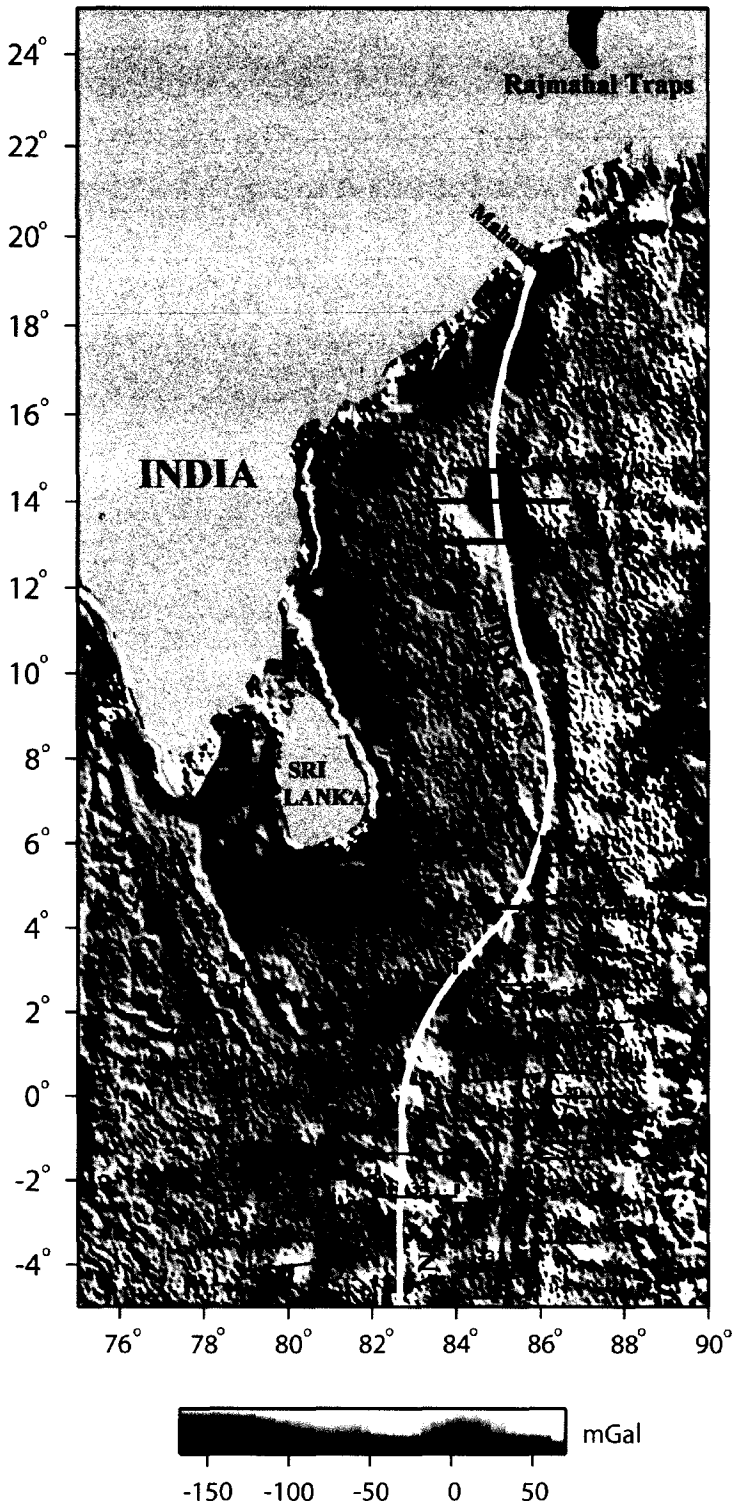


**Figure 5.2** Satellite derived free-air gravity anomaly map (Sandwell and Smith, 1997) of the northeastern Indian Ocean. Locations of 85°E (white line), seismic sections (thick line), magnetic lineations (thin line) and fracture zones (dashed line) are superposed on the map. ANS stands for Afanasy Nikitin seamount.

-1.7 s Two-Way Travel Time (TWT) Bengal Fan sediments (Figures 5.3c and d), respectively, whereas along the 14°N latitude about 0.8 s TWT thick sediment strata overlie the ridge crest. Based on seismic results of the Bay of Bengal, Curray et al. (1982) and Gopala Rao et al. (1997) have divided the entire sediment section into two sedimentary packages and interpreted that the lower package was deposited mainly from the rivers of east coast of India, whereas the upper package was deposited by the Ganges and Brahmmaputra rivers discharges after establishing the contact of the Indian subcontinent with the Asian continent. Further the packages are classified as pre- and post-collision sediments and are separated by an erosional-type unconformity developed in Paleocene age (Figures 5.3c and d) (Moore et al., 1974). The pre-collision sediment package consists of pelagic and terrigeneous sediments deposited prior to the India-Eurasia collision, whereas, the post-collision part mainly consists of Bengal Fan sediments. The 85°E Ridge acts as a structural partition for dividing the thick Bengal Fan into Western and Central basins (Curray et al., 1982).

The subsurface disposition of the ridge is quite variable as can be seen from the seismic sections shown in Figures 5.3c and d. The ridge topography has a steep westward throw and gentle eastward dip along MAN-03 and appears as a double peaked basement rise along SK107-7. Along MAN-01 the relief of the ridge is relatively less and on eastern side the ridge a prominent basement high probably associated with an oceanic fracture zone (Gopala Rao et al., 1997) is observed. Gravity anomaly plots stacked along these sections show that the ridge is associated with a prominent negative gravity anomaly (~50 mGal) flanked by regional gravity highs on either side (Figures 5.3c and d). The wavelength of the negative anomaly is relatively greater than the width of the ridge.

The morphology and gravity signature of the southern part of the ridge structure along profile 98791 at 4.5°N are distinctly different in comparison to the sections of the Bay of Bengal. The ridge structure along the profile 98791 is exposed above seafloor with an elevation of about 0.8 km (Figure 5.3d), but its flanks are buried under 2 to 3 km thick fan sediments. The pre-collision sediments are nearly absent and the thickness of fan sediments are lesser compared to the northern part of the ridge. Along this profile the ridge

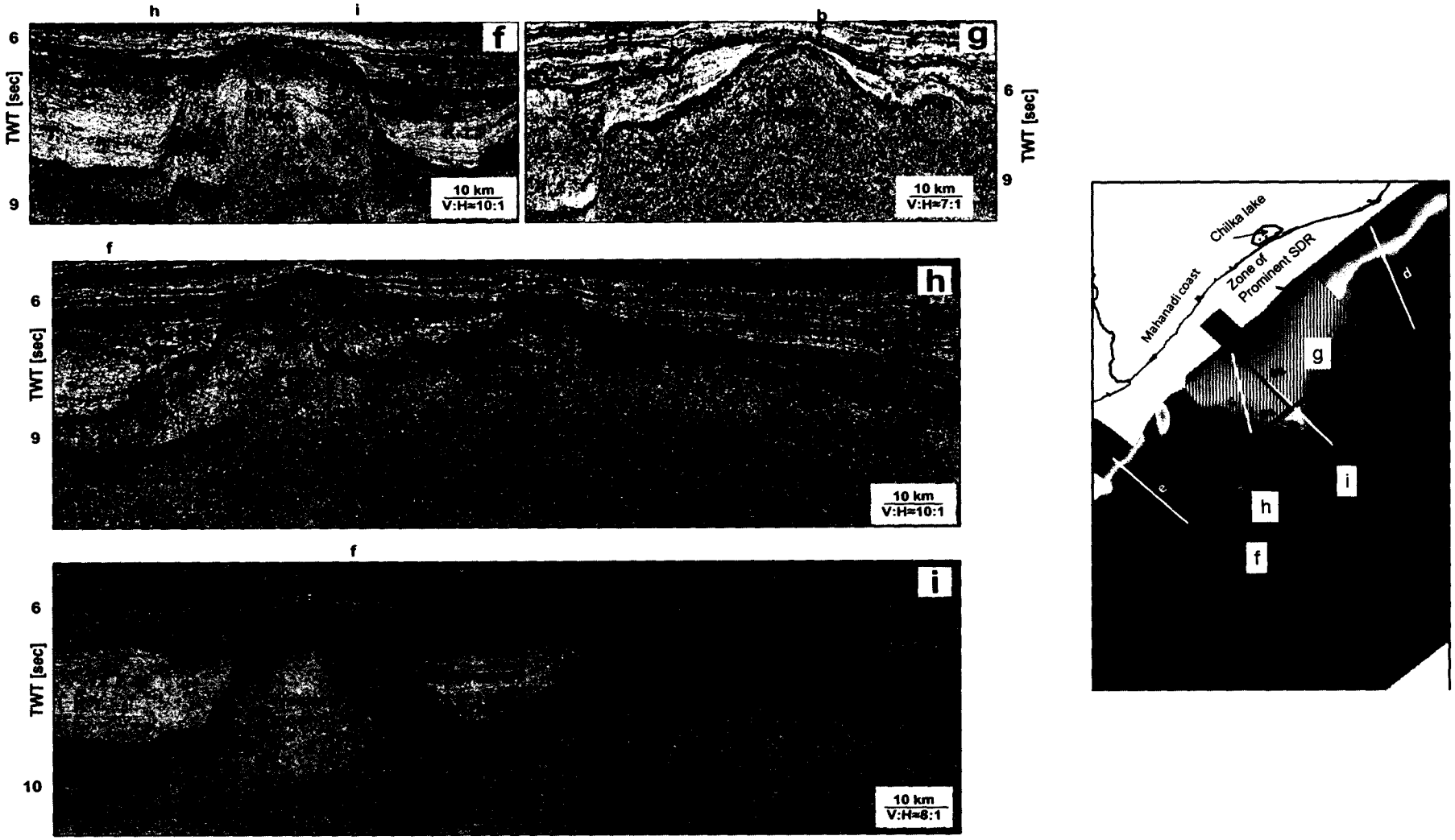


**Figure 5.3a** Seismic reflection sections depicting structure of 85°E Ridge in Mahanadi Offshore Basin (after Bastia et al., 2010)

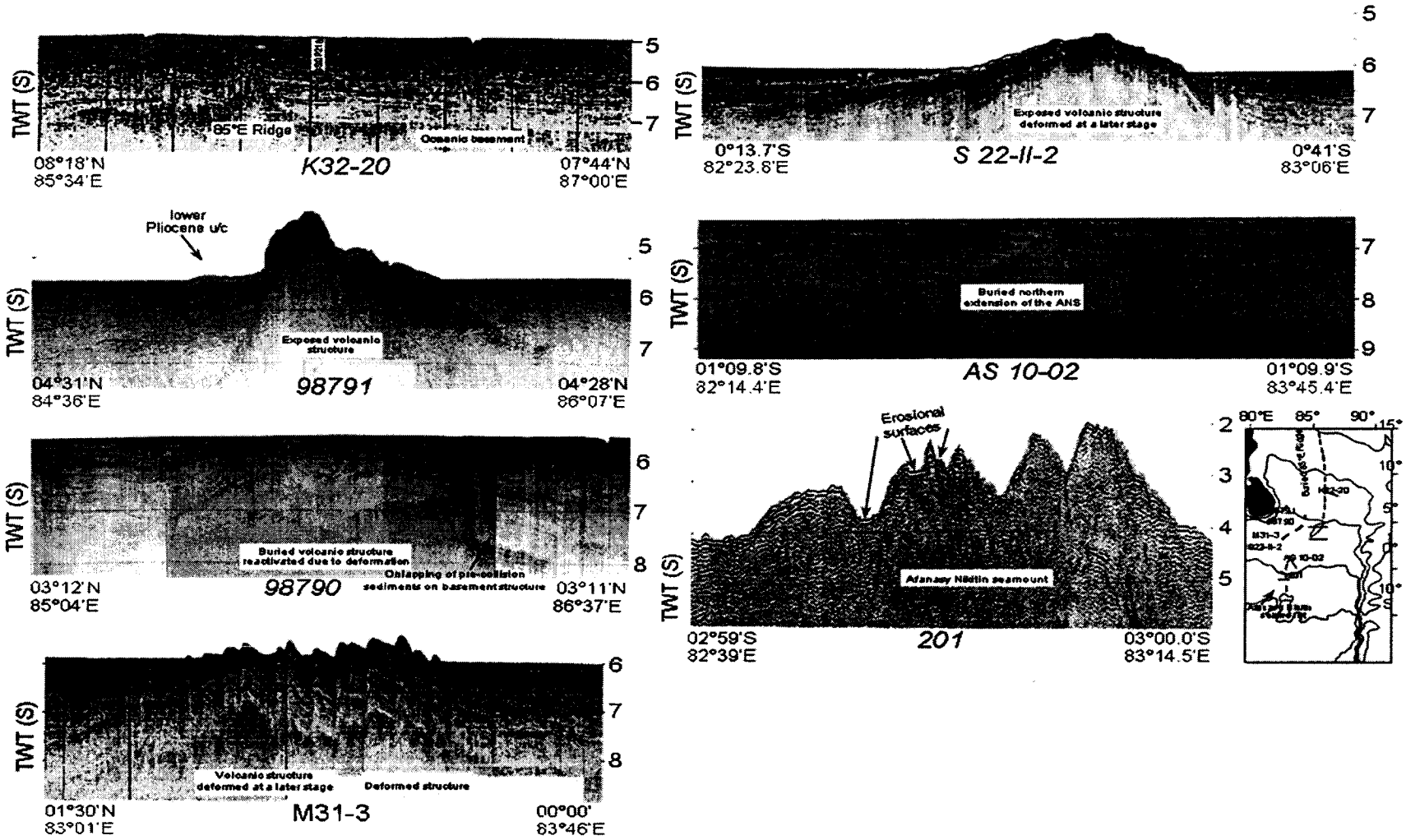


**Figure 5.3b** Seismic reflections sections depicting the structural continuity of the 85°E Ridge from 8°N (profile K-32-20) to ANS (profile 201) through buried hills (profiles S22-II-2, M31-3 and 98791), subsurface structures (profiles AS 10-02 and 98790) (after Krishna, 2003)

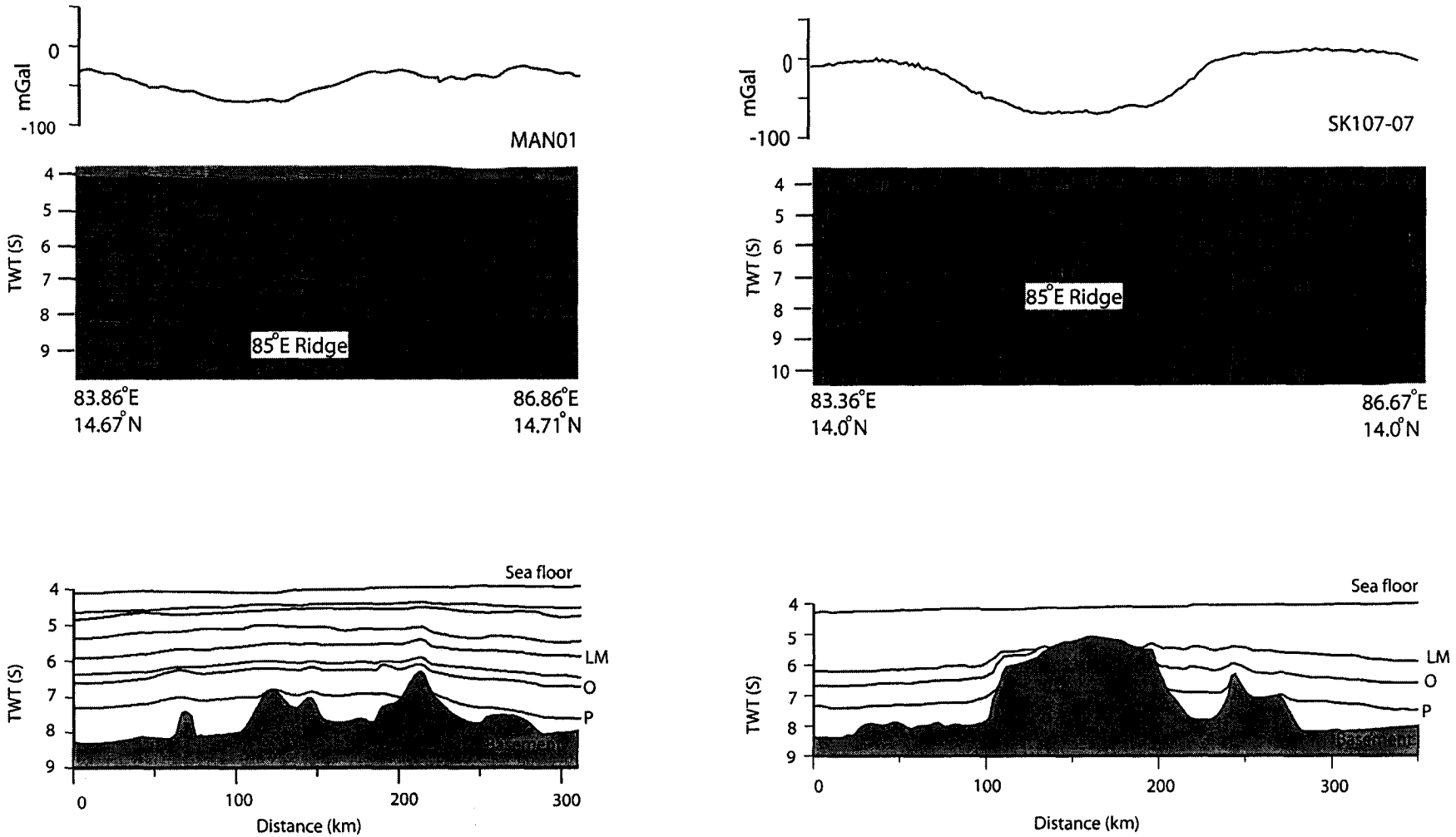


**Figure 5.3c** MAN-01 and SK107-07 seismic reflection sections and its interpreted line diagrams across 85°E Ridge stacked with gravity anomaly data. The buried 85°E ridge and associated negative gravity anomaly is clearly depicted. Paleocene (P), Oligocene (O) and lower Miocene (LM) boundaries are marked.

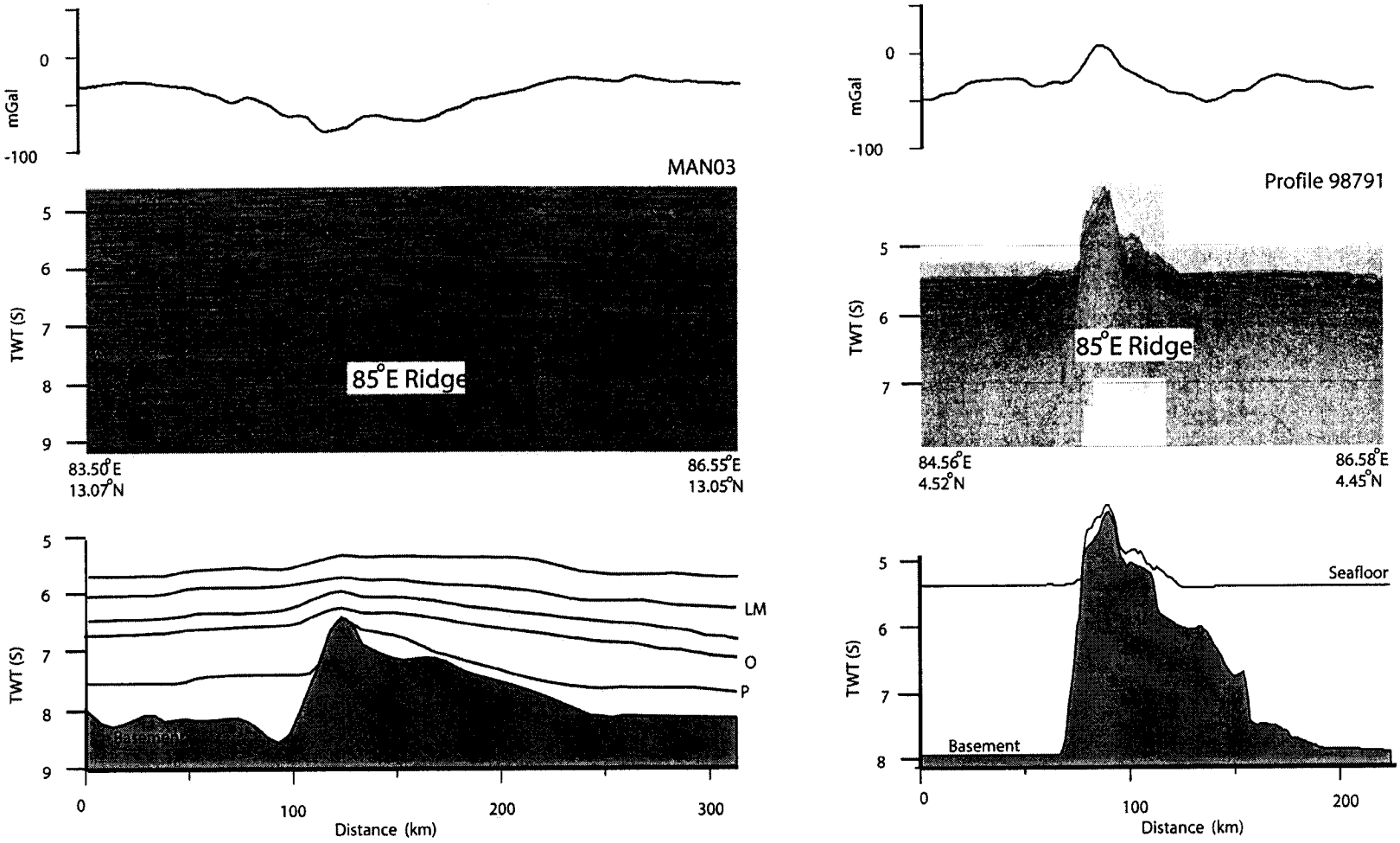


**Figure 5.3d** MAN-03 and 98791 seismic sections and its interpreted line diagrams across 85°E Ridge stacked with gravity anomaly data. The gravity anomaly along profile 98791 is satellite derived (Sandwell and Smith, 1997). Notations in figure are same as given in Figure 5.3a.

is associated with a prominent positive gravity anomaly with amplitude of about 40 mGal. The wavelength of the gravity anomaly along the profile is comparable with the width of the ridge.

## 5.5 Magnetic Response of the 85°E Ridge

The 85°E Ridge is, in general, associated with significant magnetic anomalies compared to the anomalies of the oceanic crust in the Bay of Bengal (Liu et al., 1983; Ramana et al., 1997; Gopala Rao et al., 1997). The overall strength of the magnetization of the 85°E Ridge suggests that the ridge is made of highly magnetized rocks. The asymmetry in the magnetic anomaly is attributed to the phase shift produced by the northward drift of the Indian plate (Liu et al., 1983). Recent compilation of geophysical data over the northeastern Indian Ocean (Krishna et al., 2009a; Michael and Krishna, 2011) revealed alternative stripes of high amplitude positive and negative magnetic anomalies along the 85°E Ridge track in the Bay of Bengal region. Michael and Krishna (2011) have correlated these magnetization patterns to geomagnetic time scale of Cande and Kent (1995) and assigned approximate ages to the ridge track.

## 5.6 Process Oriented Gravity Anomaly Modeling

The process oriented gravity modeling technique is highly regarded for the studies of crustal structure and tectonic evolution of geologically complex regions, like rifted continent margins (Watts, 1988; Watts and Fairhead, 1999). The modeling technique was developed based on the concept that the observed gravity anomaly is considered as sum of gravity effects of several processes, those were involved during the evolution of continental margins such as rifting, underplating, sediment loading, flexure, erosion, etc. This approach has been followed in the present study to model the gravity field and its spatial variation along the 85°E Ridge. However, the geological processes involved in the evolution of the 85°E Ridge and a rifted continent margin are different. For modeling, it is assumed that the 85°E Ridge was emplaced in an oceanic setting by a volcanic activity and the structure was eventually buried under the thick Bengal Fan sediments. The first step in the modeling is to reconstruct initial ridge topography by flexurally unloading each sedimentary layer. This is carried out by computing the flexure caused by distributed load on elastic plate and removing this effect from the

basement. Theoretical basis for the flexural computations is discussed in detail in Chapter-3. The oldest sedimentary sequence immediately above the basement in the Bay of Bengal region was deposited from early Cretaceous to Paleocene. This means that thin cover of sediments were present by the time of ridge emplacement at about ~85 Ma (Krishna, 2003; Michael and Krishna, 2011). All the sedimentary layers except a thin basal sediment layer have been backstripped for different elastic plate thickness (Te) values. The backstripped section represents the initial morphology of the ridge covered with a thin layer of sediments overlain by water. The ridge emplacement is modeled as a load on thin elastic plate and as a load on a plate with no strength (Airy), resulting in flexural and Airy type compensations, respectively at the Moho boundary. The gravity anomalies are calculated with the consideration of ridge material on both flexure and Airy Moho configurations, which gave rise to 'Ridge Anomaly'. In second stage the sedimentary layers are brought back over the ridge structure, thereby the deflections created at basement and Moho levels are considered for gravity anomaly computations. The positive contribution of the sediment load and negative effect of flexure at the Moho boundary, when added will give rise to 'Sedimentation Anomaly'. The combined gravity effect of ridge anomaly and sedimentation anomaly is compared with the observed gravity anomaly of the ridge for a specific Te value. Entire process is repeated for different Te values range from 0 to 25 km, until a good fit is obtained between the observed and calculated gravity anomalies, considering RMS error as well as amplitude and wavelength of the anomalies as the goodness of fit. A simplified flow chart diagram of the process oriented modeling is given in Figure (5.4). The model parameters used in the computations are given in Table 5.1.

## 5.7 Elastic Plate Thickness and Crustal Structure of the 85°E Ridge

Following the approach described above, individual gravity anomalies contributed by ridge structure and overlying sediments are computed for three profiles (MAN-01, SK107-07 and MAN-03) in the Bay of Bengal region and one profile (98971) in the distal Bengal Fan and shown in Figure 5.5. The ridge anomalies of the Bay of Bengal profiles are, in general, positive with variable amplitudes and wavelengths for different Te values, while the sediment anomaly is negative due to less thickness of sediments on top of the ridge compared to its flanks. The sum anomaly is calculated by adding both ridge and sediment anomalies for different Te values and compared with the observed

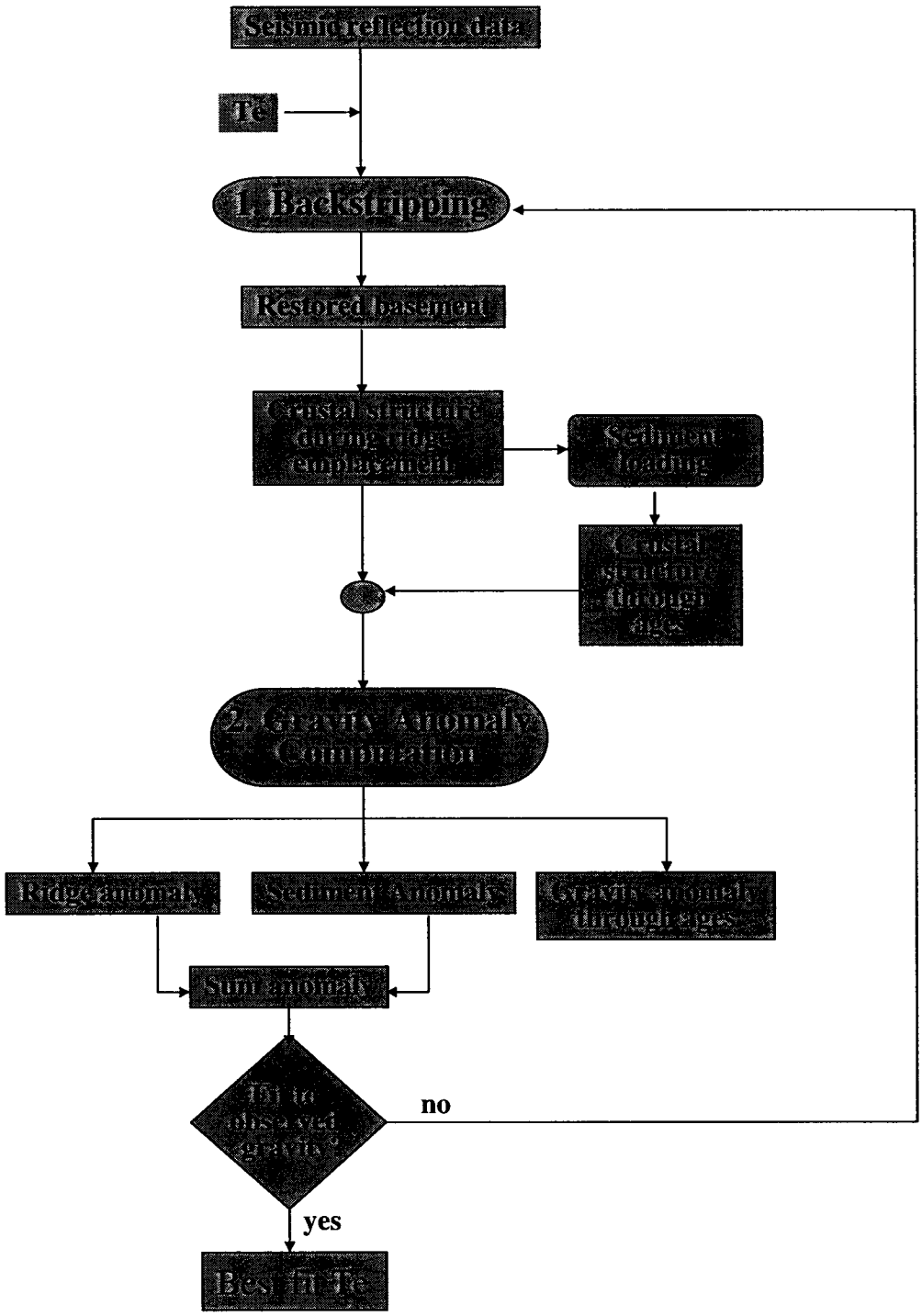


**Figure 5.4** Simplified flow diagram of process oriented modeling depicting the two major steps - 1. Backstripping and 2. Gravity anomaly computation. Crustal structure and gravity anomalies through ages (right panels) are computed with the best-fit Te (section 5.7).

**Table 5.1** Model parameters used for the flexural calculations and gravity modeling

| *Parameter* | *Value* |
|---|---|
| Density of Sea-Water ($\rho_w$) | 1.03 gm/cc |
| Density of oceanic crust ($\rho_c$) | 2.90 gm/cc |
| Density of load ($\rho_l$) | 2.65 gm/cc |
| Density of mantle($\rho_m$) | 3.30 gm/cc |
| Density of sedimentary layer1($\rho_1$) | 2.3 gm/cc |
| Density of sedimentary layer 2($\rho_2$) | 2.6 gm/cc |
| Density of metasediments ($\rho_3$) | 2.8 gm/cc |
| Average crustal thickness (t) | 6 km |
| Young's modulus (E) | 100 Gpa |
| Poisson's ratio ($\sigma$) | 0.25 |
| Universal gravitational constant (G) | $6.67.10^{-11}$ $Nm^2kg^{-2}$ |
| Acceleration due to gravity (g) | 9.8 $ms^{-2}$ |

gravity anomalies (Figure 5.5). It is observed that Te=15 km provides a better match for profiles MAN-03 and MAN-01, both in terms of amplitude and wavelength, though the RMS errors correspond to Te = 15 and 25 km are almost same. Whereas, for other profile SK107-07, Te=10 km gives a better fit with the observed anomaly. On the other hand, anomalies computed for the Airy model (Te=0 km) matches poorly with the observed anomalies and shows much smaller wavelength than the width of the ridge and more negative than the observed anomaly. The model results along the southern profile (98791) provide a best-fit for Te value 10 km (Figure 5.5) by comparing the sum anomaly with the observed anomaly. Thus, the analysis supports flexural isostatic compensation model with Te ranging from 10 to 15 km for both northern and southern parts of the 85°E Ridge.

For computations, different densities corresponding to various lithological units are used following the published seismic refraction results of the Bay of Bengal. Naini and Leyden (1973) identified a total of nine reflecting layers with velocities ranging from 2.0 to 5.78 km/s with oceanic basement having velocity of 6.2 km/s. Subsequently using seismic reflection and refraction data Curray et al. (1982) have determined velocities ranging from 1.7 to 4.85 km/s for different lithological units. Later, Curray (1991) mapped high velocity (6.0 - 6.4 km/s) pre-collision sedimentary section

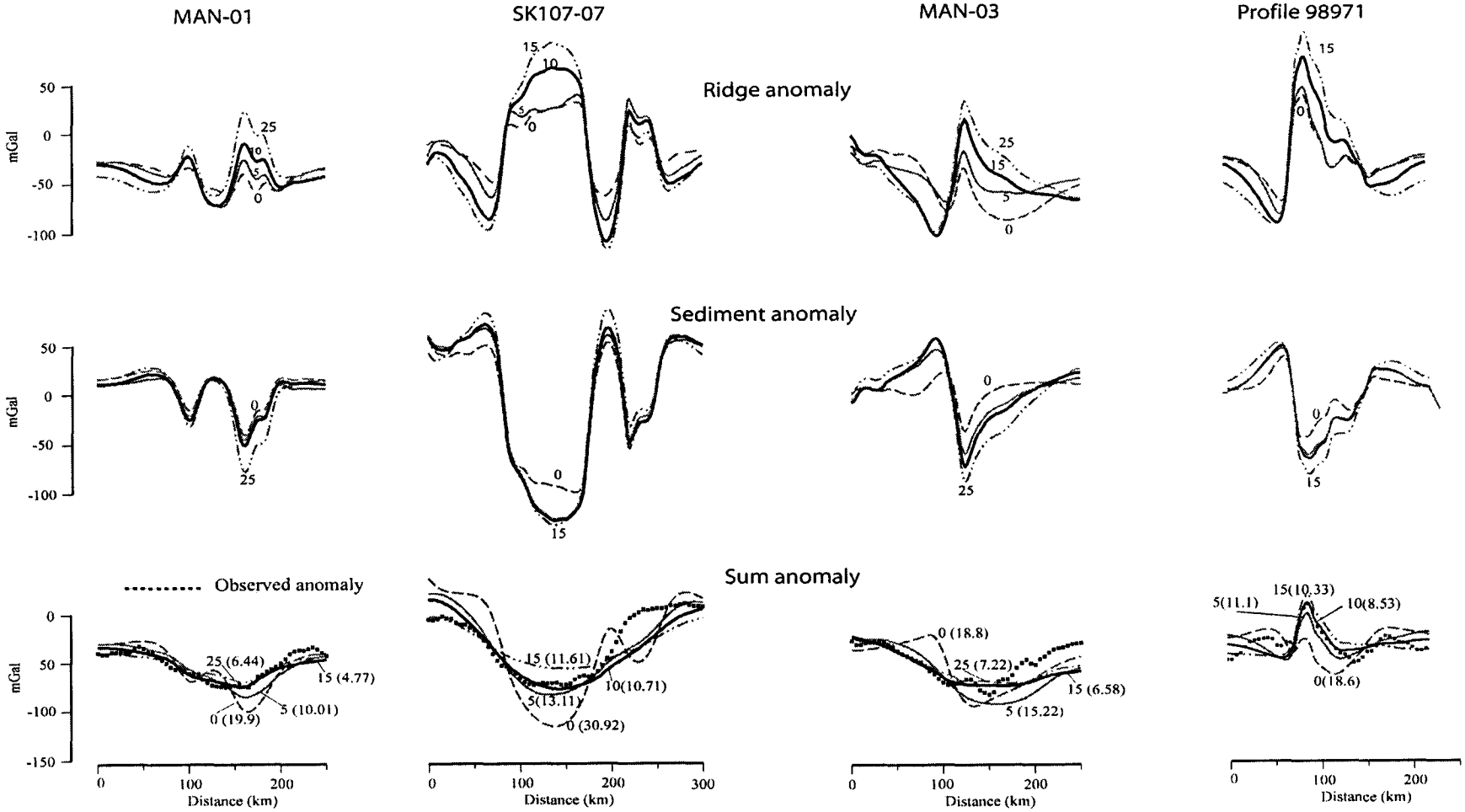


**Figure 5.5** The ridge and sedimentation anomalies computed for different Te values through process oriented gravity modeling for profiles MAN-03, MAN-01, SK107-07 and 98791. The sum anomaly of these two is compared with observed gravity anomaly with degree of fitness shown as RMS error (bracket).

(metasedimentary rocks) below the Paleocene unconformity. Velocity-depth relation of Bay of Bengal sediments derived from compilation of seismic refraction data (Radhakrishna et al., 2010) also shows high seismic velocities for deeper sediments of northern Bay of Bengal compared to the southern sediments (Figure 5.6). The observed seismic velocities were converted to density values and broadly grouped into three density distributions for consideration of gravity model studies. Density values of 2.3 and 2.6 gm/cc are considered for the upper and intermediate sedimentary layers (layer-1 and layer-2 in Table5.1), whereas higher density of 2.8 gm/cc is considered for the metasedimentary rocks (layer-3 in Table1), which is slightly higher than the density considered for the volcanic ridge (2.65 gm/cc). Density value 2.8 gm/cc considered for metasediments is not unusual as sediments undergo more compactness due to the overburden deposits than the basalts undergo.

The sediment loaded crustal structures derived for the best-fit Te values along all four profiles are presented in Figures 5.7a, b, c and d. The crustal model along the Bay of Bengal profiles suggests a broad flexure at Moho boundary with a wavelength more than the width of the ridge. For profiles MAN-01 and MAN-03 the isostatic compensation is achieved by a flexure of Moho up to 2-3 km (Figure 5.7a, c), whereas along profile SK107-07 the flexure is about 5.5 km (Figures 5.7b). The relief and width of ridge along SK107-07 quite high and lead to higher surface load, which resulted in deeper flexure at Moho boundary for isostatic compensation.

The crustal model derived along profile-98791 (Figure 5.7d) is similar to that along the northern profiles with deflection of the Moho (about 3 km) due to the loading of ridge and sediments. However, a single sediment layer with an average density of 2.3 gm/cc is only used in the modeling, as the thickness of the Bengal Fan sediments in this area is relatively less to consider the compaction effects (Figure 5.6).

### 5.7.1 Crustal Structure of the 85°E Ridge- Two-dimensional Gravity Forward Modeling

Process oriented gravity modeling of gravity profiles running across the 85°E Ridge suggests flexural isostatic compensation with an approximate crustal structure beneath the ridge. The crustal models (Figures 5.7a, b, c and d) derived so are further improved using two-dimensional gravity forward modeling in order explain the observed gravity

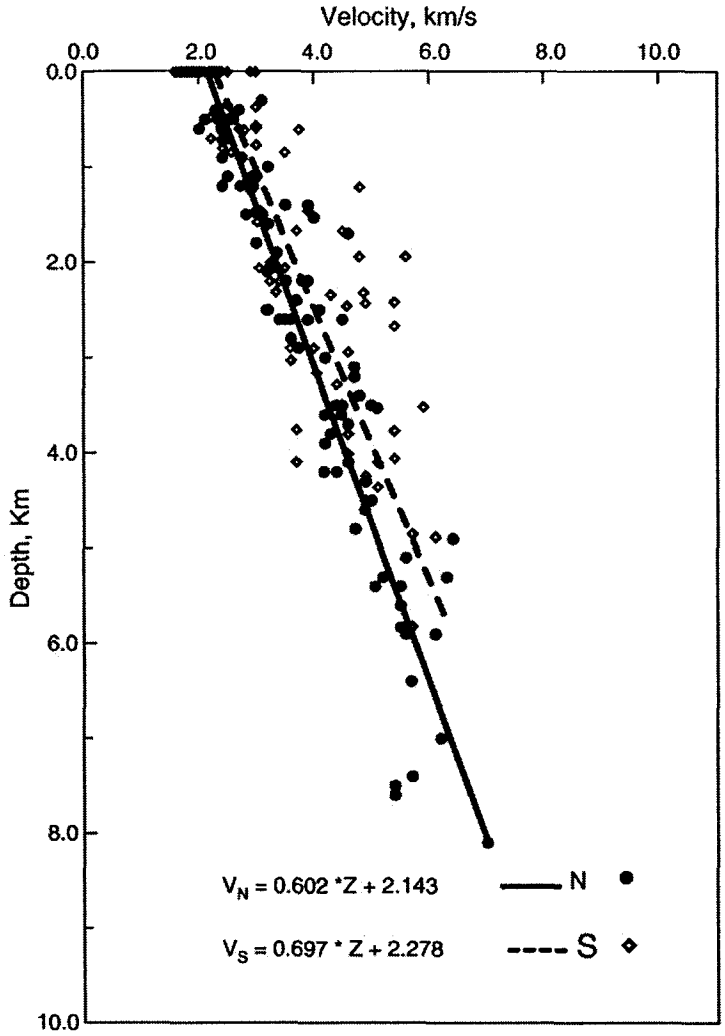


**Figure 5.6** Velocity–depth relation for sediments in the Bay of Bengal based on compilation of available seismic refraction measurements (after Radhakrishna et al., 2010). Note different burial effect for northern (N) and southern (S) Bay of Bengal sediments.

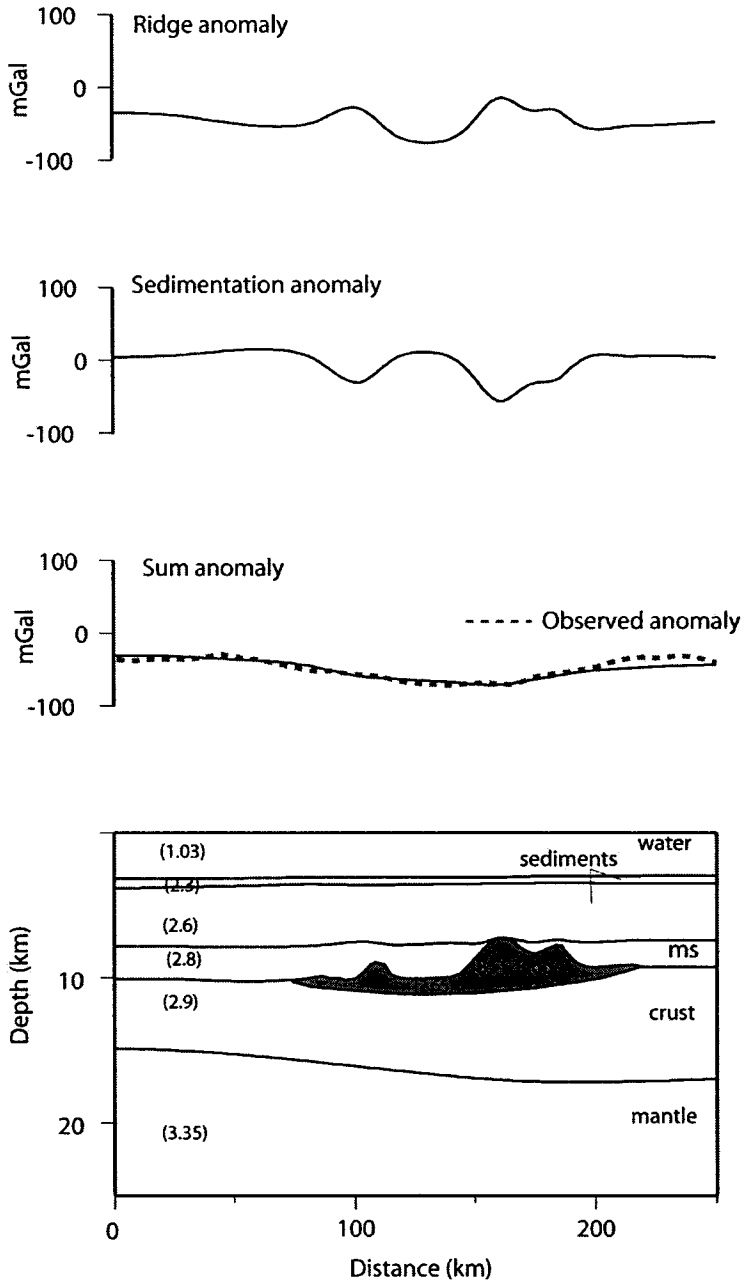


**Figure 5.7a** Crustal structure of the 85°E Ridge along profile MAN-01 along with different anomaly components (see details in text) obtained from process oriented gravity modeling. The values in bracket represent density for corresponding layer in gm/cc. The sum anomaly computed for best fitting Te (15 km) is shown along with the observed gravity anomaly. ms in Figure indicates metasediments.

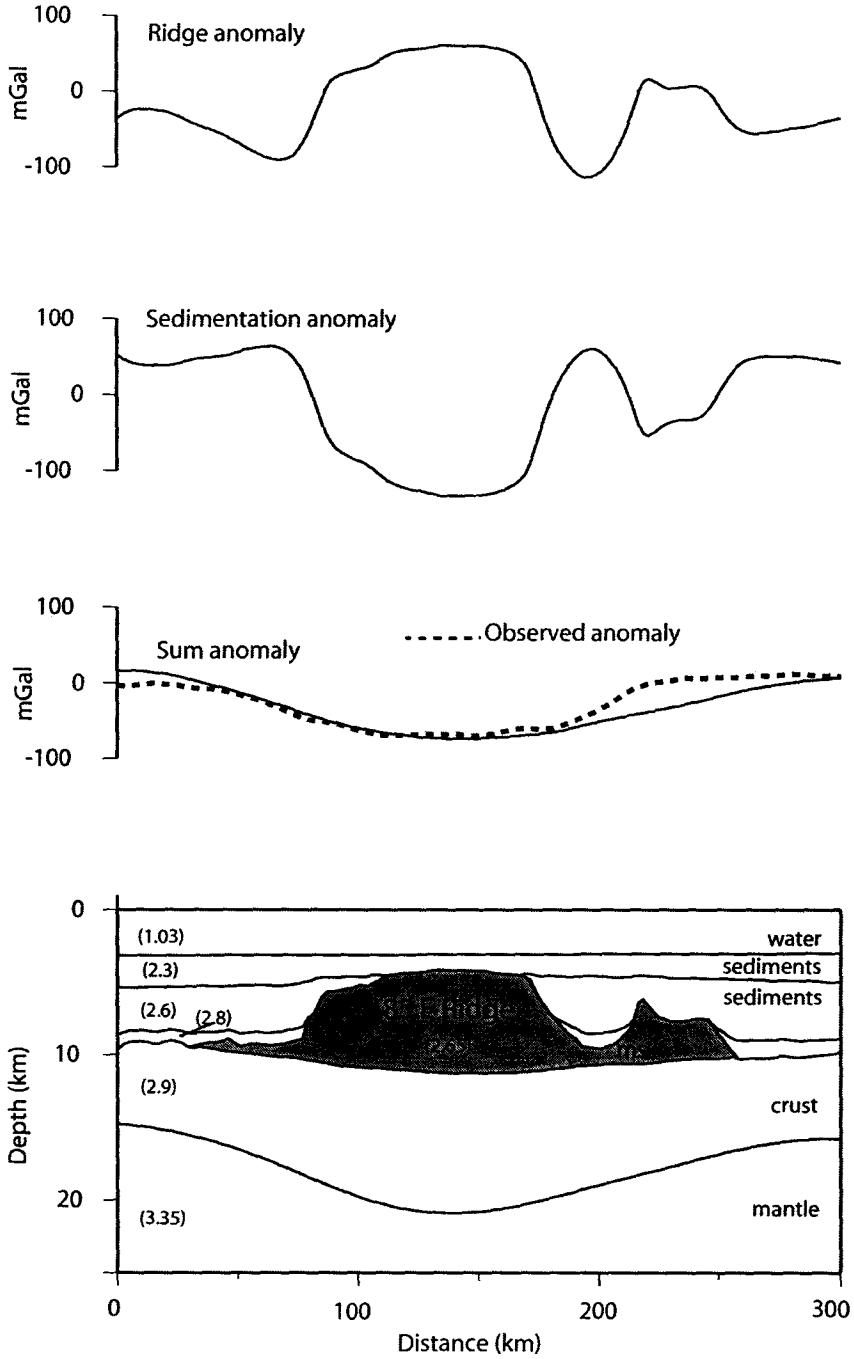


**Figure 5.7b** Crustal structure of the 85°E Ridge along profile SK107-07 along with different anomaly components obtained from process oriented gravity modeling. The sum anomaly computed for best fitting Te (10 km) is shown along with the observed gravity anomaly. Notations are same as given in Figure 5.6a.

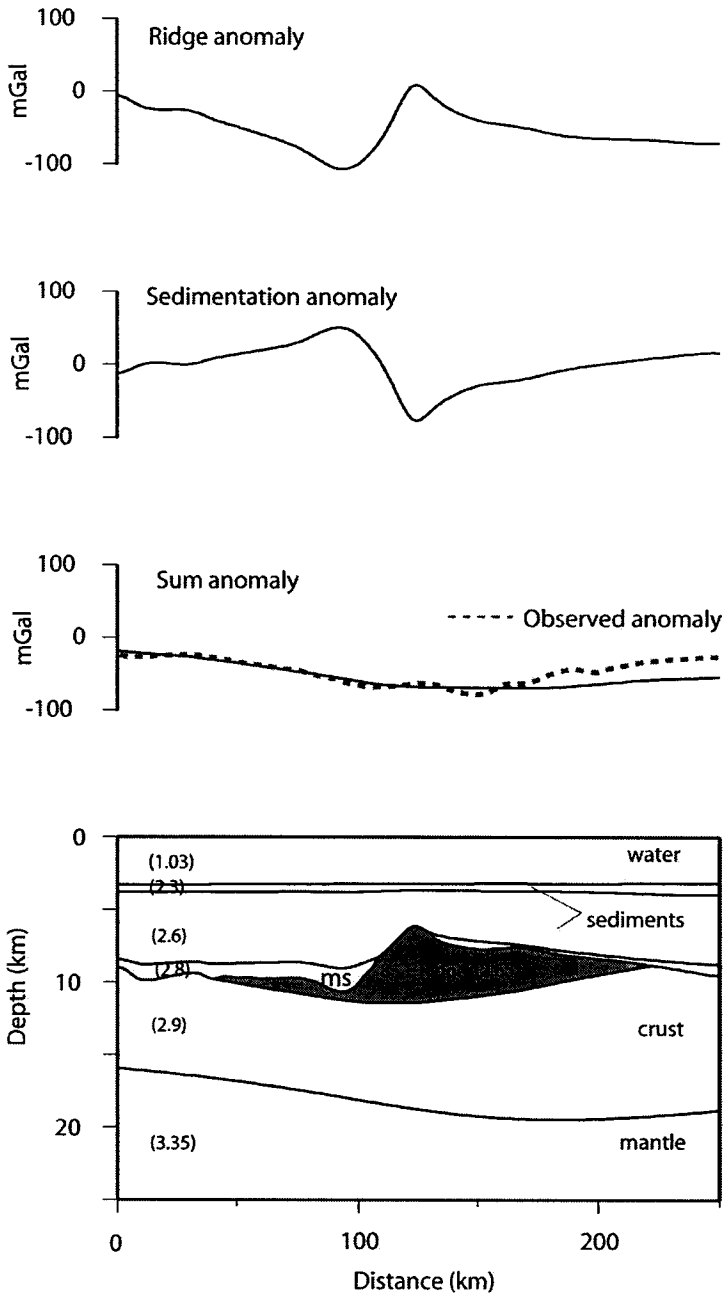


**Figure 5.7c** Crustal structure of the 85°E Ridge along profile MAN-03 along with different anomaly components obtained from process oriented gravity modeling. The sum anomaly computed for best fitting Te (15 km) is shown along with the observed gravity anomaly. Notations are same as given in Figure 5.6a.

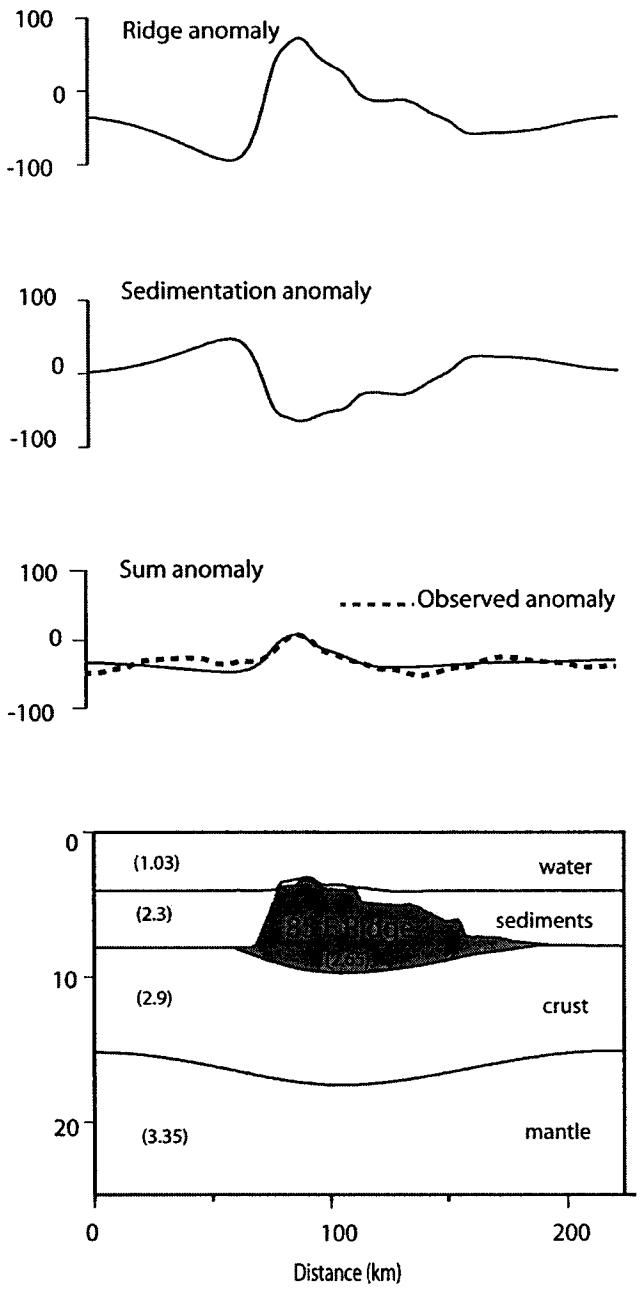


**Figure 5.7d** Crustal structure of the 85°E Ridge along profile 98791 along with different anomaly components obtained from process oriented gravity modeling. The sum anomaly computed for best fitting Te (10 km) is shown along with the observed gravity anomaly. Notations are same as given in Figure 5.6a.

field of the ridge. The forward modeling has been carried out along two profiles, MAN-03 and 98971, chosen from northern and southern parts of the ridge, respectively (Figure 5.8a and b). Oceanic crustal layers (2 and 3) with typical densities (2.7 gm/cc and 2.95 gm/cc) and thicknesses (2 km and 4 km) and mantle with density 3.35 gm/cc were considered for the model. The details of densities of sediments used in the model studies are discussed earlier in the previous section. The Moho geometry suggested by process oriented modeling is considered as initial constraints and depths to the Moho and the crustal interfaces were varied iteratively until to get a good match between observed and computed gravity anomalies.

The crustal model along the profile MAN-03 reveals that about 5 km thick volcanic material is emplaced on oceanic crust (Figure 5.8a). The crust responds to the load of the ridge and the overlying sediments by down flexing the crustal layers and Moho boundary to about 2.8 km. This is comparable to the 3 km flexure derived in process oriented model studies (Figure 5.7b). In addition, gravity forward model reveals more detailed geometry of crustal layers and Moho boundary beneath the ridge (Figure 5.8a). The gravity models derived by both the techniques conclusively suggests that the negative gravity anomaly of the 85°E Ridge could be explained by a combination of sources: the flexure at Moho boundary, presence of high density metasedimentary rocks on either side of the ridge and thick Bengal Fan sediments over the ridge

The crustal model derived along the profile 98971 is shown in Figure 5.8b. The ridge appears to be composed of volcanic material of about 6 km thick. Along this profile also, the ridge load is compensated by flexure of crustal layers as well as Moho boundary by about 3.2 km. The model is in good agreement with the model obtained by process oriented technique (Figure 5.78). The positive gravity over the ridge could be explained due to the exposition of the ridge structure above the seafloor and the absence of high-density deeper sedimentary rocks.

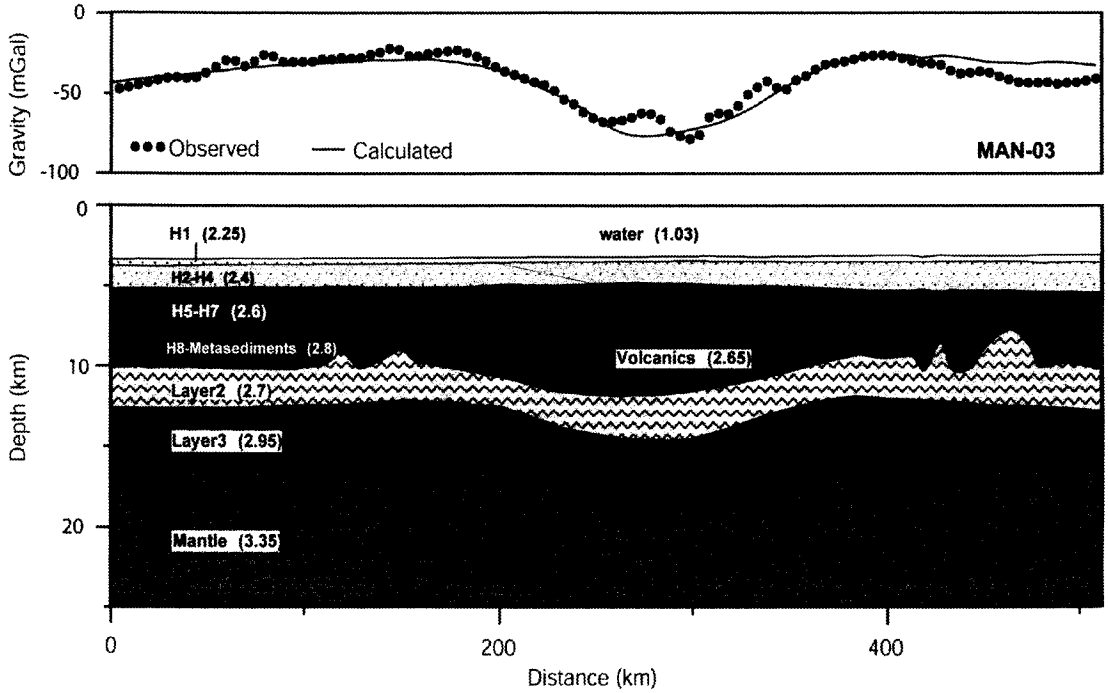


**Figure 5.8a** Two-dimensional gravity model and crustal structure along profile MAN-03. Values in bracket represent densities in gm/cc. H1, H2-H4, H5-H7 and H8 are sedimentary layers derived from the seismic sequences (H1-H8) identified along the section by Gopala Rao et al., 1997.

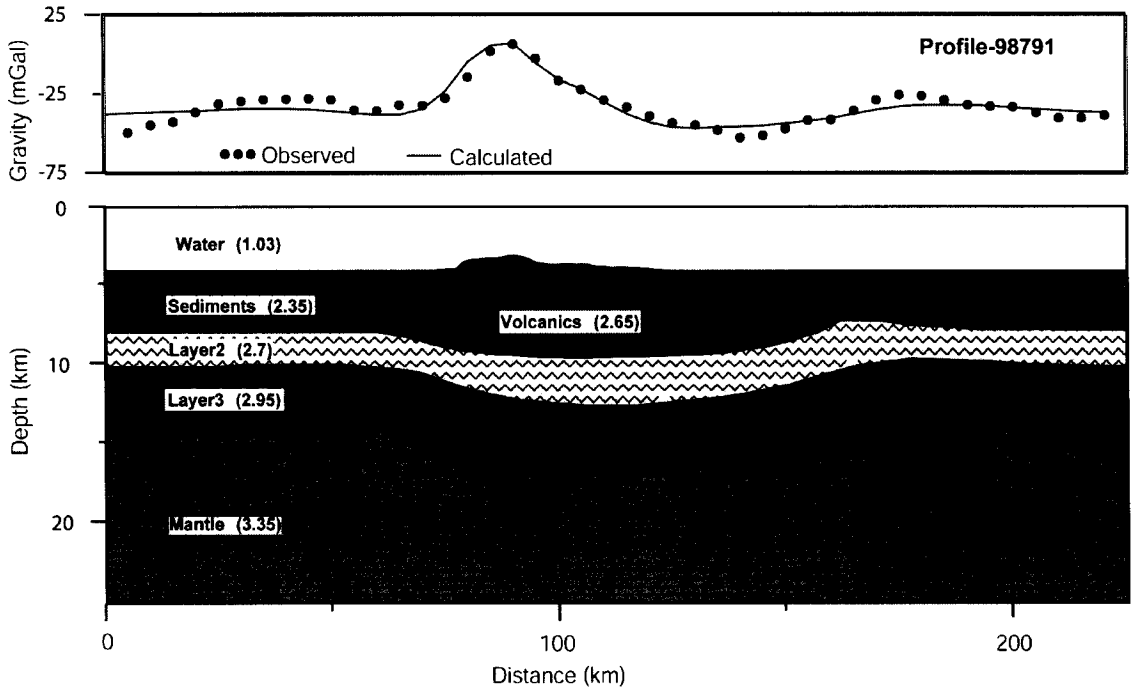


**Figure 5.8b** Two-dimensional gravity model and crustal structure along profile-98791. Values in bracket represent densities in gm/cc. A single sedimentary layer identified along the section is considered for modeling.

## 5.8 Different Stages of the 85°E Ridge – Simulation of Gravity Anomalies

As discussed in earlier sections, the initial flexural rigidity and the subsequent sediment deposition explain well the present-day negative gravity anomaly of the 85°E Ridge. Curray et al. (1982) and Gopala Rao et al. (1997) have identified several seismic horizons and unconformities within the sediments of the Bay of Bengal and discussed the sedimentation history in detail since the early Cretaceous. Keeping these results in view an attempt has been made to understand how the gravity field of the 85°E Ridge had changed through time, particularly in response to the sediments of the Bay of Bengal. In other words, gravity anomalies have been simulated at three different geologic ages since the formation of the ridge: late Cretaceous, early Miocene and Present. A simple procedure is followed- flexurally load the sediment layers phase by phase to the backstripped section and compute the gravity anomalies for each phase, particularly for the periods, late Cretaceous, early Miocene and Present. Best-fit Te value derived for each profile is used for anomaly computations. These steps are briefly described in the flow diagram of process oriented modeling (Figure 5.4). The simulated gravity anomaly and corresponding crustal model derived for three profiles of the Bay of Bengal at three different ages are presented in Figures 5.9a, b and c.

Along profiles MAN-03 and SK107-07, during the late Cretaceous the ridge structure was existing above the seafloor and associated with positive gravity anomaly due to the density contrast existed between the ridge material and water (Figure 5.9b and c). The second panel shows the crustal structure of the ridge and corresponding gravity anomaly determined for the early Miocene period, when the ridge had completely buried under the sediments. The anomaly shows a substantial reduction in amplitude, but it was still positive signature and follows the trend of the ridge topography. However, along MAN-01, by late Cretaceous the ridge structure was overlain by thin layer of sediments and hence associated with comparatively low amplitude gravity anomaly and by early Miocene the ridge got deeply buried under the sediments (Figure 5.9a). The amplitude of gravity anomaly has reduced substantially, but still remains positive over the ridge crest. After loading thick Miocene and post-Miocene sediments, the basal sediments deposited before the continental

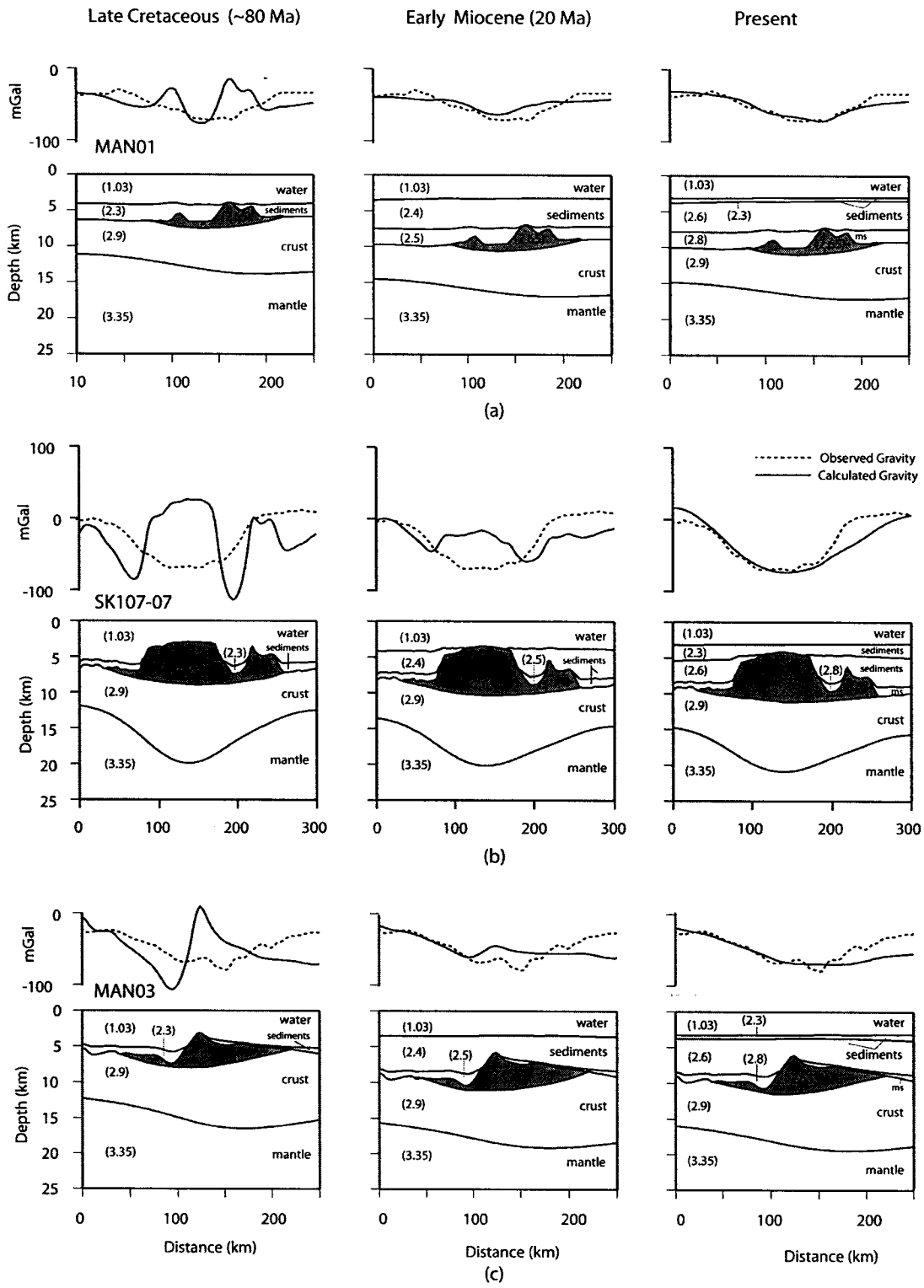


**Figure 5.9** Reconstruction of the gravity anomalies over the 85°E Ridge through geological ages for profiles a) MAN-01, b) SK 107-07, c) MAN-03. The bottom panels represent the crustal structures for the respective periods. Note the change of gravity anomaly from positive to negative. ms in figure indicates metasediments.

collision have attained higher densities equivalent to the density of metasediments (2.8 gm/cc) (third panel in Figures 5.9a, b and c). It can be observed that the gravity high over the ridge structure remains till the early Miocene age, subsequently the anomaly signature switches to negative field.

Another interesting aspect is the response of the ridge and adjacent oceanic crust to the sediment loads since the ridge emplacement. The Moho deflection produced by the ridge load during the late Cretaceous has progressively broadened with the addition of sediment material. As the thicknesses of sediments are less over the ridge crest and increases on either side of it, the sediment load flattens the flanks of the Moho deflection. The wavelength of computed gravity anomaly matches with that of the sediment loaded Moho deflection. This suggests that the sediment layers mask the gravity effect of the ridge, and the negative anomaly could be attributed to the deflection created by the ridge load and sediments on adjacent crust. These effects are more clearly visible along the profile SK107-07 as the flexure is more prominent compared to the flexure observed along other profiles (Figures 5.9)

## 5.9 Structure and Tectonics of the 85°E Ridge

Process oriented modeling of seismic and gravity data of the 85°E Ridge determines the elastic plate thickness range from 10 to 15 km for both northern and southern parts of the ridge, suggesting that the ridge emplacement was in an intraplate (off-ridge) setting. When the hotspot volcanism takes place on relatively older lithosphere, the emplaced volcanic construct would be compensated regionally. Subsequent sediment deposition led to the deeper burial of the ridge structure and adjacent oceanic basement, as a result pre-collision basal sediments have turned into metasedimentary rocks. The crustal models (Figures 5.7a, b and c, 5.8a and b, 5.9) further suggest that the 85°E Ridge and overlaying sediment load are compensated by the regional flexure of the Moho boundary. This inference is not in agreement with the earlier interpretations of the ridge structure (Liu et al., 1982; Mukhopadhyay and Krishna, 1991; Ramana et al., 1997; Subrahmanyam et al., 1999; Anand et al., 2008), wherein they favored the Airy model of isostatic compensation for the 85°E Ridge. Subrahmanyam et al. (1999) have considered underplated magmatic material

within the deep crust beneath the ridge in order to explain the negative gravity field satisfactorily; this led to believe that the 85°E Ridge was formed by a hotspot on young oceanic crust similar to the emplacement process of the Ninetyeast and Chagos-Laccadive ridges. As no deep seismic reflection or seismic refraction data are available to examine the presence of underplating or subsurface loading beneath the ridge, a simple tectonic model considered, in which the ridge includes only a surface load emplaced on a thin elastic plate. Consideration of a complex model with subsurface loading may add ambiguities in Te estimation and crustal structure as well. Also, it should be noted that plume related ridge emplacement can occur in different tectonic settings on the plate, so the structural complexities and mode of isostasy along its path (aseismic ridges) must be understood in detail, particularly in the case of deeply buried 85°E Ridge.

The results obtained in this work are combined with the earlier geophysical results of the 85°E Ridge and Conrad Rise, and with the geochronology of the rocks recovered from the ANS (Sborshchikov et al., 1995) in order to understand the evolution of the ridge and ANS in a broader perspective. Recent understanding on evolution of the conjugate oceanic regions of the Bay of Bengal and Enderby Basin (Gaina et al., 2007; Krishna et al., 2009a) enlighten that most part of the oceanic crust in the Bay of Bengal was accreted during the Cretaceous super long normal polarity phase. Hence, it is obvious that no coherent magnetic anomalies related to the Earth's magnetic reversals are probable in the Bay of Bengal. In spite of this, the 85°E Ridge is associated with alternate stripes of strong positive and negative magnetization patterns distributed for asymmetrical extents (Michael and Krishna, 2011). Following the magnetic model studies and correlations of the ridge magnetization patterns with Geomagnetic Polarity Timescale, Michael and Krishna (2011) found that the ridge was formed from 85 Ma onwards and recorded the changes of the Earth's magnetic fields, earlier to that, the underlying Bay of Bengal crust was created during the Cretaceous super-long normal polarity phase. The intermediate elastic plate thickness (10-15 km) derived from the present study strongly support the emplacement of the ridge on already evolved oceanic crust. These results when combined with the age constraint (~120 Ma) of the Bay of Bengal oceanic crust (Gopala Rao et al., 1977; Krishna

et al., 2009a) would conclusively suggest the emplacement of the ridge on an oceanic crust of about 35 m.y old.

From the recent geophysical investigations, Krishna et al. (2011a) have suggested that the ANS includes two components of volcanic materials, the main plateau and seamount highs. The main plateau was constructed along with the formation of the oceanic crust during 79-73 Ma, and seamount highs were formed subsequently in an intraplate setting. The low elastic plate thickness up to 5 km determined beneath the ANS (Paul et al., 1990), is much lower than the Te values calculated for the 85°E Ridge and is attributed to the initial on-ridge volcanism. Following the above results and discussions it is believed that the 85°E Ridge volcanism started approximately 85 Ma ago in Mahanadi Basin by a short-lived hotspot. Around this time the Conrad Rise hotspot has emplaced the main plateau of the ANS and Marion Dufresene seamount together close to the India-Antarctica Ridge (Diament and Goslin, 1986), thereafter the hotspot has moved to the Antarctica plate leaving the main plateau of the ANS as an isolated feature on the Indian plate (Figure 5.10). At other end in the Bay of Bengal the hotspot, which initiated the emplacement of the 85°E Ridge in the Mahanadi Basin, has continued its activity towards south and probably ended at ~55 Ma in the vicinity of the ANS.

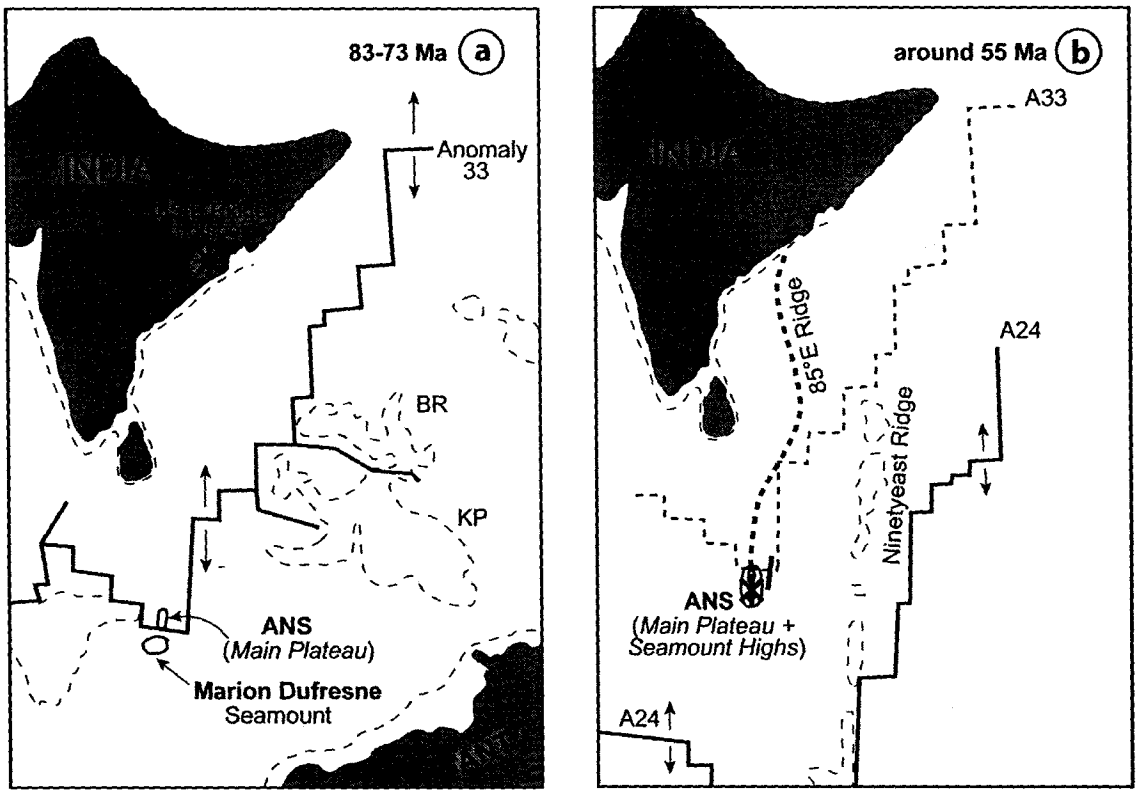


**Figure 5.10** Late cretaceous (Left) and Paleocene (Right) reconstruction of northeastern Indian Ocean (Krishna et al, 2011a). The emplacement the main plateau of ANS and initiation of 85°E Ridge emplacement at Mahanadi Basin during ~85 Ma is shown in the left panel. By ~55Ma 85°E Ridge emplaced and the causative hotspot reactivated ANS (Right). The concurrent evolution of Ninetyeast Ridge by Kerguelen hotspot activity is also shown (Right). BR and KP stands for Broken Ridge and Kerguelen Plateau respectively.

# CHAPTER 6

# Spatial Variations in Isostatic Compensation Mechanisms of the Ninetyeast Ridge and their Tectonic Implications

# Spatial Variations in Isostatic Compensation Mechanisms of the Ninetyeast Ridge and their Tectonic Implications

## 6.1 Introduction

The Ninetyeast Ridge is one of the major aseismic ridges of the World Oceans and probably the longest linear feature on planet Earth. It extends for more than 5000 km in the eastern Indian Ocean from 30°S to 17°N approximately along the 90°E meridian. The ridge edifice rises to 2-3 km from the adjacent ocean floor and separates the Central Indian Basin on the west from the Wharton Basin on the east (Figure 6.1). The morphological characteristics of the Ninetyeast Ridge and its surrounding basinal regions were well-documented (Stocks, 1960; Udinstev, 1975; Schlich, 1982), but the ridge origin was explained by different geophysical models. These include 1) horst-type structure (Francis and Raitt, 1967), 2) overriding of an oceanic plate over the other (Le Pichon and Heirtzler, 1968), 3) fracture zone (McKenzie and Sclarer, 1971), 4) hotspot trace (Bowin, 1973), and 5) excess volcanism at the junction of a transform fault and a migrating spreading center (Sclater and Fisher, 1974).

The paleolatidues derived from the DSDP Leg 26 samples (Peirce, 1978) clearly indicated that the ridge was emplaced on the Indian plate during its northward drift between the late Cretaceous and early Cenozoic by the Kerguelen the hotspot. Subsequently, geochemical (Frey et al., 1977; Weis and Frey 1991; Frey and Weis, 1995), geochronological (Duncan, 1978; Duncan, 1991) and isotopic composition (Class et al., 1993) studies brought additional evidences for the support of hotspot origin for the ridge. Currently, it is widely believed that the ridge was emplaced on the Indian plate when it was moved northward over the Kerguelen hotspot during the period 82-38 Ma following the formation of the Rajmahal traps on the Indian subcontinent, the Bunbary basalts on the Australian continent, the Broken Ridge, and the southern part of the Kerguelen Plateau.

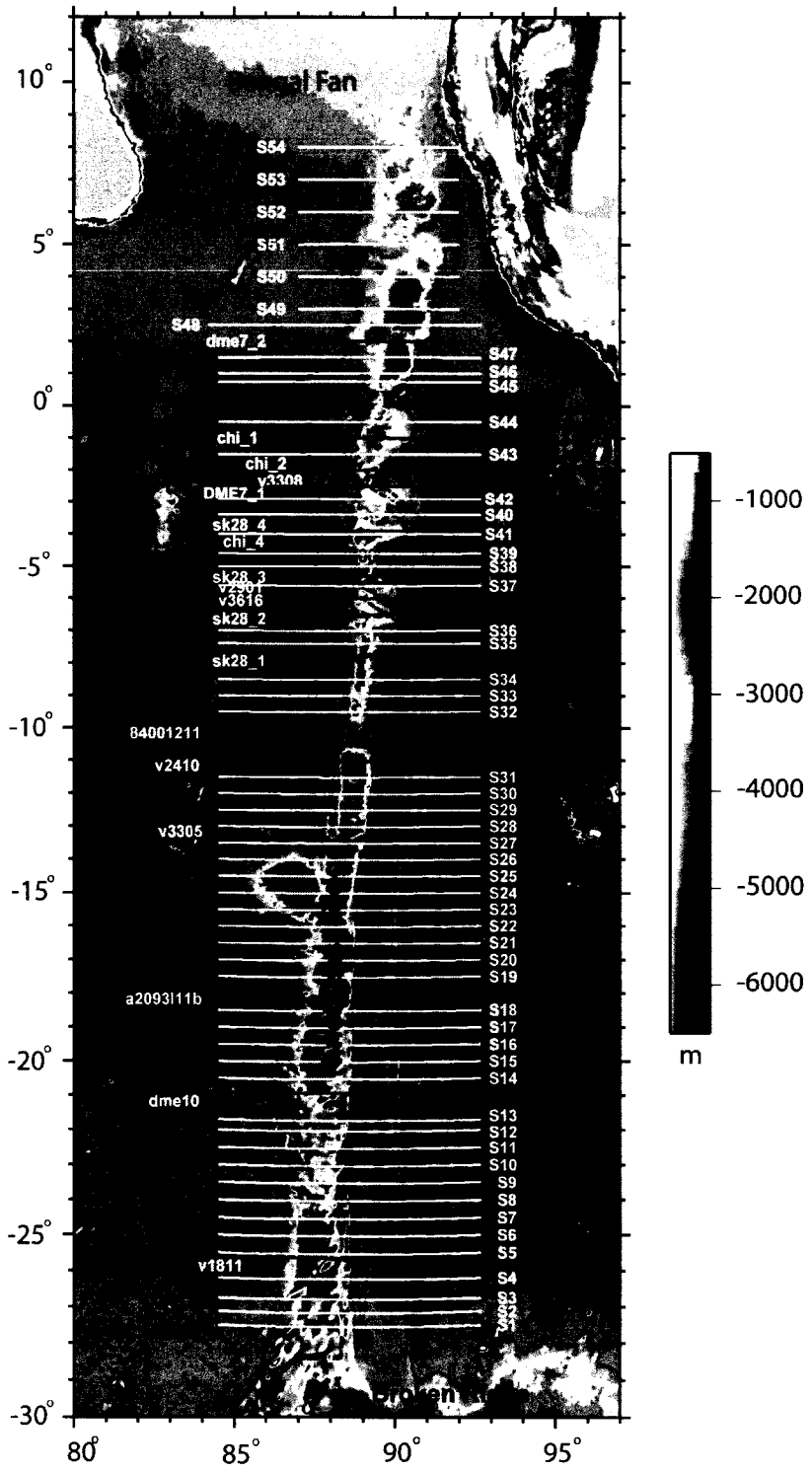


**Figure 6.1** Satellite derived bathymetry map (Smith and Sandwell, 1997) of the northeastern Indian Ocean along with 4000 m depth contour. Tracks of unprojected (dashed line) and projected (black line) ship data and satellite profiles (white lines) are shown.

Marine magnetic anomaly studies of the ocean basins surrounding the Ninetyeast Ridge revealed highly diachronous age pattern, suggesting the presence of several fossil ridge segments ceased at different ages (Figure 6.2) (Sclater and Fisher, 1974; Sandwell and Royer, 1989; Royer et al., 1991; Krishna et al., 1995, 1999). Royer et al. (1991) proposed a three phase tectonic evolution model for the emplacement of the Ninetyeast Ridge, which suggests that the northern part (north of 2°S) of the ridge was formed in intraplate setting, the central part (2.5°S 15°S) was formed at the edge of either Antarctica or a short-lived platelet and the southern part (south 15°S) was evolved along a fracture zone by the Kerguelen hotspot activity. Subsequently, Krishna et al. (1999) proposed that the central part of the Ninetyeast was formed as a result of interaction between the Kerguelen hotspot and the Wharton spreading centre. This model suggests successive southward ridge jumps and transfers lithospheric blocks originally evolved on the Antarctic plate to the Indian plate. Desa et al. (2009) have identified fossil ridge segments and presence of extra oceanic crust beneath the northern part of the Ninetyeast Ridge, suggesting on-ridge emplacement process even for the northern part of the ridge. Recent compilation of gravity, bathymetry and seismic reflection data provided evidences for spreading ridge-hotspot interactions all along the Ninetyeast Ridge and suggested that the hotspot was never far from the spreading ridge during the evolution of the entire stretch of the Ninetyeast Ridge (Sager et al., 2010).

Bowin (1973) has made the first attempt to model the crustal structure of the Ninetyeast Ridge and suggested that the Ninetyeast Ridge is isostatically compensated (local compensation) at deeper depth and supposed its origination as a result of emplacement of gabbro and serpentinized peridotite within the crust. Further, the isostasy of the Ninetyeast Ridge was examined using two-dimensional admittance analysis of ship-borne bathymetry and gravity data (Detrick and Watts, 1979; Grevemeyer and Flueh, 2000) and suggested local compensation beneath the Ninetyeast Ridge. Subsequently Detrick and Watts (1979) computed the admittance by averaging 14 profiles from equator to about 25°S, whereas Grevemeyer and Flueh (2000) used a single profile along 17°S for the analysis. Both of these studies could bring out a unique model of local isostatic compensation mechanism beneath the ridge. Subsequently Tiwari et al. (2003) have carried out three-dimensional

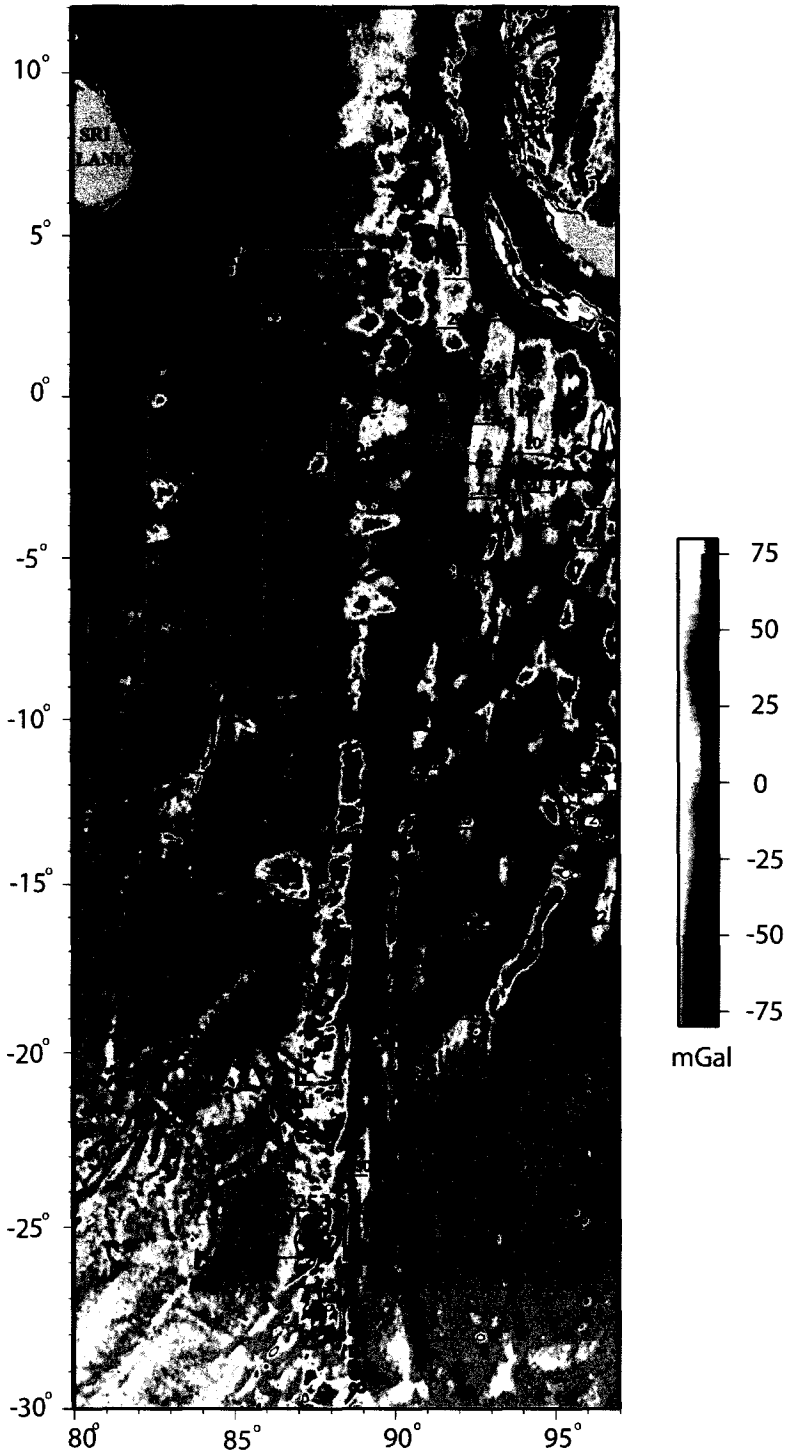


**Figure 6.2** Satellite derived free-air gravity anomaly map (Sandwell and Smith, 2009) of the northeastern Indian Ocean. Magnetic lineations (thin line), abandoned spreading centers (thick lines) and fracture zones (dashed line) are superposed on the map. Black and red colors indicate the tectonic features presented in Krishna et al., 1999, Krishna and Gopala Rao, 2000 respectively. DSDP/ ODP holes (circle) and dredging stations (square) are shown with ages in bracket.

admittance analysis using satellite-derived gravity and bathymetry grids over nine rectangular blocks from 30°S to 10°N along the ridge. Though admittance analysis using girded data can give robust elastic plate thickness (Te) estimate, its spatial variation is highly dependent on choice of size of data window. Considering the complex tectonic setting of the Ninetyeast Ridge, it is felt that analysis along closely spaced profile data would better indicate the variations in isostatic compensation mechanisms than the girded data. Hence, flexural modeling and admittance analysis were carried out along 72 profiles of ship-borne as well as satellite derived gravity and bathymetry data along the Ninetyeast Ridge from 28°S to 8°N.

## 6.2 Geophysical Data

Ship-borne gravity and bathymetry profiles crossing the Ninetyeast Ridge were chosen from the geophysical database of the eastern Indian Ocean compiled from NGDC as well as from different oceanographic cruises of Indian and Russian research programmes. In order to have even sampling along the entire ridge the larger gaps between the ship-borne profiles are filled with consideration of 54 satellite-derived gravity and bathymetry profiles (Sandwell and Smith, 2009; Smith and Sandwell, 1997) (Figure 6.1).

Free-air gravity anomaly data derived from satellite altimetry measurements have become the primary dataset for investigations of oceanic regions, where only limited number of ship-borne measurements are available (Sandwell and Smith, 2009 and references therein). The accuracy of satellite gravity in comparison to ship-borne gravity measurements, particularly in deep ocean regions is 5-10 mGal (Rapp, 1998). The satellite gravity data can resolve the geological features having wavelengths greater than 23 km (Marks, 1996). The reliability of satellite derived gravity data in the study area is tested by comparing with ship-borne gravity data along profile A2093111 (Figure 6.3a). Both the datasets match very closely with a RMS error of 4.4 mGal.

Bathymetry data from ETOPO-1 database and predicted bathymetry from satellite gravity data (Smith and Sandwell, 1997) are considered for this study. Both the datasets are

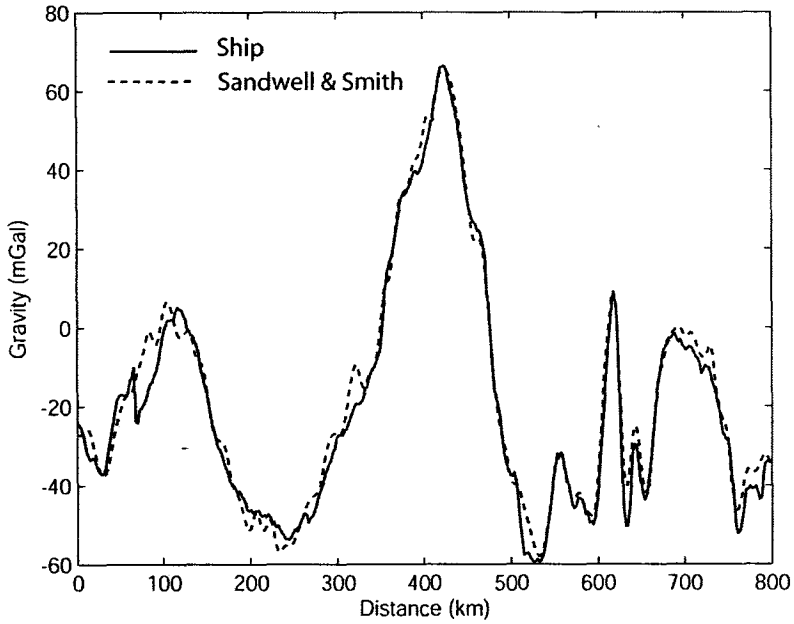


**Figure 6.3a** Comparison of gravity data along profile A2093111 with satellite derived gravity data (Sandwell and Smith, 2009) extracted along the ship track

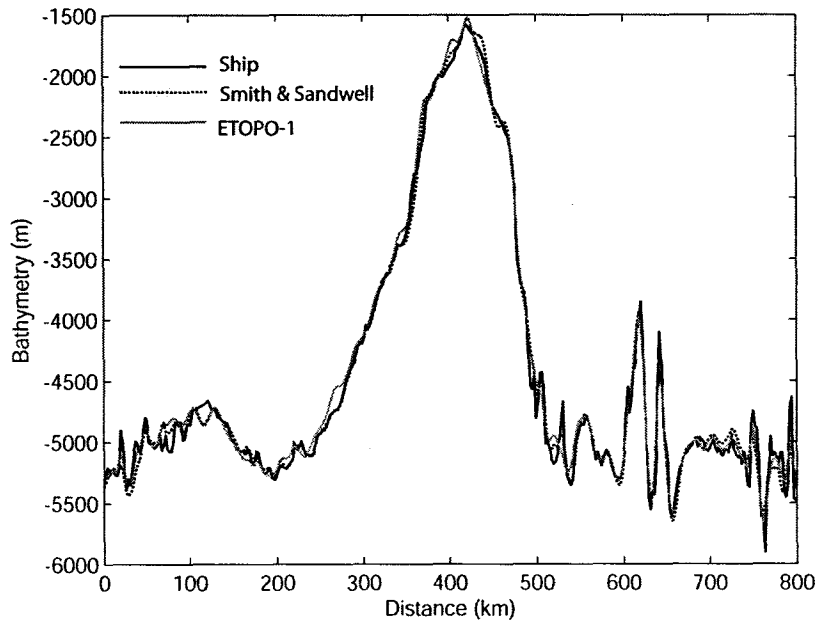


**Figure 6.3b** Comparison of bathymetry data along profile A2093111 with satellite derived gravity data (Smith and Sandwell, 1997) and ETOPO-1 data extracted along the ship track.

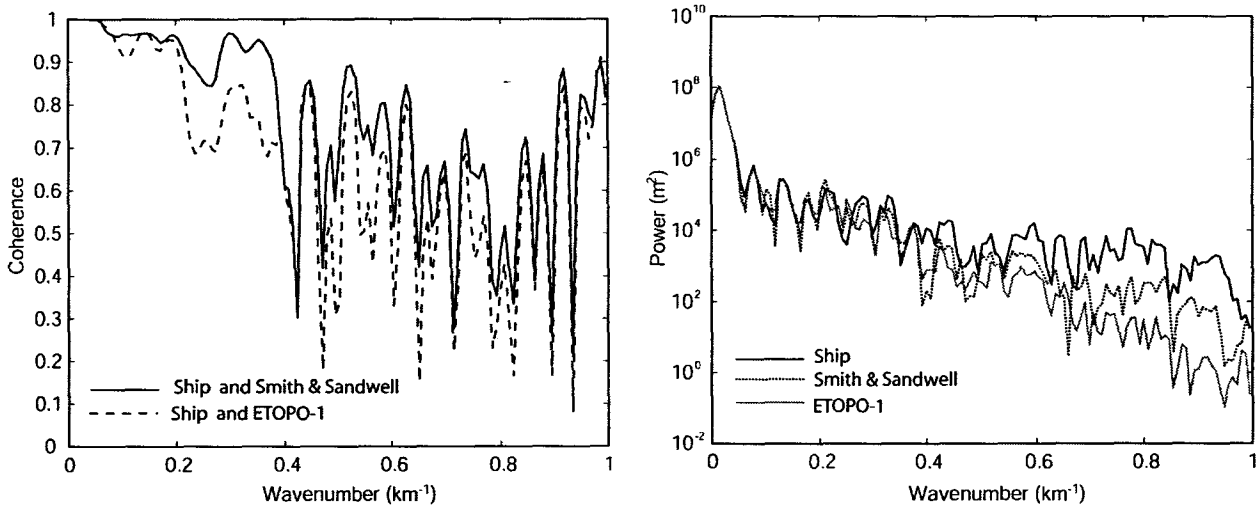


**Figure 6.3c** Comparison of power spectrum of bathymetry data along profile A2093111 with satellite derived bathymetry data (Smith and Sandwell, 1997) and ETOPO-1 data extracted along the ship track (right) and coherency between them (left).

compared with the ship-borne bathymetry along the profile A2093111. In general, both ETOPO-1 and Smith and Sandwell (1997) data match well with the ship-borne bathymetry data with RMS errors of 100 m and 103 m, respectively (Figure 6.3b). However, in spectral domain, the Smith and Sandwell (1997) data provide better coherence with ship-borne data for wavenumbers <0.4 and its power spectral density is higher than that of ETOPO-1 for wavenumbers > 0.35 (Figure 6.3c). Therefore, Smith and Sandwell (1997) bathymetry data are utilized for the analysis.

### 6.2.1 Sediment Correction

North of 2°N latitude, the Ninetyeast Ridge is partly covered by sediments; therefore it is necessary to correct bathymetry and gravity data for the sediments before attempting flexural modeling or admittance analysis. Seismic reflection results across the Ninetyeast Ridge are reasonably available north of 10°N latitude, whereas south of 10°N very few seismic sections are available. Therefore, the sediment corrections were carried out using sediment isopach maps published by Levchenko et al. (1993) and Curray (1994). The isopach maps suggest that north of 2°N, the thickness of sediments on the flanks of the Ninetyeast Ridge progressively increases from 1 to 4 km and at 10°N ridge crest is buried under the Bengal Fan sediments. The gravitational effects of the sediments were computed using Parker's method (Parker, 1972) and subtracted from the observed gravity anomaly data. The observed and corrected gravity anomaly and bathymetry data along profile S52 is shown in Figure 6.4a.

### 6.2.2 Slab Residual Gravity Anomaly Computation

The process of lithospheric subduction below an arch-trench system is known to affect gravity on the surface and also some distance away from the trench (Grow and Bowin, 1975). This is probably a consequence of thermal effects of cold oceanic lithosphere along the Benioff Zone (Minear and Toksoz, 1970), which may produce long-wavelength gravity anomalies of 50-100 mGal. Following the procedure of Furse and Kono (2003), the gravity effect of the subducting lithosphere into the Sunda Trench is computed. The subducting plate geometry considered in the present computation is similar to the one followed by

Radhakrishna et al. (2008) in their computations. The subducting lithospheric slab is assumed to be ~70 km thick below the crust of ~22 km thick (Figure 6.4b). A density contrast of 0.065 gm/cc between lithosphere and asthenosphere is considered for the computation (Radhakrishna et al., 2008). The gravity anomaly due to the subducting slab reveals a symmetrical long-wavelength anomaly with a maximum of 80 mGal (Figure 6.4b). The slab gravity effect thus computed is subtracted from the observed free-air gravity data for profiles north of 2°N.

## 6.3 Bathymetry and Gravity Anomalies of the Ninetyeast Ridge

The seafloor topography and gravity field of the Ninetyeast Ridge are clearly depicted in the satellite derived bathymetry and gravity data, respectively (Figures 6.1 and 6.2). Apart from the ridge structure, several near N-S trending fracture zones, individual seamounts, and Andaman Island Arc system are the other major tectonic features are clearly seen in the data. The width of the Ninetyeast Ridge is, in general, 200 km wide and the ridge rises to 2-3 km above the adjacent seafloor. The ridge is associated with relatively low-amplitude gravity anomalies compared to its elevation, indicating the state of isostatic compensation at deeper depths. However, the morphology and gravity anomaly signatures along the ridge are quite variable.

South of 10°S latitude, the ridge topography is very prominent with an average width and relief of ~200 km and 3 km, respectively (Figure 6.1). The southernmost part of the ridge is connected with E-W trending Broken Ridge at about 30°S. The shallowest part of the Ninetyeast Ridge is located near 25°S where the water depth is about 1500 m. The ridge continues between 20°S to 10°S with the Osborne Knoll adjoining west of the ridge at 15°S latitude. The Osborne Knoll is a flat-topped circular topographic high with approximate radius of 150 km and relief of about 3.4 km. Seismic reflection studies south of Osborne Knoll reveals that the eastern edge of the Ninetyeast Ridge is steeply faulted (Sclater and Fisher, 1974; Krishna et al., 2001b). It is also observed that the deep scarp of about 2 km fault plane observed along the eastern edge of the Ninetyeast Ridge coincides with the 89°E FZ. The gravity anomalies generally follow the trend of the bathymetry

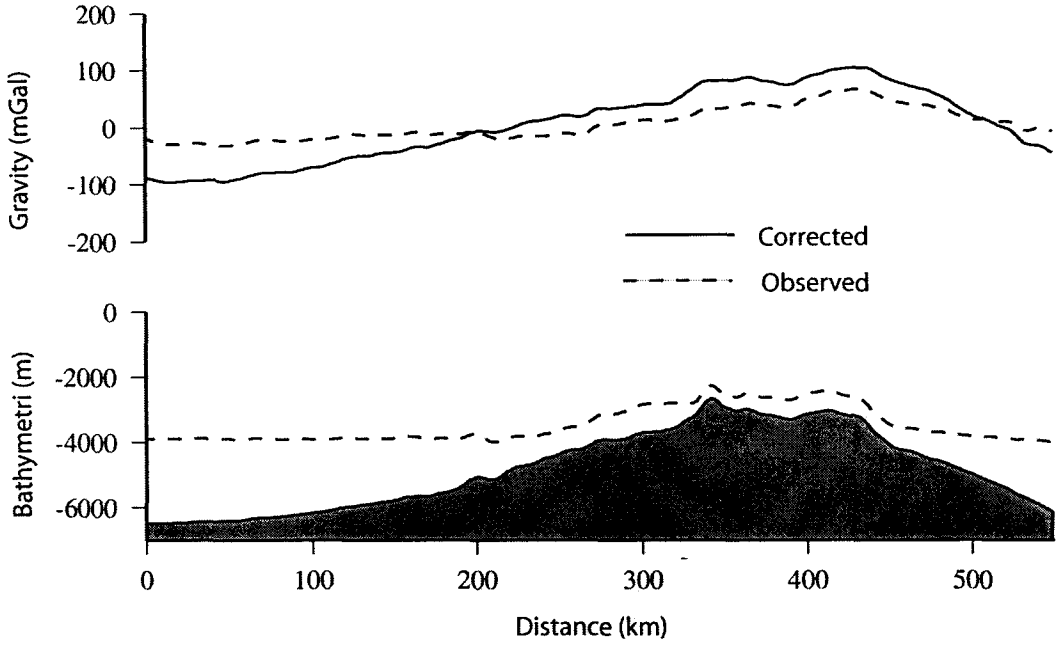


**Figure 6.4a** Observed bathymetry and gravity anomaly of Profile S52 along with sediment corrections.

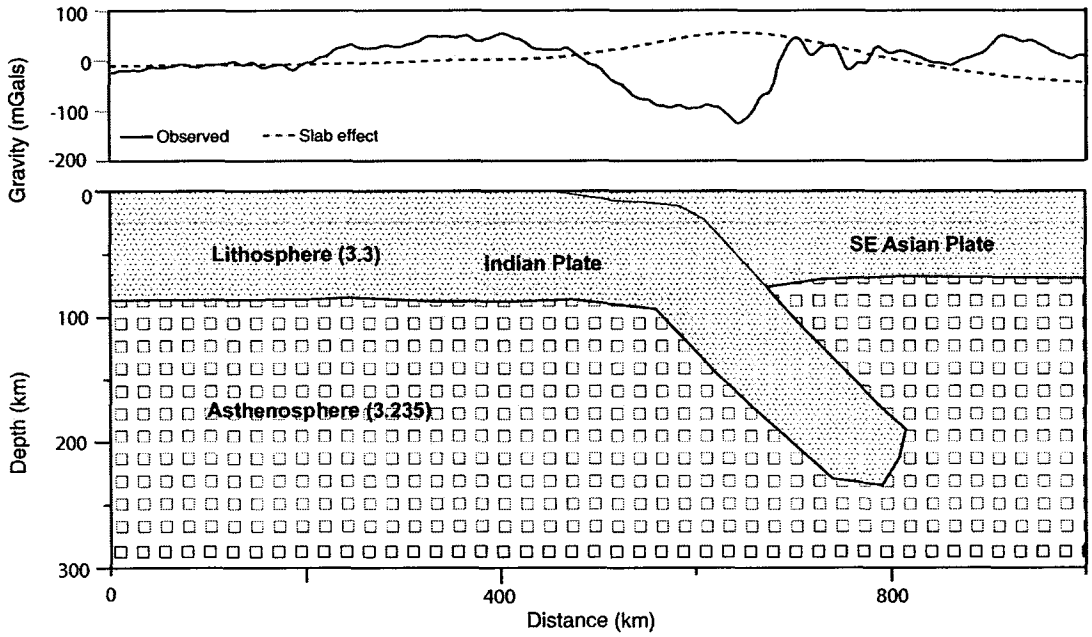


**Figure 6.4b** Computation of the gravity effect of the subducting Indian Ocean lithosphere.

(Figure 6.2) with variable amplitudes of 50-75 mGal along the ridge crest. A deep gravity low of about -75 mGal is observed on east of the Ninetyeast Ridge. N-S oriented narrow gravity lineations associated with the fracture zones along 90°E, 92°E, 94°E and 96°E longitudes are clearly seen in the satellite gravity image (Figure 6.2).

The central part of the Ninetyeast Ridge (10°S to equator) has distinct morphology with relatively smaller width (~100 km) isolated rises. The eastern edge of the central part of the ridge, unlike to the southern part, is not deeply faulted, whereas the western flank shows deeper scraps of about 1 km (Bowin, 1973; Krishna et al., 2001b). The gravity field along this part of the ridge is also highly variable corresponding to the seafloor morphology. The amplitude of the gravity anomaly as low as 25 mGal, is observed over the minimum relief (1 km) of the ridge in the central part.

North of the equator, the Ninetyeast Ridge appears as en-echelon blocks controlled by NE–SW faults. In this sector the ridge morphology is quite prominent with ~2 km relief. From the bathymetry data, the ridge is traceable up to 10°N and further north it is buried under the Bengal Fan sediments. Northward its sub-surface extension is traceable from seismic sections up to 18°N (Curray et al., 1982; Gopala Rao et al., 1997; Maurin and Rangin, 2009; Michael and Krishna 2011) and further north, the ridge seems to be vanishing. The Ninetyeast Ridge separates the Bengal Fan into two lobes: the western is the main lobe of the fan and the eastern lobe is called the Nicobar Fan (Hamilton, 1979). The gravity field along the ridge in this sector is variable with isolated peaks of amplitude >50 mGal associated with the ridge crest. North of 8°N the gravity field is subdued possibly due to sediment cover over the ridge structure. The ridge appears to impinge the subduction zone at about 6°–10° N latitude (Subrahmanyam et al., 2008).

## 6.4 Elastic Plate Thickness along the Ninetyeast Ridge

Isostatic compensation mechanisms that took place beneath the Ninetyeast Ridge are examined using two different approaches: 1) flexural modeling along closely spaced profiles to determine Te values along the ridge 2) admittance analysis to understand the

overall state of isostasy along the ridge. A total of 18 ship-borne and 54 satellite profiles of bathymetry and free-air gravity data crossing the Ninetyeast Ridge between 28°S and 10°N with an interval of about 50 km were selected for this analysis. For spectral estimations, the bathymetry and gravity profiles were projected perpendicular to the strike of the ridge and their length is restricted to 800 km keeping ridge crest in the centre. Short ship-borne profiles were extended out on both sides to this length in order to include in the study. The data were interpolated at 2.2 km and the mean including linear trend was removed. The profiles ends were tapered using a cosine window of 10% profile length prior to the spectral estimation.

### 6.4.1 Flexural Modeling

Gravity anomalies observed at the sea surface are sensitive to both the topographic loads and the deflections at the Moho boundary. The relationship between the topographic loads and underlying Moho deflections as well as the gravity response to each can be described in Fourier Domain considering the elastic plate approximations as described in Chapter 3. The gravity effect of the bathymetry and its compensation is computed for a range of Te values. The computed gravity anomalies are compared with the observed gravity anomalies and the best fitting Te values along with their lower and upper bounds are chosen by considering the wavelength, amplitude and minimum RMS error criteria. The model parameters used for the computations of flexural model is listed in Table 6.1. The flexural modeling along closely spaced gravity profiles is expected to bring the spatial variations in Te, incase exist, whereas admittance analysis requires averaging of profiles and gives the overall sate of isostasy. However, flexural modeling is more sensitive to the errors in bathymetry and gravity measurements. In this study, the quality of data is ensured by comparing different sources of data at cross over points. The Te values obtained by flexural modeling for all the profiles are summarized in Table 6.2.

The range of Te values thus, obtained along the Ninetyeast Ridge is presented in Figure 6.5. The overall parabolic trend of the curve, in general, suggests that the central part of the ridge is associated with low Te values, whereas the northern and southern parts are

associated with higher Te values (Figure 6.5). The southernmost part of the Ninetyeast Ridge between 18°S and 28°S is associated with Te values of 10-20 km. In the central part between 2°N and 20°S, the Te values are extremely variable (2-25 km). A careful examination of the curve suggests two distinct features within the central part 1. between

**Table 6.1** Model parameters used for the flexural computations

| *Parameter* | *Value* |
|---|---|
| Density of Sea-Water ($\rho_w$) | 1.03 gm/cc |
| Density of load ($\rho_l$) | 2.5 gm/cc |
| Density of oceanic crust ($\rho_c$) | 2.90 gm/cc |
| Density of mantle($\rho_m$) | 3.30 gm/cc |
| Average crustal thickness (t) | 7 km |
| Young's modulus (E) | 100 Gpa |
| Poisson's ratio ($\sigma$) | 0.25 |
| Universal gravitational constant (G) | $6.67.10^{-11}$ $Nm^2kg^{-2}$ |
| Acceleration due to gravity (g) | 9.8 $ms^{-2}$ |

18°S and 8°S, Te values of the ridge linearly decreases from 20 km to 5 km, and 2. between 8°S and 2°N, Te values are extremely variable ranging from 2 to 25 km. The northern part of the ridge (north of 2°N) is associated with high Te values of 18-30 km. Thus, based on range of Te values, the Ninetyeast Ridge between 28°S and 8°N could be divided into four distinct parts: Southern part (south of 18°S), south-central part (18°S to 8°S), north-central part (8°S to 2°N) and northern part (north of 2°N) for the discussion of isostasy of the ridge structure. Highly variable Te values for north-central part were further confirmed by Te estimations along 13 additional satellite profiles (Figure 6.5).

The results of flexural modeling carried out along eight selected profiles from the entire ridge with the consideration of two profiles from each part are shown in Figures 6.6a and b. For profiles V1811, S12, A20931 and V3305 the match between observed gravity and best-fit gravity is fairly good except along the eastern edge of the ridge (Figure 6.6a). This could be due to the effect of the 89°E FZ bounding the eastern edge of the Ninetyeast Ridge (Krishna et al., 2001b). Highly variable Te values obtained along the north-central part of the ridge is evident from the contrasting Te values obtained along SK 28-3 (Te=3

**Table 6.2** Best fit Te values along with their lower and upper bounds along Ninetyeast Ridge (south to north) obtained by flexural modeling. The latitudes given in the table are projected latitude.

| No | Profile Name | Latitude | Te (km) Lower | Best Fit | Upper |
|---|---|---|---|---|---|
| 1 | S1 | -27.5 | 13 | 14 | 15 |
| 2 | S2 | -27.13 | 12 | 13 | 14 |
| 3 | S3 | -26.75 | 15 | 15.5 | 16 |
| 4 | S4 | -26.2 | 14 | 15 | 16 |
| 5 | V1811 | -26 | 14 | 15 | 16 |
| 6 | S5 | -25.5 | 14 | 15 | 16 |
| 7 | S6 | -25 | 11 | 12 | 13 |
| 8 | S7 | -24.5 | 11 | 12 | 13 |
| 9 | S8 | -24 | 11 | 12 | 15 |
| 10 | S9 | -23.5 | 14 | 15 | 16 |
| 11 | S10 | -23 | 17 | 17.5 | 19 |
| 12 | S11 | -22.5 | 17 | 18 | 19 |
| 13 | S12 | -22 | 20 | 21 | 22 |
| 14 | S13 | -21.7 | 19 | 20 | 21 |
| 15 | DME10 | -21 | 9 | 10 | 12 |
| 16 | S14 | -20.5 | 9 | 10 | 11 |
| 17 | S15 | -20 | 11 | 12 | 13 |
| 18 | S16 | -19.5 | 11 | 12 | 13 |
| 19 | S17 | -19 | 14 | 15 | 16 |
| 20 | S18 | -18.5 | 18 | 18.5 | 19 |
| 21 | A20931 | -18 | 20 | 21 | 22 |
| 22 | S19 | -17.5 | 20 | 20.5 | 21 |
| 23 | S20 | -17 | 16 | 17 | 18 |
| 24 | S21 | -16.5 | 14 | 15 | 16 |
| 25 | S22 | -16 | 14 | 15 | 16 |
| 26 | S23 | -15.5 | 14 | 15 | 16 |
| 27 | S24 | -15 | 15 | 16.5 | 18 |
| 28 | S25 | -14.5 | 9 | 10 | 11 |
| 29 | S26 | -14 | 11 | 12 | 13 |
| 30 | S27 | -13.5 | 11 | 12 | 13 |
| 31 | V3305 | -13.4 | 10 | 10.5 | 11 |
| 32 | S28 | -13 | 11 | 12 | 13 |
| 33 | S29 | -12.5 | 10 | 12 | 13 |
| 34 | S30 | -12 | 10 | 12 | 13 |
| 35 | S31 | -11.5 | 10 | 10 | 12 |
| 36 | V2410 | -11 | 9 | 10 | 12 |
| 37 | p84 | -10.6 | 5 | 6 | 8 |
| 38 | S32 | -9.5 | 5 | 6 | 7 |
| 39 | S33 | -9 | 6 | 6.5 | 7 |
| 40 | S34 | -8.5 | 5 | 6 | 7 |
| 41 | SK28-1 | -7.8 | 5 | 5.5 | 6 |
| 42 | S35 | -7.4 | 2 | 3 | 4 |
| 43 | S36 | -7 | 13 | 13.5 | 15 |
| 44 | SK28-2 | -6.6 | 20 | 21 | 22 |
| 45 | V3616 | -6 | 14 | 17 | 19 |
| 46 | S37 | -5.6 | 1 | 2 | 4 |
| 47 | V2901 | -5.5 | 20 | 21 | 22 |
| 48 | SK28-3 | -5 | 3 | 3.5 | 4 |
| 49 | S38 | -5 | 1 | 3 | 4 |
| 50 | S39 | -4.6 | 4 | 6 | 7 |
| 51 | Chi4 | -4 | 25 | 27.5 | 30 |
| 52 | S40 | -4 | 25 | 27.5 | 30 |
| 53 | Sk28-4 | -3.9 | 25 | 27.5 | 28 |
| 54 | S41 | -3.4 | 4 | 5 | 6 |
| 55 | S42 | -2.9 | 5 | 7 | 8 |
| 56 | Dme7-1 | -2.5 | 2 | 3.5 | 5 |
| 57 | Chi2 | -2 | 3 | 4 | 5 |
| 58 | V3308 | -1.9 | 2 | 3 | 5 |
| 59 | S43 | -1.5 | 8 | 9 | 10 |
| 60 | Chi1 | -1 | 18 | 20 | 21 |
| 61 | S44 | -0.5 | 13 | 14 | 15 |
| 62 | S45 | 0.75 | 9 | 10 | 11 |
| 63 | S46 | 1 | 15 | 16 | 17 |
| 64 | S47 | 1.5 | 10 | 12 | 13 |
| 65 | Dme7-2 | 2 | 24 | 25 | 26 |
| 66 | S48 | 2.5 | 17 | 18 | 19 |
| 67 | S49 | 3 | 19 | 20 | 22 |
| 68 | S50 | 4 | 16 | 19 | 20 |
| 69 | S51 | 5 | 15 | 16.5 | 18 |
| 70 | S52 | 6 | 25 | 26 | 30 |
| 71 | S53 | 7 | 27 | 28 | 32 |
| 72 | S54 | 8 | 29 | 30 | 33 |

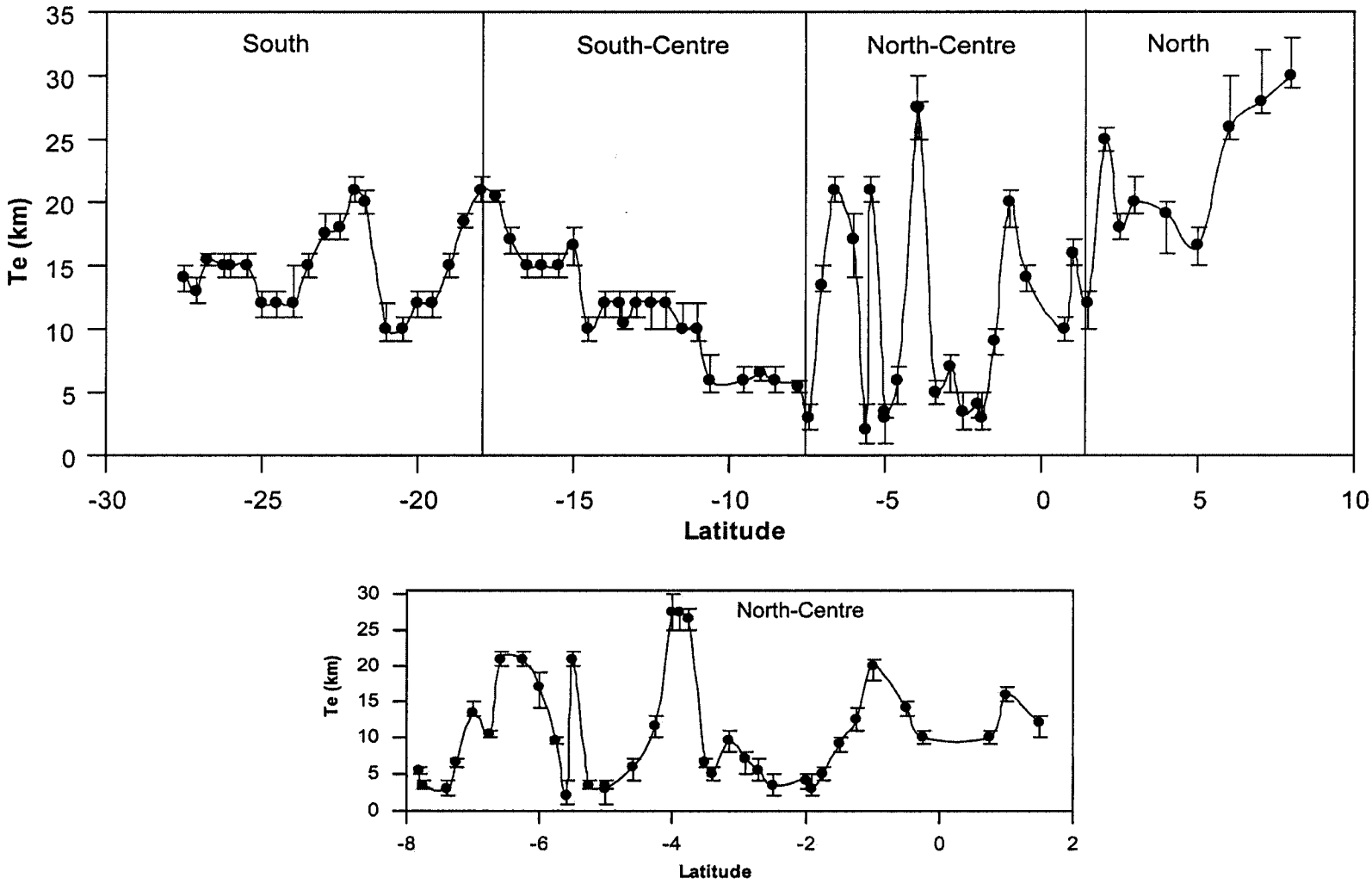


**Figure 6.5** Variations of Te values derived from flexural modeling along Ninetyeast from 28°S to 8°N. Te values derived for North-Central part using additional satellite profiles are shown separately. The error bars represents lower and upper bounds of Te estimation as given in Table (6.2).

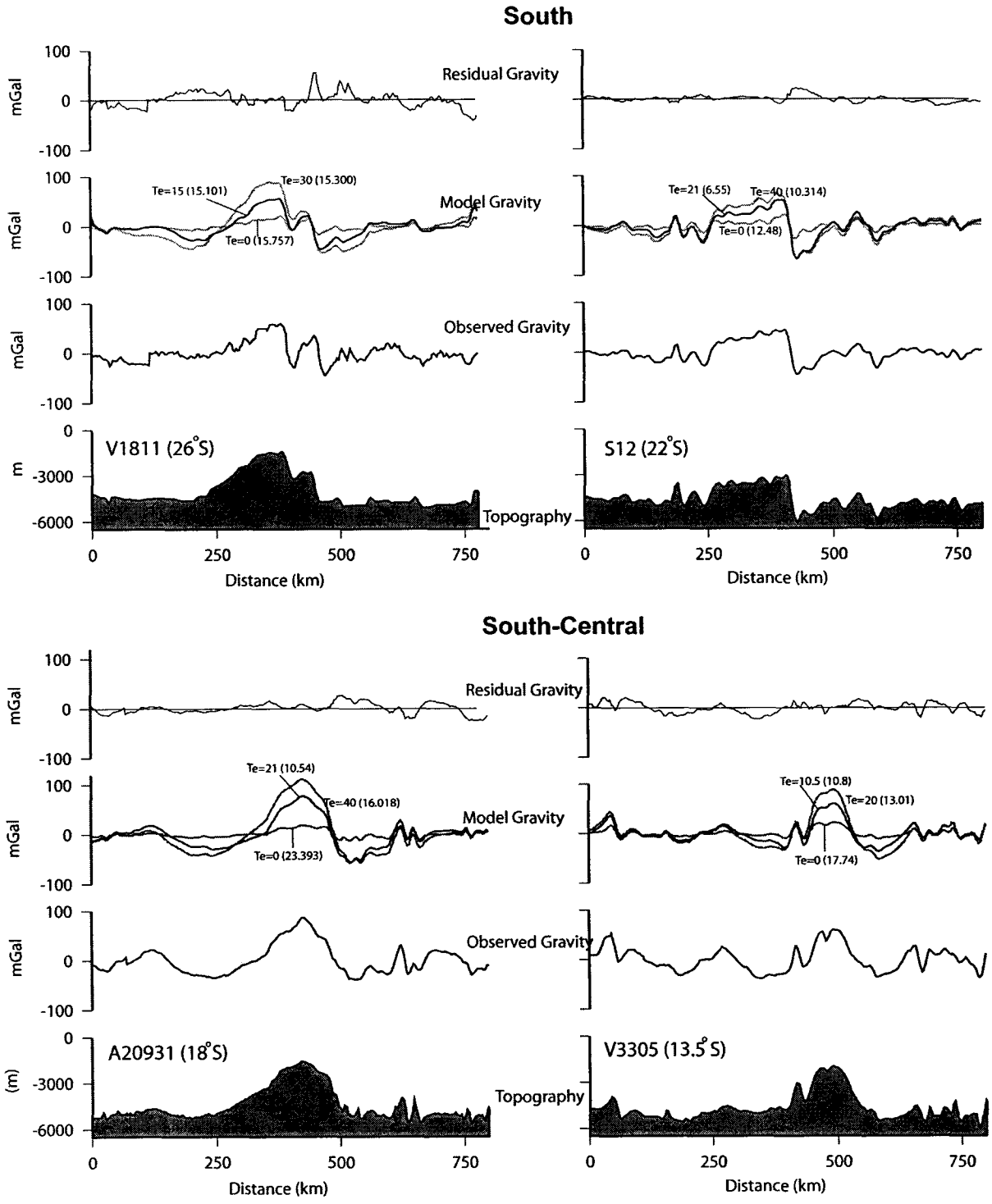


**Figure 6.6a** Flexural modeling along selected profiles from south and south-central part of the Ninetyeast Ridge. The best fitting gravity anomalies is represented by dark line. The values in bracket represent the rms error between observed and computed gravity anomalies. The residual gravity anomaly for the best fitting Te is also shown.

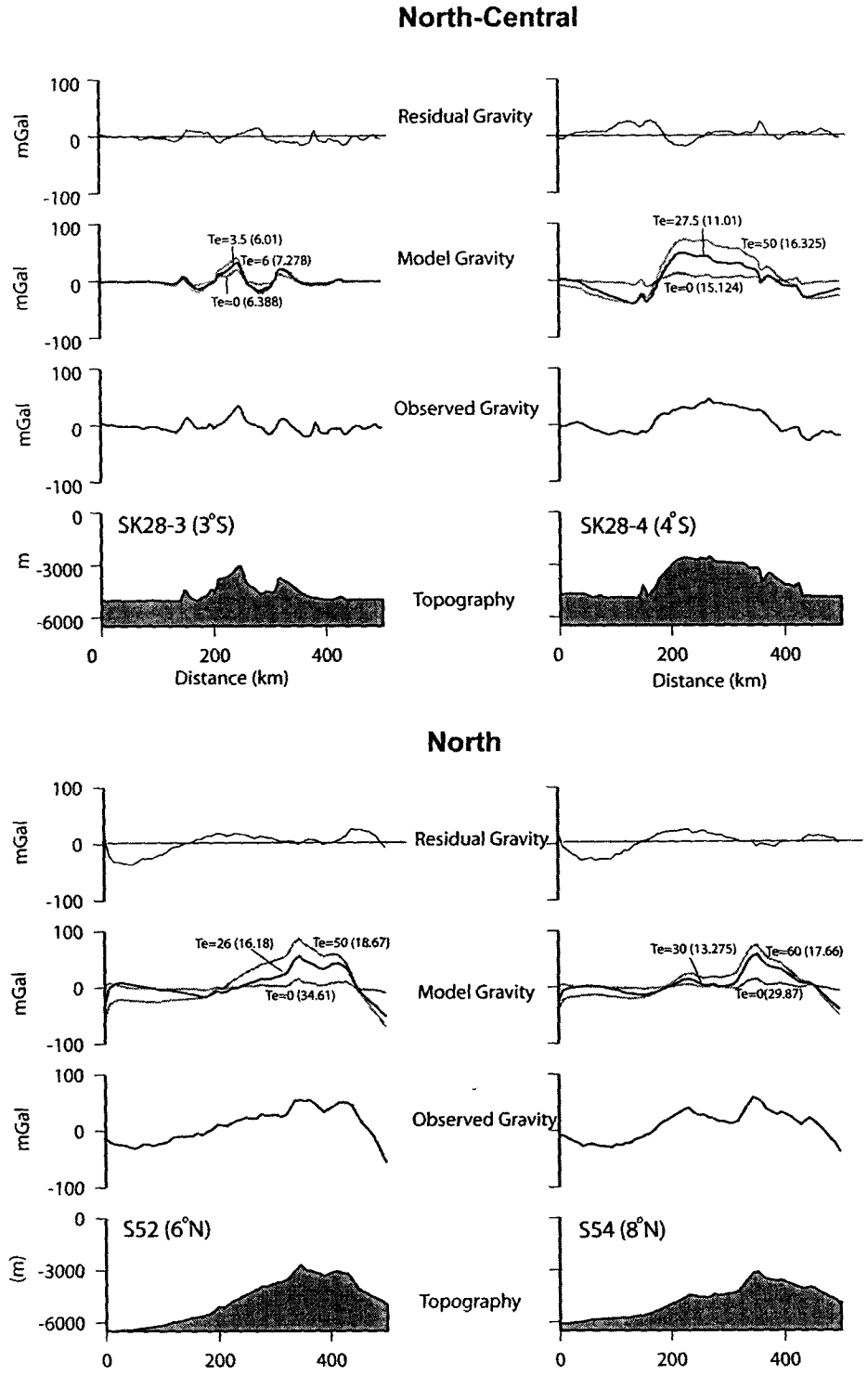


**Figure 6.6b** Flexural modeling along selected profiles from north-central and northern part of the Ninetyeast Ridge. Notations are same as given in Figure 6.6a

km) and SK 28-4 (Te=25 km) (Figure 6.6b). Compared to southern profiles the fit between observed and computed gravity anomalies in the northern part of the ridge is relatively less (Figure 6.6b). This could be due to the errors in the sediment correction applied to the bathymetry and gravity data. The variable isostatic response of the Ninetyeast Ridge and its structural and tectonic implications are discussed in detail in sections 6.5 and 6.6.

### 6.4.2 Admittance Analysis

The theory and basic computational procedures for the admittance analysis were discussed in detail in Chapters 3 and 4. The admittance estimates along each profile need to be averaged before comparing with the theoretical models. The profiles were selected according to the Te ranges estimated from flexural modeling for the purpose of averaging. The $\log_{10}$ of the amplitude of admittance, coherence and phase along with coherent and incoherent gravitational energies for each region is presented in Figures 6.7a, b, c and d. The amplitude of the admittance decreases at lower wave-numbers, indicating isostatic compensation at deeper depths. The most reliable waveband within which the observed admittance values can be compared with theoretical values, is selected based on high coherence ($\gamma_{(k)}{}^2 > 0.5$), phase close to zero and dominating coherent gravitational energy.

The mean density and water depth for each region is determined from the slope and intercept of the linear least square fit to the log-linear plot of the admittance (Table 6.3). The estimated densities (~2.36 gm/cc) are lower than the typical oceanic crustal densities (2.7 gm/cc). However, seismic refraction and Ocean Bottom Seismometer data from the central part of the Ninetyeast Ridge suggested densities of about 2.3 and 2.6 gm/cc for oceanic crustal layers 2A and 2B respectively (Krishna et al., 2001b). The densities derived from the admittance are only indicative of the densities of the upper most, fractured part of the ridge crust. Hence, for theoretical modeling an average density of 2.5 gm/cc is used and this represents the bulk density of load ($\rho_l$) (Table 6.1). The water depth derived from the admittance is in excellent agreement with the observed water depth except for the north central part of the ridge, where the difference is about 1200 m (Table 6.3).

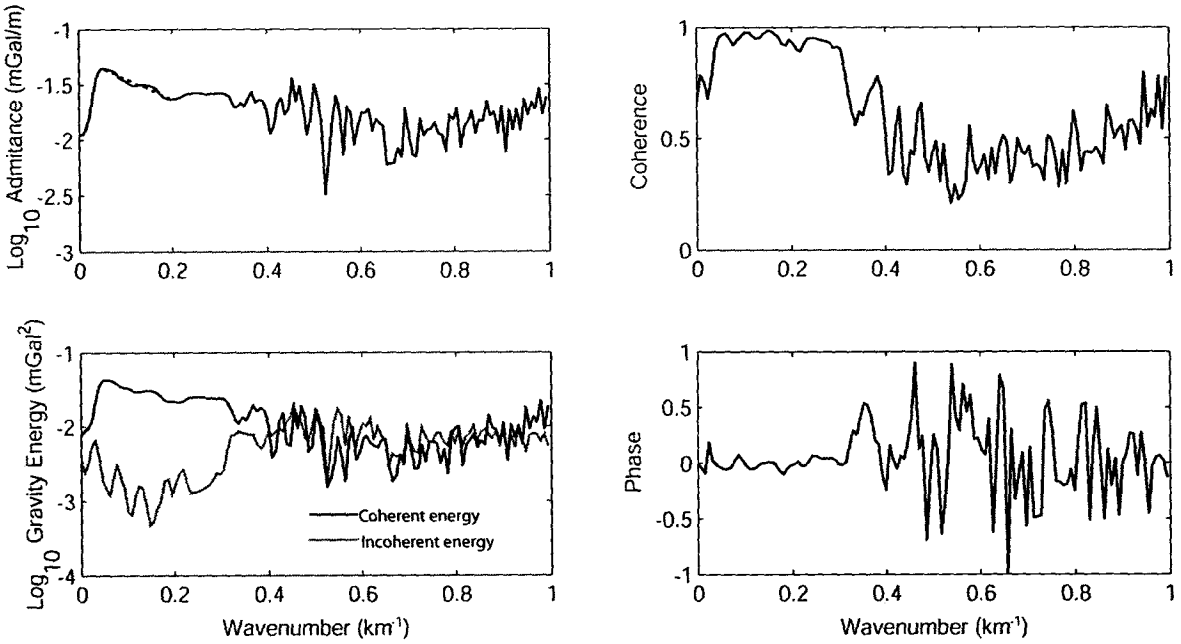


**Figure 6.7a** Observed admittance, coherence, phase and gravitational energy plots for southern part of the Ninetyeast Ridge

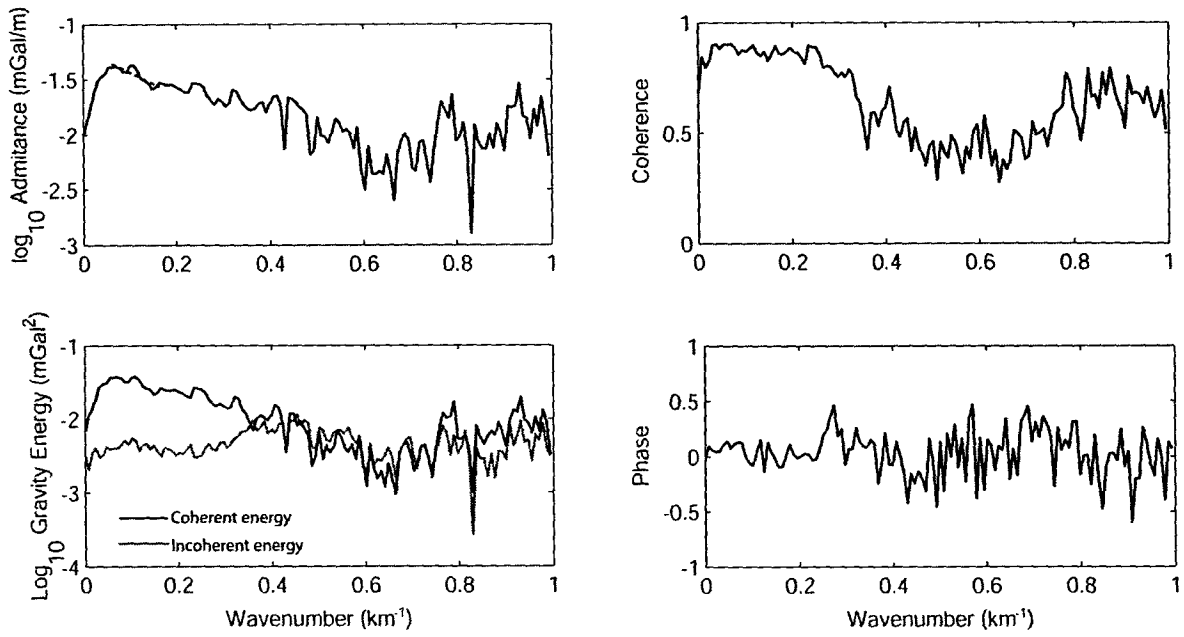


**Figure 6.7b** Observed admittance, coherence, phase and gravitational energy plots for the south-central part of the Ninetyeast Ridge

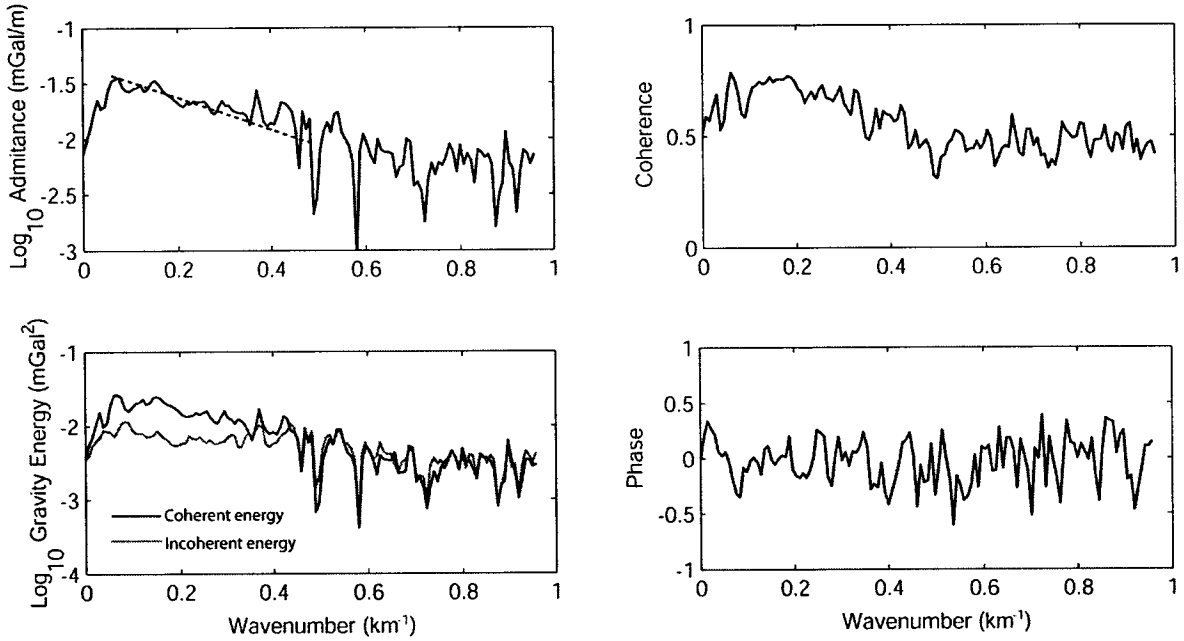


**Figure 6.7c** Observed admittance, coherence, phase and gravitational energy plots for the north-central part of the Ninetyeast Ridge.

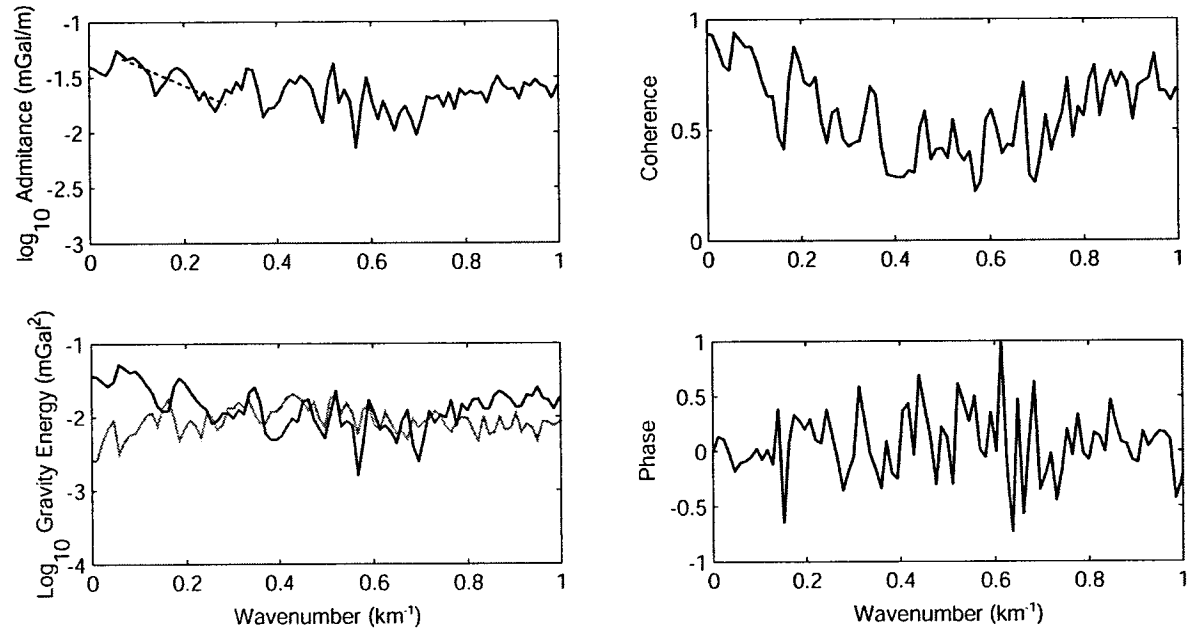


**Figure 6.7d** Observed admittance, coherence, phase and gravitational energy plots for the northern part of the Ninetyeast Ridge.

**Table 6.3** mean density and water depth derived from the slope and intercept of admittance

| *Region* | *Water depth (m)* | | | *Density (gm/cc)* | |
|---|---|---|---|---|---|
| | *Derived* | *Observed* | *Observed-Derived* | *Derived* | *Observed* |
| South | 4350 | 4277 | -73 | 2.343 | --- |
| South-Central | 4782 | 4526 | -256 | 2.450 | 2.3 (layer2A)-2.6(layer2B) |
| North-Central | 3343 | 4550 | 1207 | 2.115 | |
| North | 4324 | 4620 | 304 | 2.537 | --- |

Theoretical and observed admittance values with standard error bars are presented in Figures 6.8a, b, c and d. For southern region (Figure 6.8a), the flexure model with elastic plate thickness (Te) of 12 km appears to fit well with the observed admittance for a waveband of $0.015 < k < 0.04$. For the same waveband, the Airy model poorly fits with the admittance values for $t > 35$, therefore this model is not considered.

The observed admittance for the south-central part of the ridge is best explained by the Airy model with a crustal thickness of about 20 km (Figure 6.8b). Using seismic refraction and gravity data, Krishna et al. (2001b) and Grevemeyer et al. (2001) have found that the crust beneath the Ninetyeast Ridge in the south-central part consists of anomalous thickness of more than 20 km. On the other hand flexural modeling suggests conflicting Te values ranging from 5 to 15 km. Earlier admittance results in this part of the ridge suggested that the ridge structure has Airy isostatic compensation with a crustal thickness of 25 km (Tiwari et al., 2003) and underplating on a weak elastic plate of Te=5 km (Grevemeyer and Flueh, 2000). The present analysis is unable to distinguish between these models, but supports the Airy model of compensation.

For the north-central part of the Ninetyeast Ridge the observed admittance values are in agreement with the Airy model with a crustal thickness of about15 km (Figure 6.8c), whereas for the northern part of the ridge the observed admittance values neither match with a simple Plate model or Airy model. Hence, an attempt has been made to match the

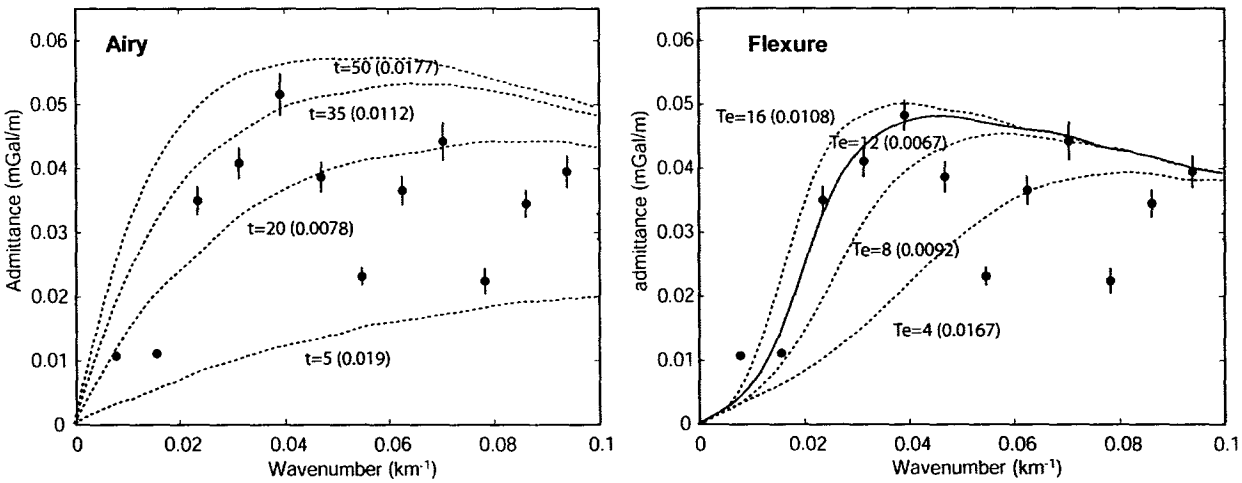


**Figure 6.8a** Observed admittance (solid dots) with standard error bars generated from profiles in the southern part of the Ninetyeast Ridge plotted with Airy and Flexure models. The RMS error in mGal/m between the observed and theoretical admittance for various t and Te values are shown in bracket. The best fit model curve is shown as continues line.

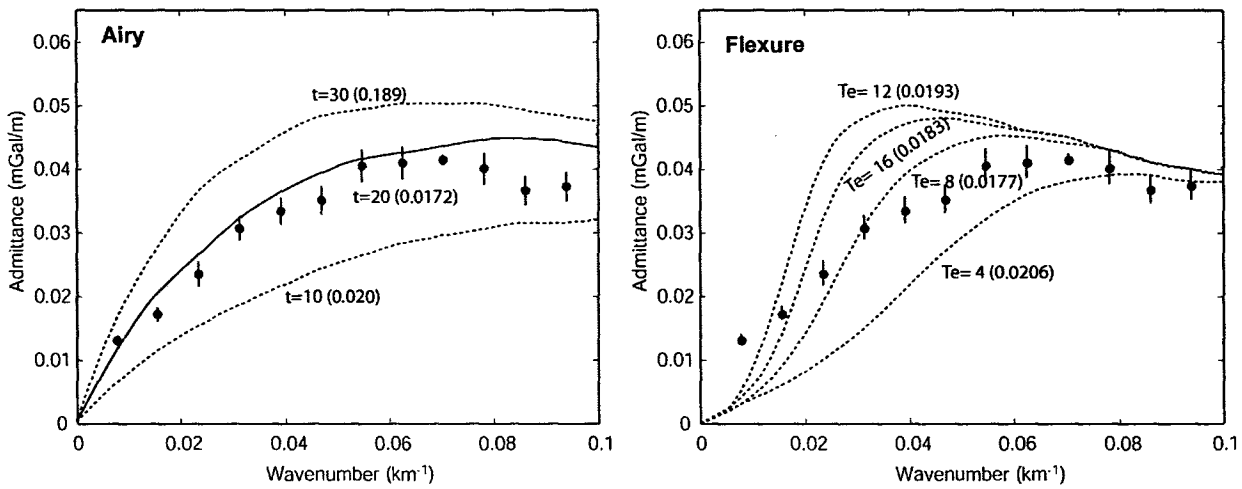


**Figure 6.8b** Observed admittance (solid dots) with standard error bars generated from profiles in the south-central part of the Ninetyeast Ridge plotted with Airy and Flexure models. Notations are same as given in Figure 6.8a

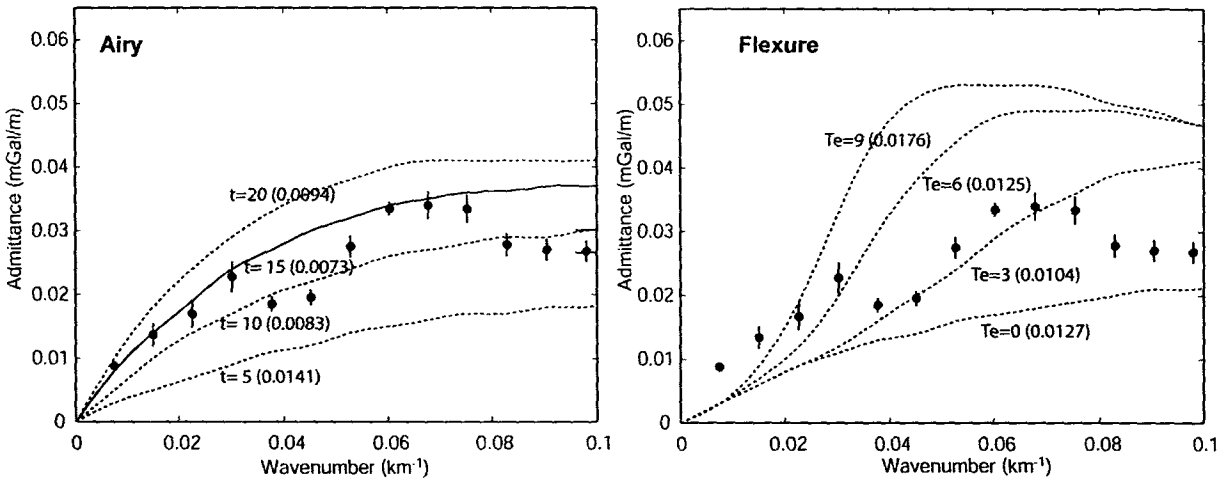


**Figure 6.8c** Observed admittance (solid dots) with standard error bars generated from profiles in the north-central part of the Ninetyeast Ridge plotted with Airy and Flexure models. Other notations are same as Figure 6.8a

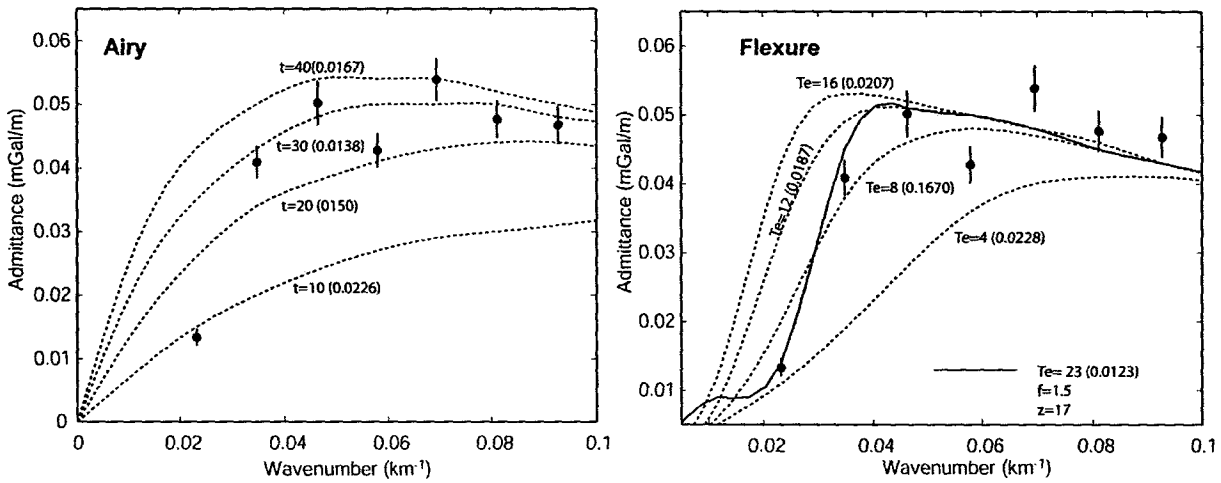


**Figure 6.8d** Observed admittance (solid dots) with standard error bars generated from profiles in the south-central part of the Ninetyeast Ridge plotted with Airy and Flexure models. Admittance values with coherence >0.5 is only shown. Notations are same as given in Figure 6.8a

observed admittance values with an elastic plate model with the consideration of both surface and subsurface loading. A reasonably good match is observed for Te=23 km with subsurface to surface loading ratio f = 1.5 and depth to the buoyant load z =18 km (Figure 6.8d).

## 6.5 Crustal Structure of the Ninetyeast Ridge

The admittance results suggest an Airy model for the central part of the Ninetyeast Ridge with t =15-20 km and flexural model for southern (Te>10) and northern (Te~23) parts of the ridge. In order to further investigate the crustal structure of the ridge two-dimensional gravity forward modeling has been carried out along five profiles: V1811, V3305, SK28-3, SK28-4 and S52. The locations of these profiles are shown in Figure 6.1 and the derived crustal models are shown in Figures 6.9 to 6.13.

For modeling of profiles V1811, V3305, SK28-3 and SK28-4 (Figures 6.9, 6.10, 6.11 and 6.12), densities and thickness of oceanic crustal layers have been considered from the published seismic refraction and OBS results of the central part of the Ninetyeast Ridge (Krishna et al., 2001b; Grevemeyer et al., 2001). Both of these studies, in general, suggest the oceanic layer 2A with anomalous velocities ranging from 3.4 to 4 km/s, and layers 2B and 3A are with velocities 4.7-5.7 and 6.4-6.8 km/s, respectively. Grevemayer et al. (2001) interpreted the layers 2A and 2B together as intrusive/ extrusive and layer 3A as pre-hotspot crustal layer. Both of these studies further reveal presence of the anomalous crustal layer 3B with velocities 7.3-7.8 km/s. In terms of thickness of crustal layers, both studies show consistent results in the Central Indian and Wharton basins adjacent to the Ninetyeast Ridge, but considerably vary beneath the ridge. For profile S52 (Figure 6.13), seismic velocity information is not available, hence only the sediment thickness details (Levchenko et al., 1993; Curray, 1994) were considered for gravity modeling.

The crustal structure along the profile V1811 derived from gravity modeling is shown in Figure 6.9. The thickness of layer 2A beneath the ridge is anomalously high (~5 km) with a low density of 2.32 gm/cc corresponding to the seismic velocities of 3.4-4.3 km/s. The

low seismic velocities of the Ninetyeast Ridge were earlier (Krishna et al., 2001b) attributed to the changes in physical properties of the ridge material due to intense weathering after its formation above sea-level followed by subsidence. The present gravity model (Figure 6.9) suggest that the crustal load is supported by down flexing of crustal layers 2A, 2B and 3A with amplitude of about 2.5-3 km. The flexure of crustal layers and Moho boundary is sliced by the 89°E FZ along the eastern edge of the ridge. This was attributed to the movement of lithospheric blocks between the fracture zones due to the extensional and compressional stresses generated by the ridge jumps (Krishna et al., 2001b). Further east, the Ninetyeast FZ is also manifested by downward flexing of the crustal and Moho boundaries. This crustal model results are in excellent agreement with the results derived by the flexural model and admittance analysis.

The gravity model of the Ninetyeast Ridge along profile the V3305 (Figure 6.10) suggests very thick (20 km) oceanic crust beneath the ridge consisting layers 2A, 2B and 3A along with underplated body of ~10 km thick. The density of underplated material is considered as 3.05 gm/cc following the earlier results (Bowin, 1973; Mukhopadhyaya and Krishna, 1991; Krishna, et al., 2001b). Normal crustal thickness of 7 km is observed for the oceanic crustal region adjacent to the Ninetyeast Ridge. The admittance analysis of the south-central part of the ridge also suggests crustal thickness of ~20 km. The ridge may have emplaced on a weak and hot lithosphere, which in turn allows accretion of magma as underplated material within the lower crustal layer. The excess magma mixes with the hot crustal rocks and becomes over-thickened crustal layer 3. Seismic refraction and OBS studies of Krishna et al. (2001b) and Grevemeyer et al., (2001) also suggest anomalous crustal thickness beneath the central part of the Ninetyeast Ridge.

The crustal structure results of the Ninetyeast Ridge along the profile SK 28-3 are almost similar to that of the profile V3305, where the observed gravity anomaly is explained by thickened crust beneath the ridge (Figures 6.11 and 6.10). Gravity model along the profile SK 28-4, which lies ~100 km north of the profile SK28-3 within the north-central region, shows altogether a different crustal structure, where the volcanic load is supported by down-flexing of crustal layers only (Figure 6.12). The crustal model results are in good

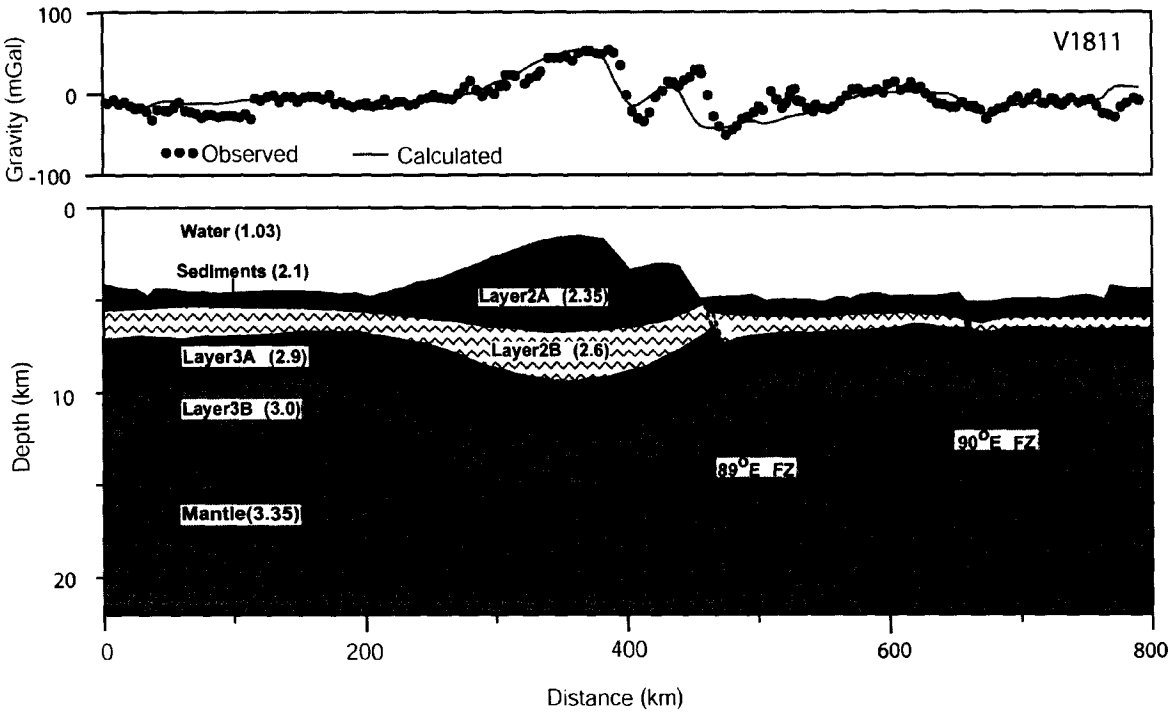


**Figure 6.9** Two-dimensional gravity model with interpreted crustal structure along profile V1811. Depth and densities of oceanic crustal layers 2A, 2B, 3A are considered from seismic refraction results of Krishna et al., (2001b) and Grevemeyer et al., (2001). Numerical values within brackets indicate the densities (gm/cc) of different strata.

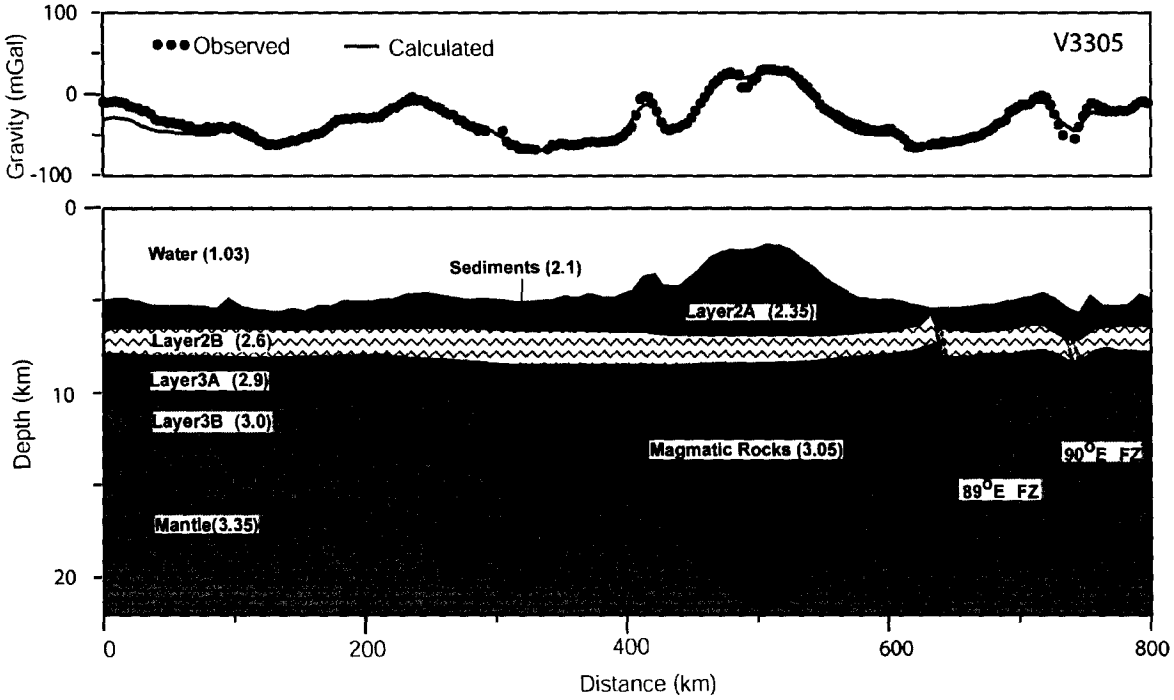


**Figure 6.10** Two-dimensional gravity models with interpreted crustal structure along profile V3305.

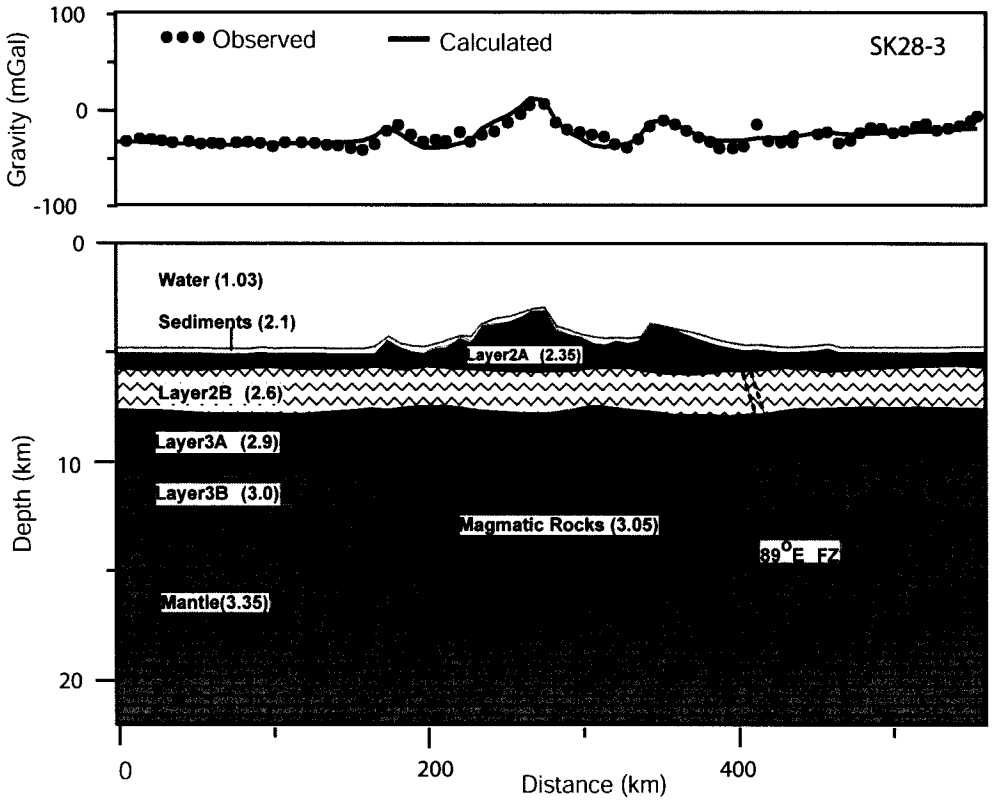


**Figure 6.11** Two-dimensional gravity models with interpreted crustal structure along profile SK28-3.

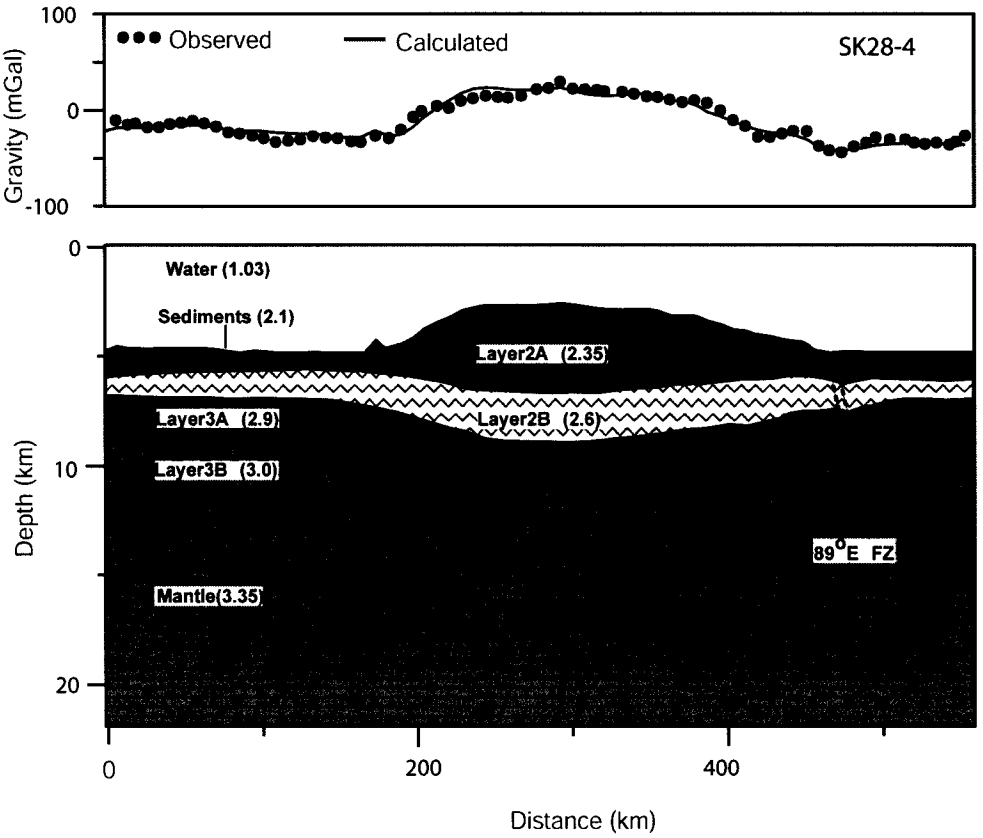


**Figure 6.12** Two-dimensional gravity models with interpreted crustal structure along profile SK28-4.

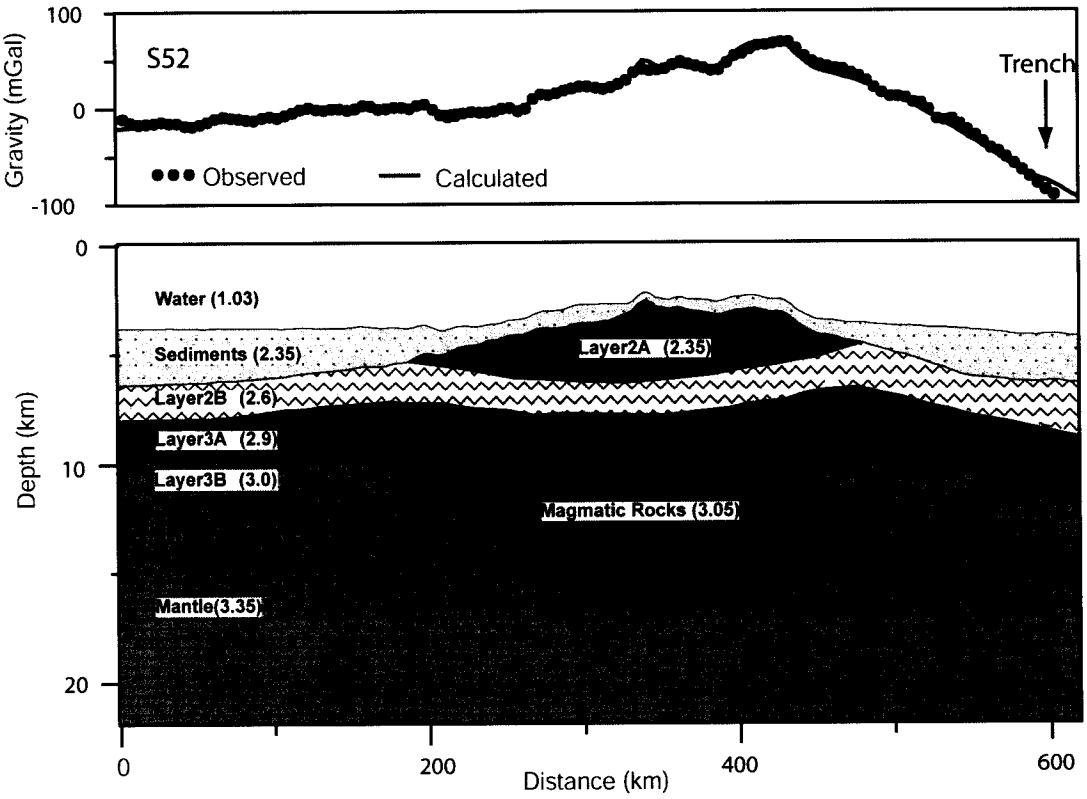


**Figure 6.13** Two-dimensional gravity models with interpreted crustal structure along profile S52. The sediment thickness data along the profile where extracted from the isopach maps of Levchenko et al. (1993) and Curray (1994).

agreement with low and high Te values (3 and 25 km) determined for the profiles SK28-3 and SK28-4 respectively using flexural modeling (Figure 6.6b).

The Ninetyeast Ridge along the Profile S52 in the Bay of Bengal region (6°N) is buried under the Bengal Fan sediments. The thickness of the sediments ranges from 0.5 km over the ridge to about 3 km on either side in basinal regions (Figure 6.13). For gravity anomaly modeling along the profile, average densities of 2.35, 2.7 and 2.95 gm/cc have been considered for sediments, crustal layers 2 and 3, respectively. The model results suggest that the volcanic load (ridge material) is compensated by a broad flexure of the crustal layers with wavelengths greater than that of the ridge. The gravity anomaly trend along the eastern side of the ridge merges with that of the Sunda trench. This is reflected as up-warp of the crustal layers ridge followed by dip toward the trench. The model also suggests presence of low-density mantle rocks of thickness ~4.5 km beneath the ridge. This model is in good agreement with the results of admittance analysis of the northern part of the ridge, which clearly suggest flexural model with surface and subsurface loading. The depth to the buoyant load (z) derived from the admittance analysis matches well with the depth to the low-density mantle.

## 6.6 Variations of Te values along the Ninetyeast Ridge and Geodynamic Implications

Both admittance analysis and flexural modeling of southern part of the Ninetyeast Ridge reveal flexural compensation with Te values >10 km, suggesting an emplacement of volcanic rocks on an intermediately strong lithosphere. Present Te values are differing from the Te values derived by Tiwari et al., (2003), where they have estimated Te=22 km and indicated off-ridge emplacement of the ridge. Their model requires both surface and sub-surface loading. However, the two-dimensional crustal model developed along profile V1811 (~26°S) suggest that the load of the ridge is supported by down flexing of crustal layers with amplitude of about 2.5-3 km with out any subsurface loading (Figure 6.9). It should be noted that "off-ridge" emplacement requires emplacement on a strong plate, which can support the enormous load created by the hotspot as in the case of the Hawaiian Ridge emplacement on the Pacific plate (Watts, 1989; Watts et al., 2006). Plate

reconstruction models of eastern Indian Ocean suggest that south of 11°S the Ninetyeast Ridge evolved along the 89°E FZ (Royer et al., 1991). This fracture zone kept growing along with the northward migration of Wharton spreading centre and acted as a structural and thermal boundary for the magma erupted by the Kerguelen hotspot. This clearly indicates that the eruption must have occurred along a plate which has been weekend by the 89°E FZ and it is difficult to reconcile "off-ridge" scenario for the emplacement of the ridge. The crustal model and isostatic response of the ridge (Figures 6.6a and 6.9) support emplacement on an intermediately strong plate plausibly along the edge of the Indian plate (Royer et al., 1991; Krishna et al., 1999).

The northern part of the Ninetyeast Ridge is also flexurally compensated with high Te values of >20 km, suggesting emplacement of the ridge on a strong lithosphere. The model also includes subsurface loading. The crustal model derived using gravity forward modeling (Figure 6.13) suggests that the magmatic material generated by the Kerguelen hotspot has accreted below the crust providing up-ward bouncy forces, which further support the load of the ridge. It is interesting to note that the underplated material never becomes a part of the crust as observed in the central part of the Ninetyeast Ridge (Figure 6.11). Mukhopadhyay and Krishna (1995) also observed anomalous mass beneath the ridge and opined that they act like "cushion" for the isostatic compensation. Further, using geoid and gravity data analysis Rajesh and Majumdar (2009) observed presence of large volume of hotspot related underplated material below the northern part of the Ninetyeast Ridge. Watts et al. (1985) observed that flexed oceanic crust (Te=25 km) beneath the Hawaiian-Emperor seamount is underlain by a 4 km thick body of anomalous seismic velocities of 7.4-7.8 km/s. The northern part of the Ninetyeast Ridge also seems to possess similar crustal structure.

The plate reconstruction models suggest that the northern part of the Ninetyeast Ridge was emplaced by the Kerguelen hotspot on a relatively old lithosphere formed during the Cretaceous Magnetic Quite Period (Royer et al., 1991). However, based on E-W lineations in the vertical gravity field corresponding to the extrusive features over the Ninetyeast Ridge, Sager et al., (2010) suggested an emplacement of ridge near spreading axis with

successive ridge jumps towards south. This idea probably supports the proposed fossil ridge segments near to the Ninetyeast Ridge suggesting discrete ridge jumps (Desa et al., 2009). However, the idea of ridge jumps beneath the northern part of the Ninetyeast Ridge remains elusive as the magnetic anomalies over the ridge are highly disturbed (Desa et al., 2009).

In contrast to southern and northern parts of the Ninetyeast Ridge, Airy model is suggested for the central part of the ridge with crustal thickness (t) ranging from 15-20 km. This implies that the Te values within this region should be consistently very low. Interestingly, highly variable Te values are observed for the central part of the Ninetyeast Ridge. It is well established that the Te values are dependent on the age of the oceanic crust during the formation of the ridge. Therefore, age data along the ridge track and adjacent oceanic crust are further investigated in detail for better understanding.

A new compilation of geochronology data along the Ninetyeast Ridge obtained by precise Ar/Ar dating of rock samples of DSDP Sites 214, 216, 254 and ODP Sites 756-758 along with newly dredged rock samples from sites Dr 7, Dr 16, Dr 32 and Dr 33 revealed linear north-south age progression from 80 to 40 Ma (Pringle et al., 2007, 2008). Studies of marine magnetic anomalies suggests that the age of oceanic crust west of 86°E FZ increases systematically from south to north, whereas on east of the 90°E FZ there is no regular age pattern (Krishna et al., 1999; Krishna et al., 2011b). Pairs of crustal age pattern east of the Ninetyeast Ridge led to the identification of an east-west fossil spreading centers in the Wharton Basin, which were ceased at about 42 Ma followed by the initiation of spreading activity along the Southeast Indian Ridge (Liu et al., 1983; Royer and Sandwell, 1989; Royer et al., 1991; Krishna et al., 1995). The Wharton spreading centers close to the Ninetyeast Ridge are believed to have jumped several times towards south and the process led to extend the length of the Ninetyeast Ridge (Royer and Sandwell, 1989; Royer et al., 1991). Subsequently, Krishna et al. (1995) and Krishna and Gopala Rao (2000) identified abandon spreading centers (ASCs) between the 86°E FZ and Ninetyeast Ridge and interpreted them as western extension of the Wharton spreading ridge.

The magnetic anomaly pattern between the 86°E FZ and the 90°E FZ suggests highly variable age pattern with traces of Abandoned Spreading Centers (ASC) of ages 65 and 42 Ma. The ridge segments within the corridor ceased spreading and jumped southward several times, thus the spreading ridge segments have maintained a minimum distance with the Kerguelen hotspot location. In other words, during the evolution of the Ninetyeast Ridge, whenever the spreading centre reached a critical distance from the hotspot it moved towards the hotspot by southward ridge jumps. These ridge jumps resulted capturing of crust segments initially belonged to the Antarctica plate and adding them to the Indian plate. Evidences for successive ridge jumps are obtained from the extrusive faulted structures obtained from seismic data and corresponding E-W trending vertical gravity gradients (Sager et al., 2010). Further, Krishna et al. (2011b) noticed that the rate of accretion of Ninetyeast Ridge between ODP 758 (77 Ma) and 756 (43 Ma) is higher by at least a factor of two than that of the adjacent basins.

As discussed earlier the 89°E FZ has acted as a thermo-mechanical boundary for the volcanic outpour of the Kerguelen hotspot. This fracture zones which bounds the eastern edge of the southern part of the Ninetyeast Ridge crosses the ridge at about 11°S, and thereafter borders the western edge of the ridge towards north (Figure 6.2). Interestingly, this ridge-fracture zone junction separates the north-central part from the south-central part of the Ninetyeast Ridge. The random Te values in the north-central part of the ridge can be due to the emplacement of the ridge on lithosphere of complex age pattern resulted from the series of southward ridge jumps. The successive ridge jumps must have resulted mechanically heterogeneous lithosphere of variable age. The Kerguelen hotspot eruption on such lithosphere may lead to variable isostatic compensation of the ridge. This is evident from the contrasting Te estimates and gravitational response of the ridge as observed in the flexural as well as two-dimensional gravity forward models along profiles SK 28-3 and SK 28-4 (Figures 6.6b, 6.11 and 6.12).

Geochemical studies of rock samples from ODP Site 757 and DSDP Site 214, which lie within the south-central part of the ridge suggests interaction between Kerguelen hotspot and spreading centre (Weis and Frey 1991; Frey and Weis, 1995). The first ridge jump at

about 65 Ma brought the spreading centre close to the hotspot leading to on-axis emplacement of the ridge. This hypothesis is supported by a low Te values (< 5 km) obtained for the south-central part of the Ninetyeast Ridge form the present analysis. However, towards south the Te values increases and reaches a maximum value of 20 km near 18°S latitude, suggesting a progressive increase in age of lithosphere during the emplacement. This could be explained by hotspot eruption on transferred crustal blocks of Antarctica Plate as a result of a major ridge at about 42 Ma (Krishna et al., 2011b). Similar to this observation, Lyons et al., (2000) observed that the Te values consistently increases from southeast to northwest along the Louisville Ridge in Pacific Ocean with a marked discontinuity associated with an extinct spreading centre.

It is widely known that Te values are in general sensitive to the age of the lithosphere at the time of the formation of the load ( $\Delta t$ ). The empirical relationship between them (discussed in detail in Chapter 4) is widely used to predict the age of volcanic loads when the age of crust is known and to predict the age of the crust when the age of load is known (Calmant et al., 1990). The age progression along the Ninetyeast Ridge between ODP Sites 756 (43 Ma) and 758 (77 Ma) is well constrained from the dating of rock samples, whereas the age of the surrounding ocean floor is poorly known. Hence, an attempt has been made to predict the approximate age of the oceanic crust beneath/ close to the Ninetyeast Ridge. The predicted age beneath the Ninetyeast Ridge along with age of seafloor obtained by marine magnetic anomalies west of the 86°E FZ, east of 90°E FZ and between 86°FZ and Ninetyeast Ridge is presented in Figure 6.14. In general, the predicted age beneath the ridge follows an increasing trend from south to north following the age of seafloor west of the 86°E FZ. The variations in age due to the transferred crust could be clearly observed, particularly in the central part of the ridge. It should be noted that the predicted age may have considerable inaccuracies due to the uncertainties in Te estimations and the possible scatter in Te-age relationship beyond the error bounds given in the empirical equation. This is evident from the unrealistic ages (>120 Ma) predicted for the central and northern part of the Ridge (Figure 6.14). Nevertheless, the present results suggest that Ninetyeast Ridge, especially the central part from 20°S to 2°N was evolved on a much complex tectonic setting than previously thought.

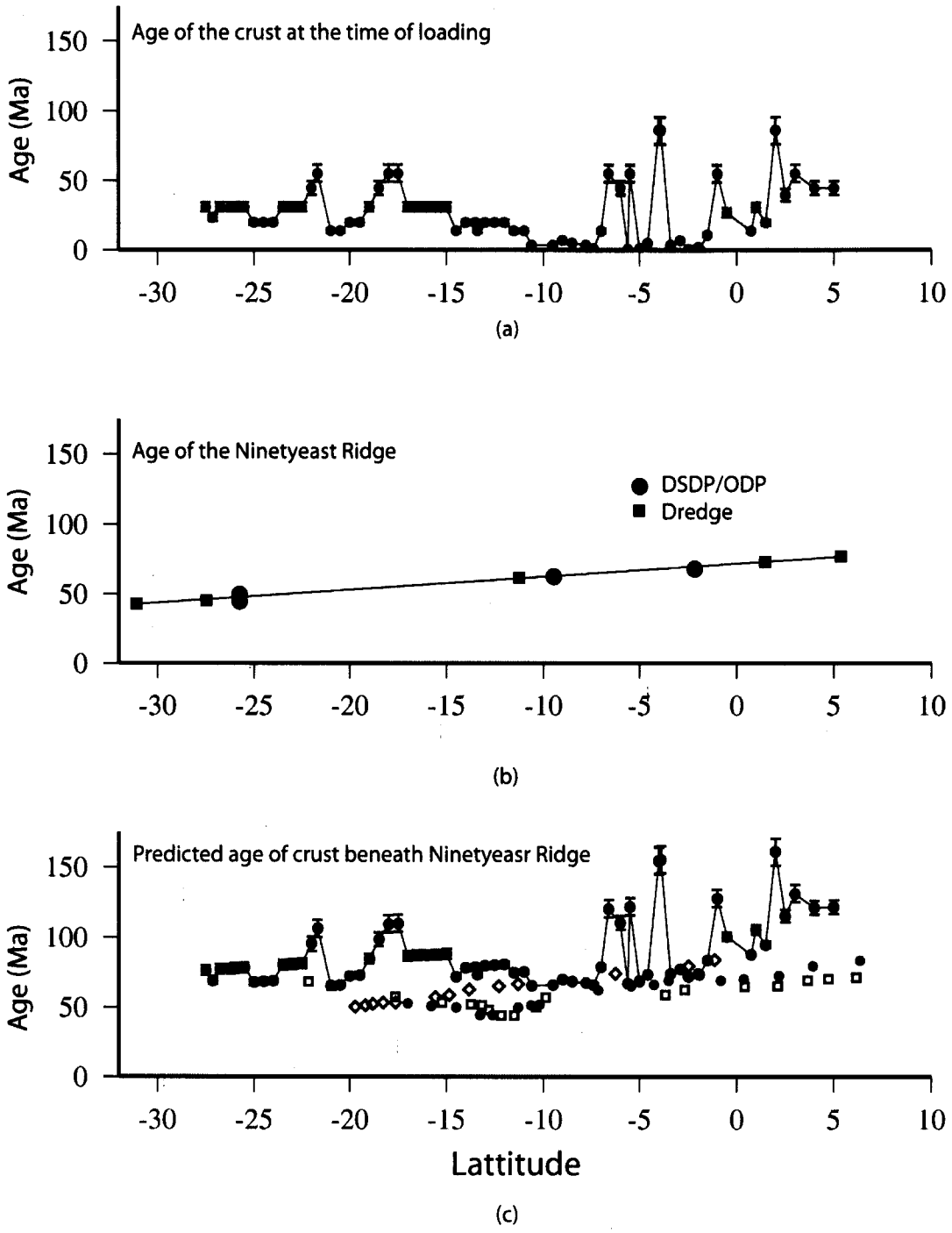


**Figure 6.14** Age verses latitude plots for the Ninetyeast Ridge. a) Age of the crust at the time of loading with error bars determined using the Te-age empirical relation. b) Age of the Ninetyeast Ride determined from Ar/Ar dating). c) Predicted age of the crust beneath Ninetyeast Ridge (solid black) compared with the age of oceanic crust west of 86°E FZ (green diamond), between the 86°E FZ and the Ninetyeast Ridge (red circle) and east of the 90°E FZ (blue square).

The tectonic model for the evolution of the Ninetyeast Ridge based on the present study is compared with the existing models in Figure 6.15. The evolutionary model for the southern and northern part of the ridge agrees with that of Royer et al., (1991) and Krishna et al., (1999), whereas for the central part a more complex model with interaction of spreading centre with hotspot along with multiple ridge jumps beneath the Ninetyeast Ridge is proposed. The north-central part must have emplaced on a crust of highly variable age produced by multiple southward ridge jumps, whereas the south-central part was emplaced on a crust of uniformly increasing age produced as a result of a major southward ridge jump.

# CHAPTER 7

# Summary and Conclusions

# Summary and Conclusions

The present research work dealt with the investigations of bathymetry, gravity and seismic reflection data of three important aseismic ridges: Comorin Ridge, 85°E Ridge and Ninetyeast Ridge, of the northeastern Indian Ocean for determining the internal structure and isostatic compensation mechanisms. The study brought out important constraints with regard to crustal architecture, isostatic compensation mechanisms and evolutionary models for all three aseismic ridges, and the results provided new insights to the understanding of geodynamics of the northeastern Indian Ocean in a broad perspective. Summary of the work reported in this thesis and the conclusions arrived at are as follows.

## 7.1 The Structure and isostatic model of the Comorin Ridge

The Comorin Ridge is one of the least studied aseismic ridges in the Indian Ocean, in spite of its location close to the Indian Continental Margin. Ship-borne bathymetry, gravity and magnetic data of the Comorin Ridge were investigated to map the ridge extent, morphology and its gravity anomaly signatures. Further, the structure and isostasy of the Comorin Ridge were studied using transfer function technique and forward modeling of gravity and bathymetry data. The important conclusions derived from this study are as follows.

1. The Comorin Ridge extends for about 500 km in NNW-SSE direction in north central Indian Ocean, close to the southern tip of India and western continental margin of Sri Lanka. The ridge topography has variable reliefs along its strike and uneven gradients on both sides of the ridge flanks. The southern part of the ridge (between 1.5°N and 3°N) has an elevation of up to 0.5 km from the adjacent seafloor of about 4 km deep; in the central part (between 3°N and 5°N) the ridge has a maximum elevation of up to 1 km from the surrounding water depths ranging from 3 to 4 km, and in the north (between 5°N and 6.5°N) the ridge elevates mostly on eastern side of the ridge, ranging from 0.4 to 0.7 km from adjacent water depths of about 2.5 km. Across the

southern part of the ridge the western flank extends for more than 100 km with relatively smooth gradient and the eastern flank steeply deepens with a scrap of about 1.2 km within a horizontal distance of about 50 km.

2. Geophysical profile data of the Comorin Ridge show that the ridge is associated with relatively low-amplitude gravity anomalies of about 25 mGal in southern part (1.5°N – 5°N) and 30 mGal in northern part (5°N – 6.5°N) compared to its elevations. There is a significant inference to note that a less-raised north part of the ridge is associated with relatively higher (30 mGal) gravity anomaly, suggesting that this part of the ridge is relatively less compensated in comparison to that of south part of the ridge. On the eastern flank of the ridge the gravity profiles data show a sudden regional shift in anomaly by about 50 mGal, which may indicate the location of Continent-Ocean Boundary (COB) on the western continental margin of Sri Lanka. The seafloor spreading-type magnetic anomaly 34 is identified on profiles V2902-a and C1215, besides there are other anomalies with short-wavelength and low-amplitude observed on oceanic crust evolved during the period of pre anomaly 34, that is during the Cretaceous Magnetic Quiet Period. It is also observed that the Comorin Ridge is not associated with any specific magnetic anomaly signatures.

3. Admittance analysis of the Comorin Ridge suggested that the southern part of the ridge (south of 5°N) is compensated with Airy model or local compensation with an elastic plate thickness (Te) of about 3 km and crustal thickness (t) of 15-20 km, while the northern part is compensated with flexural plate model with an elastic thickness of about 15 km. Two-dimensional gravity forward model studies suggest that the crust beneath the southern part of the ridge is ~ 17 km thick, which consist of 2 km thick volcanic rocks as surface load, 6 km thick oceanic crust and 9 km thick underplated magmatic rocks as subsurface load. While the gravity model across the northern part of the ridge shows that the ridge was emplaced on continental crust with a thickness of about 20 km. About 3 km thick volcanic rocks were emplaced as surface load on top of the crust, which seems to have contributed to flexure of the crustal layers and Moho boundary to the magnitude of about 3 km. The results further suggest that the

southern part of the ridge was emplaced on relatively weak oceanic lithosphere, while the northern part was emplaced on continental lithosphere.

4. The east side of the Comorin Ridge all along is controlled by different tectonic elements, southernmost part by the 79°E FZ, central part by the COB and northernmost part by termination of the Gulf of Mannar Basin. Gravity model studies have determined relatively thin (~ 21 km) continental crust on western margin of Sri Lanka, which may have evolved due to the crustal stretching during the rift processes that took place during the breakup of eastern Gondwanaland fragments and early spreading activity.

5. The present results of the Comorin Ridge together with published plate kinematic models of the north Indian Ocean led to infer that the Comorin Ridge was evolved at about 90 Ma during the rift stage of the Madagascar from the southwest of India.

## 7.2 The Structure and Evolution of the 85°E Ridge

The 85°E Ridge extends for about 2500 km long from the Mahanadi Basin in the north to the Afanasy Nikitin seamount in south in the Central Indian Basin. The ridge associates with two contrasting gravity anomaly signatures: negative anomaly over the north part (up to 5°N latitude), where the ridge structure is buried under thick Bengal Fan sediments, and positive anomaly over the south part, where the structure is intermittently exposed above the seafloor. Origin of the 85°E Ridge is enigmatic due to its characteristic negative gravity anomaly and complex magnetic signatures. In this study, the morphology, trend, extent, and characteristic negative gravity anomaly signature are studied in detail using seismic reflection, satellite and ship-borne gravity data. The ridge structure and isostasy aspects are further investigated using process oriented modeling of gravity and seismic reflection data. The important conclusions of this study are as follows.

1. The 85°E Ridge extends from 19°N to 5°S with variable widths range from 100 to 180 km. The width of the ridge is greater in the vicinity of 14°N latitude and this part is associated with a significant gravity low of ~ 80 mGal. Further north between 15°N and 16.5°N latitudes, the gravity anomaly of the ridge is not apparently clear, but reappears anomaly signature again near 17°N latitude and continues further north up to 19°N, in to the region of offshore Mahanadi Basin. Towards south between 11°N and 2°N, the ridge track turns in clockwise direction, then continues straight-down to join the Afanasy Nikitin seamount (ANS). The prominent negative gravity anomaly signature associated with the 85°E Ridge in the Bay of Bengal region changes to positive south of 5°N and in further south, the ANS is associated with significant positive gravity anomaly.

2. Seismic reflection sections crossing the 85°E Ridge in the Bay of Bengal region suggests that the subsurface disposition of the ridge is quite variable. The ridge topography has a steep westward throw and gentle eastward dip at 13°N latitude and appears as a double peaked basement rise at 14°N, whereas at 14.7°N the relief of the ridge is much less with eastern side of the ridge dominated by a prominent basement high probably associated with a oceanic fracture zone. Gravity anomalies along these sections show that the ridge is associated with a prominent negative gravity anomaly (~50 mGal) flanked by regional gravity highs on either side. In the south, the morphology and gravity anomaly signature of the ridge structure are distinctly different in comparison to the sections of the Bay of Bengal. Along 4.5°N latitude, the ridge is characterized by shallower basement and exposed above the seafloor with a prominent positive gravity anomaly of 40 mGal amplitude.

3. Process oriented modeling of seismic and gravity data of the 85°E Ridge revealed that the ridge was emplaced on a lithosphere, whose elastic plate thickness was approximately 10-15 km and suggest the off-ridge tectonic emplacement. This result is consistent for both northern and southern parts of the ridge in spite of contrasting gravity signatures associated with the ridge.

4. The isostatic model of the 85°E Ridge suggests that the ridge structure and the overlaying sediments are supported by a broad flexure of the Moho boundary. Two-dimensional gravity forward modeling also suggests flexural compensation beneath both northern and southern parts of the ridge. The gravity models derived by both the methods conclusively suggest that the negative gravity anomaly over the 85°E Ridge could be explained by a combination of sources: the flexure at Moho boundary, thick Bengal Fan sediments over the ridge and the presence of high density metasedimentary rocks on both sides of the ridge flanks.

5. The gravity anomalies of the 85°E Ridge are reconstructed since the ridge formation with possible crustal structures prevailed at different geological ages. At the time of ridge emplacement, that is during the late Cretaceous the ridge was associated with a significant positive anomaly with a compensation generated by a regional flexure of the Moho boundary. By early Miocene the ridge was approximately covered by post-collision sediments and led to alteration of initial gravity anomaly to a small positive anomaly. At present, the ridge is buried by approximately 3 km thick Bengal Fan sediments on its crestal region and about 8 km thick pre- and post-collision sediments on the ridge flanks. This geological setting had changed physical properties of the sediments and led to alter the minor positive gravity anomaly of early Miocene to distinct negative gravity anomaly.

6. Present results together with published plate reconstruction constraints suggest that the 85°E Ridge was emplaced by a short-lived hotspot from 85 to 55 Ma in an intraplate geological setting.

## 7.3 The Structure and Tectonics of the Ninetyeast Ridge

The Ninetyeast Ridge is one of the classic aseismic ridges of the World Oceans and probably the longest linear feature on planet Earth. It stretches for more than 5000 km in the eastern Indian Ocean from 30°S to 17°N approximately along the 90°E meridian. The Ninetyeast Ridge was emplaced on the Indian plate during its northward drift between the

late Cretaceous and early Cenozoic by the Kerguelen hotspot volcanism. In this study, an attempt was made to understand the isostatic compensation mechanisms along the Ninetyeast Ridge using flexural modeling and admittance analysis of closely spaced bathymetry and gravity profiles. Further, two-dimensional gravity forward modeling was carried out along five representative profiles of different parts of the ridge in order to determine the crustal structure of the ridge. The important conclusions of this study are as follows

1. Elastic plate thickness (Te) of the Ninetyeast Ridge between latitudes 28°S and 8°N has been determined using flexural modeling and admittance analysis of 72 gravity and bathymetry profiles distributed at approximately equal interval. The results suggest that, southern (south of 18°S) and northern (north of 2°N) parts of the ridge are flexurally compensated with elastic plate thickness values of >10 and >18km, respectively. Admittance analysis further suggests that the central part (20°S to 2°N) of the ridge has Airy type compensation with crustal thickness of 15-20 km. However, Te values derived in flexural modeling of the profiles revealed that that central part of the ridge may further divided into 1) south-central part (18°S to 8°S), where the Te values constantly decreases from 20 km to 5 km and 2) north-central part (8°S to 2°N), where Te values randomly varies between 2 and 25 km.

2. Crustal structure of the Ninetyeast Ridge are determined using two-dimensional gravity forward modeling along five east-west gravity profiles, representing from different parts of the ridge possesses variable elastic plate thickness values, under the constraints from seismic results, particularly from the point of corroboration of ridge variable isostatic compensations. The models suggest that the crustal structure of the Ninetyeast Ridge show considerable internal variations. In the southern part along ~26°S latitude, the ridge topography is compensated by down-flexing of crustal layers 2A, 2B and 3A with amplitude of about 2.5-3 km. In the south-central part (~13.5°S), the model suggests very thick crust (~20 km) beneath the ridge, which includes ~10 km thick underplated body. In north-central part gravity models at 3°N suggest thickening of crust beneath the ridge topography, in contrast at 4°N the ridge shows a

different crustal structure, where the volcanic load is supported by down-flexing of crustal layers. These crust mantle configuration derived from the two-dimensional gravity forward modeling is in good agreement with the Te values obtained along the respective profiles.

3. Over the north part of the Ninetyeast Ridge, where the ridge structure is buried under the Bengal Fan sediments, the model results suggest that the volcanic load (ridge material) is compensated by a broad flexure of the crustal layers with wavelengths greater than that of the ridge. The model also suggests the presence of low-density mantle rocks of ~ 4.5 km thick beneath the ridge. The model results are fairly in good agreement with the results of admittance analysis of the northern part of the ridge, and they together obviously suggest the flexural compensation with both surface and subsurface loading. The depth to the buoyant load (z) derived from the admittance analysis matches well with the depth to the low-density mantle rocks in the model.

4. Based on present results and available plate reconstruction model results a plausible tectonic model is proposed for the formation of Ninetyeast Ridge. The southern part of the ridge was emplaced on a lithosphere of intermediate strength possibly along the edge of the Indian plate, whereas the northern part was emplaced clearly in an intraplate setting. The highly variable isostatic compensation mechanisms in the central part of the ridge could be a manifestation of the complex interactions of the Kerguelen hotspot and Wharton spreading ridge segments. The north-central part may have emplaced on a crust of highly variable age produced by multiple southward ridge jumps, whereas the south-central part was emplaced on a crust of uniformly increasing age produced as a result of a major southward ridge jump.

## 7.4 Future Research

During the investigation of present research problems, particularly understanding the isostatic compensation mechanisms beneath three important aseismic ridges: Comorin Ridge, 85°E Ridge and Ninetyeast Ridge, it is found that there are some interesting

research aspects related to the evolution of the ridges. Those aspects, mentioned below, may further be investigated in future research for better understanding.

### 7.4.1 Continent-Ocean Boundary on Western Margin of Sri Lanka and Southern Tip of India

Demarcation of Continent-Ocean Boundary (COB), crustal structure, stretching rates during the margin evolution, etc., along the passive continental margins provides useful geological information on creation of early oceanic crust, evolution of rifted and deep water basins, ridges, etc. The COB and associated geophysical anomaly signatures may further reveal how the segments of continental margin split from its conjugate margin, whether those were in transform motion before they complete the rifting and imitates drifting or in normal rift phase for longer periods. It was discussed in Chapter 4 that, the northern part of the Comorin Ridge was emplaced on rigid continental lithosphere and the central part was evolved nearly in the vicinity of continent-ocean adjoining region and the southern part on a weak oceanic crust. Based on this study, the COB on the ridge and off western margin of Sri Lanka and southern tip of India were cautiously demarcated. However, exact demarcation of COB in this region is an important geophysical constraint, which can provide new insights to the rifting history of Sri Lanka from the Indian landmass and formation of the Mannar Basin in between.

Admittance analysis of gravity and bathymetry profiles of the continental margin regions of southern India and western margin of Sri Lanka may also provide constraints associated with continental rift processes. Further, flexural backstripping analysis of seismic reflection profiles from the Mannar Basin may be used to understand the basin evolution and demarcation of the COB. This is particularly interesting to the oil industries in view of the hydrocarbon prospects of the basin.

### 7.4.2 Origin of the 85°E Ridge

In the present study, crustal structure and isostatic compensation mechanism of the 85°E Ridge are determined using process oriented modeling of gravity and seismic reflection

data. The derived results of the ridge together with previously published geophysical results led to interpret that the ridge was emplaced by volcanic activity. However, following the analogy of the negative gravity anomaly signature of the Laxmi Ridge in the Arabian Sea and its continental sliver interpretation, it may also be possible to think in the direction of assigning continental origin to the 85°E Ridge. Deep seismic refraction studies may possibly resolve this ambiguous issue and lead to better understanding of the nature of the ridge.

The present study further suggests that the 85°E Ridge was emplaced by a hotspot in an intraplate geological setting. However, several issues related to the ridge evolution are yet to be understood very clearly such as, which hotspot was responsible for the emplacement of the 85° E Ridge? What is the exact timing of the emplacement? Why the clock-wise turn exists in the ridge track? etc. Some of the researchers believe that the ridge was emplaced by the Crozet hotspot (Curray and Munasinghe, 1991), while others opine that it is a product of the Kerguelen hotspot (Bastia et al., 2010). In the later case, the extension of the ridge towards Rajmahal Traps needs to be established by geophysical and geochemical studies. Also, a plate reconstruction model, which allows emplacement of both the 85°E Ridge and the Ninetyeast Ridge, needs to be developed and tested. In unison, integrated geophysical and geochemical studies are essential to be carried out to unravel the complexities associated with the origin of the 85°E Ridge.

### 7.4.3 Variable Isostatic Compensation Mechanisms beneath the Ninetyeast Ridge and its Complex Tectonic Evolution

As discussed in Chapter 6, the isostatic response of the Ninetyeast Ridge all along its track is highly variable, especially in the central part of the ridge. This is interpreted as a product of interaction between hotspot and spreading centers and also with multiple ridge jumps beneath the Ninetyeast Ridge during the evolution of the ridge. In other words, whenever the spreading centre reached a critical distance away from the hotspot, the spreading centre moved towards the hotspot by southward ridge jump. Although recent geophysical studies of the Ninetyeast Ridge support the idea of southward ridge jumps (Sager et al., 2010; Krishna et al., 2011b), the dynamics involved in the process are yet to

be known clearly. The Ninetyeast Ridge is a unique feature and provides the opportunity to study the ridge-plume interactions, which have great implications in global plate tectonics.

The role of the 89°E FZ in the emplacement process of the Ninetyeast Ridge is another important geophysical aspect. This fracture zone, which bounds the eastern edge of the southern part of the Ninetyeast Ridge crosses the ridge at about 11°S, and thereafter borders the western edge of the ridge towards north. Interestingly, this ridge-fracture zone junction separates the north-central part, which was emplaced on a crust produced by multiple southward ridge jumps from the south-central part, which was emplaced on a crust produced as a result of a major southward ridge jump. How the 89°E FZ acted as a thermo-mechanical boundary for the volcanic outpour of the Kerguelen hotspot need to be further investigated.

# REFERENCES

Airy G.B., 1855. On the computation of the effect of the attraction of mountain-masses as disturbing the apparent astronomical latitude of stations of geodetic surveys. Philos. Trans. R. Soc. London, 145, 101-104.

Anand, S.P., Rajaram, M., Majumdar, T.M., Bhattacharyya, R., 2009. Structure and tectonics of 85_E Ridge from analysis of Geopotential data. Tectonophysics, 478 (1-2), 100-110.

Anderson, D.L., 2007. New theory of the earth. 384p, Cambridge university press, New York, United States.

Anil Kumar, Pande, K., Venkatesan, T.R., Baskar Rao, Y.J., 2001. The Karnataka Late Cretaceous dykes as products of the Marion hot spot at the Madagascar-India breakup event: evidence from $^{40}Ar$-$^{39}Ar$ geochronology and geochemistry. Geophy. Res. Lett., 28, 2715-2718.

Ashalatha, C., Subrahmanyam, C., Singh, R.N., 1991. Origin and compensation of Chagos-Laccadive ridge, Indian Ocean, from admittance analysis of gravity and bathymetry data. Earth. Plant. Sci. Lett., 105, 47-54.

Avraham, Z.B., Bunce, E.T., 1977. Geophysical study of the Chagos-Laccadive Ridge, Indian Ocean, J. Geophys. Res., 82, 1295-1305. J. Geophys. Res., 82 (8), 1295-1305.

Backman,J., R.A. Duncan et al., 1988. Proc. ODP ini. Repts., College Station, TX (Ocean Drilling Program), 115, 5-15.

Bansal A.R., Fairhead, J.D., Green, C.M., Fletcher, K.M.U., 2005. Revised gravity for offshore India and the isostatic compensation of submarine features. Tectonophysics, 404, 1-22.

Barrel, J., 1914. The strength of earths crust. 1. Regional distribution of isostatic compensation. J. Geol., 22, 145-165.

Bastia, R., Radhakrishna, M., Das, S., Kale, A.S., Catuneanu, O., 2010. Delineation of the 85°E Ridge and its structure in the Mahanadi Offshore Basin, Eastern Continntal Margin (ECMI), from seismic reflection imaging. Mar. Petro. Geol., 27, 1841-1848.

Besse, J., Courtillot, V., 1988. Paleogeographic maps of the continents bordering the Indian Ocean since the Early Jurassic. J. Geophys. Res., 93 (B10), 11,791-11,808.

Bhattacharya, G.C., Chaubey, A.K., 2001. Western Indian Ocean - A Glimpse of the tectonic scenario. In: Gupta, R.S., Desa, E. (Eds), The Indian Ocean-A perspective. 2, 691-729.

Borissova, I.M.F., Coffin, P. Charvis, Operto, S., 2003. Structure and development of a microcontinent: Elan Bank in the southern Indian Ocean. Geochem. Geophys. Geosyst., 4(9), 1071, doi:10.1029/2003GC000535.

Bowin, C., 1973.Origin of the Ninetyeast Ridge from studies near the equator, J. Geophys. Res., 78, 6029-6043.

Bull, J.M., Scrutton, R.A., 1990. Sediment velocities and deep structure from wide-angle reflection data around Leg 116 sites. In: Cochran, J.R. et al (Eds), Proc. Ocean Drill Program, Sci. Results, 211-316.

Calmant, S., Cazenave, A., 1987. Anomalous elastic thickness of the oceanic lithosphere in the south-central Pacific. Nature, 328, 236-238.

Calmant, S., Francheteau, J., Cazenave, A. 1990. Elastic layer thickening with age of the oceanic lithosphere: a tool for prediction of the age of volcanoes or oceanic crust. Geophys. J. Int., 100, 59-67.

Cande, S.C., Mutter, J.C., 1982. A revised identification of the oldest sea-floor spreading anomalies between Australia and Antartica, Earth. Planet. Sci. Lett., 58, 151-160.

Cande, S.C., Kent, D.V., 1995. Revised calibration of the geomagnetic polarity time scale for the late Cretaceous and Cenozoic. J. Geophys. Res., 100, 6093-6095.

Chand, S., Radhakrishna, M., Subrahmanyam, C., 2001. India-East Antarctica conjugate margins: rift-shear tectonic setting inferred from gravity and bathymetry data. Earth. Plant. Sci. Lett., 185, 225-236.

Chand, S., Subrahmanyam, C., 2003. Rifting between India and Madagascar-mechanism and isostasy. Earth. Plant. Sci. Lett., 210, 317-332.

Chaubey, A.K., Gopala Rao, D., Srinivas, K., Ramprasad, T., Ramana, M.V., Subrahmanyam, V., 2002. Analysis of multichannel seismic reflection, gravity and magnetic data along a regional profile across the central-western continental margin of India. Mar. Geol., 182, 303-323.

Chaubey, A.K , Srinivas, K., Ashalatha, B, Gopala Rao, D., 2008. Isostatic response of the Laccadive Ridge from admittance analysis of gravity and bathymetry data. J. Geodynam., 46, 10-20.

Christensen, N.I., 1977. Seismic velocities and elastic moduli of igneus and metamorphic rocks from Indian Ocean. In: Heirtzler et al. (Eds), Indian Ocean Geology and Biostratigraphy, AGU, Washington D.C., 279-299.

Class, C., Goldstein, S.L, Galer, S.J.G, Weis. D., 1993. Young formation age of a mantle plume source. Nature, 362, 715-721.

Coffin, M., Pringle, M.S., Duncan, R.A., Gladczenko, T.P., Storey, M., Mueller, R.D, Gahagan, L.A., 2002. Kerguelen hotspot magma output since 130 Ma. J. Petrol., 43, 1121-1139, doi:10.1093/petrology/ 43.7.1121.

Courtillot, V., Davaille, A., Besse, J., Stock, J., 2003. Three distinct types of hotspots in the Earth's mantle. Earth. Planet. Sci. Lett., 205, 295-308.

Cox, A., Hart, R.B., 1986. Plate Tectonics How it works. 392p, Blackwell Scientific Publications.

Curray, J.R., Emmel, F.J., Moore, D.G., Russel, W.R., 1982. Structure, tectonics, and geological history of the northeastern Indian Ocean. In: Nairn A.E., Stheli, F.G. (Eds), The Ocean Basins and Margins-The Indian Ocean, 6, 399-450, Plenum, New York.

Curray, J.R., 1984. Sri Lanka: is a Mid-Plate Platelet?. J. Natio. Acqua. Resour. Agen., 31, 30-50.

Curray, J.R., 1991. Possible greenschist metamorphism at the base of a 22-km sedimentary section, Bay of Bengal. Geology, 19, 1097-1100.

Curray, J.R., Munasinghe, T., 1991. Origin of the Rajmahal Traps and the 85°E Ridge: preliminary reconstructions of the trace of the Crozet hotspot. Geology, 19, 1237-1240.

Curray, J.R., 1994. Sediment volume and mass beneath the Bay of Bengal. Earth Planet. Sci. Lett., 125, 371-383.

Curray J.R., Emmel, F.J., Moore, D.G., 2003. The Bengal Fan: morphology, geometry, stratigraphy, history and processes. Mar. Petrol. Geol., 19, 1191-1223.

Desa, M., Ramana, M.V., Ramprasad, T. 2006. Seafloor spreading magnetic anomalies south off Sri Lanka. Mar. Geol., 229, 227-240.

Desa, M., Ramana, M.V., Ramprasad, T. 2009. Evolution of the Late Cretaceous crust in the equatorial region of the Northern Indian Ocean and its implication in understanding the plate kinamatics. Geophy. J. Int., 177, 1265-1278.

Detrick, R.S., Watts, A.B., 1979. An analysis of Isostasy in the world's oceans 3. Aseismic ridges. J. Geophys. Res., 84, 3637-3653.

Diament, M., Goslin, J., 1986. Emplacement of the Marion Dufresne, Lena and Ob seamounts (South Indian Ocean) from a study of isostasy. Tectonophys. 121, 253-262.

Dietz, R.S., 1961. Continent and ocean basin evolution by spreading of the sea floor. Nature, 190, 854-857.

Duncan, R.A., 1978. Geochronology of Basalts from the Nine- tyeast Ridge and Continental Dispersion in the Eastern Indian Ocean. J. Volcanol. Geotherm. Res., 4, 283-305.

Duncan,R.A., 1981. Hotspots in the southern Oceans: An absolute frame of reference motion of the Gondwana Continents. Tectonophysics, 74, 29-42.

Duncan, R.A., 1990. The volcanic record of the Reunion hotspot. In: Duncan, R.A., Backman, J., Peterson, L.C., et al. (Eds.), Proceedings of the Ocean Drilling Program, Scientific Results. 115, College Station, TX (Ocean Drilling Program), 3-10.

Duncan, R.A., 1991. The age distribution of volcanism along aseismic ridges in the eastern Indian Ocean, Proc. Ocean Drill. Program Sci. Results, 121, 507-517.

Dutton, C.E., 1889. On some of the greater problems of physical geology. Bull. Phi. Soc., Washington, 2, 51-64.

Everest, G., 1857-59. Rectification of logarithemic errors in the measurements of two sections of the meridional arc of India. Royal Soc. Proc., 9, 620-626.

Francis, T.J.G., Raitt, R.W., 1967. Seismic refraction measurements in the southern Indian Ocean. J. Geophys. Res., 72, 3015-3042.

Frey F.A, Dickey, J.S., Thompson, G., Bryan, W.B., 1977. Eastern Indian Ocean DSDP Sites: correlations between petrography, geochemistry, and tectonic setting: In Heirtzler, J.R, Bolli, H.M., Davis, T.A., Saunders, J,B., Sclater J.G. (Eds), A synthesis of deep sea drilling in the Indian Ocean, Washington D.C.: U.S. Government printing office 189-257.

Frey, F., Weis, D., 1995. Temporal evolution of the Kerguelen plume; Geochemical evidence from approximately 38 to 82 Ma lavas forming the Ninetyeast Ridge, Contrib. Mineral. Petrol., 121, 12-28.

Frey F.A., et al., 2000. Origin and evolution of a submarine large igneous province: the Kerguelen Plateau and Broken Ridge, southern Indian Ocean. Earth and Planet. Sci. Lett., 176, 73-89.

Furuse, N., Kono, Y., 2003. Slab residual gravity anomaly: gravity reduction due to subducting plates beneath the Japanese Islands. J. Geodyn., 36, 497-514.

Gaina, C., Müller, R.D., Brown, B., Ishihara, T., 2003. Microcontinent formation around Australia, In: Hillis, R.R., Müller, R.D. (Eds), Evolution and Dynamics of the Australian Plate, Spec. Pap. Geol. Soc. Am., 372, 405-416.

Gaina, C., Müller, R.D., Brown, B., Ishihara, T., 2007. Breakup and early seafloor spreading between Indian and Antarctica. Geophys. J. Int. 170, 151-169.

Gopala Rao, D., Krishna, K.S., Sar, D., 1997. Crustal evolution and sedimentation history of the Bay of Bengal since the Cretaceous. J. Geophys. Res., 102, 17747-17768.

Gordon, R.G., DeMets, C., Royer, J.-Y., 1998. Evidence for long-term diffuse deformation of the lithosphere of the equatorial Indian Ocean. Nature, 395, 370–374, doi: 10.1038/26463.

Gopala Rao, D., Krishna, K.S., Neprochnov, Yu.P., Grinko, B.N., 2004. Satellite gravity anomalies and crustal features of the central Indian Ocean basin. Curr. Sci., 86, 948-957.

Grevemeyer, I., Flueh, E.R., 2000. Crustal Underplating and its implications for subsidence and state of isostasy along the Ninetyeast Ridge hotspot trail. Geophys. J. Int., 142, 643-649.

Grevemeyer, I., Flueh, E.R., Reichert, C., Bialas, J., Klaschen, D., Kopp, C., 2001. Crustal architecture and deep structure of the Ninetyeast Ridge hotspot trail from active-source ocean bottom seismology. Geophys. J. Int., 144, 414- 431.

Grow, J.A., Bowin, C.O., 1975. Evidence for High-Density Crust and Mantle Beneath the Chile Trench Due So the Descending Lithosphere. J. Geophys. Res., 80, 1449-1,458.

Hamilton, W., 1979. Tectonics of the Indonesian Region, U.S. Geol. Surv., Prof Pap. 1078, Washington, 345p.

Hayford, J.F., 1909. The figure of the Earth and isostasy from measurements in the United States, 178p, Government Printing Office, Washington DC.

Heezen, B.C., Tharp, M., 1964. Physiographic diagram of the Indian Ocean, map, Geol. Soc. America. Boulder, Colorado.

Heiskanen, W.A., 1931. Isostatic tables for reduction of gravimetric observations calculated on the basis of Airy's hypothesis. Bull. Geod., 30, 110-129.

Hess, H.H., 1960. Evolution of ocean basins: Report to Office of Naval Research on research supported by ONR contract Number 1858, 149-150.

Hess, H.H., 1962. History of the Ocean Basins. In: Engel, A.E.G, James, H.L., Leonard B.F. (Eds), Petrologic studies. Geol. Soc. Am., 559-620.

Holmes, M.A., Watkins, D.K., 1992. Middle and Upper Cretaceous history of the Indian. Ocean. In: Duncan, R.A et al. (Eds.), Synthesis of Results from Scientific Drilling in the Indian Ocean. Geophysical Monograph, 70, American Geophysical Union, 225-244.

Houtz, R.E., Hayes, D.E., Mark], R.G., 1977. Kerguelen Plateau bathymetry sediment distribution and crustal structure. Mar. Geol., 25, 95-130.

Hubbert, King, M., 1948. A line-integral method of computing the gravimetric effects of two-dimensional masses. Geophysics, 13, 215-225.

Jokat, W., Nogi, Y., Leinweber, V., 2010. New aeromagnetic data from the western Enderby Basin and consequences for Antarctica-India break-up. Geophy. Res. Lett., 37, L21311, doi:10.1029/2010GL045117.

Kahle, H.G., Naini, B.R., Talwani, M., Eldholm, O., 1981. Marine geophysical study of the Comorin ridge, north central Indian basin. J. geophys. Res., 86, 3807-3814.

Kamesh Raju, K.A., Ramprasad, T., Kodagali, V.N., Nair, R.R., 1993. Multibeam bathymetry, gravity and magnetic studies over 79°E Fracture Zone, Central Indian Basin. J. Geophys. Res., 98, 9605-9618.

Kamesh Raju, K.A., Ramprasad, T., Rao, P.S., Ramalingeswara Rao, B., Varghese, J., 2004. New insights into the tectonic evolution of the Andaman basin, northeast Indian Ocean. Earth. Earth Planet. Sci. Lett., 221, 145-162.

Kenneth, J.P., 1982. Marine Geology. 813p, Prentice-Hall, Inc, Englewood Cliffs, N.P.

Kent, R.W., Pringle, M.S., Müller, R.D., Saunders, A.D., Ghose, N.C., 2002. $^{40}Ar/^{39}Ar$ Geochronology of the Rajmahal basalts, India, and their relationship to the Kerguelen plateau. J. Petrology, 43, 1141-1153.

Kious, W.J., Tilling, R.I., 2008. This Dynamic Earth: the Story of Plate Tectonics. 108p, USGS, online edition, http://pubs.usgs.gov/gip/dynamic/dynamic.html

Koppers, A.A.P., Morgan, J.P., Morgan, J.W., Staudigel, H., 2001. Testing the fixed hotspot hypothesis using 40Ar/39Ar age progressions along seamount trails, Earth Planet. Sci. Lett., 185, 237-252.

Krishna, K.S., Gopal Rao, D., Ramana, M.V., Subrahmanyam, V., Sarma, K.V.L.N.S., Pilipenko, A.I., Shcherbakov, V.S., Radhakrishna Murthy, I.V., 1995. Tectonic model for the evolution of oceanic crust in the northeastern Indian Ocean from the Late Cretaceous to the early Tertiary. J. Geophys. Res., 100, 20,011-20,024.

Krishna, K.S., Ramana, M.V., Gopala Rao, D., Murthy, K.S.R., Malleswara Rao, M.M., Subrahmanyam, V., Sarma, K.V.L.N.S., 1998. Periodic deformation of oceanic crust in the central Indian Ocean. J. Geophy. Res., 103, 17,859-17,875, doi: 10.1029/98JB00078.

Krishna, K.S., Gopal Rao, D., Subba Raju, L.V., Chaubey, A.K., 1999. Paleocene on-spreading-axis hotspot volcanism along the Ninetyeast Ridge: An interaction between the kerguelen hotspot and the Wharton spreading center, Proc. Indian Acad. Sci. Earth Planet. Sci., 108, 255-267.

Krishna, K. S., Gopala Rao, D. 2000. Abandoned Paleocene spreading center in the northeastern Indian Ocean: Evidence from magnetic and seismic reflection data. Mar. Geol., 162, 215-224, doi:10.1016/S0025- 3227(99)00085-7.

Krishna, K.S., Bull, J.M., Scrutton, R.A., 2001a. Evidence for multiphase folding of the central Indian Ocean lithosphere. Geology, 29, 715-718.

Krishna, K.S., Neprochnov, Y.P., Gopala Rao, D., Grinko, B.N., 2001b. Crustal structure and tectonics of the Ninetyeast Ridge from seismic and gravity studies. Tectonics, 20, 416-433.

Krishna, K.S., 2003. Structure and evolution of the Afanasy Nikitin seamount, buried hills and 85°E Ridge in the northeastern Indian Ocean. Earth Planet. Sci. Lett., 209, 379-394, doi:10.1016/S0012-821X(03) 00081-5.

Krishna, K.S., Gopala Rao, D., Sar, D., 2006. Nature of the crust in the Laxmi Basin (14°-20°N) western continental margin of India. Tectonics, 25, TC1006, doi: 10.1029/ 2004TC001747.

Krishna, K.S., Michael, L., Bhattacharyya, R., Majumdar, T.J., 2009a. Geoid and gravity anomaly data of conjugate regions of Bay of Bengal and Enderby Basin: New constraints on breakup and early spreading history between India and Antarctica. J. Geophys. Res. 114, B03102 doi: 10.1029/2008JB005808.

Krishna, K.S., Bull, J.M., Scrutton, R.A., 2009b. Early (pre-8 Ma) fault activity and temporal strain accumulation in the central Indian Ocean. Geology, 37, 3, 227-230.

Krishna, K.S., Scrutton, R.A., Bull, J.M., Jaisankar, S., Banakar, V.K., 2011a. Growth of the Afanasy Nikitin seamount, central Indian Ocean: the product of short-lived hotspots. (submitted)

Krishna, K.S., Abraham, H., Sager, W.W., Gopala Rao, D., Levchenko., 2011b. Tectonics of the Ninetyeast Ridge derived from the spreading records of the contiguous oceanic basins and age constraints of the ridge. J. Geophy. Res. (Submitted).

Kumar, A., Pande, K., Venkatesan, T.R., Baskar Rao, Y.J., 2001. The Karnataka Late Cretaceous dykes as products of the Marion hot spot at the Madagascar-India breakup event: evidence from 40Ar-39 Ar geochronology and geochemistry. Geophys. Res. Lett., 28, 2715-2718.

Laughton, A.S., Matthews, D.H., Fisher, R.L., 1970. The structure of the Indian Ocean. In: Maxwell, A.E (Ed.). The Sea, Wiley-Interscience, New York, 4, part II, 543-585.

Lawver, L.A., Gahagan, L.M., Dalziel, I.W.D., 1998. A Tight fit-Early Mesozoic Gondwana, A Plate Reconstruction Perspective, Origin and Evolution of Continents: Proceedings of the International Symposium "Origin and Evolution of Continents," In:

Motoyoshi, Y, Shiraishi, K. (Eds.), Origin and Evolution of Continents. Memoirs of National Institute of Polar Research, special issue No. 53, 214-229.

Le Pichon, X., Heirtzler, J.R., 1968. Magnetic Anomalies in the Indian Ocean and Sea Floor Spreading. J. Geophyz Res., 73, 2101-2117.

Levchenko, O.V., Milanovskiy V.Ye., Popov A.A., 1993. A sediment thickness map and tectonics of the distal Bengal Fan. Oceanology, 33, 2, 232-238.

Li, X., Gőtze, H.-J., 2001. Ellipsoid, geoid, gravity, geodesy and geophysics. Geophysics, 66, 6, 1660-1668.

Liu, C.S., Sandwell, D.T., Curray, J.R, 1982. The negative gravity field over the 85°E Ridge. J. Geophys. Res., 87, 7673-7686.

Liu, C.S., Curray, J.R, McDonald, J.M., 1983. New constraints on the tectonic evolution of the eastern Indian Ocean. Earth Planet. Sci. Lett., 65, 331-342, doi:10.1016/0012-821X(83)90171-1.

Louden, K.E., 1981. A comparison of the isostatic response of bathymetric features in the north Pacific Ocean and Philippine Sea. Geophys. J. R. Astron. Soc., 64, 393-424.

Lowrie, W., 2007. Fundamentals of Geophysics. 381p, Cambridge University Press, Cambridge, United Kingdom.

Lyons, S. N., Sandwell, D. T., Smith, W. H. F., 2000. Three-dimensional estimation of elastic thickness under the Louisville ridge. J. Geophys. Res., 105, 13,239-13,252.

Mahoney, J.J., White, W.M., Upton, B.G.J., Neal, C.R., Scrutton, R.A., 1996. Beyond EM-1: Lavas from Afanasy-Nikitin Rise and the Crozet Archipelago, Indian Ocean. Geology, 24, 615-618.

Marks K.M. 1996. Resolution of the Scripps/NOAA marine gravity field from satellite altimetry. Geophy. Res. Lett. 23, 2069-2072.

Maurin, T., Rangin C., 2009. Impact of the 90°E ridge at the Indo-Burmese subduction zone imaged from deep seismic reflection data. Mar. Geol., 266,143-155.

McAdooD.C., Sandwell, D.T., 1989. On the source of cross-grain lineations in the central Pasific gravity field. J. Geophy. Res., 94, 9341-9352.

McKenzie, D.P., Sclater, J.G., 1971. The evolution of the Indian Ocean since late Cretaceous. Geophys. J. R. Astron. Soc., 25, 437-528.

McKenzie, D., Bowin, C., 1976. The relationship between bathymetry and gravity in Atlantic Ocean. J. Geophys. Res., 81, 1903-1915.

Michael, L., Krishna, K.S., 2011. Dating of the 85°E Ridge (northeastern Indian Ocean) using marine magnetic anomalies. Curr. Sci., 100, 1314-1322.

Minear, J. H., Toksoz, M.N., 1970. Thermal Regimes of a Downgoing Slab and Now Global Tectonics. J. Geophys. Res., 75, 1397-1419.

Molnar, P., Stock, J., 1985. A method for bounding uncertainties in combined plate reconstructions. J. Geophys. Res., 90, 12537-12544.

Molnar, P., Stock, J., 1987. Relative motions of hotspots in the Pacific, Atlantic and Indian oceans since late Cretaceous time. Nature, 327, 587-591.

Moore, D.G., Curray, J.R., Raitt, R.W., F.J., Emmel, 1974. Stratigraphic-seismic section corrlations and implications to Bengal Fan history. Init. Rep. Deep Sea Drill. Proj. 22, 403-412.

Morgan, W.J., 1971. Convection Plumes in the Lower Mantle. Nature, 230, 42-43.

Morgan W.J., 1972. Plate motions and deep convection. Geol. Soc. Am. Mem., 132, 7-22.

Morgan, W.J., 1981. Hotspot tracks and the opening of the Atlantic and Indian Oceans. In: C. Emiliani (Ed.), The Sea (Vol. 7): The Oceanic Lithosphere. Wiley-Interscience, NewYork, 443-487.

Moritz, H., 1980. Geodetic reference system 1980. Bulletin Géodésique, 54, 395-405.

Mukhopadhyay, M., Krishna, M.R., 1991. Gravity field and deep structure of the Bengal Fan and its surrounding continental margins, northeast Indian Ocean. Tectonophysics, 186, 365-386.

Mukhopadhyay, M., Radhakrishna, M., 1995. Gravity Anomalies and Deep Structure of the Ninetyeast Ridge North of the Equator, Eastern Indian Ocean - A Hot Spot Trace Model, Mar. Geophy. Res. 17, 201-216.

Müller, R.D., Royer, J.-Y., Lawver, L.A., 1993. Revised plate motions relative to the hotspots from combined Atlantic and Indian Ocean hotspot tracks. Geology, 21, 275-278.

Müller, R.D., Roest, W.R., Royer, J.-Y., Gahagan, L.M., Sclater, J.G., 1997. Digital isochrones of the world's ocean floor. J. Geophys. Res., 102, 3211-3214.

Müller, R.D., Gaina, C., Tikku, A.A., Mihut, D., Cande, S.C., Stock, J.M., 2000. Mesozoic/ Cenozoic tectonic events around Australia. In: Richards, M.A., Gordon, R., van der Hilst, R. (Eds.), The History and Dynamics of Global Plate Motions, AGU Geophysical Monograph, 161-188.

Mutter, J.C., Cande, S.C., 1983. The early opening between Broken Ridge and Kerguelen Plateau. Earth planet. Sci. Lett., 65, 369-376.

Naini, B.R, Leyden, R., 1973. Ganges Cone: A wide angle seismic reflection and refraction study. J. Geophys. Res., 78, 8711-8720.

Naini, B.R., Talwani, M., 1983. Structural framework and the evolutionary history of the continental margin of western India, In: Watkins, J. S., Drake, C. L. (Eds), Studies in Continental Margin Geology, AAPG Mem., 34 167-191.

National Geophysical Data Centre (NGDC), 1998. GEODAS CD-ROM, 98-MGG-04, Worldwide Marine Geophysical Data, up-dated 4th edn., National Oceanic and Atmospheric Administration , US Department of Commerce, Washington, DC.

Nayak, G.K., Rama Rao, Ch., 2002. Structural configuration of Mahanadi offshore Basin, India: An aeromagnetic study. Mar. Geophys. Res., 23, 471-479.

Neprochnov, Yu.P., Gopala Rao, D., Murthy, K.S.R., Subrahmanyam, C., 1998. Intraplate deformation in the Central Indian Ocean Basin. Geol. Soc. India. Memoir, 39, 71-86, GSI, Bangalore, India.

Nettleton, L.L, 1976. Gravity and magnetics in oil prospecting. 464p, McGraw-Hill international series in the earth and planetary sciences, USA.

Nogi, Y., Nishi, K., Seama, N., Fukuda, Y., 2004. An interpretation of the seafloor spreading history of the west Enderby basin between initial breakup of Gondwana and anomaly C34. Mar. Geophy. Res., 25, 219-229.

Norton, I.O., Sclater, J.G., 1979. A model for the evolution of th Indian Ocean and the breakeup of Gondwanaland. J. Geophys. Res., 84 (B12), 6803-6830.

O'Neill, C., Muller, D., Steinberger, B., 2003. Geodynamic implications of moving Indian Ocean hotspots. Earth Planet. Sci. Lett., 215, 151-168.

Parker, R.L., 1972. The rapid calculation of potential anomalies. Geophy. J. R. Astr. Soc., 31, 447-455.

Paul, J., Singh, R.N., Subrahmanyam, C., Drolia, R.K., 1990. Emplacement of Afanasy-Nikitin seamount based on transfer function analysis of gravity and bathymetry data. Earth Planet. Sci. Lett., 96, 419-426.

Peirce, J.W., 1978. The Northward Motion of India since the Late Cretaceous. Royal Astro. Soc. Geophys. J., 52, 277-311.

Plummer, PhS, Belle, E.R., 1995, Mesozoic tectono-stratigraphic evolution of the Seychelles microcontinent. Sedimentary Geology, 96, 73-91.

Pratt, J. H., 1855. On the attraction of the Himalaya Mountains and of the elevated regions beyond them, upon the plumb line in India. Philos. Trans.R. Soc. London, 145, 53-100.

Pringle, M.S., Frey, F.A., Mervine, E.M., Sager, W.W., 2007. New Ar/Ar ages from the Ninetyeast Ridge, Indian Ocean: Beginning of a robust Indo-Atlantic hotspot reference frame. AGU, 88(52), Fall Mtg. Suppl. Abstract, U13A-0871.

Pringle, M.S., Frey, F.A., Mervine, E.M., 2008. A simplr linear age progression for the Ninetyeast Ridge, Indian Ocean: New constraints on Indian Plate motion and hotspot dynamics. EOS, trans. AGU, 89(53), Fall Mtg, Suppl. Abstract, T54B-03.

Putnam, G. R., 1912. Condition of the Earth's crust. Science, 36, 869-871.

Radhakrishna, M., Lasitha S., Mukhopadhyay, M. 2008. Seismicity, gravity anomalies and lithospheric structure of the Andaman arc, NE Indian Ocean. Tectonophysics, 460, 248-262,doi:10.1016/j.tecto.2008.08.021.

Radhakrishna, M., Subrahmanyam,C., Twinkle Damodharan. 2010. Thin oceanic crust below Bay of Bengal inferred from 3-D gravity interpretation. Tectonophysics, 493, 93-105.

Radhakrishna, T., Dallmeyer, R.D., Josheph, M., 1994. Palaeomagnetism and $^{36}Ar/^{40}Ar$ isotope correlation ages of dyke swarms in central Kerala, India: tectonic implications. Earth. Plant. Sci. Lett., 121, 213-226.

Rajesh, S., Majumdar, T.J., 2009. Geoid height versus topography of the northern Ninetyeast Ridge: implications on crustal compensation. Mar. Geophy. Res., 30, 251-264.

Ramana, M.V., Subrahmanyam, V., Chaubey, A.K, Ramprasad, T., Sarma, K.V.L.N.S, Krishna, K.S., Maria Desa, Murty, G.P.S, 1997. Structure and origin of the 85°E Ridge. J. Geophys. Res., 102, 17995-18012.

Rapp, R.H., 1998. Comparison of altimetry derived and ship gravity anomalies in the vicinity of the Gulf of California. Mar. Geod., 21, 245-259.

Raval, U., Veeraswamy, K., 2003a. India-Madagascar separation: breakup along a pre-existing mobile belt and chipping of the craton. Gondwana Res., 6, 467-485.

Raval, U., Veeraswamy, K., 2003b. Modification of geological and geophysical regimes due to interaction of mantle plume with Indian lithosphere. J. Virtual Explorer, 12, 117-143.

Recq, M., Charvis, P., 1986. A seismic refraction survey in the Kerguelen Isles, southern Indian Ocean. Geophys. J. R. Astr. Soc., 84, 529-559.

Rotstein, Y., Munschy, M., Bernard, A., 2001. The Kerguelen province revisited: additional constraints on the development of the southeast Indian Ocean. Mar. Geophys. Res., 22, 81-100.

Royer, J.-Y., Sandwell, D.T., 1989. Evolution of the eastern Indian Ocean since the late Cretaceous: Constraints from Geosat altimetry. J. Geophys. Res., 94, 13,755-13,782, doi:10.1029/JB094iB10p13755.

Royer, J.Y., Peirce, J.W., Weissel, J.K., 1991. Tectonic constraints on the hotspot formation of Ninetyeast Ridge, Proc. Ocean Drill. Program Sci. Results, 121, 763-775.

Royer. J.-Y., Coffin, M.F., 1992. Jurassic to Recent plate tectonicreconstructions in the Kerguelen Plateau region. Proc. Ocean Drill. Program Sci. Results. 120, 917-928.

Royer, J-Y., Sclater, J.G., Sandwell, D.T., Cande, S.C., Schlich, R., Munschy, M., Dyment, J., Fisher, R.L., Muller, R.D., Coffin, M.F., Patriat, P. and Bergh, H., 1992. Indian Ocean plate reconstructions since the Late Jurassic. In: Duncan, R.A., Rea, D.K., Kidd, R.B., Von Rad, U., Weissel, J.K. (Eds.), Synthesis of Results from Scientific Drilling in the Indian Ocean. AGU Geophysical Monograph, 70, 70471-475, Washington DC, USA.

Royer, J.-Y., Gordon, R.G., 1997. The motion and boundary between the Capricorn and Australian plates. Science, 277, 1268–1274, doi:10.1126/science.277.5330.1268.

Royer, J.-Y., Chaubey, A.K., Dyment, J., Bhattacharya, G.C., Srinivas, K., Yatheesh, V., Ramprasad, T., 2002. Paleogene plate tectonic evolution of the Arabian and Eastern Somali basins. In: Clift, P.D., Kroon, D., Gaedicke, C., Craig, J. (Eds.), The Tectonic and Climatic Evolution of the Arabian Sea Region, 195. Geological Society, London, 7-23 (Special Publications).

Sager, W.W., Paul, C.F., Krishna, K.S., Pringle, M., Eisin, A.E., Frey, F.A., Gopala Rao, D., Levchenko, O. 2010. Large Fault Fabric of the Ninetyeast Ridge Implies Near-Spreading Ridge Formation. Geophy. Res. Lett., 37, L17304, 5, doi:10.1029/2010GL044347.

Sandwell, D.T., Smith, W.H.F., 1997. Marine gravity from Geosat and ERS-1 satellite altimetry. J. Geophys. Res., 102, 10039-10054.

Sandwell, D.T., Smith, W.H.F., 2009. Global marine gravity from retracked Gosat and ERS-1 altimetry: Ridge segmentation versus spreading rates, J. Geophys. Res., 114, B01411, doi: 10.1029/2008JB006008.

Sborshchikov, I.M., Murdmaa, I.O., Matveenkov, V.V, Kashintsev, G.L., Glomshtock, A.I. Al'mukhamedov, A.I., 1995. Afanasy Nikitin seamount within the intraplate deformation zone, Indian Ocean. Mar. Geol. 128, 115-126.

Schlich, R., 1982. The Indian Ocean: Aseismic ridges, spreading centers, and oceanic basins, In: Nairn, A.E.M. Stehli, F.G (Eds), The Ocean Basins and Margins, vol. 6, The Indian Ocean, 51-148, Plenum, New York.

Schubert, G., Sandwell, D., 1989. Crustal volumes of the continents and of oceanic and continental submarine plateaus. Earth. Planet. Sc. Lett., 92, 234-246.

Sclater, J.G., Fisher, R.L., 1974. Evolution of the East Central Indian Ocean, with Emphasis on the Tectonic Setting of the Ninety East Ridge. Geol. Soc. Am. Bull., 86, 683-702.

Sheena, V.D., Radhakrishna, M., Subrahmanyam, C., 2007. Estimates of effective elastic thickness along the Southwest Continental Margin of Inida using coherence analysis of gravity and bathymetry data-geodynamical implications. J. Geol. Soc. India., 70, 475-487.

Smith, W. H. F., Sandwell, D.T., 1997. Global seafloor topography from Satellite altimetry and ship depth soundings. Science, 277, 1956-1962.

Stagg, H.M.J., Calwell, J.B., Direen, N.G., O' Brien, P.E, Bernardel, G., Borissova, I., Brown, B.J., Ishihara, T., 2004, Geology of the continental margin of Enderby and Mac. Robertson Lands, East Antarctica : insights from a regional data set. Mar. Geophys. Res., Doi: 10.1007/S11001-005-1316-1.

Stocks, Th., 1960. Zur Bodengestalt des Indischen Ozeans; Erdkunde, Archiv fur wiss. Geogr., 14, 161-170.

Storey, M., Mahoney, J.J., Saunders, A.D., Duncan, R.A., Kelley, S.P., Coffin, M.F., 1995. Timing of hot spot-related volcanism and the breakup of Madagascar and India. Science, 267, 852-855.

Storey, M., Mahoney, J.J., Saunders, A.D., 1997. Cretaceous basalts in Madagascar and the transition between plume and continental lithosphere mantle sources. In: Mahoney J.J., Coffin M. (Eds), Large Igneous provinces: Continental, Oceanic, and Planetary Flood Volcanism. Am. Geophys. Union, Monogr, 95-122.

Subrahmanyam, C., Thakur, N.K., Gangadhara Rao, T., Khanna, R., Ramana, M.V, Subrahmanyam, V., 1999. Tectonics of the Bay of Bengal: new insights from satellite-gravity and ship-borne geophysical data. Earth Planet. Sci. Lett., 171, 237-251.

Subrahmanyam, C., Chand, S., 2006. Evolution of the passive continental margins of India-a geophysical appraisal. Gondwana Res., 10, 167-178.

Subrahmanyam, C., Gireesh, R., Chand, S., Kamesh Raju, K.A., Gopala Rao, D. 2008. Geophysical characteristics of the Ninetyeast Ridge-Andaman island arc/trench convergent zone. Earth Planet. Sci. Lett., 266, 29-45.

Subrahmanyam, V. Krishna, K.S., Radhakrishna Murty, I.V., Sarma, K.V.L.N.S., Maria Desa, Ramana, M.V., Kamesh Raju, K.A., 2001. Gravity anomalies and crustal structure of the Bay of Bengal. Earth. Plant. Sci. Lett., 192, 447-456.

Subrahmanyam,V., Subrahmanyam,A.S., Murty,G.P.S., Murthy, K.S.R., 2008. Morphology and tectonics of Mahanadi Basin, northeastern continental margin of India from geophysical studies. Mar. Geol., 253, 63-72.

Talwani, M., Worzel, J.L., Landisman, M. 1959. Rapid gravity computations for two-dimensional bodies with application to the Mendocino submarine fracture zone. J. Geophys. Res., 64, 49-59.

Talwani, M., Reif C., 1998. Laxmi Ridge—A continental sliver in the Arabian Sea. Mar. Geophys. Res., 20, 259-271.

Telford, W.M., Geldart, L.P., Sheriff, R.E., 1990. Applied Geophysics, second edition. 770p, Cambridge University Press, United Kingdom.

Tiwari, V.M., Diament, M., Sing, S.C., 2003. Analysis of satellite gravity and bathymetry data over Ninety-East Ridge: variation in the compensation mechanism and implication for emplacement processes. J. Geophys. Res., 108, 2109, doi: 10.1029/2000JB000047.

Torsvik, T.H., Tucker, R.D., Ashwal, L.D., Eide, E. A., Rakotosolofo, N.A., Dewit, M.J., 1998. Late cretaceous magmatism in Madagascar: paleomagnetic evidence for a stationary Marion hotspot. Earth. Plant. Sci. Lett., 164, 221-232.

Torsvik, T.H., Tucker, R.D., Ashwal, L.D., Carter, L.M., Jamtveit, B., Vidyadharan, K.T., Venkataramana, P., 2000. Late Cretaceous India-Madagascar fit and timing of break-up related magmatism. Terra Nova, 12, 220-224.

Turcotte, D.L., Schubert, G., 2002. Geodynamics. 456p, Cambridge University Press, Cambridge, United Kingdom.

Udintsev, G.B., 1975. Geological-Geophysical Atlas of the Indian Ocean, 151p, Pergamon, New York.

Vanney, J.R., Johnson, G. L., 1982. Marine geomorphology of Kerguelen-Antartica Passage (southern Indian Ocean). In: Scrutton, R.A., Talwani, M. (Eds), The Sea Floor, Wiley, London, 237-254.

Veevers, J.J., 1986. Breakeup of Australia and Antartica estimated as Mid-Cretaceous (95±5 Ma) from magnetic and seismic data at continental margins. Earth. Planet. Sci. Lett., 77, 91-99.

Vening-Meinesz, F.A., 1939. Tables fondamentales pour la réduction isostatique régionale. Bull. Geod., 63, 711-776.

Vine, F.J., Matthews, D.H., 1963. Magnetic anomalies over oceanic ridges. Nature, 199, 947-949.

Watts, A.B., 1978. An analysis of isostasy in the world's oceans: Hawaiian-Emperor Seamount Chain. J. Geophy. Res., 83, 5989-6004.

Watts, A.B., 1982. Seamounts and flexure of the lithosphere. Nature, 297, 182-183.

Watts, A.B., ten Brink, U.S., Buhl, P., Brocher T.M., 1985. A multi channel seismic study of lithospheric flexure across the Hawaiian-Emperor seamount chain. Nature, 315, 105-111.

Watts, A.B., 1988. Gravity anomalies, crustal structure and flexure of the lithosphere at the Baltimore Canyon Trough. Earth Planet. Sci. Lett., 89, 221-238.

Watts, A.B., ten Brink, U.S., 1989. Crustal structure, flexure and subsidence history of the Hawaiian Islands, J. Geophys. Res., 94, 10,473-10,500.

Watts, A.B, Fairhead, J.D, 1999. A Process-oriented approach to modeling the gravity of continental margins. The Leading Edge, February, 258-263.

Watts, A.B., 2001. Isostasy and flexure of the lithosphere, 458p, Cambridge University Press, UK.

Watts, A.B., Sandwell, D.T., Smith, W.H.F., Wessel, P., 2006. Global gravity, bathymetry, and the distribution of submarine volcanism through space and time. J. Geophy. Res., 111, B08408, doi: 10.1029/2005JB004083.

Wegener, A,. 1922. Die Entstehung der Kontinente und Ozeane. 3rd edn, Hamburg: Vieweg, Braunschweig.

Weis, D., Frey, F.A., 1991. Isotope geochemistry of Ninetyeast Ridge basement basalts: SR, ND, and PB evidence for involvement of the Kerguelen hotspot: In Proceedings of the Ocean Drilling Program, Scientific Results, College Station, Texas, Ocean Drilling Program, 121, 591-610.

Weissel J., Karner, G., 1989. Flexural Uplift of Rift Flanks Due to Mechanical Unloading of the Lithosphere during extension. J. Geophys., Res., 94, B10, doi: 10.1029/JB094iB10p13919.

Welch, P., 1967. The use of fast Fourier transform for the estimation of power spectra: A method based on time averaging over short, modified periodograms. IEEE Trans. Audio Electroacoustics, 15, 70-73.

Wessel, P., Smith, W.H.F., 1995. New version of the Generic Mapping Tools released. EOS Trans., American Geophysical Union, 76, 329.

White, R., McKenzie, D., 1989. Magmatism at rift zones - The generation of volcanic continental margins and flood basalts. J. Geophys. Res., 94, 7685-7729.

Whitmarsh, R.B. et al., 1974. Sites 219, 220 and 221. In: Whitmarsh R.B,. Weser, O.E and others (Eds), Initial Reports of the Deep-Sea Drilling Project, 23, U.S. Government Printing Office, Washington D.C., 35-210.

Wilson, J. T., 1963. A possible origin of the Hawaiian Islands. Can. J. Phys., 41, 863-870.

Wilson J.T., 1965. Evidence from oceanic islands suggesting movement in the Earth. Philos. Trans. R. Soc. London Ser., 258, 145-167.

Wilson, J. T,. 1966. Did the Atlantic close and then reopen?. nature, 211, 676-681.

Yatheesh, V., Bhattacharya, G.C., Mahender, K., 2006. The terrace like feature in the mid-continental slope region off Trivandrum and plausible model for India-Madagascar juxtaposition in immediate pre-drift scenario. Gondwana Res., 10, 179-185.

# List of Publications from the Present Research Work

Sreejith, K.M., Krishna, K.S. Bansal, A.R., 2008. Structure and isostatic compensation of the Comorin Ridge, north central Indian Ocean. Geopy. J. Int., 175, 729-741.

Sreejith, K.M., Radhakrishna, M., Krishna, K.S., Majumdar, T.J., 2011. Development of the negative gravity anomaly of the 85°E Ridge, northeastern Indian Ocean – a process oriented modeling approach. J. Earth Syst. Sci. (in press).

Sreejith K.M., Krishna, K.S., 2011. Structure and isostasy of the Ninetyeast Ridge and its tectonic implications. (Under preparation).

*Geophys. J. Int.* (2008) **175**, 729–741 doi: 10.1111/j.1365-246X.2008.03905.x

# Structure and isostatic compensation of the Comorin Ridge, north central Indian Ocean

K. M. Sreejith,[1] K. S. Krishna[1] and A. R. Bansal[2]

[1]*National Institute of Oceanography, Dona Paula, Goa* 403004, *India. E-mail: sreejith81@gmail.com*
[2]*National Geophysical Research Institute, Uppal Road, Hyderabad* 500007, *India*

Accepted 2008 June 30. Received 2008 June 18; in original form 2007 April 4

## SUMMARY

Bathymetry, gravity and magnetic data (about 9200 lkm) of the Comorin Ridge, north central Indian Ocean were investigated using the transfer function and forward model techniques to understand the mode of isostatic compensation and origin of the ridge. The ridge extends for about 500 km in NNW–SSE direction and associates with low-amplitude gravity anomalies ranging from 25 to 30 mGal compared to the ridge relief, suggesting that the anomalies are compensated at deeper depths. From Admittance analysis an Airy model or local compensation with an elastic plate thickness ($T_e$) of about 3 km and crust thickness ($t$) of 15–20 km are suggested for the southern part of the Comorin Ridge (south of 5°N), whereas for the northern part a flexural plate model with an elastic thickness of about 15 km is obtained. Admittance analysis together with the results from gravity forward modelling reveal that the south part was emplaced on relatively weak oceanic crust with both surface and subsurface loading, while the north part was emplaced on the continental crust. Based on present studies and published plate kinematic models we interpret that the Comorin Ridge was evolved at about 90 Ma during the rift stage of Madagascar from the southwest of India. We have also demarcated the continent–ocean boundary (COB) west of Sri Lanka and southern tip of India, which runs across the strike of the ridge, placing the northern part of the ridge on continent and southern part on oceanic crust. On the southern part of the ridge eastern flank is steep-faulted up to 0.6 km and is controlled by the 79°E FZ and then by COB.

**Key words:** Gravity anomalies and Earth structures; Continental margins: divergent; Oceanic hotspots and intraplate volcanism; Dynamics: gravity and tectonics; Lithospheric flexure; Indian Ocean.



## 1 INTRODUCTION

The Indian Ocean seafloor consists of numerous aseismic ridges, plateaus, seamounts, etc. Aseismic ridges which were evolved by the mantle plumes provide histories of the Indian plate motion and major tectonic events the plate underwent. The Comorin Ridge, an important aseismic ridge in the northern Indian Ocean, is relatively less understood in terms of structure, emplacement and nature of underneath crust compared to Ninetyeast, Chagos-Laccadive and 85°E ridges.

The Comorin Ridge was first reported from the compilation of echo-sounding data (Heezen & Tharp 1964) acquired during the International Indian Ocean Expedition (IIOE). The ridge trends in NNW–SSE direction in the deep-water region west of Sri Lanka and south of India, was named Comorin Ridge because of its vicinity to the place called Cape Comorin, southern tip of India (Fig. 1). Using marine geophysical data Kahle *et al.* (1981) have suggested that the Comorin Ridge was formed on oceanic crust with Airy type compensation and opined that the eastern edge of the Comorin Ridge could denote a boundary between oceanic crust and rifted or altered continental crust. Further they concluded that the ridge seems to act as a barrier to the passage of Ganges sediments to the west. Southeast of the Comorin Ridge Krishna *et al.* (2001a) have also mapped steep isolated basement rises in seismic reflection data and attributed the limiting of the western extent of Bengal Fan sediments to the rises which act as a barrier. All these structures together have encircled the western margin of Sri Lanka and contributed to the formation of a small basin within the Gulf of Mannar (Fig. 1).

In this study we have analysed ship-borne bathymetry and gravity data across the Comorin Ridge using transfer function technique and forward modelling. The main objectives of the study are (1) to determine the effective elastic plate thickness ($T_e$) and crustal thickness ($t$) across the south and north parts of the ridge, (2) to discuss the mode of isostatic compensation, nature of the underneath crust and its response to the ridge material, (3) to demarcate the continent–ocean boundary (COB) on the southwest margin of Sri Lanka and southern tip of India and (4) to outline the tectonic setting of the ridge, particularly on its eastern flank.

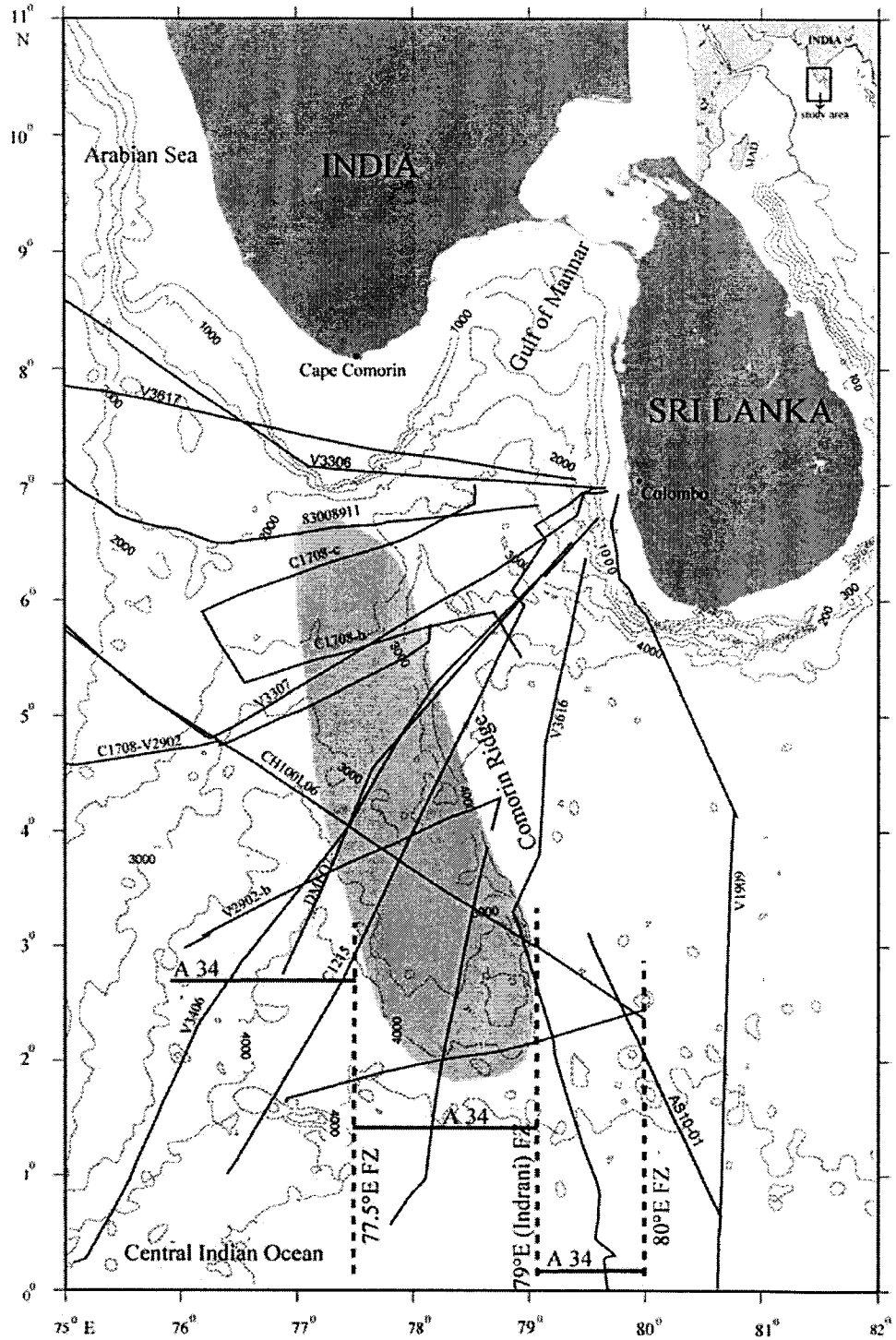


**Figure 1.** General bathymetry of the southern tip of India and south and west margins of Sri Lanka (ETOPO5). Light shaded region shows the location of the Comorin Ridge. Solid lines indicate the geophysical profiles acquired onboard various research vessels. Magnetic lineation A34 and fracture zones shown in this figure are after Müller *et al.* (1997) and Krishna and Gopala Rao (2000).

## 2 GEOLOGICAL SETTING OF THE REGION

The eastern margins of India and Sri Lanka were formed in the early Cretaceous after the break up from Mac. Robertson Land–Enderby Land, east Antarctica (Rotstein *et al.* 2001; Kent *et al.* 2002; Gaina *et al.* 2007). At a subsequent stage, after 124 Ma a continental fragment called Elan Bank was detached from the northeastern margin of India (Gaina *et al.* 2003). The southwest margin of Sri Lanka and southern margin of India seem to have

been rifted initially at around 127 Ma from east Gunnerus Ridge, east Antarctica. At a stage, before the commencement of the first major change in spreading direction in the Indian Ocean, there was a probable ridge jump towards India–Sri Lanka region similar to the ridge jump which occurred on the northeast margin of India. This implies that the earliest oceanic crust formed near the India–Sri Lanka region was transferred to the west Enderby Basin (Nogi *et al.* 2004). Therefore, the oceanic crust adjacent to India–Sri Lanka region appears to be evolved during the long Cretaceous normal polarity reversal.

The western margin of India presumably rifted from the eastern margin of Madagascar during the Late Cretaceous period (White & McKenzie 1989; Storey *et al.* 1995, 1997; Torsvik *et al.* 1998, 2000; Raval & Veeraswamy 2003a). The rifting process was associated with the Marion hotspot volcanism which occurred at Volcan de l'Androy, southeast Madagascar and caused the eruption of widespread basalts and rhyolites in Madagascar and Fe-Ti-enriched tholeiites in southwest India. The hotspot might have formed the Comorin Ridge and some basaltic flows and dykes in the southwestern margin of India (Radhakrishna *et al.* 1994; Anil Kumar *et al.* 2001) as well as in Madagascar (Storey *et al.* 1995; Torsvik *et al.* 1998) before shifting its activity entirely to the African plate. The Comorin Ridge extends in NNW–SSE direction between latitudes 1.5°N and 6.5°N (Fig. 1) with an average width of 150 km. The southern part of the ridge lies on the oceanic crust evolved earlier than the seafloor magnetic anomaly A34 and is bounded by the 77.5°E and 79 E (Indrani) FZs. The nature of the crust beneath the northern part of the ridge is not clearly known.

## 3 GEOPHYSICAL DATA

Bathymetry, gravity and magnetic data along 17 profiles totalling to 9200 lkm across the Comorin Ridge and in its adjacent parts, acquired during the cruises of Conrad 17, Vema 29, 33, 34, Chain L06, Jean Charcot 83008911 and Dimitry Mendeleev 07 (NGDC 1998) and A. A. Sidorenko (AS 10), are used in this study to investigate the mode of compensation and origin of the ridge. Additionally, ETOPO-5 bathymetric data (3-D image) are used to study the morphology of the ridge. Sediment isopachs of this region published by Kahle *et al.* (1981) are also considered for 2-D forward modelling of gravity anomalies to constrain the sediment thickness along profiles C1215 and V3307. Profiles considered from Vema and Conrad cruises, were acquired using GSS-2 and Bell gravimeters and satellite navigation system, which have an accuracy of 2–5 mGal. For Chain profile (CHI00L06) the details of navigation and gravity instruments used in the survey are not available. Profiles Jean Charcot 83008911 and Dimitry Mendeleev 07, used satellite navigation system but the information on type of gravimeter used is not available. The reliability of the data has been examined at available cross over points, and we feel that the accuracy is fair enough for carrying out regional studies.

## 4 BATHYMETRY, GRAVITY AND MAGNETIC ANOMALIES OF THE RIDGE

A 3-D topographic map of the seafloor is shown in Fig. 2 for better visualization of the Comorin Ridge morphology and for its comparison with the adjacent seafloor. Bathymetry, gravity and magnetic profiles have been stacked with reference to axis of the Comorin Ridge and are shown in Fig. 3. The depth to the seafloor along the profiles (Fig. 3) varies from 2 to 4.2 km. The important geomorphic features in the study area are the Comorin Ridge, another ridge-like structure in the northwest quarter of the region, a steep scarp of up to 1.2 km on the eastern flank of the ridge, and 77.5°E and 79°E (Indrani) FZs. In general the water depth adjacent to the Comorin Ridge is decreasing towards north from 4 to 2.5 km (Figs 2 and 3). The southern part of the ridge between 1.5°N and 3°N has an elevation of up to 0.5 km compared to that of adjacent seafloor. In the central part between 3°N and 5°N the ridge has maximum elevation of 1 km from the surrounding water depths, and in the north between 5°N and 6.5°N the ridge has an elevation mostly on eastern side ranging from 0.4 to 0.7 km (Fig. 3). On the northern part of the ridge, the western flank does not have any distinct bathymetric expression as it probably merges with the continental rise of the southern tip of India (Fig. 2). While in the southern part, the western flank extends for more than 100 km with relatively smooth gradient, the eastern flank comes to an end about 50 km distance with a steep scarp of about 1.2 km (Fig. 3). North of the ridge, north of 5.5°N the eastern steep scarp is not obviously seen.

The free-air gravity anomalies of the study area in general follow the topography of the seafloor with variable amplitudes (Fig. 3). From satellite gravity data of the central Indian Ocean, Gopala Rao *et al.* (2004) found NW trending elongated gravity high closures associated with the Comorin Ridge. From the profile data it is evident that the ridge is associated with relatively low amplitude gravity anomalies of about 25 mGal in southern part (1.5°N–5 N) and 30 mGal in northern part (5°N–6.5°N) corresponding to its variable elevations. The less elevated northern part of the ridge is associated with relatively high-amplitude 30 mGal gravity anomaly, suggesting that this part of the ridge is relatively less compensated in comparison to its southern part. Along the profiles C1215, V2902-b, V3406, DME07, C1708-V2902, V3307 and C1708-b a significant regional gravity anomaly of more than 50 mGal is observed on the eastern flank of the Comorin Ridge (Fig. 3). Such significant anomaly is absent on other profiles, CH100L06 and C1708-a, in spite of sharp increase in depths to the seafloor (about 500 m) on eastern side of the ridge. Northern most profiles, V3306 and V3617 show bathymetric rise and associated high gravity anomalies (Figs 1 and 3), which are related to southern the tip of continental margin of India and not associated with the Comorin Ridge.

Most of the study area underlined by oceanic crust was evolved during the period from post-anomaly 34 to younger part of the long Cretaceous magnetic quiet period. The seafloor magnetic anomaly 34 is identified on profiles V2902-a and C1215 (Fig. 3). The rest of the anomalies are short-wavelength and low amplitude and may have been formed during the Cretaceous magnetic quiet period. The anomaly identifications (A34) are reasonably acceptable as they are found to be compatible with the earlier anomaly identifications of adjacent region (Krishna & Gopala Rao 2000). It is observed that the Comorin Ridge is not associated with any specific magnetic anomaly signatures.

## 5 GRAVITY AND TOPOGRAPHY—ADMITTANCE ANALYSIS

Admittance analysis (Transfer function technique) is regarded as one of the important geophysical approaches for quantitative study of isostatic compensation mechanism beneath aseismic ridges, seamounts, etc., whereby to understand the evolution of geological structures (McKenzie & Bowin 1976; Watts 1978; Detrick &

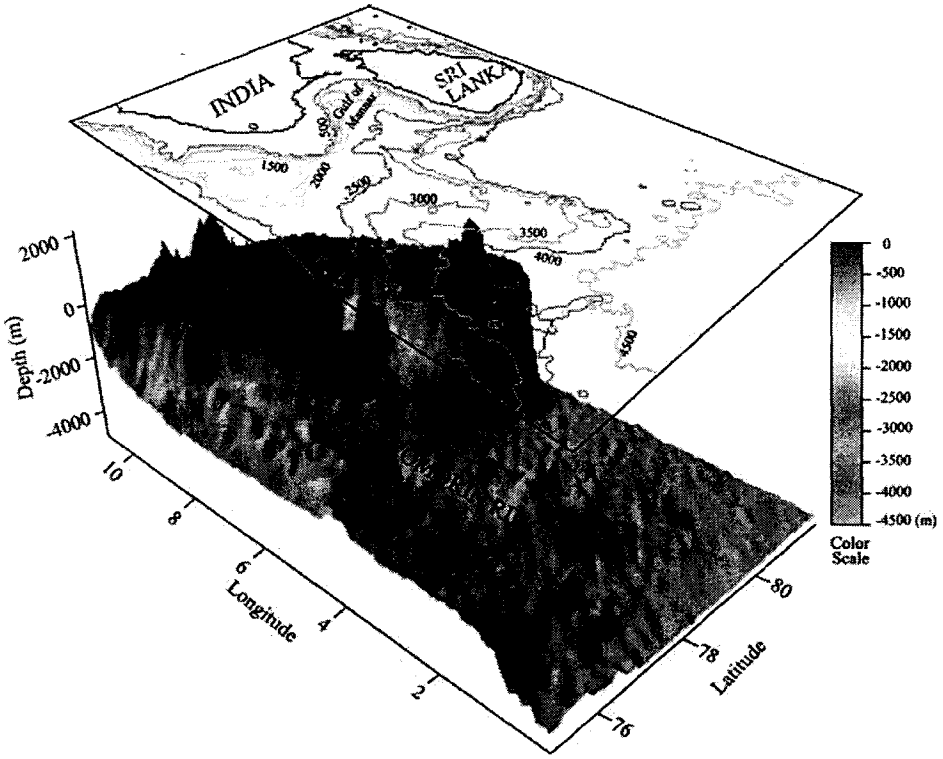


**Figure 2.** 3-D topography of the Comorin Ridge generated from ETOPO5 data.

Watts 1979). The technique was employed earlier on different geological features of the Indian Ocean to obtain important geophysical details regarding their formation and evolution (Paul *et al.* 1990; Ashalatha *et al.* 1991; Tiwari *et al.* 2003; Bansal *et al.* 2005). The admittance analysis derives isostatic parameters such as effective elastic plate thickness, average crustal thickness, mean depth to seafloor and density of oceanic crust; mode of compensation and tectonic setting, whether the volcanic emplacement was near the spreading ridge or in intraplate situation.

The admittance between gravity and bathymetry data can be calculated as suggested by McKenzie & Bowin (1976),

$$Z(k) = \frac{C(k)}{E_t(k)}, \tag{1}$$

where $k$ is the wavenumber, $Z(k)$ is gravitational admittance between gravity and topography, $C(k)$ is cross spectrum of the gravity and topography and $E_t(k)$ is power spectrum of the topography.

The Welch's averaged periodogram method was used to compute cross spectrum and power spectrum because of its improvement over the conventional fast Fourier transform (FFT) method (Welch 1967). The method has the advantage of having less variance, hence it produces smooth admittance. In this method, bathymetry and gravity data are divided into overlapping segments and each of them is detrended, windowed using Hanning window and discrete Fourier transformed. Two more additional parameters, coherence and phase of admittance, are also calculated. The coherence is a measure of gravity produced by seafloor topography. The phase of admittance is an indicator of the coherence between free-air gravity and seafloor topography, where zero value of phase indicates high coherence (Watts 2001). The coherence can be calculated as:

$$\gamma_0^2 = \text{coherence} = \frac{C(k)C^*(k)}{E_g(k)E_t(k)}, \tag{2}$$

where $C(k)$ is cross-spectrum between free-air gravity and seafloor topography, $C^*(k)$ is conjugate of cross spectrum between free-air gravity and seafloor topography and $E_g(k)$ and $E_t(k)$ are power spectrum of free-air gravity field and seafloor topography, respectively.

The phase of admittance is given by

$$\theta = \arctan[\text{Im}\, Z(k)/\text{Re}\, Z(k)]. \tag{3}$$

Theoretical basis for the calculation of admittance of Airy and Flexure models has been discussed in detail earlier by McKenzie & Bowin (1976) and Watts (2001), hence not presented here. The model parameters used for the calculation of theoretical admittance are given in Table 1.

**Table 1.** Model parameters used for the calculation of theoretical admittance.

| Parameter | Notation | Value |
|---|---|---|
| Density of sea water | $\rho_w$ | 1030 Kg m$^{-3}$ |
| Density of oceanic layer 2 | $\rho_2$ | 2700 Kg m$^{-3}$ |
| Density of oceanic layer 3 | $\rho_3$ | 2900 Kg m$^{-3}$ |
| Density of mantle | $\rho_m$ | 3350 Kg m$^{-3}$ |
| Thickness of oceanic layer 2 | $t_2$ | 2 km |
| Thickness of oceanic layer 3 | $t_3$ | 5 km |
| Young's modulus | $E$ | 100 Gpa |
| Poissons ratio | $\sigma$ | 0.25 |

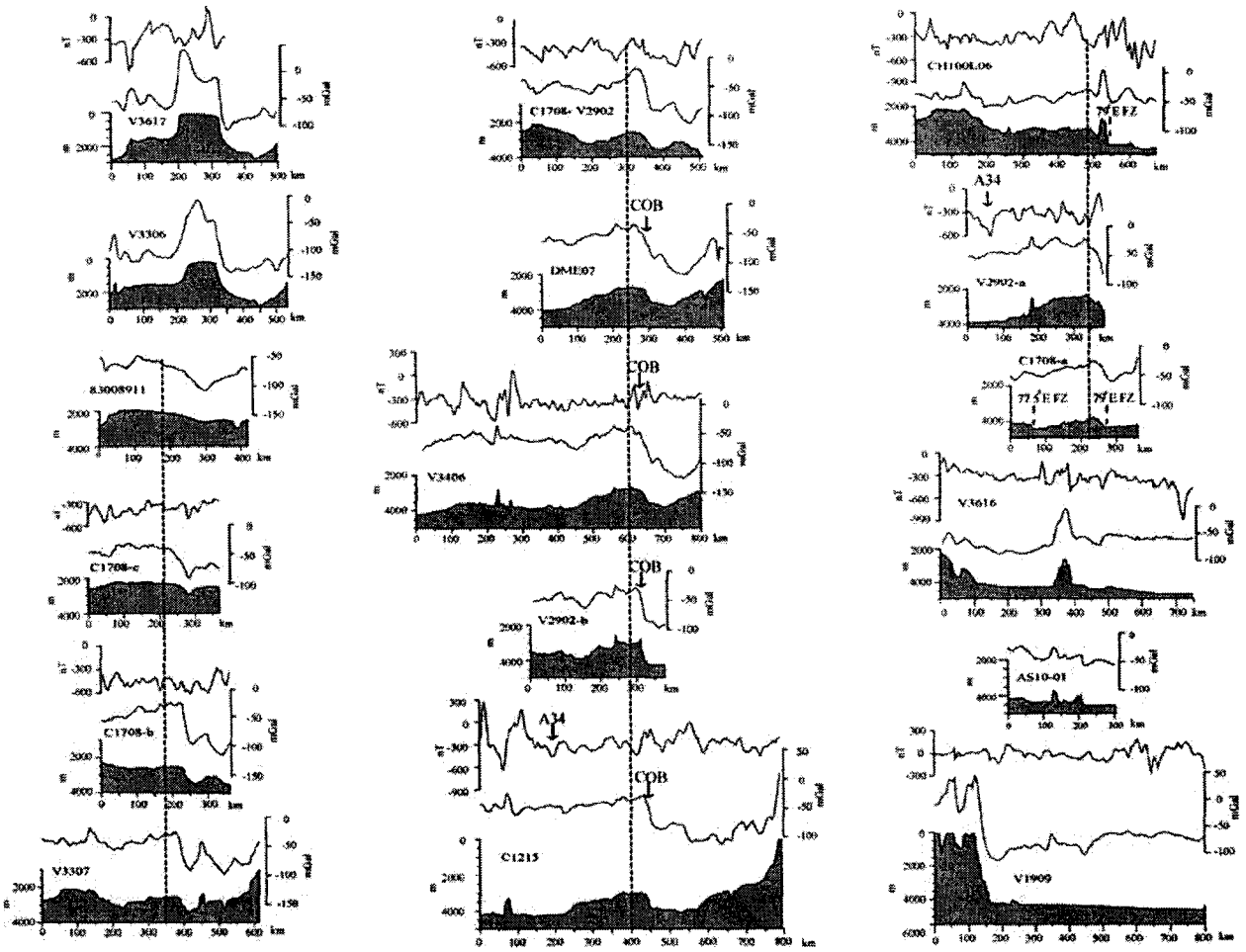


**Figure 3.** Composite plots of bathymetry, gravity and magnetic profile data across the Comorin Ridge and its vicinity. The dashed line marks the axis of the Comorin Ridge.

### 5.1 Elastic plate thickness ($T_e$) and crustal thickness ($t$)

Bathymetry and gravity profiles across the ridge are projected perpendicular to the strike of the ridge and their length is limited to 300 km keeping the apex of the ridge in the centre for the purpose of analysis. Each profile has been sampled at an interval of 1.172 km representing a spatial wavenumber range of $0.0105 < k < 2.6805$ km$^{-1}$ ($600 > \lambda > 2.344$ km). Finally, ends of the profiles were tapered using a cosine window of 10 per cent profile length prior to the spectral estimation. Rough estimates of elastic plate thickness ($T_e$) and crustal thickness ($t$) along each profile were obtained by comparing with theoretical models (Table 2). On the basis of $T_e$- and $t$-value ranges we have combined the profiles into two groups: southern profiles ($T_e$ range 1–5 km, $t$ range 15–20 km) and northern profiles ($T_e$ range 9–20 km and $t$ more than 30 km) with a view to calculate smoothed admittance by averaging individual spectra.

The admittance, coherence and phase for southern and northern profiles of the ridge are presented in Figs 4(a) and (b), respectively. For $k < 0.314$ ($\lambda > 20.01$ km), coherence is high ($\gamma_2^0 > 0.5$), phase is low ($\theta$), admittance is smooth and appears to be significant. Presence of sediments may reduce the coherence of short-wavelength admittance, but will not affect the analysis of the intermediate and long-wavelength admittance. It is also reported that thick sedimentary cover may affect the calculation of gravity anomalies from bathymetry and admittance filter. Sedimentary cover over the Comorin Ridge is not thick not (<0.4 km) and nearly uniform, hence we believe that the sedimentary cover has no significant effect on the admittance analysis for southern and northern parts of the ridge.

Average water depth and density of the crust are calculated from slope and intercept of the linear least-square fit to the log10 admittance for $0.11 < k < 0.8167$ and $0.04 < k < 0.44$ for the southern and northern parts of the ridge. These wavebands represent the portion where the admittance linearly decreases with wavenumber and the coherence is much above zero. For the southern part the mean calculated water depth, 3.52 km is in agreement with observed water depth of 3.5 km and the estimated density of 2.5 g cc$^{-2}$ is less than the density of normal oceanic crust. Estimated water depth (2.7 km) and density (2.75 g cc$^{-2}$) for the northern part are comparable with the observed water depth of 2.6 km and density of normal oceanic crust. Theoretical admittance values and observed admittance values with standard error bars are plotted and shown in Figs 5(a) and (b). Root mean square (rms) errors between the observed and theoretical admittance for different $t$ and $T_e$ values have been presented in Figs 5(a) and (b). We explain the fit between

**Table 2.** Elastic plate thickness ($T_e$) and crustal thickness ($t$) are determined from admittance analysis and approximate age of lithosphere at the time of ridge emplacement is determined for each profile following the relationship of Calmant & Cazenave (1987).

| S. No. | Profile ID | $T_e$ (km) | $t$ (km) | Approximate age (Myr) | Remarks |
|---|---|---|---|---|---|
| 1 | C1708-a | 4–5 | 15 | 2.2–3.5 | Low $T_e$ and high $t$ values |
| 2 | CH100L06 | 1–3 | No match | 0.13–1.2 | Low $T_e$ value |
| 3 | C1215 | 2–3 | 10–15 | 0.6–1.2 | Low $T_e$ and high $t$ values |
| 4 | V2902-b | 3–4 | 20 | 1.2–2.2 | Same as above |
| 5 | V3406 | 3–4 | 20 | 1.2–2.2 | Same as above |
| 6 | C1708-V2902 | 9–15 | 30–40 | 11–31 | High $T_e$ and exceptionally high $t$ values |
| 7 | V3307 | 10–15 | 40 | 14–31 | Same as above |
| 8 | C1708-c | 10–15 | >40 | 14–31 | Same as above |
| 9 | 84000411 | 15–20 | >50 | 31–55 | Same as above |

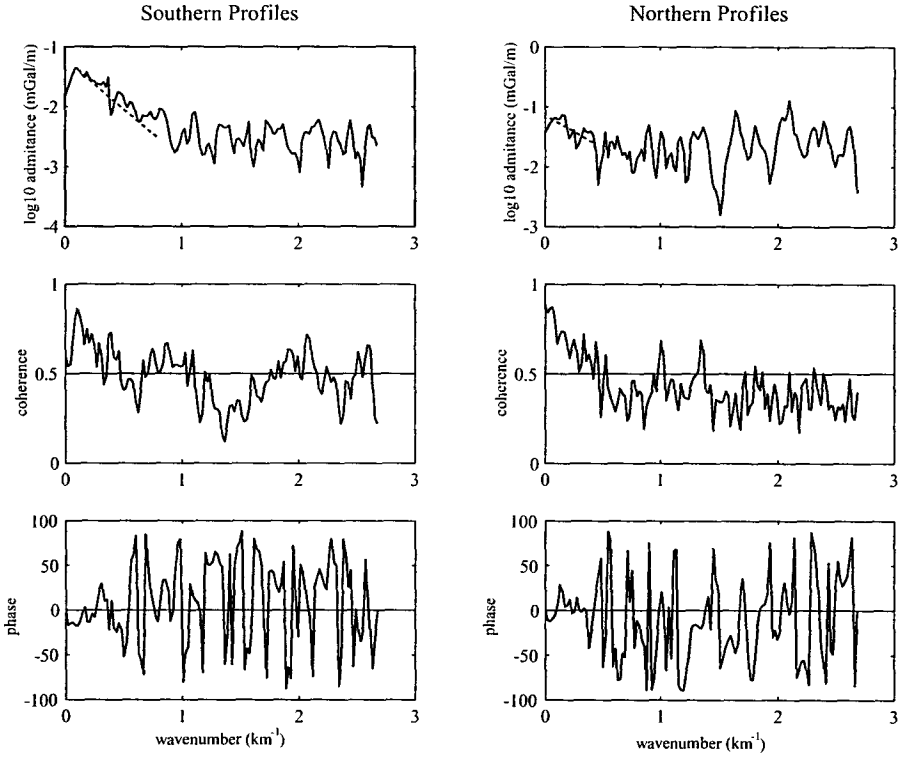


**Figure 4.** log10 of the amplitude of admittance, coherence and phase in degree generated from (a) southern and (b) northern set profiles. The dashed line represents the best fit to the observed admittance for (a) $0.11 < k < 0.8167$ and (b) $0.04 < k$ 0.44.

observed and theoretical curves based on both minimum rms error condition and error bounds in the admittance calculation.

Admittance values calculated for southern part of the ridge (Fig. 5a) are suitable for Airy model of isostatic compensation with a crustal thickness ($t$) of 15–20 km and for flexural model with a $T_e$ value of ~3 km, indicating that the southern part of the ridge has Airy model compensation and was emplaced on a young and weak oceanic crust. The results are confirmed by 2-D forward model studies, carried out along profile, C1215 (Fig. 6). The model studies infer that the surface load is compensated beneath the ridge at a depth of 18–20 km from sea surface, which is comparable with the average crustal thickness of 15 km obtained for the Airy model. The observed admittance for the northern part of the ridge is too high to be explained by the Airy model compensation. Crustal thickness of about 40 km is required for explaining the observed admittance, which is very unlikely to be there beneath the ridge. On the other hand, a simple flexural model with $T_e$ value of ~15 km is reasonably in agreement with the observed admittance (Fig. 4b). The nature of the underneath crust may be interpreted either as an old oceanic crust or rifted/altered continental crust.

## 6 CRUSTAL STRUCTURE BENEATH THE COMORIN RIDGE

Two gravity anomaly profiles, C1215 from southern part and V3307 from northern part of the Comorin Ridge have been chosen to determine the crustal structure using 2-D forward modelling technique. The profiles were selected as the admittance results broadly suggested that the ridge was emplaced in two geological settings: southern part of the ridge was formed on weak oceanic crust and the northern part was formed either on old oceanic crust or continental crust. Sediment layer and oceanic crust layers (2 and 3) thicknesses

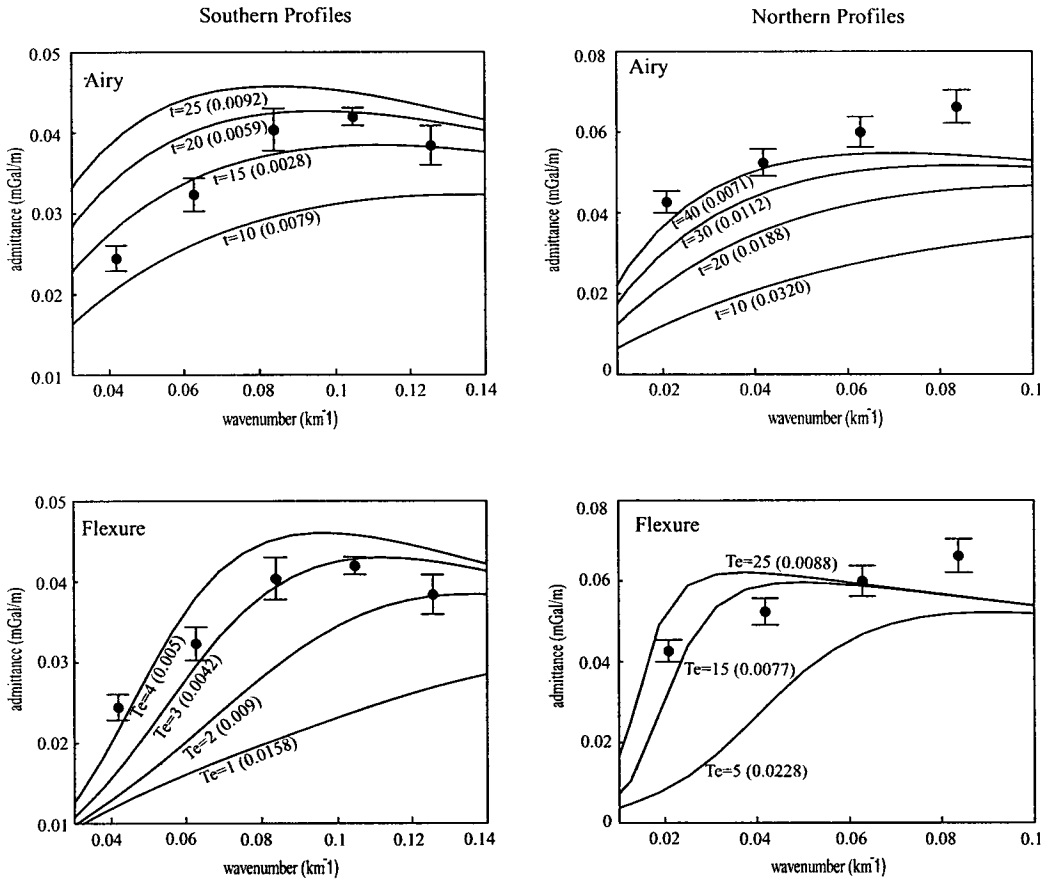


**Figure 5.** Observed admittance (solid dots) with standard error bars generated from (a) southern and (b) northern set profiles plotted with theoretical curves based on Airy and Flexure models. The rms error in mGal $m^{-1}$ between the observed and theoretical admittance for various $t$ and $T_e$ values are shown in bracket.

are considered from sediment isopach map of Kahle *et al.* (1981) and seismic refraction results of equatorial region published by Bull & Scrutton (1990) and Neprochnov *et al.* (1998), respectively as initial constraints. The crustal layers are refined moderately to determine the crustal structure beneath the Comorin Ridge. We have used the seismic velocities obtained from the refraction studies of the equatorial region, 1°S–2°N (Bull & Scrutton, 1990; Neprochnov *et al.* 1998) to determine the densities for oceanic crust, whereas for densities of continental crust, seismic velocity results of western continental margin of India (Naini & Talwani, 1983) were used. Then these velocities were converted to densities following the velocity–density relationship (Christensen 1977). Using these densities and thicknesses of crustal layers, we have modelled the gravity anomalies along the profiles C1215 and V3307 and determined crustal structures are shown in Fig. 6.

The gravity model studies reveal that the crust beneath the southern part of the Comorin Ridge is ~17 km thick consisting of 2-km-thick volcanic rocks, 6-km-thick oceanic crust and 9-km-thick underplated magmatic rocks (Fig. 6). The crust is comparatively thicker than oceanic crust thickness (7–8 km) lying west of the ridge and nearly equals the thickness of continental crust extending from the southwest of Sri Lanka. The continental crust-off southwest of Sri Lanka terminates at eastern flank of the Comorin Ridge, revealing that the ridge was basically emplaced on the oceanic crust lying adjacent to the continental crust. A small flexure to the magnitude of up to 1 km is observed at interfaces within the crust. Beneath other geological features of the Indian Ocean such as Ninetyeast Ridge and Afanasy Nikitin seamount thick anomalous crustal structures including volcanic and magmatic rocks were determined (Krishna *et al.* 2001b; Krishna 2003) and they are comparable with the results of crustal structure of the southern part of the Comorin Ridge. We made an attempt to model the gravity anomalies of the profile V3307 running across the northern part of the ridge, with two types of crust (continental or old oceanic) to determine the nature of crust beneath the ridge. In the first computation we assumed the underneath crust as continental and could achieve a reasonably good fit between observed and computed gravity anomalies (Fig. 6). The crustal structure indicates that the northern part of the ridge was emplaced on continental crust with a crustal thickness of about 20 km. About 3-km-thick volcanic rocks are determined on top of the crust, which had eventually contributed to flexure the crustal layers and Moho boundary with a magnitude of about 3 km (Fig. 6).

In the second computation we assumed the underneath crust as old oceanic crust with the consideration of similar geometry for upper/ lower crust and Moho interfaces obtained in the earlier model, but with greater densities and reduced thickness of crustal layers. Even in this situation we could get reasonable fit with a crustal thickness of about 15 km beneath the ridge and its westward component, but towards east crust thickness increases up to

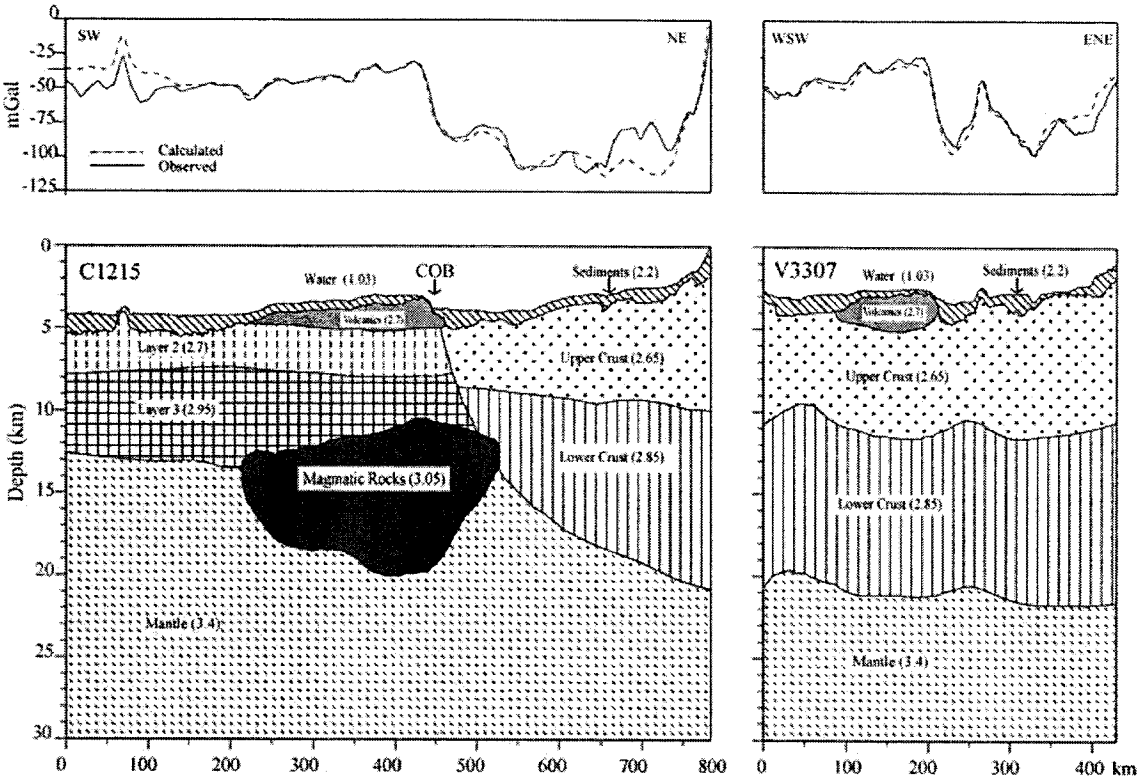


**Figure 6.** 2-D gravity model with interpreted crustal structure along profiles C1215 and V3307. Numerical values within brackets indicate the densities (gm $cc^{-1}$) of different strata.

18 km. This crustal model has two difficulties for acceptance: (1) it is difficult to consider such over thick oceanic crust beneath the north part of the ridge against usual thickness of 7 km oceanic crust and (2) high $T_e$ value of about 15 km and oceanic crust age of about 30 Myr (determined from $T_e$ value) at the time of volcanic emplacement are not in accordance with the plate motion data particularly with reference to the evolution of the south part of the ridge.

## 7. CONTINENT-OCEAN BOUNDARY ON WESTERN MARGIN OF SRI LANKA AND SOUTHERN TIP OF INDIA

Demarcation of COB along the continental margins, in general, provides useful geological information for understanding the evolution of basins, ridges, etc., lying in the vicinity of margins or oceanward. The boundary and associated geophysical signatures may further reveal how the segments of continental margin split from its conjugate margin, whether those were in transform motion before they drifted away or in rift phase for longer periods. A steep scarp on seafloor topography and rapid decrease in gravity anomaly are, in general, observed with variable amplitudes on eastern edge of the Comorin Ridge. The 79°E FZ in the central Indian Ocean, south of this study area possess a distinct step-like structure with rapid increase in water depths by about 0.3 km and sudden fall in gravity anomalies by about 20 mGal on eastern side of the FZ (Kamesh Raju *et al.* 1993). Keeping these signatures in view we have mapped the northward continuity of the 79°E FZ on profiles C1708-a and CH100L06 (Figs 1 and 3). Further north along profiles C1215, V2902-b, V3406 and DME07 steep scarp of about 1.2 km on eastern side of the ridge is seen associated with the lateral shift of ~50 mGal in regional gravity field. But no significant magnetic anomaly is seen coinciding with the steep scarp of the seafloor topography and lateral shift of the gravity field as the oceanic crust of the study area may have evolved during the long interval of Cretaceous Magnetic Quiet Period. The shift in gravity field may be interpreted due to the presence of high-density oceanic rocks beneath the volcanic rocks of the Comorin Ridge (Fig. 6) between latitudes 3.5°N and 5°N. Earlier, following the same criterion of lateral shift in gravity field, Chaubey *et al.* (2002) and Krishna *et al.* (2006) have demarcated the COB west of the Laccadive Ridge and Laxmi Ridge, respectively. On close observation we found that the amplitude of the gravity anomaly along the eastern edge of the Comorin Ridge varies from ~55 mGal in the central part between 3.5°N and 5°N to ~65 mGal in the northern part between 5°N and 6° N, although the depth to the seafloor is nearly constant (~0.9 km). The gravity anomaly on northern part is independently controlled by the undulations of seafloor topography, whereas in the central part the anomaly is contributed by multiple sources such as seafloor undulation and geometry between the Moho, lower crust and magmatic body at deeper depth. In other words the northern part of the ridge was emplaced on rigid continental lithosphere and the central part was evolved nearly in the vicinity of continent–ocean adjoining region, hence the gravity anomaly of the central part of the ridge is compensated.

From Admittance and forward modelling studies it is found that continental crust lies below the north part of the Comorin Ridge (north of 5°N latitude), allowing COB to run across the strike of

the ridge. The boundary permits the north part of the ridge on continent and south part on oceanic crust. Earlier Kahle *et al.* (1981) have related the eastern edge of the Comorin Ridge to the place of significant change in crustal structure, which they have cautiously attributed to the boundary between oceanic crust on the seaward side and rifted or altered continental crust on the landward side.

We have compared the COB and associated magnetic and gravity anomalies of this study area with that of eastern and western margins of India (Gopala Rao *et al.* 1997; Krishna *et al.* 2006) (Fig. 7), with a view to discussing the possible geological processes associated in COB evolution (Fig. 7). On eastern margin of India the COB was located at about 70–80 km seaward of the shelf edge, where as on western margin of India the COB was placed along the west of

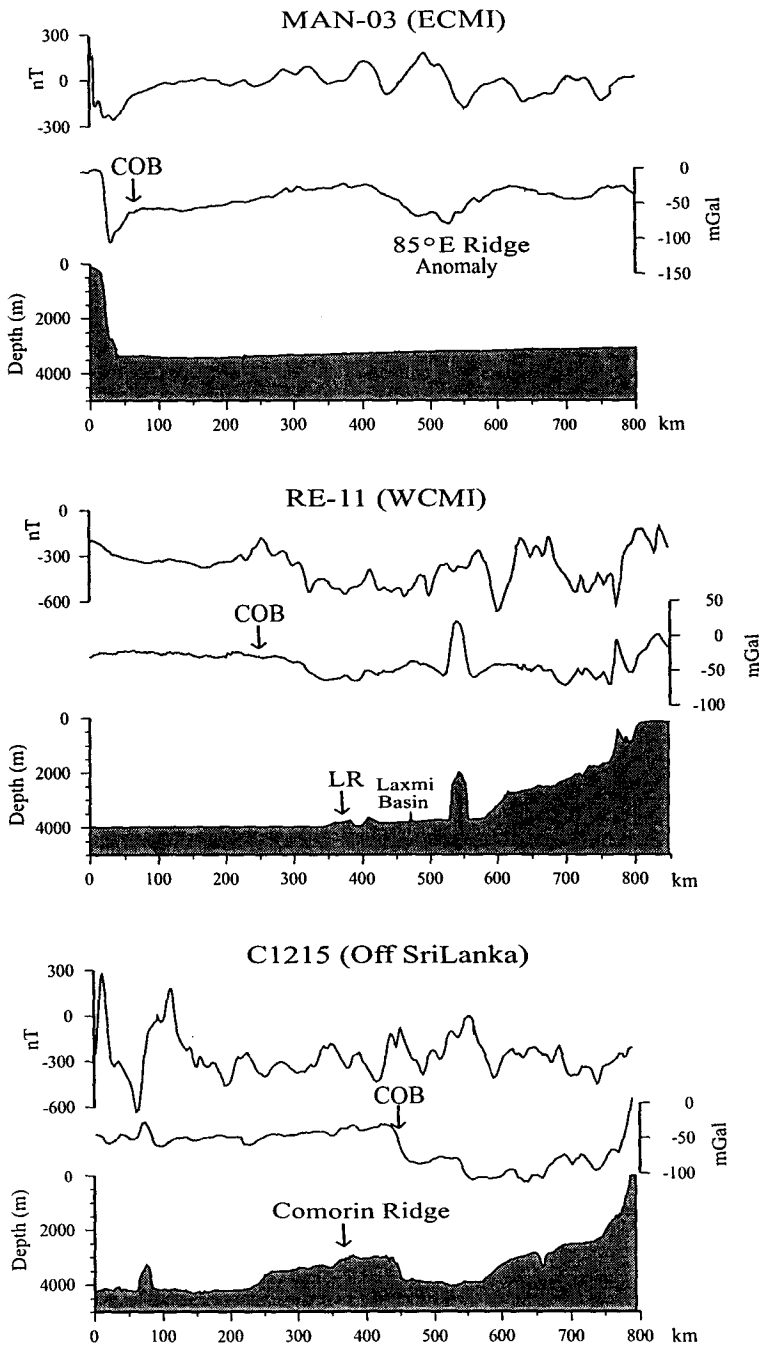


**Figure 7.** A comparison of bathymetry, gravity and magnetic profile data from western continental margin of India (WCMI), eastern continental margin of India (ECMI) and western margin of Sri Lanka. The diagnostic character of regional shift in gravity anomaly for demarcation of COB is observed in western margin of Sri Lanka and WCMI.

the Laxmi Ridge about 400 km away from the shelf edge. In this study area we found that the COB lies about 250 km off southwest of Sri Lanka and about 300 km off southern tip of India (Fig. 9). The gravity signature having a lateral shift in regional field is seen associated with the COB on both western margins of India and Sri Lanka, while on the eastern margin of India the COB associates with a different gravity signature of high-amplitude, short-wavelength negative gravity anomaly that rapidly changes to low-amplitude broad regional anomaly (Gopala Rao *et al.* 1997; Subrahmanyam *et al.* 2001). South of Sri Lanka we have placed the COB about 250 km away from the coastline following the changes in regional character of the gravity field on profiles (V3616 and V1909 in Fig. 3) as well as in satellite gravity image (Fig. 9). The boundary is tentatively shown, but needs to be confirmed by other geophysical results. Off Kron Prinz Olav Kyst and Gunnerus Ridge region, east Antarctica (conjugate part of Sri Lanka), Stagg *et al.* (2004) have marked the COB below the Enderby Basin, which is about 250 km away from the coastline and lying in water depths of around 4000 m. Thus the COB on southwest and southern parts of Sri Lanka and their conjugate region, off east Antarctica has evolved approximately in similar geological processes.

## 8 TECTONICS AND EVOLUTION OF THE COMORIN RIDGE

Marine geophysical data of the Comorin Ridge was investigated using transfer function and forward modelling techniques in order to obtain the elastic plate thickness and crustal structure beneath the ridge. Admittance analysis suggested that an Airy model or local compensation with an elastic plate thickness of about 3 km and crustal thickness of about 15–20 km best explains the southern part of the ridge, whereas a flexural model with a plate thickness of about 15 km explains the regional compensation beneath the northern part of the ridge. From 2-D gravity model studies we found that the southern part of the ridge (south of 5°N) was emplaced on 2–3 Myr old weak lithosphere and reaches a crustal thickness of about 17 km including 2-km-thick volcanic rocks as surface load and 9-km-thick magmatic rocks as subsurface load. No magmatic rocks are found lying beneath the northern part of the ridge and it is regionally compensated with a flexure of about 3 km at upper/lower crust interface and at Moho boundary. Thus the Comorin Ridge possesses two modes of isostatic compensation with Airy model beneath the southern part of the ridge and plate model beneath the northern part.

Considering the Airy isostatic model beneath the southern part of the ridge, proximity of seafloor spreading magnetic anomaly 34 between 77.5°E FZ and 79°E FZ and plate kinematic models we conjecture that the ridge was formed during the Late Cretaceous period. Volcanic rocks, erupted during the Late Cretaceous were found on the southwest coast of India (Radhakrishna *et al.* 1994; Kumar *et al.* 2001) and southeast of Madagascar (Storey *et al.* 1995; Torsvik *et al.* 1998, 2000) and the rocks were considered as products of the Marion hotspot formed during the rift stage of western margin of India from Madagascar. Earlier investigations: plate motions relative to the Indian Ocean hotspots (Müller *et al.* 1993), plate reconstructions (Storey *et al.* 1995; Torsvik *et al.* 2000) and submarine morphological structures of India and Madagascar (Yatheesh *et al.* 2006) suggest that the breakup between Madagascar and India occurred at around 90 Ma. The probable location of the Marion hotspot with reference to the continental masses of India, Madagascar, Seychelles and Africa for the Late Cretaceous period just prior to the emplacement of the Comorin Ridge is shown in Fig. 8 (Torsvik *et al.* 2000). Keeping these inferences and present geophysical results in view, we opine that the Comorin Ridge may have been emplaced by the Marion hotspot volcanic activity in a span of about 6 Myr from north (88–90 Ma) to south (82–84 Ma).

Isostatic compensation of the plate model with elastic plate thickness of about 15 km beneath the northern part of the Comorin Ridge suggests that the ridge was emplaced either on approximately 30 Myr old oceanic crust following the simple age–$T_e$ relationship of Calmant & Cazenave (1987) or on rifted/altered continental crust. Whereas the southern part of the ridge was emplaced on 2–3-Myr-old oceanic crust. It is difficult to reconcile the presence of old oceanic crust beneath the northern part of the ridge as the age spans for the formation of the oceanic crust from north to south beneath the ridge (about 28 Myr) and for emplacement of the ridge by the

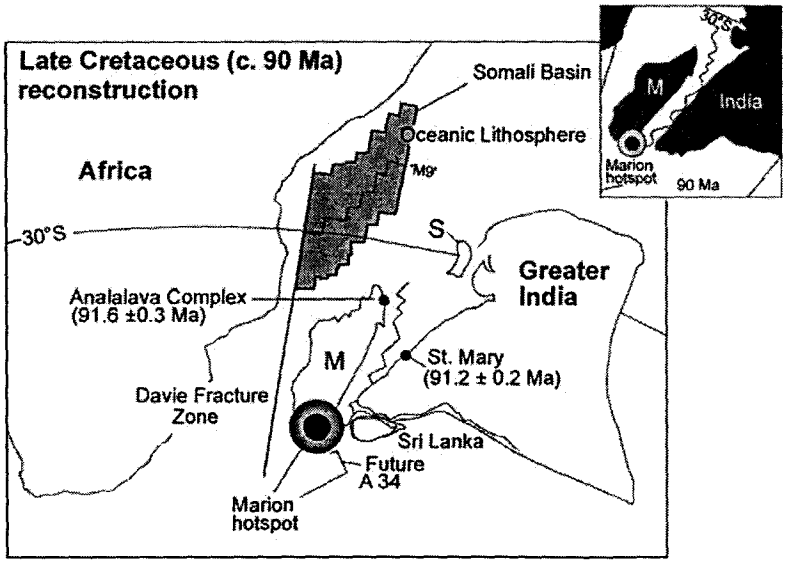


**Figure 8.** Late Cretaceous reconstruction of India, Madagascar (M), Seychelles (S) and Africa with reference to the Marion hot spot position before emplacement of the Comorin Ridge, reproduced from Torsvik *et al.* (2000).

Marion hotspot (about 6 Myr) are not in accordance with the plate motion data with reference to Indian Ocean hotspots. We, therefore, believe that the northern part of the Comorin Ridge was emplaced on rifted continental crust. The gravity model studies across the northern part of the ridge (along profile V3307) also suggest the continental nature of the crust beneath this part of the ridge (Fig. 6).

Geophysical profiles: C1215, V292b, V3406 and DME 07, across the Comorin Ridge show a distinct character of steep downward-scarp on eastern flank of the ridge. The geophysical characters such as steep seafloor topography and lateral shift in regional gravity field (Figs 3 and 6) allow us to place the COB on eastern side of the central part of the ridge (Fig. 9). The eastern side of the ridge (entire) is controlled by different tectonic elements, southernmost part (up to 3.5°N) by the 79°E FZ, central part (3.5°N to 5°N) by the COB and northernmost part by the termination of the Gulf of Mannar Basin (Fig. 9). From geophysical signatures we interpret that continental crust extends on western margin of Sri Lanka up to eastern side of the ridge and off the southern tip of India up to 5°N latitude, which includes northernmost part of the ridge (Fig. 9). Model studies of the gravity anomalies suggest that about

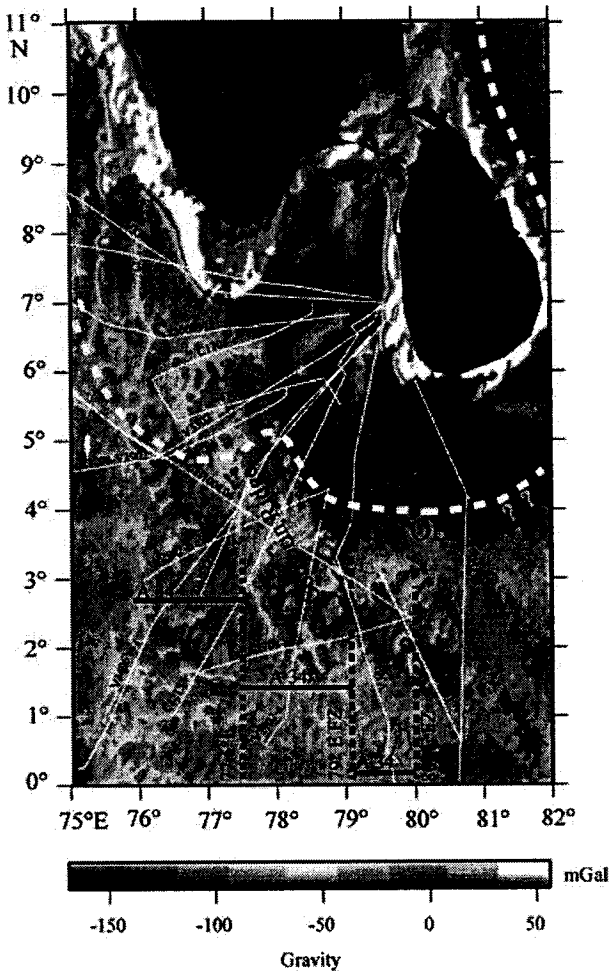


**Figure 9.** Interpreted COB on western margin of Sri Lanka and southern tip of India, geophysical profiles used in this study, fracture zones and magnetic lineation A34 are superimposed on satellite gravity field (Sandwell & Smith 1997). Eastern margin of Comorin Ridge is bounded by different tectonic elements.

21-km-thick continental crust lie on the western margin of Sri Lanka that is relatively thinner than the normal continental crust. This thin continental crust may have evolved due to the crustal stretching during the rift processes that took place between Sri Lanka and the Gunnerus Ridge part of east Antarctica (Rotstein *et al.* 2001; Kent *et al.* 2002) and between India and Madagascar (Storey *et al.* 1995; Torsvik *et al.* 2000). Demarcation of the COB on the western margin of Sri Lanka (Fig. 9) could provide new constraints on the nature of the crust beneath the Gulf of Mannar Basin. Western part of the Greater India (India–Madagascar–Seychelles) had experienced continental rifts several times in the geological past; thereby new basins have formed on continent as well as in offshore regions of western India (Krishna *et al.* 2006). The stretching process that eventually led to continental splitting contributed to the evolution of the rifted basins both on western and eastern margins of India. The basins underlined by thin continental crust did not extend further for continental breakups. For example Cambay and Kutch rifts on western India (Raval & Veeraswamy 2003b) and Laxmi Basin on western margin of India (Krishna *et al.* 2006) have remained as failed rifts due to some changes in geological settings. On the basis of subsidence rates, particularly higher rates during the Neogene, in the Gulf of Mannar Basin and folded and uplifted Bengal Deep-Sea Fan sediments off the SSE continental margin of Sri Lanka Curray (1984) has suggested the possible continuation of continental stretching in the basin. The stretching process between India and Sri Lanka may have contributed for the initiation of basin in Gulf of Mannar and the basin appears to be widening due to the continuing process of stretching. We, therefore, believe that the basin in the Gulf of Mannar had evolved by extensional tectonics, but underlained by relatively thin continental crust.

On comparison of geophysical signatures of COB obtained from this study area with those from western margin of India (Krishna *et al.* 2006) and eastern margin of India (Gopala Rao *et al.* 1997) we found that western margins of India and Sri Lanka have rifted margin character and eastern margin of India, south of 15°N latitude has transform-rift character. These observations are supported by earlier results obtained from admittance analysis of bathymetry and gravity data of conjugate margins of southeastern margin of India and Enderby Land of Antarctica (low elastic plate thickness of less than 5 km) (Chand *et al.* 2001; Subrahmanyam & Chand 2006) and conjugate margins of India and Madagascar ($T_e$ values ranging from 8 to 15 km) (Chand & Subrahmanyam 2003).

## 9 CONCLUSION

Analyses of bathymetry, magnetic and gravity data of the Comorin Ridge provide new insights regarding the structure and isostatic compensation of the ridge. The results were discussed for understanding the emplacement of the ridge, for determining the nature of the underneath crust and for demarcation of COB. Important observations are as follows.

1. The Comorin Ridge stretches for about 500 km in NNW–SSE direction in north central Indian Ocean. The ridge has variable relief along the strike and gradients across the flanks. The southern part of the ridge (between 1.5°N and 3°N) has an elevation of up to 0.5 km compared to the adjacent seafloor of about 4 km; in the central part (between 3°N and 5°N) the ridge has a maximum elevation of up to 1 km from the surrounding water depths ranging from 3 to 4 km, and in the north (between 5°N and 6.5°N) the ridge has elevation mostly on the eastern side ranging from 0.4 to 0.7 km from adjacent water depths of about 2.5 km. In the southern part of the ridge the

western flank extends for more than 100 km with relatively smooth gradient and the eastern flank steeply deepens with a scrap of about 1.2 km in a horizontal distance of about 50 km.

2. Geophysical profile data show that the ridge is associated with relatively small amplitude gravity anomalies of about 25 mGal in southern part (1.5°N–5°N) and 30 mGal in northern part (5°N–6.5°N) compared to its elevation. It is interesting to note that the less-elevated north part of the ridge is associated with 30 mGal anomaly, suggesting that this part of the ridge is relatively less compensated in comparison to that of south part of the ridge. On the eastern flank of the ridge the gravity profiles (C1215, V2902-b, V3406 and DME07) show a sudden regional shift by about 50 mGal, which may indicate the location of COB on the western margin of Sri Lanka. The seafloor magnetic anomaly 34 is identified on profiles V2902-a and C1215 and many of the other anomalies having short-wavelength and low amplitude may have formed during the Cretaceous magnetic quiet period. It is observed that the Comorin Ridge is not associated with any specific magnetic anomaly signatures.

3. Admittance analysis suggested that the southern part of the ridge (south of 5°N) is compensated with Airy model or local compensation with an elastic plate thickness of about 3 km and crustal thickness of 15–20 km, while the northern part is compensated with flexural plate model with an elastic thickness of about 15 km. 2-D forward gravity model studies suggest that the crust beneath the southern part of the Comorin Ridge is ~17 km thick with 2-km-thick volcanic rocks as surface load, 6-km-thick oceanic crust and 9-km-thick underplated magmatic rocks as subsurface load. While the gravity model across the northern part of the ridge shows that the ridge was emplaced on continental crust with a thickness of about 20 km. About 3-km-thick volcanic rocks were emplaced as surface loads on top of the crust, which had contributed to flexure the crustal layers and Moho boundary to the magnitude of about 3 km. The results further suggest that the southern part of the ridge was emplaced on relatively weak oceanic crust, while the northern part was emplaced on the continental crust.

4. The eastern side of the ridge is controlled by different tectonic elements, southernmost part by the 79°E FZ, central part by the COB and northernmost part by the termination of the Gulf of Mannar Basin. Gravity model studies have determined relatively thin ~21-km-thick continental crust on western margin of Sri Lanka, which may have evolved due to the crustal stretching during the rift processes that took place between eastern Gondwanaland fragments.

## ACKNOWLEDGMENTS

The work was jointly carried out under NIO-NGRI collaborative project. We thank Directors, NIO and NGRI for the encouragement in this joint research work. Authors are thankful to Dr D. Gopala Rao, CSIR Emeritus Scientist for his constructive comments at various stages of the manuscript. K. M. Sreejith is thankful to CSIR, New Delhi for awarding JRF position. Department of Science & Technology, New Delhi (project: ESS/16/174/2002) has supported the work. The figures were prepared with GMT software (Wessel & Smith 1991). This is NIO contribution number 4334.

## REFERENCES

Ashalatha, C., Subrahmanyam, C. & Singh, R.N., 1991. Origin and compensation of Chagos-Laccadive ridge, Indian Ocean, from admittance analysis of gravity and bathymetry data, *Earth. planet. Sci. Lett.*, **105**, 47–54.

Bansal, A.R., Fairhead, J.D., Green, C.M., Fletcher, K.M.U., 2005. Revised gravity for offshore India and the isostatic compensation of submarine features, *Tectonophysics*, **404**, 1–22.

Bull, J.M. & Scrutton, R.A., 1990. Sediment velocities and deep structure from wide-angle reflection data around Leg 116 sites, in *Proceedings of the Ocean Drill Program, Sci. Results*, pp. 211–316, eds Cochran, J.R. *et al.*, Ocean Drilling Program, College Station, TX, USA.

Calmant, S. & Cazenave, A., 1987. Anomalous elastic thickness of the oceanic lithosphere in the south-central Pacific, *Nature*, **328**, 236–238.

Chand, S. & Subrahmanyam, C., 2003. Rifting between India and Madagascar-mechanism and isostasy, *Earth. planet. Sci. Lett.*, **210**, 317–332.

Chand, S. Radhakrishna, M. & Subrahmanyam, C., 2001. India-East Antarctica conjugate margins: rift-shear tectonic setting inferred from gravity and bathymetry data, *Earth. planet. Sci. Lett.*, **185**, 225–236.

Chaubey, A.K., Gopala Rao, D., Srinivas, K., Ramprasad, T., Ramana, M.V. & Subrahmanyam, V., 2002. Analysis of multichannel seismic reflection, gravity and magnetic data along a regional profile across the central-western continental margin of India, *Mar. Geol.*, **182**, 303–323.

Christensen, N.I., 1977. Seismic velocities and elastic moduli of igneus and metamorphic rocks from Indian Ocean, in *Indian Ocean Geology and Biostratigraphy*, eds Heirtzler, J.R., Bolli, H.M., Davis, T.A., Savnders, J.B.L. & Sclater, J.G., pp. 279–299, AGU, Washington DC.

Curray, J.R., 1984. Sri Lanka: is a Mid-Plate Platelet? *J. Natio. Acqua. Resour. Agen.*, **31**, 30–50.

Detrick, R.S. & Watts, A.B., 1979. An analysis of Isostasy in the world's oceans 3. Aseismic ridges, *J. geophys. Res.*, **84**, 3637–3653.

Gaina, C., Müller, R.D., Brown, B. & Ishihara, T., 2003. Microcontinent formation around Australia, in *The Evolution and Dynamics of the Australian Plate*, Pap. 22, pp. 399–410, eds Hillis, R. & Müller, R.D., Joint Geol. Soc. of Aust. Am. Spec.

Gaina, C., Müller, R.D., Brown, B. & Ishihara, T., 2007. Breakup and early spreading between India and Antarctica, *Geophys. J. Int.*, **170**, 151–169.

Gopala Rao, D., Krishna, K.S. & Sar, D., 1997. Crustal evolution and sedimentation history of the Bay of Bengal since the Cretaceous, *J. geophys. Res.*, **102**, 17 747–17 768.

Gopala Rao, D., Krishna, K.S., Neprochnov, Yu.P. & Grinko, B.N., 2004. Satellite gravity anomalies and crustal features of the central Indian Ocean basin, *Curr. Sci.*, **86**, 948–957.

Heezen, B.C. & Tharp, M., 1964. Physiographic diagram of the Indian Ocean, *Map*, Geol. Soc. America, Boulder, Colorado.

Kamesh Raju, K.A., Ramprasad, T., Kodagali, V.N. & Nair, R.R., 1993. Multibeam bathymetry, gravity and magnetic studies over 79°E Fracture Zone, Central Indian Basin, *J. geophys. Res.*, **98**, 9605–9618.

Kahle, H.G., Naini, B.R., Talwani, M. & Eldholm, O., 1981. Marine geophysical study of the Comorin ridge, north central Indian basin, *J. geophys. Res.*, **86**, 3807–3814.

Kent, R.W., Pringle, M.S., Müller, R.D., Saunders, A.D. & Ghose, N.C., 2002. $^{40}Ar/^{39}Ar$ Geochronology of the Rajmahal basalts, India, and their relationship to the Kerguelen plateau, *J. Petrol.*, **43**, 1141–1153.

Krishna, K.S., 2003. Structure and evolution of the Afanasy Nikitin seamount, buried hills and 85°E Ridge in the northern Indian Ocean, *Earth. planet. Sci. Lett.*, **209**, 379–394.

Krishna, K.S. & Gopala Rao, D., 2000. Abandoned Paleocene spreading center in the north eastern Indian Ocean: evidence from magnetic and seismic reflection data, *Mar. Geol.*, **162**, 215–224.

Krishna, K.S., Bull, J.M. & Scrutton, R.A., 2001a. Evidence for multiphase folding of the central Indian Ocean lithosphere, *Geology*, **29**, 715–718.

Krishna, K.S., Neprochnov, Y.P., Gopala Rao, D. & Grinko, B.N., 2001b. Crustal structure and tectonics of the Ninetyeast Ridge from seismic and gravity studies, *Tectonics*, **20**, 416–433.

Krishna, K.S., Gopala Rao, D. & Sar, D., 2006. Nature of the crust in the Laxmi Basin (14°-20°N) western continental margin of India, *Tectonics*, **25**, TC1006, doi: 10.1029/ 2004TC001747.

Kumar, A., Pande, K., Venkatesan, T.R. & Baskar Rao, Y.J., 2001. The Karnataka Late Cretaceous dykes as products of the Marion hot spot at the

Madagascar-India breakup event: evidence from $^{40}$Ar-$^{39}$ Ar geochronology and geochemistry, *Geophys. Res. Lett.*, **28,** 2715–2718.

McKenzie, D. & Bowin, C., 1976. The relationship between bathymetry and gravity in Atlantic Ocean, *J. geophys. Res.*, **81,** 1903–1915.

Müller, R.D., Royer, J.-Y. & Lawver, L.A., 1993. Revised plate motions relative to the hotspots from combined Atlantic and Indian Ocean hotspot tracks, *Geology,* **21,** 275–278.

Müller, R.D., Roest, W.R., Royer, J.-Y., Gahagan, L.M. & Sclater, J.G., 1997. Digital isochrones of the world's ocean floor, *J. geophys. Res.*, **102,** 3211–3214.

Naini, B.R., & Talwani, M., 1983. Structural framework and the evolutionary history of the continental margin of western India, in *Studies in Continental Margin Geology,* Vol. 34, pp. 167–191, eds Watkins, J.S., & Drake, C.L., AAPG Mem., Tulsa, OK, USA.

National Geophysical Data Centre (NGDC), 1998. *GEODAS CD-ROM, 98-MGG-04, Worldwide Marine Geophysical Data,* Up-dated 4th edn, National Oceanic and Atmospheric Administration, US Department of Commerce, Washington, DC.

Neprochnov, Yu.P., Gopala Rao, D., Murthy, K.S.R. & Subrahmanyam, C., 1998. Intraplate deformation in the Central Indian Ocean Basin, *Geol. Soc. India. Memoir.,* Vol. 39, pp. 71–86, GSI, Bangalore, India.

Nogi, Y., Nishi, K., Seama, N. & Fukuda, Y., 2004. An interpretation of the seafloor spreading history of the west Enderby basin between initial breakup of Gondwana and anomaly C34, *Mar. Geophys. Res.*, **25,** 219–229.

Paul, J., Singh, R.N., Subrahmanyam, C. & Drolia, R.K., 1990. Emplacement of Afanasy-Nikitin seamount based on transfer function analysis of gravity and bathymetry data, *Earth. planet. Sci. Lett.*, **96,** 419–426.

Radhakrishna, T., Dallmeyer, R.D. & Josheph, M., 1994. Palaeomagnetism and $^{36}$Ar/$^{40}$Ar isotope correlation ages of dyke swarms in central Kerala, India: tectonic implications, *Earth. planet. Sci. Lett.*, **121,** 213–226.

Raval, U. & Veeraswamy, K., 2003a. India-Madagascar seperation: breakup along a pre-existing mobile belt and chipping of the craton, *Gondwana Res.*, **6,** 467–485.

Raval, U. & Veeraswamy, K., 2003b. Modification of geological and geophysical regimes due to interaction of mantle plume with Indian lithosphere, *J. Virtual Explor.,* **12,** 117–143.

Rotstein, Y., Munschy, M. & Bernard, A., 2001. The Kerguelen province revisited: additional constraints on the development of the southeast Indian Ocean. *Mar. Geophys. Res.*, **22,** 81–100.

Sandwell, D.T. & Smith, W.H.F., 1997. Marine gravity from Geosat and ERS-1 satellite altimetry, *J. geophys. Res.*, **102,** 10 039–10 054.

Stagg, H.M.J., Calwell, J.B., Direen, N.G., O' Brien, P.E., Bernardel, G., Borissova, I., Brown, B.J. & Ishihara, T., 2004. Geology of the continental margin of Enderby and Mac. Robertson Lands, East Antarctica: insights from a regional data set, *Mar. Geophys. Res.* doi:10.1007/S11001–005-1316–1.

Storey, M., Mahoney, J.J., Saunders, A.D., Duncan, R.A., Kelley, S.P. & Coffin, M.F., 1995. Timing of hot spot-related volcanism and the breakup of Madagascar and India, *Science,* **267,** 852–855.

Storey, M., Mahoney, J.J. & Saunders, A.D., 1997. Cretaceous basalts in Madagascar and the transition between plume and continental lithosphere mantle sources, in *Large Igneous provinces: Continental, Oceanic, and Planetary Flood Volcanism,* pp. 95–122, eds Mahoney, J.J. & Coffin, M., Am. Geophys. Union, Monogr, Washington, DC.

Subrahmanyam, C. & Chand, S., 2006. Evolution of the passive continental margins of India-a geophysical appraisal, *Gondwana Res.*, **10,** 167–178.

Subrahmanyam, V. Krishna, K.S., Radhakrishna Murty, I.V., Sarma, K.V.L.N.S., Maria, Desa, Ramana, M.V. & Kamesh Raju, K.A., 2001. Gravity anomalies and crustal structure of the Bay of Bengal, *Earth. planet. Sci. Lett.*, **192,** 447–456.

Tiwari, V.M., Diament, M. & Sing, S.C., 2003. Analysis of satellite gravity and bathymetry data over Ninety-East Ridge: variation in the compensation mechanism and implication for emplacement processes. *J. geophys. Res.*, **108,** 2109, doi:10.1029/2000JB000047.

Torsvik, T.H., Tucker, R.D., Ashwal, L.D., Eide, E.A., Rakotosolofo, N.A. & Dewit, M.J., 1998. Late cretaceous magmatism in Madagascar: paleomagnetic evidence for a stationary Marion hotspot, *Earth. planet. Sci. Lett.*, **164,** 221–232.

Torsvik, T.H., Tucker, R.D., Ashwal, L.D., Carter, L.M., Jamtveit, B., Vidyadharan, K.T. & Venkataramana, P., 2000. Late Cretaceous India-Madagascar fit and timing of break-up related magmatism, *Terra Nova,* **12,** 220–224.

Yatheesh, V., Bhattacharya, G.C. & Mahender, K., 2006. The terrace like feature in the mid-continental slope region off Trivandrum and plausible model for India-Madagascar juxtaposition in immediate pre-drift scenario, *Gondwana Res.*, **10,** 179–185.

Watts, A.B., 1978. An analysis of isostasy in world's Oceans 1. Hawaiian-Emperor seamount chain, *J. geophys. Res.*, **83,** 5989–6004.

Watts, A.B., 2001. *Isostasy and Flexure of the Lithosphere,* pp. 458, Cambridge University Press, UK.

Welch, P., 1967. The use of fast Fourier transform for the estimation of power spectra: a method based on time averaging over short, modified periodograms, *IEEE Trans. Audio Electroacoust.*, **15,** 70–73.

Wessel, P. & Smith, W.H.F., 1991. Free software helps map and display data, *EOS Trans. AGU,* **72,** 44–446.

White, R. & McKenzie, D., 1989. Magmatism at rift zones—the generation of volcanic continental margins and flood basalts, *J. geophys. Res.*, **94,** 7685–7729.

Journal of
EARTH SYSTEM SCIENCE
HOME • LOGIN • HELP • REGISTER • UPDATE MY INFORMATION • JOURNAL OVERVIEW
MAIN MENU • CONTACT US • SUBMIT A MANUSCRIPT • INSTRUCTIONS FOR AUTHORS

# Development of the negative gravity anomaly of the 85°E Ridge, northeastern Indian Ocean – a process oriented modeling approach

**K.M. Sreejith[1#], M. Radhakrishna[2], K.S. Krishna[3] and T. J. Majumdar[1]**

[1]Geosciences Division, Marine, Geo and Planetary Sciences Group, Space Applications Centre, Indian Space Research Organization, Ahmedabad-380 015, India

[2]Department of Earth Sciences, Indian Institute of Technology Bombay, Powai, Mumbai-400 076, India

[3]National Institute of Oceanography, Council of Scientific and Industrial Research, Dona Paula, Goa-403 004, India

[#]Corresponding author (E-mail: sreejith81@gmail.com; Phone: +91 79 26914103)



**Abstract**

The 85°E Ridge extends from the Mahanadi Basin, off northeastern margin of India to the Afanasy Nikitin seamount in the Central Indian Basin. The ridge is associated with two contrasting gravity anomalies: negative anomaly over the north part (up to 5°N latitude), where the ridge structure is buried under thick Bengal Fan sediments and positive anomaly over the south part, where the structure is intermittently exposed above the seafloor. Ship-borne gravity and seismic reflection data are modeled using process oriented method and this suggest that the 85°E Ridge was emplaced on approximately 10-15 km thick elastic plate (Te) and in an off-ridge tectonic setting. We simulated gravity anomalies for different crust-sediment structural configurations of the ridge that were existing at three geological ages, such as late Cretaceous, early Miocene and Present. The study shows that the gravity anomaly of the ridge in the north has changed through time from its inception to present. During the late Cretaceous the ridge was associated with a significant positive anomaly with a compensation generated by a broad flexure of the Moho boundary. By early Miocene the ridge was approximately covered by the post-collision sediments and led to alteration of the initial gravity anomaly to a small positive anomaly. At present, the ridge is buried by approximately 3 km thick Bengal Fan sediments on its crestal region and about 8 km thick pre- and post-collision sediments on the flanks. This geological setting had changed physical properties of the sediments and led to alter the minor positive gravity anomaly of early Miocene to the distinct negative gravity anomaly.

**Keywords**: 85°E Ridge; elastic plate thickness; lithospheric flexure; process oriented modeling; Bengal Fan; northeastern Indian Ocean